



RESEARCH

2009-06

Implementation of the MEPDG for New and Rehabilitated
Pavement Structures for Design of Concrete and
Asphalt Pavements in Minnesota



Take the



steps...

Research...Knowledge...Innovative Solutions!

Transportation Research

Technical Report Documentation Page

1. Report No. MN/RC 2009-06	2.	3. Recipients Accession No.	
4. Title and Subtitle Implementation of the MEPDG for New and Rehabilitated Pavement Structures for Design of Concrete and Asphalt Pavements in Minnesota		5. Report Date January 2009	
		6.	
7. Author(s) Raul Velasquez, Kyle Hoegh, Iliya Yut, Nova Funk, George Cochran, Mihai Marasteanu, Lev Khazanovich		8. Performing Organization Report No.	
9. Performing Organization Name and Address Department of Civil Engineering University of Minnesota 500 Pillsbury Dr. SE Minneapolis, Minnesota 55455-0220		10. Project/Task/Work Unit No.	
		11. Contract (C) or Grant (G) No. (c) 81655 (wo) 121	
12. Sponsoring Organization Name and Address Minnesota Department of Transportation 395 John Ireland Boulevard, Mail Stop 330 St. Paul, Minnesota 55155		13. Type of Report and Period Covered Final Report	
		14. Sponsoring Agency Code	
15. Supplementary Notes http://www.lrrb.org/PDF/200906.pdf			
16. Abstract (Limit: 200 words) <p>The recently introduced Mechanistic-Empirical Pavement Design Guide (MEPDG) and related software provide capabilities for the analysis and performance prediction of different types of flexible and rigid pavements. An important aspect of this process is the evaluation of the performance prediction models and sensitivity of the predicted distresses to various input parameters for local conditions and, if necessary, re-calibration of the performance prediction models. To achieve these objectives, the Minnesota Department of Transportation (MnDOT) and the Local Road Research Board (LRRB) initiated a study "Implementation of the MEPDG for New and Rehabilitated Pavement Structures for Design of Concrete and Asphalt Pavements in Minnesota."</p> <p>This report presents the results of the evaluation of default inputs, identification of deficiencies in the software, sensitivity analysis, and comparison of results to the expected limits for typical Minnesota site conditions, a wide range of pavement design features (e.g. layer thickness, material properties, etc), and the effects of different parameters on predicted pavement distresses. Since the sensitivity analysis was conducted over a span of several years and the MEPDG software underwent significant modifications, especially for flexible pavements, various versions of the MEPDG software were run. Performance prediction models of the latest version of the MEPDG 1.003 were evaluated and modified or recalibrated to reduce bias and error in performance prediction for Minnesota conditions.</p>			
17. Document Analysis/Descriptors MEPDG, pavement design, pavement performance, distress models, cracking, rutting, faulting, local calibration		18. Availability Statement No restrictions. Document available from: National Technical Information Services, Springfield, Virginia 22161	
19. Security Class (this report) Unclassified	20. Security Class (this page) Unclassified	21. No. of Pages 229	22. Price

Implementation of the MEPDG for New and Rehabilitated Pavement Structures for Design of Concrete and Asphalt Pavements in Minnesota

Final Report

Prepared by

Raul Velasquez
Kyle Hoegh
Iliya Yut
Nova Funk
George Cochran
Mihai Marasteanu
Lev Khazanovich

Department of Civil Engineering
University of Minnesota

January 2009

Published by

Minnesota Department of Transportation
Research Services Section
395 John Ireland Boulevard, MS 330
St. Paul, Minnesota 55155-1899

This report represents the results of research conducted by the authors and does not necessarily represent the views or policies of the Minnesota Department of Transportation and/or the Center for Transportation Studies. This report does not contain a standard or specified technique.

The authors and the Minnesota Department of Transportation and/or Center for Transportation Studies do not endorse products or manufacturers. Trade or manufacturers' names appear herein solely because they are considered essential to this report.

Acknowledgements

The research described in this paper is sponsored by the Minnesota Department of Transportation, Contract No. 81655, Work Order 133. This research study would not have been possible without the contribution of a number of individuals. The authors would like to acknowledge the significant efforts of the technical advisory panel members Jerry Geib (technical liaison), Maureen Jensen, Curtis Turgeon, Dave VanDeusen, Shongtao Dai, Tom Burnham, Matthew Oman, Bruce Chadbourn, Graig Gilbertson, Dennis Iverson, Chris Dulan, and Dan Warzala (administrative liaison). The authors also would like to thank engineers and computer programmers from ARA, Inc. for their cooperation.

Table of Contents

Chapter 1 Introduction.....	1
Chapter 2 Evaluation of Typical MEPDG Inputs	3
2.1 Introduction	3
2.2 Major MEPDG Inputs	3
2.3 Asphalt Characterization	16
2.4 PCC Material Characterization.....	27
2.5 Unbound Material Properties	32
Chapter 3 Evaluation of the Design Guide Performance Prediction.....	34
3.1 Introduction	34
3.2 Flexible Pavements.....	34
3.3 Rigid Pavements.....	80
Chapter 4 Special Topics.....	89
4.1 Introduction	89
4.2 Subgrade Characterization.....	89
4.3 Stabilized Base Characterization.....	117
4.4 Asphalt Binder Characterization	122
4.5 Asphalt Binder Characterization	126
Chapter 5 Recalibration of MEPDG Prediction Models	130
5.1 Introduction	130
5.2 Flexible Pavements.....	130
5.3 Rigid Pavements.....	153
5.4 Calibration Conclusions	158
Chapter 6 Conclusions.....	159
References	161
Appendix A: Examples of Predicted Distresses for Rigid Pavements	

List of Tables

Table 2.1	Minnesota truck seasonal adjustment factors.	8
Table 2.2	Minnesota ICM weather station locations and region names.	10
Table 2.3	Mn/DOT pavement selection process & design options.	12
Table 2.4	A and VTS defaults for select Superpave grades.	21
Table 2.5	PCC unit weight and Poisson's ratio for the Minnesota LTPP sections.	28
Table 3.1	10 million ESAL's summary inputs	35
Table 3.2	1 million ESAL's summary inputs	36
Table 3.3	Maximum values of the predicted distresses for 10 million ESAL's	37
Table 3.4	Maximum values of the predicted distresses for 1 million ESAL's	37
Table 3.5	P-values for 10 million ESAL's	54
Table 3.6	P-values for 1 million ESAL's	55
Table 3.7	Coding of input parameters for 10 million ESAL's	56
Table 3.8	Coding of input parameters for 1 million ESAL's	57
Table 3.9	Correlation matrix for 10 million ESAL's	57
Table 3.10	Correlation matrix for 1 million ESAL's	57
Table 3.11	Sensitivity summary for 10 million ESAL's	58
Table 3.12	Sensitivity summary for 1 million ESAL's	59
Table 3.13	Factorial of input parameters – First phase.	81
Table 3.14	Factorial of input parameters – Second phase.	82
Table 3.15	Cracking correlation matrix.	87
Table 3.16	Faulting correlation matrix.	88
Table 4.1	Summary of correlations to estimate material properties.(4).	91
Table 4.2	Resilient moduli recommended by the MEPDG based on the soil classification.	91
Table 4.3	k_1 , k_2 and k_3 parameters for the materials tested by CRREL.	95
Table 4.4	k_1 - k_2 - k_3 parameters for MnROAD materials obtained from MnDOT test results.	97
Table 4.5	k_1 - k_2 - k_3 parameters obtained in the Arizona DOT-sponsored study.	98
Table 4.6	Typical ranges of values for each of the k parameters for coarse grained and fine grained materials.	98
Table 4.7	Sets of k parameters chosen for the unbound layers and subgrade of the pavement structure examined in the sensitivity analysis.	102
Table 4.8	Resilient moduli.	113
Table 4.9	Coefficients of the effective stiffness -- subgrade resilient modulus correlations.	116
Table 4.10	Typical values for modulus of rupture (AASHTO 2008).	120
Table 4.11	Example of new flexible pavement designed in MEPDG for analysis.	121
Table 4.12	$ G^* $ and δ at $\omega = 10$ rad/sec for PG 58-28 binder.	123
Table 4.13	Input Summary for pavement structure.	126
Table 4.14	Percent slabs cracked for locations in Minnesota.	128
Table 5.1	Design parameters of the measured and predicted rutting cells (MnROAD 2008).	132
Table 5.2	Seasonal FHWA vehicle class distribution.	136

Table 5.3 Base material properties.....	136
Table 5.4 Subgrade material properties.	137

List of Figures

Figure 2.1	Design life and pavement type input screen.....	4
Figure 2.2	Distribution of flexible pavement ages at reconstruction.....	5
Figure 2.3	Distribution of rigid pavement ages at reconstruction.....	5
Figure 2.4	Traffic input screen.....	6
Figure 2.5	AADTT calculator.....	6
Figure 2.6	Number of lanes on Minnesota roads (WIM sites).....	7
Figure 2.7	Truck traffic monthly adjustment input screen (Urban MN).....	7
Figure 2.8	Hourly truck traffic distribution input screen (Urban MN).....	8
Figure 2.9	Hourly percent of the 24-hr period based on the 2000-2003 vehicle class tube counts-trunk highways rural and urban.....	9
Figure 2.10	Virtual weather station generation screen.....	10
Figure 2.11	Predicted rutting vs. climate.....	11
Figure 2.12	Mn/DOT pavement design standards.....	12
Figure 2.13	Pavement cross section input screen: Mn/DOT design standard no. 2.....	13
Figure 2.14	Pavement cross section input screen: Mn/DOT design standard no. 4.....	13
Figure 2.15	Distribution of AC surface thicknesses in the Mn/DOT PMS database.....	14
Figure 2.16	Distribution of PCC surface thicknesses in the Mn/DOT PMS database.....	14
Figure 2.17	Distribution of joint spacing for Minnesota JPCP pavements.....	15
Figure 2.18	Asphalt layer thickness input screen.....	16
Figure 2.19	Average percent passing for Minnesota asphalt mix gradation.....	17
Figure 2.20	Predicted rutting vs. % passing #200 sieve.....	18
Figure 2.21	Asphalt binder: Superpave binder grading.....	19
Figure 2.22	Asphalt binder: conventional viscosity grade.....	19
Figure 2.23	Asphalt binder: conventional penetration grade.....	20
Figure 2.24	Predicted rutting vs. PG grade.....	20
Figure 2.25	Asphalt general properties input screen (Level 3).....	22
Figure 2.26	Thermal cracking.....	23
Figure 2.27	Asphalt binder: Superpave binder test data.....	24
Figure 2.28	Asphalt binder: conventional binder test data.....	25
Figure 2.29	Level 2: thermal cracking input screen.....	26
Figure 2.30	Level 1: asphalt mix properties input screen.....	27
Figure 2.31	PCC material properties input screen.....	29
Figure 2.32	PCC mix properties input screen.....	30
Figure 2.33	PCC strength properties input screen (Level 3).....	30
Figure 2.34	PCC strength properties input screen (Level 2).....	31
Figure 2.35	PCC strength properties input screen (Level 1).....	32
Figure 2.36	EICM inputs for unbound materials.....	33
Figure 3.1	Alligator cracking after 20 years for 10 million ESAL's.....	38
Figure 3.2	Longitudinal cracking after 20 years for 10 million ESAL's.....	40
Figure 3.3	Transverse cracking after 20 years for 10 million ESAL's.....	41
Figure 3.4	Total rutting after 20 years for 10 million ESAL's.....	42
Figure 3.5	AC rutting after 20 years for 10 million ESAL's.....	43
Figure 3.6	IRI after 20 years for 10 million ESAL's.....	45
Figure 3.7	Alligator cracking after 20 years for 1 million ESAL's.....	46

Figure 3.8	Longitudinal cracking after 20 years for 1 million ESAL's	47
Figure 3.9	Transverse cracking after 20 years for 1 million ESAL's	49
Figure 3.10	Total rutting after 20 years for 1 million ESAL's	50
Figure 3.11	AC rutting after 20 years from 1 million ESAL's	51
Figure 3.12	IRI after 20 years for 1 million ESAL's	52
Figure 3.13	Comparison for predicted distresses between 0.615 and 0.900 version for alligator cracking	60
Figure 3.14	Comparison for predicted distresses between 0.615 and 0.900 version for longitudinal cracking	60
Figure 3.15	Comparison for predicted distresses between 0.615 and 0.900 version for AC rutting	61
Figure 3.16	Comparison for predicted distresses between 0.615 and 0.900 version for total Rutting	61
Figure 3.17	Alligator cracking comparison	62
Figure 3.18	Longitudinal cracking comparison	63
Figure 3.19	Total rutting comparison	63
Figure 3.20	Transverse cracking comparison	64
Figure 3.21	IRI comparison	64
Figure 3.22	Alligator cracking comparison	65
Figure 3.23	Longitudinal cracking comparison	66
Figure 3.24	Total rutting comparison	67
Figure 3.25	AC rutting	67
Figure 3.26	Transverse cracking comparison	68
Figure 3.27	IRI comparison	69
Figure 3.28	Alligator cracking comparison	70
Figure 3.29	Longitudinal cracking comparison	71
Figure 3.30	Total rutting comparison	72
Figure 3.31	AC rutting	72
Figure 3.32	Transverse cracking comparison	73
Figure 3.33	IRI comparison	73
Figure 3.34	Longitudinal cracking after 20 years for 10 million ESAL's	75
Figure 3.35	Transverse cracking after 20 years for 10 million ESAL's	76
Figure 3.36	AC Rutting after 20 years for 10 million ESAL's	77
Figure 3.37	Total rutting after 20 years for 10 million ESAL's	78
Figure 3.38	IRI after 20 years for 10 million ESAL's	79
Figure 4.1	Correction factor as a function of the degree of saturation	93
Figure 4.2	Comparison between the CRREL's M_R Model and the k_1 - k_2 - k_3 M_R Model, for different levels of octahedral shear stress	96
Figure 4.3	A pavement system assumed for calculation with BISAR	101
Figure 4.4	Effect of the asphalt layer thickness on predicted resilient moduli	103
Figure 4.5	Effect of base thickness on predicted resilient moduli	103
Figure 4.6	Effect of subbase thickness on predicted resilient moduli	104
Figure 4.7	Effect of base k_1 on predicted resilient moduli	105
Figure 4.8	Effect of base k_2 on predicted resilient moduli	105
Figure 4.9	Effect of subbase k_3 on predicted resilient moduli	106
Figure 4.10	Effect of subbase k_1 on predicted resilient moduli	106

Figure 4.11	Effect of subbase k2 on predicted resilient moduli.	107
Figure 4.12	Effect of subgrade k3 on predicted resilient moduli.	107
Figure 4.13	Effect of subgrade k1 on predicted resilient moduli.	108
Figure 4.14	Effect of subgrade k2 on predicted resilient moduli.	108
Figure 4.15	Effect of subgrade k3 on predicted resilient moduli.	109
Figure 4.16	Predicted subgrade and base moduli for various AC thicknesses. Base modulus is not constrained.....	110
Figure 4.17	Predicted subgrade and base moduli for various AC thicknesses. The minimum allowed value for the base modulus is equal to 30,000 psi.	111
Figure 4.18	Predicted resilient modulus for the A ₇₋₆ subgrade material St. Louis 1.	114
Figure 4.19	Predicted resilient modulus for the A ₆ subgrade material Silty Loam 1.	115
Figure 4.20	MEPDG user interface of cement stabilized layer for (a) flexible pavement and (b) rigid pavement.	118
Figure 4.21	Warning screen for CTB layer in flexible pavement.....	119
Figure 4.22	Warning messages for modulus of rupture values.	120
Figure 4.23	MEPDG screenshot illustrating presence of reflective cracking models in AC overlay analysis.	120
Figure 4.24	MEPDG screenshot suggesting absence of reflective cracking models in flexible analysis.	121
Figure 4.25	Absence of any degradation of the modulus of elasticity of a CTB layer in a new flexible system after 10 years and 60 million flexible ESALs from MEPDG version 1.00.....	122
Figure 4.26	Rutting vs. time for AC pavement located in Columbus, Ohio.....	124
Figure 4.27	Alligator cracking vs. time for AC pavement located in Columbus, Ohio.	124
Figure 4.28	Longitudinal cracking vs. time for AC pavement located in Columbus, Ohio.....	125
Figure 4.29	IRI vs. time for AC pavement located in Columbus, Ohio.	125
Figure 4.30	Additional locations selected between MSP and STC.	127
Figure 4.31	Location of weather stations listed by MEPDG for Minnesota.	127
Figure 4.32	MEPDG interface showing error for missing data.	128
Figure 4.33	MEPDG interface showing number of missing months.....	129
Figure 5.1	MnROAD test sections with design details of the asphalt sections, updated August 2005 (MnROAD 2008).	131
Figure 5.2	Straightedge method for measuring rut depth (Mulvaney and Worel 2002).....	135
Figure 5.3	Group A measured and predicted rutting over the pavement age (Cell 1).	138
Figure 5.4	Group B measured and predicted rutting over the pavement age (Cell 2).	138
Figure 5.5	Cell 2 predicted and measured rutting versus pavement age using equation 2.....	140
Figure 5.6	Cell 1 predicted rutting using equation 2.	141
Figure 5.7	Measured versus predicted rutting after 10 years without subtraction of the initial base and subgrade rutting jump.	142
Figure 5.8	10 year total rutting after the correction for the initial subgrade and base rutting.....	142
Figure 5.9	Total rutting predictions from 5.1 and 5.2 vs measured rutting after five years.	143
Figure 5.10	Predicted versus measured total rutting after five and 10 years.....	143

Figure 5.11 Truck and passing lane predicted and measured rutting after five and 10 years.....	144
Figure 5.12 Predicted rutting for cell 4 with 50% reliability using equation 5.1.....	145
Figure 5.13 Predicted rutting for cell 4 at 50% reliability using equation 5.2.....	146
Figure 5.14 Predicted rutting for cell 4 at 90% reliability using equation 5.2.....	147
Figure 5.15 Measured and predicted alligator cracking for HMA MnROAD cells	149
Figure 5.16 Fatigue damage comparison of MnPAVE and MEPDG.....	150
Figure 5.17 Adjustment of local calibration settings in the MEPDG software.....	151
Figure 5.18 Measured and predicted transverse cracking.....	152
Figure 5.19 Measured and predicted longitudinal cracking.....	153
Figure 5.20 Measured vs predicted PCC cracking. Nationally calibrated model.....	156
Figure 5.21 Measured vs recalibrated predicted PCC cracking.....	157
Figure 5.22 IRI as function of the age of PCC pavement.....	158

Executive Summary

The recently introduced Mechanistic-Empirical Pavement Design Guide (MEPDG) and related software provide capabilities for the analysis and performance prediction of different types of flexible and rigid pavements. In this study, the evaluation of default inputs, identification of deficiencies in the software, sensitivity analysis, and evaluation of the prediction capabilities of the MEPDG were conducted for Minnesota conditions, and performance prediction models were modified or recalibrated.

The rigid pavement sensitivity analysis confirmed the robustness of the design procedure. The flexible pavement sensitivity analysis and comparison of predictions to expected limits resulted in the identification of several MEPDG software bugs which were reported to the software developers, thus improving the MEPDG program. In addition, during the analysis conducted in this study, multiple issues, related to MEPDG subgrade characterization, stabilized base characterization, asphalt binder characterization, and climate inputs, were encountered. These issues will need to be addressed in future versions of the MEPDG software.

The MEPDG performance predictions were evaluated using field performance data obtained from MnROAD pavement sections as well as other pavement sections located in Minnesota and neighboring states. A need for recalibration of the cracking models for rigid and flexible pavements for Minnesota conditions was identified and a recalibration was conducted. In addition, it was found that the rutting models for the base and subgrade of flexible pavements could not be properly calibrated by adjusting the model parameters and thus appropriate modifications were proposed. This resulted in a reduction of bias and error in the design procedure performance prediction for Minnesota conditions. These models should be further evaluated and validated in future studies. However, it is anticipated that AASHTO will sponsor a significant upgrade of the software in the near future. It is recommended to repeat the calibration process and conduct verification and validation with the professional grade software. Meanwhile, the current version of the software, with the proposed recalibrated models adjustment and modified calibration coefficients, can be used for pilot evaluation of the MEPDG along with the current design procedures. The MEDPG can be implemented completely for the design of rigid pavements and partially (without the longitudinal cracking and IRI models) for the design of flexible pavements.

Chapter 1 Introduction

The AASHTO interim Mechanistic-Empirical Pavement Design Guide (MEPDG) Manual of Practice, also known as the MEPDG, was recently introduced in the United States (AASHTO 2008). The development of such a procedure was conducted by the National Cooperative Highway Research Program (NCHRP) under sponsorship by the American Association of State Highway and Transportation Officials (AASHTO). The MEPDG and related software provide capabilities for the analysis and performance prediction of different types of flexible and rigid pavements.

The MEPDG uses mechanistic-empirical numerical models to analyze input data for traffic, climate, materials and proposed structure. The models estimate damage accumulation over service life. The MEPDG is applicable for designs of both flexible and rigid pavements. The concept of pavement performance accounts for structural and functional performance, which the Guide is primarily concerned with. Performance predictions are made in terms of pavement distresses and ride quality. Prediction of the following distresses is included in the MEPDG:

- Flexible or AC pavements:
 - Rutting (El-Basyouny et al. 2005a, El-Basyouny et al. 2005b)
 - Bottom-up AC fatigue cracking (Witczak and Mirza 2000, El-Basyouny and Witczak 2005a, Basyouny and Witczak 2005b, Basyouny and Witczak 2005c)
 - Top-down AC fatigue cracking (Witczak and Mirza 2000, El-Basyouny and Witczak 2005a, El-Basyouny and Witczak 2005d)
 - Thermal cracking (Roque et al. 1995)
- Jointed plain concrete pavement (JPCP):
 - Joint faulting (Darter et al. 2001, Khazanovich et al. 2004)
 - Transverse cracking (Darter et al. 2001)
- Continuously reinforced rigid pavements (CRCP):
 - Punchouts (Selesneva et al 2004)

For all pavement types, mechanistic-empirical distress predictions are empirically correlated to the International Roughness Index (IRI). The IRI is employed as a functional criterion in the design process.

The Design Guide is a significant innovation in the way pavement design is performed—design inputs include traffic (full load spectra for single, tandem, tridem, and quad axles), material and subgrade characterization, climatic factors, performance criteria and many others. Many state transportation agencies began the evaluation of this procedure with the ultimate goal of its adaptation and calibration for local conditions. An important aspect of this process is the evaluation of the performance prediction models and sensitivity of the predicted distresses to various input parameters for local conditions and, if necessary, re-calibration of the performance prediction models.

To achieve these objectives, the Minnesota Department of Transportation (MnDOT) and the Local Road Research Board (LRRB) initiated a study “Implementation of the MEPDG for New

and Rehabilitated Pavement Structures for Design of Concrete and Asphalt Pavements in Minnesota.” The following activities were executed in this study:

- Evaluation of MEPDG default inputs
- Identification of deficiencies in the MEPDG software
- Evaluation of prediction capabilities of the MEPDG performance prediction models for Minnesota conditions
- Re-calibration of the MEPDG performance models for Minnesota conditions.

The activities performed under this study are documented in this report.

Chapter 2 Evaluation of Typical MEPDG Inputs

2.1 Introduction

An evaluation of typical design guide inputs is given in this chapter. The research team evaluated both typical Minnesota pavement sections and inputs of the MEPDG for Minnesota roads, and developed recommendations for default values of these parameters. The MEPDG inputs were divided into two groups, *design parameters* and *default values*, as defined below:

- *Design Parameters*: the parameters that are typically changed from project to project.
- *Default Values*: the remaining MEPDG inputs that will be assumed to be the same for all Minnesota Asphalt Concrete (AC) and portland cement concrete (PCC) pavements.

The user has the option of determining the level of analysis in the MEPDG. A level 3 analysis uses more default values. Level 2 analysis requires an intermediate level of accuracy. This level is recommended when appropriate tests are not available for a level 1 analysis. Inputs would typically be user defined from an agency database or derived values from a limited testing program. Level 1 requires the highest level of accuracy. This type of analysis would typically be used in heavy trafficked areas or where there is dire safety or economic consequences of early failure. Level 1 inputs require laboratory testing. Determination of the analysis level determines the required input values from the user.

2.2 Major MEPDG Inputs

The following are MEPDG parameters have to be supplied by the user:

- Design Life
- Traffic Information
- Climatic Parameters and Regional Information
- Pavement Cross Section
- ✓ For AC pavements
 - AC Thickness
 - Asphalt Mix Properties
 - Asphalt Binder
 - Thermal Cracking Inputs
- ✓ For PCC pavements
 - PCC Thickness
 - PCC properties
 - Shoulder type
 - Slab width
 - Base erodibility
 - Joint design
 - Joint spacing
 - Dowel diameter

The following sections give a description of the parameters and defaults listed above.

2.2.1 Design Life

The MEPDG defines the pavement life as the length of time a pavement structure is being designed for, including the time from construction until major rehabilitation. Mn/DOT defines the design life of an asphalt pavement as 20 years and the design life of a concrete pavement as 30 years. The input screen for the design life is shown in Figure 2.1.

The screenshot shows a software dialog box titled "General Information". It contains several input fields and sections:

- Project Name:** A text box containing "Project1".
- Description:** A large empty text area.
- Design Life (years):** A dropdown menu with "20" selected.
- Base/Subgrade Construction Month:** A dropdown menu with "September" selected and a "Year" dropdown with "2003" selected.
- Pavement construction month:** A dropdown menu with "September" selected and a "Year" dropdown with "2003" selected.
- Traffic open month:** A dropdown menu with "October" selected and a "Year" dropdown with "2003" selected.
- Type of Design:** A section with three radio button options:
 - New Pavement:** Includes "Flexible Pavement", "Jointed Plain Concrete Pavement (JPCP)", and "Continuously Reinforced Concrete Pavement (CRCP)".
 - Restoration:** Includes "Jointed Plain Concrete Pavement (JPCP)".
 - Overlay:** Includes "Asphalt Concrete Overlay" and "PCC Overlay", each with a dropdown menu below it.
- Buttons:** "OK" and "Cancel" buttons at the bottom.

Figure 2.1 Design life and pavement type input screen.

Figures 2.2 and 2.3 show distributions, provided by Mn/DOT in February 2005, of ages at reconstruction for Minnesota flexible and rigid pavements, respectively.

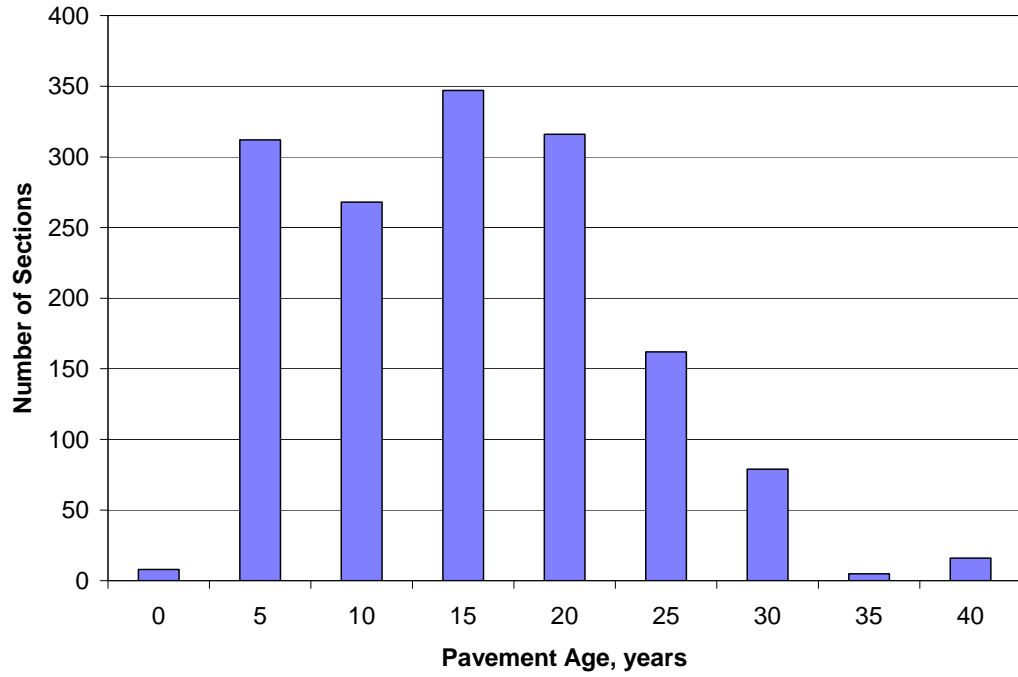


Figure 2.2 Distribution of flexible pavement ages at reconstruction.

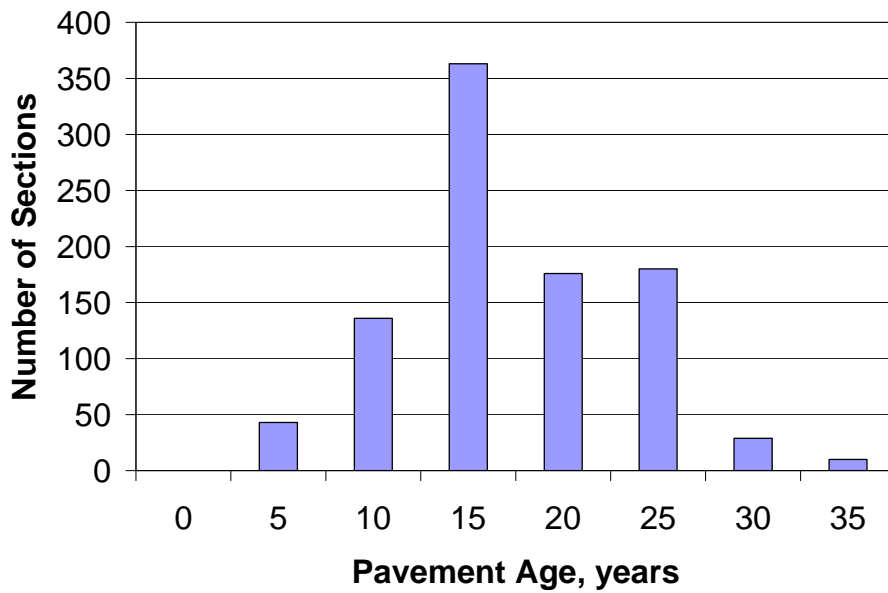


Figure 2.3 Distribution of rigid pavement ages at reconstruction.

2.2.2 Traffic Information

In the MEPDG, traffic is input either directly as AADTT (Average Annual Daily Truck Traffic) or in an AADTT calculator, where AADT (Average Annual Daily Traffic) and percentage of heavy vehicles (class 4 and higher) are multiplied. Figure 2.4 shows the traffic input screen and Figure 2.5 shows the AADTT multiplier screen. Figure 2.4 is also the input screen for the number of lanes in the design direction.

The screenshot shows a window titled "Traffic" with the following fields and controls:

- Design Life (years): 20
- Opening Date: October, 2003
- Initial two-way AADTT: [Empty field]
- Number of lanes in design direction: 2
- Percent of trucks in design direction (%): 50.0
- Percent of trucks in design lane (%): 95.0
- Operational speed (mph): 60
- Traffic Volume Adjustment: [Checked] Edit
- Axle load distribution factor: [Checked] Edit
- General Traffic Inputs: [Checked] Edit
- Traffic Growth: Compound, 4%
- Buttons: OK, Cancel

Figure 2.4 Traffic input screen.

The screenshot shows a window titled "AADTT Calculator" with the following fields and controls:

- Two-way annual average daily traffic (AADT): [Empty field]
- Percent of heavy vehicles (Class 4 or higher): [Empty field]
- Buttons: OK, Cancel

Figure 2.5 AADTT calculator.

While figure 2.4 shows the Design Guide input screen for the number of lanes in the design direction, figures 2.6 and 2.7 show data from twenty-eight Minnesota Weigh-in-Motion (WIM) sites, provided by Mn/DOT in February 2005. Figure 2.6 shows the frequency of roads with 2, 4, and 6 lanes. Four lanes per road is the most common occurrence at the WIM sites.

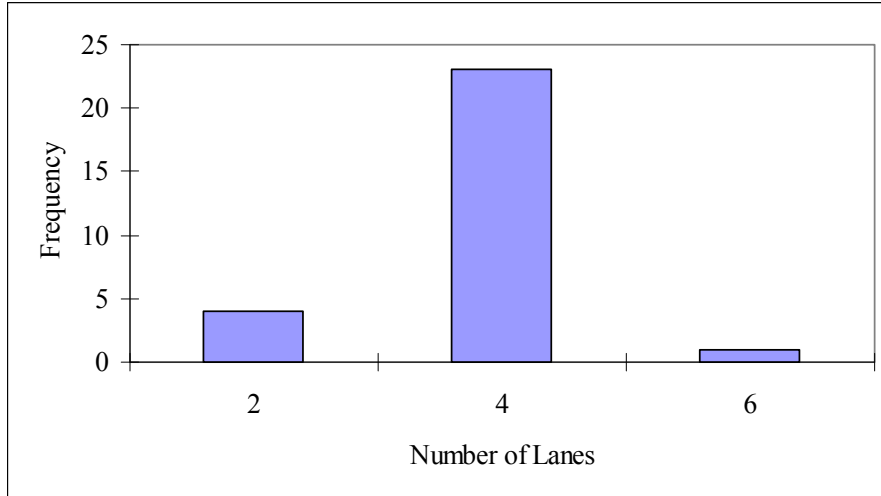


Figure 2.6 Number of lanes on Minnesota roads (WIM sites).

In addition to inputting the AADTT, the user may adjust the distribution of truck traffic on a monthly basis. The MEPDG's current default is set at 1.00 for all months and all truck classes. Figure 2.7 shows the MEPDG input screen for truck monthly adjustment factors. A spike in truck traffic may be observed in some seasons on certain roads, and the monthly adjustment may need to be utilized. Table 2.1 shows typical Minnesota monthly truck adjustment factors for both urban and rural road systems, as supplied by Mn/DOT in February 2005.

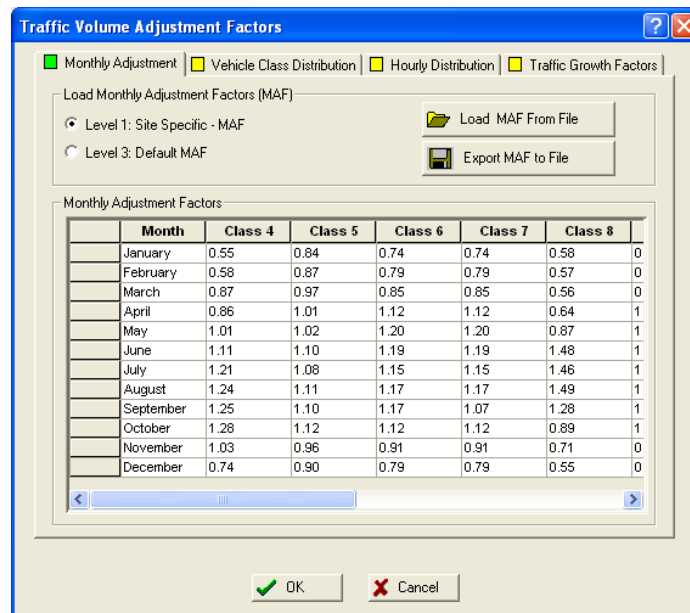


Figure 2.7 Truck traffic monthly adjustment input screen (Urban MN).

Table 2.1 Minnesota truck seasonal adjustment factors.

Fed #	System	Vehicle Type	Jan	Feb	Mar	Apr	May	Jun	Jul	Aug	Sep	Oct	Nov	Dec
4	Urban	Buses	0.55	0.58	0.87	0.86	1.01	1.11	1.21	1.24	1.25	1.28	1.03	0.74
5	Urban	2 Axle 6 Tire	0.84	0.87	0.97	1.01	1.02	1.10	1.08	1.11	1.10	1.12	0.96	0.90
6	Urban	3 Axle Single Unit	0.74	0.79	0.85	1.12	1.20	1.19	1.15	1.17	1.17	1.12	0.91	0.79
7	Urban	4 Axle Single Unit	0.74	0.79	0.85	1.12	1.20	1.19	1.15	1.17	1.17	1.12	0.91	0.79
8	Urban	3 Axle Semi (TST)	0.58	0.57	0.56	0.64	0.87	1.48	1.46	1.49	1.28	0.89	0.71	0.55
9	Urban	5 Axle Semi (TST)	0.75	0.80	0.89	1.11	1.04	1.16	1.14	1.17	1.12	1.06	0.91	0.77
10	Urban	6 Axle Semi (TST)	0.75	0.80	0.89	1.11	1.04	1.16	1.14	1.17	1.12	1.06	0.91	0.77
11	Urban	Twin Trailers	0.89	0.82	0.88	1.04	0.98	1.11	1.06	1.07	1.08	1.15	0.99	0.87
12	Urban	Twin Trailers	0.89	0.82	0.88	1.04	0.98	1.11	1.06	1.07	1.08	1.15	0.99	0.87
13	Urban	Twin Trailers	0.89	0.82	0.88	1.04	0.98	1.11	1.06	1.07	1.08	1.15	0.99	0.87
4	Rural	Buses	0.50	0.59	0.61	0.86	1.00	1.16	1.14	1.22	1.42	1.26	0.88	0.53
5	Rural	2 Axle 6 Tire	0.75	0.79	0.87	0.93	0.99	1.06	1.14	1.37	1.23	1.05	0.92	0.86
6	Rural	3 Axle Single Unit	0.59	0.71	0.87	0.92	0.86	1.15	1.18	1.15	1.41	1.29	0.80	0.73
7	Rural	4 Axle Single Unit	0.59	0.71	0.87	0.92	0.86	1.15	1.18	1.15	1.41	1.29	0.80	0.73
8	Rural	3 Axle Semi (TST)	0.46	0.50	0.61	0.73	0.83	0.98	1.23	1.47	1.68	1.11	0.60	0.49
9	Rural	5 Axle Semi (TST)	0.88	0.93	1.00	1.03	1.01	1.12	1.05	1.08	1.11	0.99	0.88	0.94
10	Rural	6 Axle Semi (TST)	0.88	0.93	1.00	1.03	1.01	1.12	1.05	1.08	1.11	0.99	0.88	0.94
11	Rural	Twin Trailers	0.88	0.92	0.97	1.10	0.98	1.00	1.06	0.94	1.10	1.08	0.94	1.07
12	Rural	Twin Trailers	0.88	0.92	0.97	1.10	0.98	1.00	1.06	0.94	1.10	1.08	0.94	1.07
13	Rural	Twin Trailers	0.88	0.92	0.97	1.10	0.98	1.00	1.06	0.94	1.10	1.08	0.94	1.07

Figure 2.8 shows the input screen in the MEPDG for hourly truck distribution. The percentage of truck traffic is input for every hour in the 24-hour day. Figure 2.9 shows the percentage of trucks on both rural and urban Minnesota trunk highways during the average 24-hr day, provided by Mn/DOT in February 2005. This information was used for local calibration of the MEPDG models presented in chapter 5 of this report.. As would be expected, the roads see a peak in truck traffic between the times of 8:00am and 5:00pm.

Traffic Volume Adjustment Factors

Monthly Adjustment
 Vehicle Class Distribution
 Hourly Distribution
 Traffic Growth Factors

Hourly truck traffic distribution by period beginning:

Midnight	0.68	Noon	7.5
1:00 am	0.57	1:00 pm	7.6
2:00 am	0.57	2:00 pm	7.7
3:00 am	0.67	3:00 pm	7.4
4:00 am	1.0	4:00 pm	6.1
5:00 am	2.7	5:00 pm	4.9
6:00 am	5.0	6:00 pm	3.6
7:00 am	6.5	7:00 pm	2.4
8:00 am	7.5	8:00 pm	1.7
9:00 am	7.6	9:00 pm	1.4
10:00 am	7.4	10:00 pm	1.1
11:00 am	7.6	11:00 pm	0.83

Note: The hourly distribution must total 100%

Total: 100

OK Cancel

Figure 2.8 Hourly truck traffic distribution input screen (Urban MN).

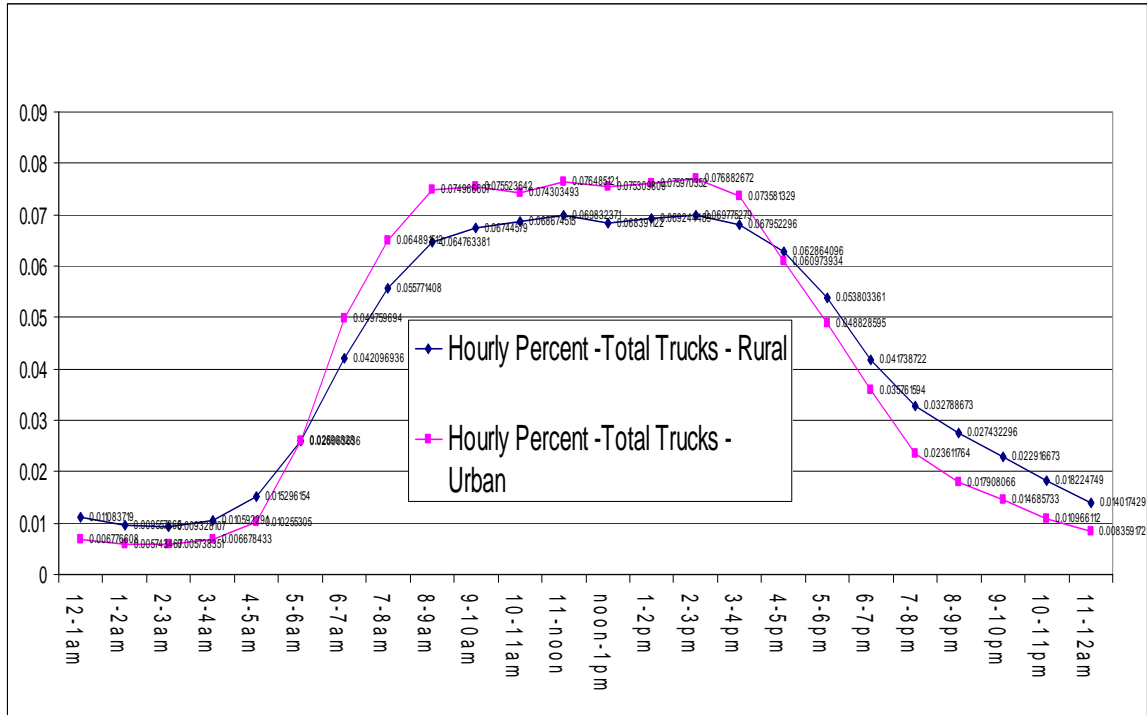


Figure 2.9 Hourly percent of the 24-hr period based on the 2000-2003 vehicle class tube counts-trunk highways rural and urban.

2.2.3 Climatic Parameters and Regional Information

The MEPDG software simulates temperature and moisture profiles in the pavement structure and subgrade over the design life of a pavement using the *Enhanced Integrated Climatic Model (EICM)*. EICM is incorporated into the MEPDG software. To simplify the input of numerous climatic inputs, such as historic data of precipitation, air temperature, sunshine, etc., the MEPDG software also contains a climatic database, that provides hourly data from 800 weather stations across the United States. Fifteen of these stations are located in Minnesota. Table 2.2 presents a list of weather stations available with MEPDG software for the Minnesota climate.

For a specific location, the Integrated Climatic Model (ICM) can create a virtual weather station by interpolating the climatic data from neighboring weather stations. Figure 2.10 shows an input screen of the MEPDG software used in the virtual weather station generation.

As can be observed in Figure 2.10, in addition to the location of the weather station, the elevation and the depth of the water table should be provided to generate a new climatic file. For water table and elevation, the online USGS (United States Geological Survey) database is used to obtain representative average of seasonal water table variation and elevation for each Mn/DOT district.

Table 2.2 Minnesota ICM weather station locations and region names.

Name	Station Location	Latitude (degrees.minutes)	Longitude (degrees.minutes)	Elevation (ft)
Alexandria	Municipal Airport	45.53	-95.23	1421
Baudette	Baudette International Airport	48.44	-94.37	1080
Brainerd	Brainerd-Crow Wing County	46.24	-94.08	1222
Duluth	International Airport	46.50	-92.11	1426
Grand Marais	The Bay of Grand Marais	47.45	-90.2	613
Hibbing	Chisholm-Hibbing Airport	47.23	-92.5	1352
International Falls	Falls International Airport	48.34	-93.24	1182
Minneapolis	Crystal Airport	45.04	-93.21	869
Minneapolis	Flying Cloud Airport	44.50	-93.28	919
Minneapolis-St. Paul	International Airport	44.53	-93.14	817
Park Rapids	Park Rapids	46.54	-95.04	1450
Redwood Falls	Municipal Airport	44.33	-95.05	1021
Rochester	Municipal Airport	43.54	-92.29	1323
St. Cloud	Municipal Airport	45.32	-94.03	1021
St. Paul	Downtown Holman Field	44.56	-93.03	708

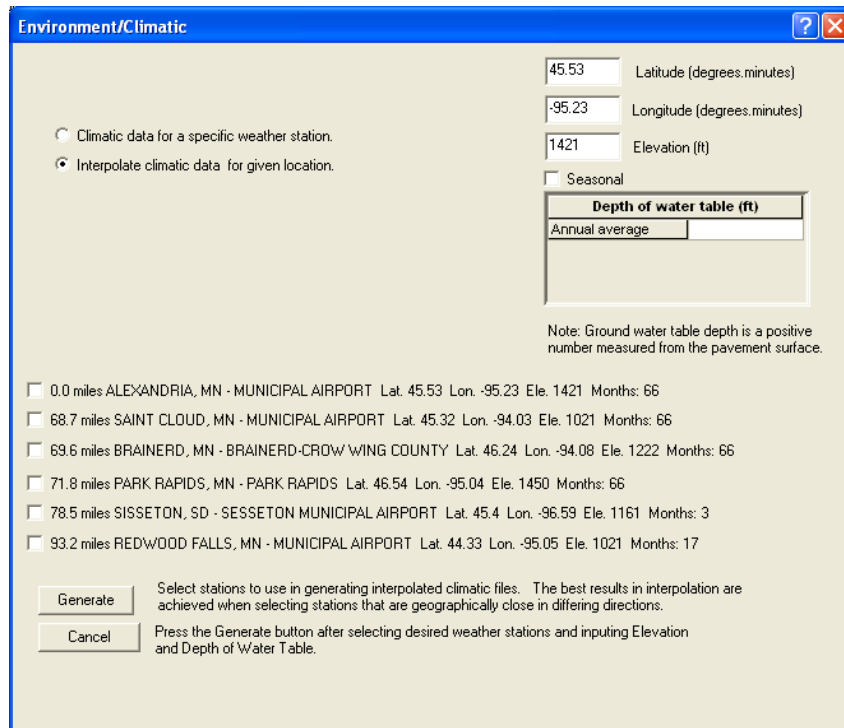


Figure 2.10 Virtual weather station generation screen.

Figure 2.11 shows the predicted rutting of the exact same road in seven different climates. Clearly, the environment in which the road is constructed has a huge impact on the future distresses seen in the pavement. The MEPDG allows the user to input the location of the project either directly by choosing a city such as those seen below in figure 2.11 or by interpolating between several weather stations.

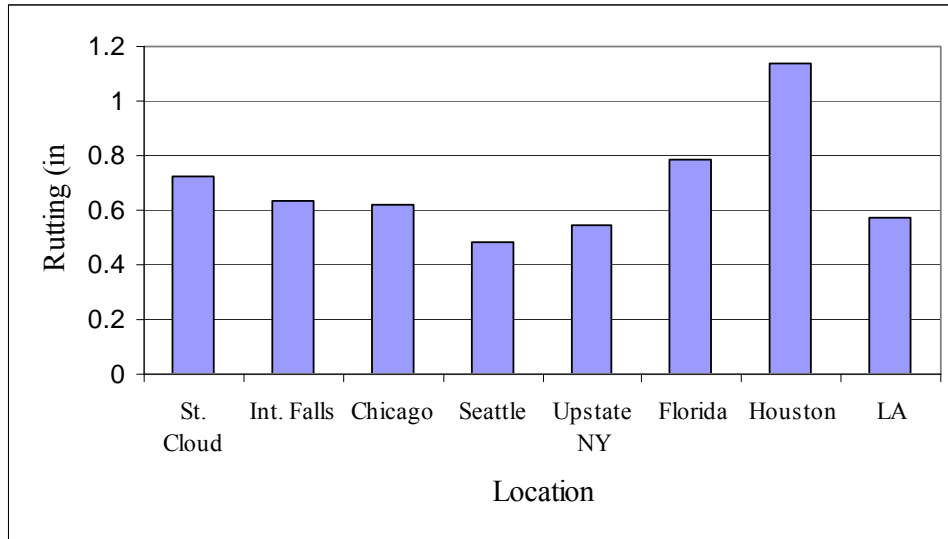


Figure 2.11 Predicted rutting vs. climate.

2.2.4 Pavement Cross Section

Mn/DOT uses their *Geotechnical Manual* for selection of pavement cross sections. Table 2.3 is a guide for selection of designs based on 20-yr design lane bituminous ESALs, referring to several design types. Design types 1-6 are found in figure 2.12. Table 2.3 and figure 2.12 are from Mn/DOT's *Geotechnical Manual*.

Table 2.3 Mn/DOT pavement selection process & design options.

20-Year Design Lane BESALs	Subgrade Soil R-Value	Process Type Design(s)	Description of Design(s)
1,000,000 or less	> 40	Informal – Flexible Design #6	Flexible – Aggregate Base (BAB) Flexible – Deep Strength (BDS)
	≤ 40	Formal Design #3 & 6	Rigid – Aggregate Base Flexible – Aggregate Base (BAB) Flexible – Deep Strength (BDS)
1,000,001 to 7,000,000	> 40	Informal – Flexible Design #4 & 5	Flexible – Aggregate Base (BAB) Flexible – Deep Strength (BDS)
	≤ 40	Formal Design #1, 2, 4, & 5	Rigid – Open Graded Base Rigid – Select Granular Flexible – Aggregate Base (BAB) Flexible – Deep Strength (BDS)
7,000,001 to 10,000,000	All Values	Formal Design #1, 2, 4, & 5	Rigid – Open Graded Base Rigid – Select Granular Flexible – Aggregate Base (BAB) Flexible – Deep Strength (BDS)
Over 10,000,000	All Values	Informal – Rigid Design #1 & 2	Rigid – Aggregate Base Rigid – Open Graded Base

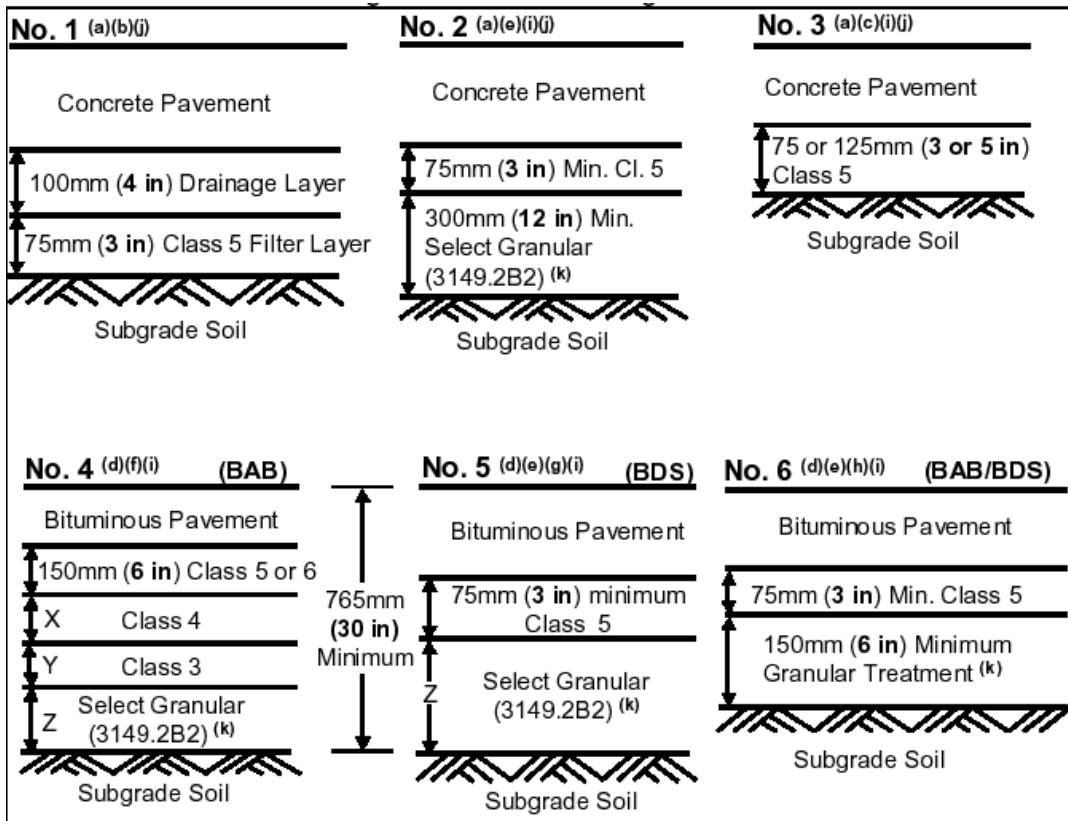


Figure 2.12 Mn/DOT pavement design standards.

Figures 2.13 and 2.14 show the software input screen for the pavement cross section and Mn/DOT's no. 2 and no. 4 pavement design standards, respectively, as inputs.

Structure

Layers

Layer	Type	Material	Thickness (in)
1	PCC	JPCP	6.0
2	Granular Base	A-1-a	3.0
3	Granular Base	A-1-b	12.0
4	Subgrade	A-7-6	Semi-infinite

Insert Delete Edit

Opening Date: Design Life (years): ...

Figure 2.13 Pavement cross section input screen: Mn/DOT design standard no. 2.

Structure

Layers

Layer	Type	Material	Thickness (in)	Interface
1	Asphalt	Asphalt concrete	10.0	1
2	Granular Base	A-1-a	6.0	1
3	Granular Base	A-1-b	14.0	1
4	Subgrade	A-7-6	Semi-infinite	n/a

Insert Delete Edit

Opening Date: Design Life (years): ...

Figure 2.14 Pavement cross section input screen: Mn/DOT design standard no. 4.

Figures 2.15 and 2.16 present distributions of AC and PCC surface thicknesses, respectively, for the pavement sections from the Mn/DOT pavement management database. One can observe that the AC thickness varies from 3 to 13 in, but the majority of the flexible pavements have AC thickness from 3 to 6 in. For rigid pavements, the PCC thickness may vary from 6 to 14 inches, but the typical thickness is from 8 to 9 inches.

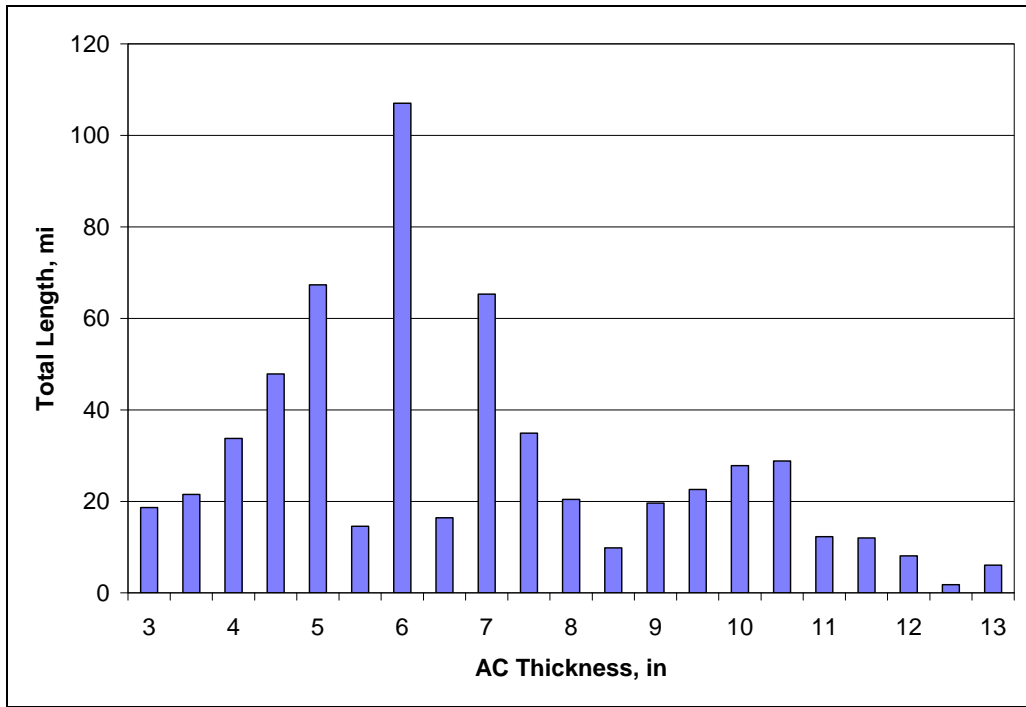


Figure 2.15 Distribution of AC surface thicknesses in the Mn/DOT PMS database.

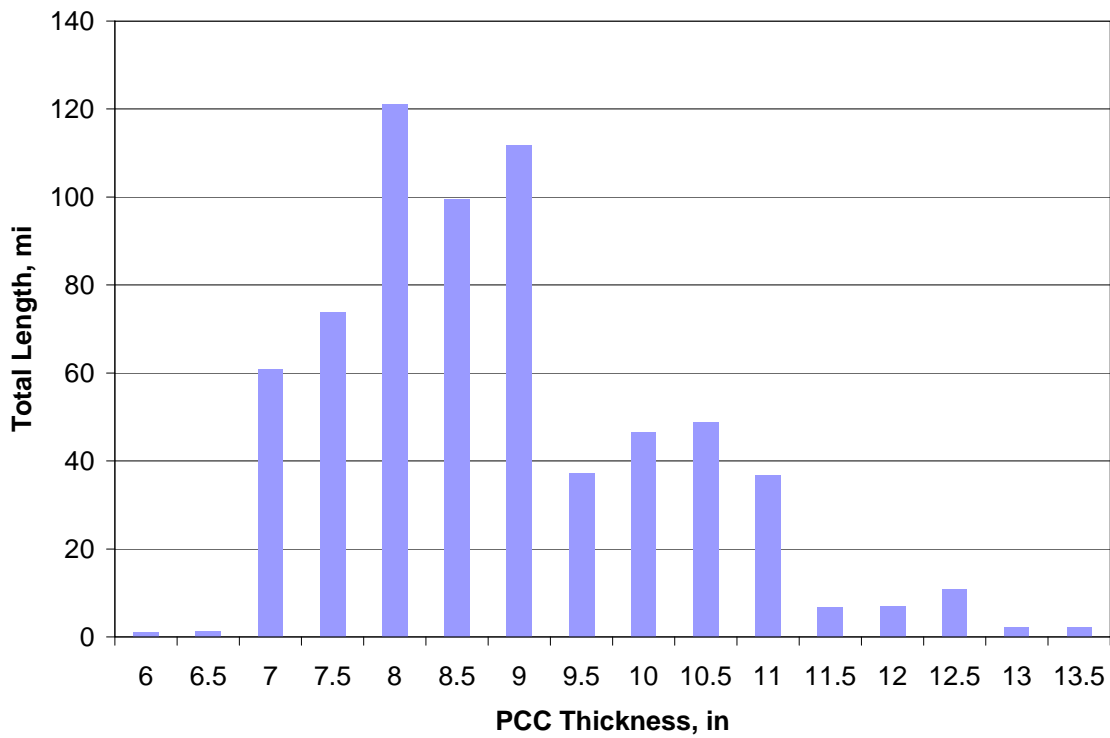


Figure 2.16 Distribution of PCC surface thicknesses in the Mn/DOT PMS database.

2.2.5 Pavement Width and Shoulder Type

Pavement width and shoulder type are important input parameters for the design of rigid pavements but do not affect the design of flexible pavements. The standard lane width is 12 ft, but only about one third (245 mi out of 667 mi) of Minnesota concrete pavements have the truck slab width equal to 12 ft. The majority of the concrete pavement sections in Minnesota have either 14 or 15-ft wide truck lane slab (347 mi).

Shoulder type also affects performance prediction. AC shoulder is the most typical type of shoulders whereas concrete shoulders are used only for about 15 percent of Minnesota concrete pavements (105 mi out of 667 mi).

2.2.6 Joint Spacing

Joint spacing is another important parameter affecting curling stresses in PCC pavements. Three joint spacings (15, 16, and 20 ft) are typically used in Minnesota jointed plain concrete pavements. Figure 2.17 presents the lane mile length distribution obtained from the Mn/DOT pavement management systems (PMS) database. One can observe that more than 75 percent of pavements have 15-ft joint spacing.

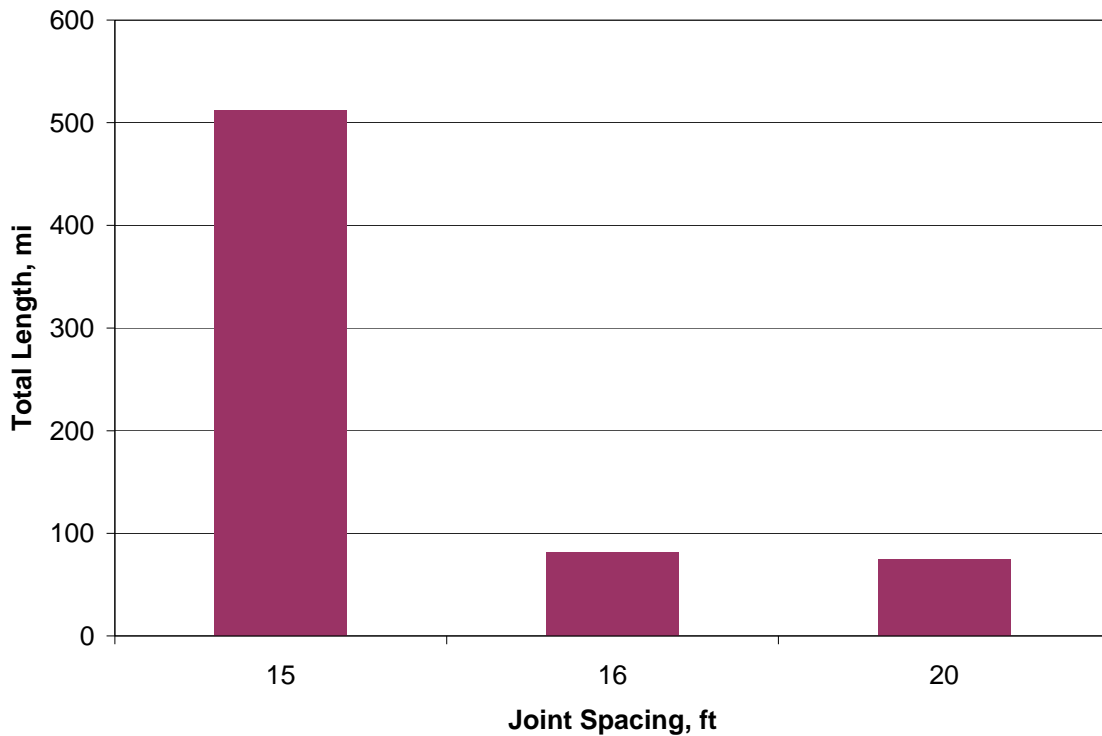


Figure 2.17 Distribution of joint spacing for Minnesota JPCP pavements.

2.2.7 Asphalt Thickness

Figure 2.18 shows the MEPDG input screen for asphalt layer thickness. Thickness is given in inches.

The screenshot shows the 'Asphalt Material Properties' dialog box. The 'Level' is set to 3, the 'Asphalt material type' is 'Asphalt concrete', and the 'Layer thickness (in)' is 10. The 'Asphalt Mix' radio button is selected. The 'Aggregate Gradation' section contains the following values:

Parameter	Value
Cumulative % Retained 3/4 inch sieve	0.2
Cumulative % Retained 3/8 inch sieve	14.9
Cumulative % Retained #4 sieve	33.8
% Passing #200 sieve	5.4

Figure 2.18 Asphalt layer thickness input screen.

Figure 2.15 shows distributions for typical flexible pavement thicknesses in Minnesota, provided by Mn/DOT in February 2005. Flexible pavement thicknesses typically range between 3 and 6-in. Very few asphalt pavements are seen with thicknesses exceeding 9-in.

2.3 Asphalt Characterization

The following parameters must be supplied by the user to characterize the asphalt layers:

- Asphalt mix properties
- Asphalt binder
- Asphalt material properties
- Thermal cracking model inputs

The specifics of the required information for each MEPDG input level is presented below.

2.3.1 Level 3 Input Characterization

Asphalt mix properties - These inputs include basic information on the asphalt mix, specifically, the aggregate gradation. Figure 2.18 shows the input screen from the MEPDG software.

Figure 2.19 shows an average mix gradation for Minnesota asphalt roads. The average mix gradation was provided by Mn/DOT in February 2005 and is an average of several mix gradations. Mix gradations include a Marshall mix with various maximum aggregate sizes, a Gyratory mix with various maximum aggregate sizes, and a Superpave mix. Figure 2.20 shows the effect of changing mix gradation in the MEPDG. It can be observed when comparing total rutting after a design life of 20 years to the percentage of the asphalt mix passing the No. 200 Sieve, that as the percentage of fines in the mix increases, so does the predicted rutting. The plot with 5.4% passing the No. 200 sieve is the overall mix gradation for Minnesota asphalt roads shown in figure 2.19. The exception is when the asphalt mix contains no fines. It can be observed that predicted rutting is slightly higher when no particles pass the No. 200 Sieve, than when approximately 5% of particles pass the No. 200 Sieve.

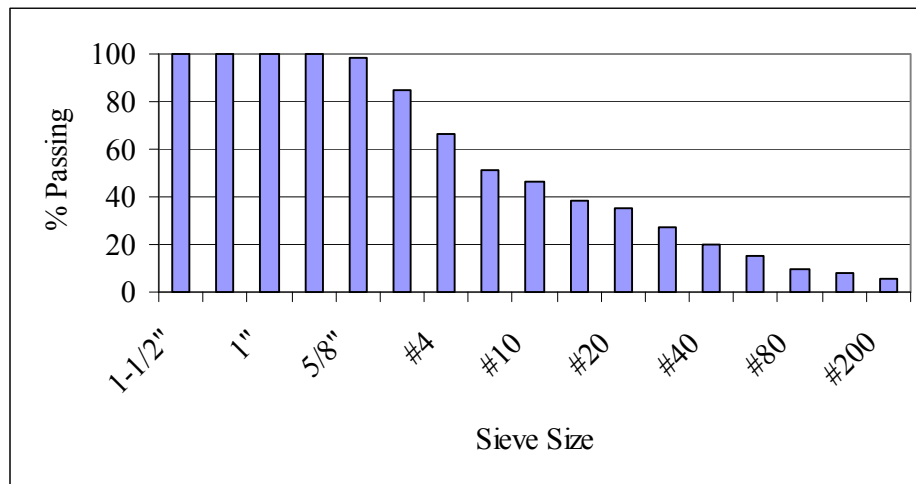


Figure 2.19 Average percent passing for Minnesota asphalt mix gradation.

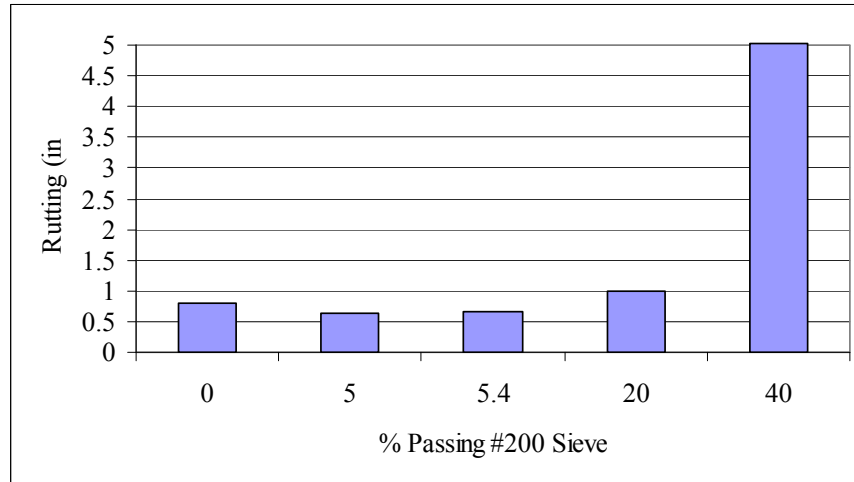


Figure 2.20 Predicted rutting vs. % passing #200 sieve.

Asphalt binder - This input includes an option for the user to choose how the asphalt binder properties are determined. The three available methods are:

- Superpave binder grading
- Conventional viscosity grade
- Conventional penetration grade

Figures 2.21, 2.22, and 2.23 show the MEPDG software input screen for the Superpave, viscosity, and penetration methods, respectively. With Superpave binder grading, the user selects a PG grade (i.e. PG58-34) from a list supplied by the MEPDG Software. The most common Superpave binders used in Minnesota are:

- PG58-28
- PG58-34
- PG64-34

Other, less common Superpave binders used in Minnesota include:

- PG52-34
- PG52-40
- PG58-40
- PG64-22
- PG64-28

Conventional viscosity grading requires the user to select a viscosity grade (i.e. AC 10) from a list of six grades. Penetration grade requires the user to select from a list of five penetration grades (i.e. Pen 85-100) for the asphalt binder.

Asphalt Material Properties

Level: 3 Asphalt material type: Asphalt concrete
 Layer thickness (in): 10

Asphalt Mix Asphalt Binder Asphalt General

Options:

- Superpave binder grading
- Conventional viscosity grade
- Conventional penetration grade

High Temp (°C)	Low Temp (°C)					
	-10	-16	-22	-28	-34	-40
46						
52						
58						
64						
70						
76						
82						

A: 11.0100 VTS: -3.7010

OK Cancel

Figure 2.21 Asphalt binder: Superpave binder grading.

Asphalt Material Properties

Level: 3 Asphalt material type: Asphalt concrete
 Layer thickness (in): 10

Asphalt Mix Asphalt Binder Asphalt General

Options:

- Superpave binder grading
- Conventional viscosity grade
- Conventional penetration grade

Viscosity Grade:

- AC 2.5
- AC 5
- AC 10
- AC 20
- AC 30
- AC 40

A: VTS:

OK Cancel

Figure 2.22 Asphalt binder: conventional viscosity grade.

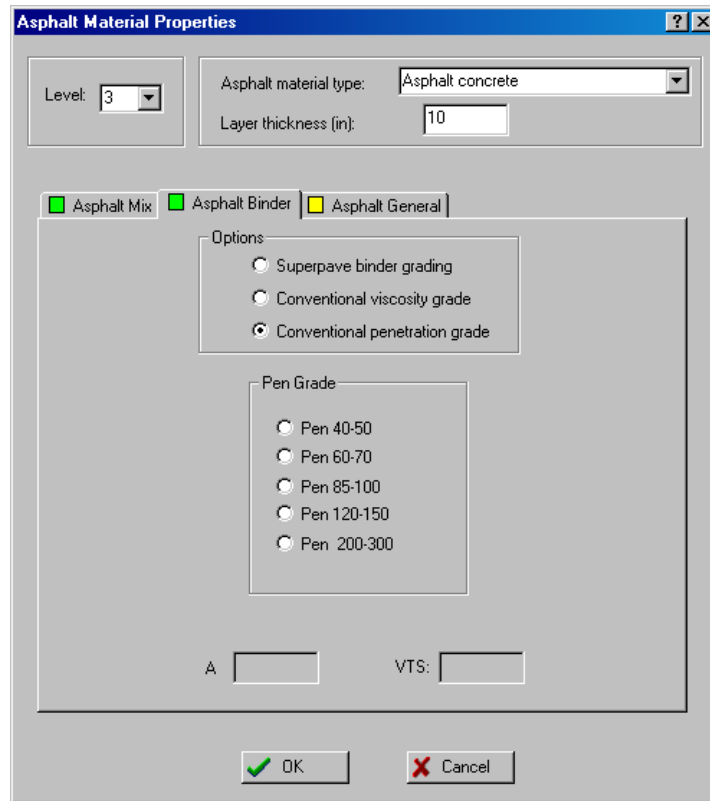


Figure 2.23 Asphalt binder: conventional penetration grade.

Mn/DOT uses only Superpave binders when designing asphalt pavements. For that reason, only the Superpave binder grading system will be further studied in this project. Figure 2.26 shows the results of estimated rutting from the MEPDG when only the asphalt binder is changed.

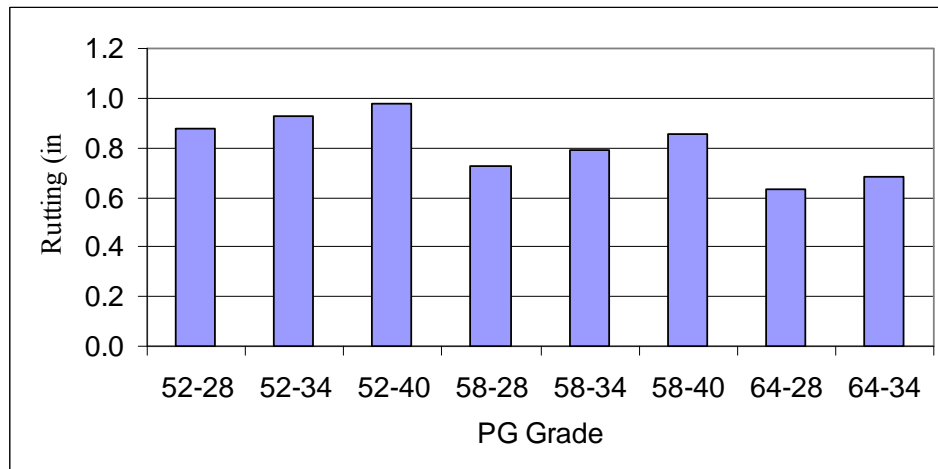


Figure 2.24 Predicted rutting vs. PG grade.

In Level 3 analysis, the MEPDG uses A and VTS values to relate a Superpave binder to viscosity by equation 2.1. A and VTS values for select Superpave binders can be seen in Table 2.4.

$$\text{LogLog}(\eta) = A + (\text{VTS})\text{Log}T_R \quad (2.1)$$

where:

- η = viscosity, cP
- T_R = Temperature, Rankine
- A = Regression Intercept
- VTS = Regression slope of Viscosity temperature susceptibility

Table 2.4 A and VTS defaults for select Superpave grades.

High Temp Grade	Low Temperature Grade													
	-10		-16		-22		-28		-34		-40		-46	
	VTS	A	VTS	A	VTS	A	VTS	A	VTS	A	VTS	A	VTS	A
46									-3.901	11.504	-3.393	10.101	-2.905	8.755
52	-4.570	13.386	-4.541	13.305	-4.342	12.755	-4.012	11.840	-3.602	10.707	-3.164	9.496	-2.736	8.310
58	-4.172	12.316	-4.147	12.248	-3.981	11.787	-3.701	11.010	-3.350	10.035	-2.968	8.976		
64	-3.842	11.432	-3.822	11.375	-3.680	10.980	-3.440	10.312	-3.134	9.461	-2.798	8.524		
70	-3.566	10.690	-3.548	10.641	-3.426	10.299	-3.217	9.715	-2.948	8.965	-2.648	8.129		
76	-3.331	10.059	-3.315	10.015	-3.208	9.715	-3.024	9.200	-2.785	8.532				
82	-3.128	9.514	-3.114	9.475	-3.019	9.209	-2.856	8.750	-2.642	8.151				

Viscosity is then used in the prediction equation 2.2 to obtain the dynamic modulus of the mixture.

$$\text{Log}|E^*| = \delta + \frac{\alpha}{1 + e^{\beta + \gamma \text{Log}t_R}} \quad (2.2)$$

where:

- E^* = Dynamic Modulus
- $\delta = -1.249937 + 0.02932 P_{200} - 0.001767(P_{200})^2 - 0.002841 P_4 - 0.05097V_a - 0.802208 \left[\frac{Vb_{eff}}{Vb_{eff} + V_a} \right]$
- $\alpha = 3.871977 - 0.0021 P_4 + 0.003958 P_{38} - 0.000017(P_{38})^2 + 0.005470 P_{34}$
- $\beta = 0.603313 - 0.393532 \text{log}(\eta_{Tr})$
- $\text{log}(t_r) = \text{log}(t) - 1.255882(\text{log}(\eta) - \text{log}(\eta_{Tr}))$
- $\gamma = 0.313351$
- t = time of loading
- η = viscosity at the age and temperature of interest
- η_{Tr} = viscosity at the reference temperature
- Vb_{eff} = effective binder content, % by volume
- V_a = air void content
- P_{34} = cumulative % retained on the 3/4-in sieve
- P_{38} = cumulative % retained on the 3/8-in sieve
- P_4 = cumulative % retained on the No. 4 sieve
- P_{200} = % passing the No. 200 sieve

Asphalt material properties - Default values in the MEPDG software for four asphalt material properties are used in Level 3 analysis are set as follows:

- Reference Temperature of 70 degree Fahrenheit
- 0.35 Poisson's Ratio
- 11% Effective Binder Content (by volume)
- 8.5% Air Voids
- 148-pcf Total Unit Weight of Asphalt Mix

The thermal properties include the thermal conductivity of the mix, set at 0.67-BTU/hr-ft-F^o, and the heat capacity of the mix, set at 0.23-BTU/lb-F^o. The volumetric properties of asphalt include asphalt air voids, effective binder content and total unit weight. Figure 2.25 shows the input screen in the MEPDG software for asphalt general properties.

The screenshot shows the 'Asphalt Material Properties' dialog box. At the top, 'Level' is set to 3, 'Asphalt material type' is 'Asphalt concrete', and 'Layer thickness (in)' is 10. The 'Asphalt Mix' tab is active, showing 'Reference temperature (F°)' as 70, 'Effective binder content (%)' as 11, 'Air voids (%)' as 8.5, and 'Total unit weight (pcf)' as 148. The 'Poisson's Ratio' section has 'Use predictive model to calculate Poisson's ratio.' unchecked, 'Poisson's ratio:' as 0.35, and empty fields for 'Parameter a:' and 'Parameter b:'. The 'Thermal Properties' section at the bottom shows 'Thermal conductivity asphalt (BTU/hr-ft-F°)' as 0.67 and 'Heat capacity asphalt (BTU/lb-F°)' as 0.23. 'OK' and 'Cancel' buttons are at the bottom.

Figure 2.25 Asphalt general properties input screen (Level 3).

Thermal cracking model inputs - Level 3 analysis of thermal cracking in the MEPDG software allows the user to select creep compliance values at three temperatures, Low Temp (-4°F), Mid Temp (14°F), and High Temp (32°F) for a loading time of either 100 seconds (default value) or 1000 seconds. Creep compliance default values are set based on the asphalt binders for tests of 100. For a test of 1000 seconds, the user must provide creep compliance values for loading times of 200 seconds, 500 seconds, and 1000 seconds.

The default average tensile strength at 14°F is currently set at 350-psi. The MEPDG allows the user to either input the mix coefficient of thermal contraction (in/in/°F) or let the software compute it by providing the mixture VMA (%) and the aggregate coefficient of thermal expansion. Figure 2.26 shows the MEPDG input screen for thermal cracking at Level 3.

Loading Time sec	Creep Compliance (1/psi)		
	Low Temp (°F)	Mid Temp (°F)	High Temp (°F)
	-4	14	32
1	1.456e-007	1.674e-007	2.868e-007
2	1.547e-007	1.857e-007	3.131e-007
5	1.682e-007	2.035e-007	3.661e-007
10	1.77e-007	2.214e-007	4.145e-007
20	1.857e-007	2.392e-007	4.896e-007
50	1.941e-007	2.657e-007	6.171e-007
100	2.12e-007	2.738e-007	7.307e-007

Figure 2.26 Thermal cracking.

2.3.2 Level 2 Analysis

Asphalt mix properties - The input for the asphalt binder in Level 2 requires more information than in Level 3. In Level 2, the user is given two options: to perform Superpave binder tests or to perform conventional binder tests.

Selecting Superpave binder test data requires the user to select the number of temperatures (°F), from one to ten, and conduct testing at those temperatures to determine the binder complex shear modulus $|G^*|$ in Pascals and the binder phase angle, δ , in degrees. The angular frequency is set at 10 rads/sec in all tests. Figure 2.27 shows the input screen for Superpave binder test data.

Asphalt Material Properties

Level: Asphalt material type:

Layer thickness (in):

Asphalt Mix Asphalt Binder Asphalt General

Options - At Short Term Aging - RTFO

Superpave binder test data
 Conventional binder test data

Number of temperatures:

Temperature (°F)	Angular frequency = 10 rad/sec	
	G' (Pa)	Delta (°)

OK Cancel

Figure 2.27 Asphalt binder: Superpave binder test data.

Asphalt binder - Conventional binder testing allows the user to determine binder properties using penetration or binder viscosity tests. The user must input the number of penetrations and the number of Brookfield viscosities tested. Both values can range from zero to six. The software provides default values for softening point, absolute viscosity, kinematic viscosity, and specific gravity. Figure 2.33 shows the input screen for conventional binder test data.

Asphalt Material Properties

Level: 2 Asphalt material type: Asphalt concrete
 Layer thickness (in): 10

Asphalt Mix Asphalt Binder Asphalt General

Options - At Short Term Aging - RTFO

Superpave binder test data
 Conventional binder test data

Number of penetrations: 3 Number of Brookfield viscosities: 3

Test	Temperature (°F)	Binder property
Softening point (P)	0	13000
Absolute viscosity (P)	140	0
Kinematic viscosity (CS)	275	0
Specific gravity	77	0
Penetration		
Brookfield viscosity		

OK Cancel

Figure 2.28 Asphalt binder: conventional binder test data.

Asphalt material properties - This parameter is identical to Level 3 analysis.

Thermal cracking model inputs - Level 2 analysis of thermal cracking requires laboratory testing, unlike Level 3 analysis. Default values are provided (Level 3 default values) but should be replaced with testing results. Level 3 analysis provides default values for three temperatures. Level 2 requires testing at only one temperature, the Mid Temp (14°F). Figure 2.29 shows the input screen for level 2 thermal cracking.

Figure 2.29 Level 2: thermal cracking input screen.

2.3.3 Level 1 analysis

Asphalt mix properties - Unlike Levels 2 and 3 where aggregate gradation of the asphalt mix is the only information required, Level 1 required that the user performs dynamic modulus $|E^*|$ testing of the asphalt mix. The software requires the user to perform tests at 10, 40, and 70°F, but also allows up to five more temperatures for testing. There frequencies, 0.1, 1, and 10-Hz, are required with the option of adding five more frequencies. Figure 2.35 shows the input screen for asphalt mix in Level 1 analysis.

Level: 1

Asphalt material type: Asphalt concrete

Layer thickness (in): 10

Asphalt Mix Asphalt Binder Asphalt General

Dynamic Modulus Table

Number of temperatures: 8

Number of frequencies: 3

Temperature (°F)	Mixture E' (psi)		
	0.1	1	10
10			
40			
70			

Import Export

OK Cancel

Figure 2.30 Level 1: asphalt mix properties input screen.

Asphalt binder - This parameter is identical to Level 2 analysis.

Asphalt material properties - This parameter is identical to both Level 2 and Level 3 analyses.

Thermal cracking model inputs - Level 1 analysis of thermal cracking is similar to Level 2 analysis and assumes testing will be conducted. Again, the Level 3 default values are present but are not to be used without testing. Thermal cracking in Level 1 requires creep compliance testing at the same three temperatures seen in Level 3 (Low Temp (-4°F), Mid Temp (14°F), and High Temp (32°F)). Figure 2.36 shows the Level 3 input screen, which is identical with Level 1.

2.4 PCC Material Characterization

This contains several sub-categories, which are briefly discussed as outlined below.

- ◆ Unit weight and Poisson's ratio
- ◆ Cement concrete thermal properties
- ◆ Concrete mix properties
- ◆ Concrete strength properties

2.4.1 Level 3 Inputs

Unit weight and Poisson's ratio – Cement concrete unit weight and Poisson's ratio is required to be used as a general design value. Current default cement concrete unit weight and Poisson's ratio values are set to *150-pcf* and *0.20*, respectively.

Analysis of these parameters for the Minnesota LTPP sections was performed in this study. Table 2.5 presents the results of this analysis. One can observe that although a significant variation exists in PCC unit weight and Poisson's ratio, the mean values are close to the MEPDG default values. Therefore, it is reasonable to use these values as the default parameters.

Table 2.5 PCC unit weight and Poisson's ratio for the Minnesota LTPP sections.

	Unit weight, lb/ft ³	Poisson's ratio
Mean	149.8	0.195
Min	144	0.12
Max	154	0.27
Number of observations	22	22

PCC thermal properties – Thermal properties include *coefficient of thermal expansion, thermal conductivity, and heat capacity*. The current default values for thermal expansion, thermal conductivity, and heat capacity are set to *5.5 per °F x 10e-6, 1.25 BTU/hr-ft-°F, and 0.28 BTU/lb-°F*, respectively.

Since no experimental values are available for the PCC thermal conductivity, and heat capacity, it is recommended to adopt the MEPDG default values. Analysis of the coefficients of thermal expansion for the Minnesota LTPP sections has shown that they vary from 4.89×10^{-6} to 6.67×10^{-6} $1/^\circ\text{F}$ with an average value equal to 5.86×10^{-6} $1/^\circ\text{F}$. This confirms that the MEPDG default value for the coefficient of thermal expansion, 5.5×10^{-6} $1/^\circ\text{F}$ is a reasonable default value for the Minnesota concrete pavements.

Figure 2.36 shows the input screen for PCC material properties. Properties include layer thickness, unit weight, Poisson's ratio, and thermal properties.

PCC Material Properties - Layer #1

Thermal
 Mix
 Strength

General Properties

PCC material: JPCP

Layer thickness (in): 10

Unit weight (pcf): 150

Poisson's ratio: 0.20

Thermal Properties

Coefficient of thermal expansion (per F° x 10- 6): 5.5

Thermal conductivity (BTU/hr-ft-F°): 1.25

Heat capacity (BTU/lb-F°): 0.28

OK Cancel

Figure 2.31 PCC material properties input screen.

Concrete mix properties – This group contains information regarding *cement type, cement content (lb/yd³), water/cement ratio, aggregate type, and curing method*. Default value for cement type, cement content, and water/cement ratio is set to *Type 1, 600 lb/yd³, and 0.42*, respectively. These values were used as default for this study. Figure 2.37 shows the input screen for PCC mix properties.

PCC Material Properties - Layer #1

Thermal
 Mix
 Strength

Cement type:

Cementitious material content (lb/yd³):

Water/cement ratio:

Aggregate type:

PCC zero-stress temperature (F°):

Ultimate shrinkage at 40% R.H. (microstrain):

Reversible shrinkage (% of ultimate shrinkage):

Time to develop 50% of ultimate shrinkage (days):

Curing method:

OK
 Cancel

Figure 2.32 PCC mix properties input screen.

Concrete strength properties – The default value for concrete 28-day compressive strength (Comp.) that will be used is 3900-lb/in². Figure 2.38 shows the input screen for PCC strength properties.

PCC Material Properties - Layer #1

Thermal
 Mix
 Strength

Input Level:

 Level 1

 Level 2

 Level 3

28-day PCC modulus of rupture (psi):

28-day PCC compressive strength (psi):

28-day PCC elastic modulus (psi):

OK
 Cancel

Figure 2.33 PCC strength properties input screen (Level 3).

2.4.2 Level 2 Inputs

Unit weight and Poisson's ratio – This parameter is identical to Level 3 analysis.

PCC thermal properties – This parameter is identical to Level 3 analysis.

Concrete mix properties – This parameter is identical to Level 3 analysis.

Concrete strength properties – The default values for concrete 7-, 14-, 28-, and 90-day compressive strength (Comp.), as well as the 20 year/28-day compressive strength are given in figure 2.34. Figure 2.34 also shows the input screen for PCC strength properties.

Time	Comp.(psi)
7 Day	3560
14 Day	3900
28 Day	4200
90 Day	4700
20 Year/28 Da	1.44

Figure 2.34 PCC strength properties input screen (Level 2).

2.4.3 Level 1 Inputs

Unit weight and Poisson's ratio – This parameter is identical to both Level 2 and Level 3 analyses.

PCC thermal properties – This parameter is identical to both Level 2 and Level 3 analyses.

Concrete mix properties – This parameter is identical to both Level 2 and Level 3 analyses.

Concrete strength properties – The concrete modulus of elasticity (E), modulus of rupture (MR), and split tensile strength (S.T.) are given for the same time values as in level 2 analysis can be observed in figure 2.35. Figure 2.34 also shows the input screen for PCC strength properties.

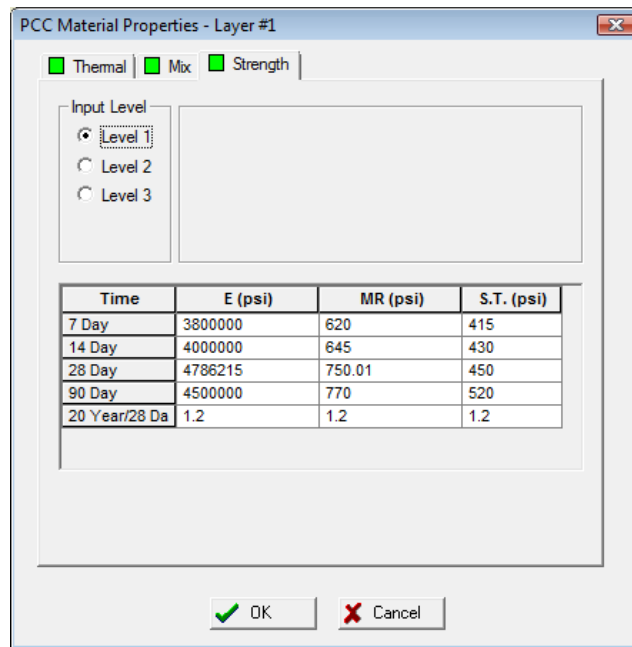


Figure 2.35 PCC strength properties input screen (Level 1).

2.5 Unbound Material Properties

The properties for the unbound materials (base and subgrade) can be divided into two groups:

- Strength properties
- ICM materials properties

The MEPDG procedure characterizes strength properties of unbound materials through resilient modulus at the optimum moisture content and Poisson's ratio. These properties can be obtained from laboratory testing or through correlation with other material properties or material classification. Although the MEPDG provides correlations to estimate the resilient modulus from CBR, DCP, and R-values, this study concluded that use of those correlations is not recommended. The resilient modulus can be assigned either based on AASHTO soil classification or results of resilient modulus testing (see Chapter 4 of this report for more details). For the granular base layer, it recommended to use AASHTO subgrade defaults for A-1-a and A-3 to characterize MnDOT class 5 and class 3 bases according to materials classification based on Mn/DOT Grading and Base Manual, Specification 3138.

Soil properties for EICM – The following input parameters are required by the EICM to predict temperature distribution in the PCC layer and moisture distribution in the unbound layers:

- Plasticity Index
- Liquid Limit
- Gradation

- Index properties from the sieve analysis
- Maximum dry unit weight
- Specific gravity and other parameters as shown in figure 2.36.

Unbound Layer - Layer #2

Unbound Material: Thickness(in): Last layer

Strength Properties ICM

Range Mean

Sieve	Percent Passing
0.001mm	
0.002mm	
0.020mm	
#200	8.7
#100	
#80	12.9
#60	
#50	
#40	20.0
#30	
#20	
#16	
#10	33.8
#8	
#4	44.7
3/8"	57.2
1/2"	63.1
3/4"	72.7
1"	78.8
1 1/2"	85.8
2"	91.6
2 1/2"	
3"	
3 1/2"	97.6

Plasticity Index (PI)	1
Liquid Limit (LL)	6
Compacted Layer	<input checked="" type="checkbox"/> Yes
Index Properties from Sieve Analysis	
% Passing #200	8.7
% Passing #40	20.0
% Passing #4	44.7
D10 (mm)	0.1035
D20 (mm)	0.425
D30 (mm)	1.306
D60 (mm)	10.82
D90 (mm)	46.19
User Overridable Index Properties	
Maximum Dry Unit Weight(pcf)	<input type="checkbox"/> 127.7
Specific Gravity, Gs	<input type="checkbox"/> 2.70
Sat. Hydraulic Conductivity(ft/hr)	<input type="checkbox"/> 0.051
Optimum gravimetric water content(%)	<input type="checkbox"/> 7.4
Degree of Saturation at Optimum(%)	62.2
User Overridable Soil Water Characteristic Curve	
af	<input type="checkbox"/> 7.255
bf	<input type="checkbox"/> 1.333
cf	<input type="checkbox"/> 0.8242
hr	<input type="checkbox"/> 117.4

Figure 2.36 EICM inputs for unbound materials.

Chapter 3 Evaluation of the Design Guide Performance Prediction

3.1 Introduction

This chapter documents the results of sensitivity runs using various versions of MEPDG software for typical Minnesota site conditions and a wide range of pavement design features (e.g. layer thickness, material properties, etc). An evaluation of the predicted pavement performance with respect to expected limits, and performance trends (change in predicted performance with change in design features) are presented as well. The results of the flexible pavements will be presented first, followed by the rigid pavement results.

3.2 Flexible Pavements

As recommended by MnDOT engineers, two different traffic levels, 10 and 1 million ESAL's, were considered separately in the analysis for flexible pavements. The following parameters were changed in the sensitivity analysis:

- Climate
- AC thickness
- Asphalt binder grading
- Gradation of the asphalt mix
- Base thickness
- Subbase thickness
- Subgrade type

The following distresses were investigated: alligator cracking, longitudinal cracking, transverse cracking, total rutting, AC rutting and IRI.

For the 10 million ESAL's traffic level a total of 648 simulations were run. The parameters used in this analysis are presented in Table 3.1. For the 1 million ESAL's traffic level a total of 120 simulations were run. Table 3.2 contains the input parameters used in this analysis.

Table 3.1 10 million ESAL's summary inputs.

Parameter	Cases	Description
Climate	2	NW - Grand Forks, ND SE – Rochester
AC thickness	3	6" 8" 10"
Binder PG*	3*	PG 58-28 (A) PG 58-34 (B) PG 64-34 (C)
Mix gradation	2	fine mix coarse mix
Other layers	18**	See details below

*The PG for the two sublayers of equal thickness are as follows:

Thickness	Case 1	Case 2	Case 3
6"	C + A	B + A	B + B
8"	C + A	B + A	B + B
10"	C + A	B + A	B + B

** The “other layers” combinations are as follows:

Layer	Height	Type	Modulus
Base	3"	Class 6	25ksi
	6"		
	9"		
Subbase	0"	Class 3 Select granular	20ksi
	12"		
	24"		
Soil		A3	20ksi
		A6	10ksi

Table 3.2 1 million ESAL's summary inputs.

Parameter	Cases	Description
Climate	2	NW - Grand Forks, ND SE - Rochester
AC thickness	3	4" - base $M_R = 25\text{ksi}$ 4" - base $M_R = 40\text{ksi}$ 6" - base $M_R = 25\text{ksi}$
Binder PG	3*	PG 58-28 (A) PG 58-34 (B) PG 64-34 (C)
Mix gradation	2	fine mix coarse mix
Other layers	4**	See details below

* The PG for the two layers of equal thickness are as follows:

Thickness	Case 1	Case 2	Case 3
4"	C + C	B + B	A + A
6"	C + A	B + A	B + B

** The other layers combinations are as follows:

Layer	Height	Type	Modulus
Base	3" 6"	Class 6	25ksi or 40ksi see mixture thickness
Soil		A3 A6	20ksi 10ksi

Since the project was conducted over the span of several years, the MEPDG software underwent significant modifications, especially for flexible pavements, partially due to feedback from this project. A detailed analysis of the results from MEPDG version 0.615 is presented first. This will be followed by comparisons of the predictions from the updated MEPDG software versions and a summary of the predictions from the latest version, 1.003.

3.2.1 MEPDG Version 0.615 Results

For 10 million ESAL's the maximum values for the predicted distresses from all of the simulations are presented in table 3.3. All the predicted maximum values are larger than the limits suggested in the design guide. The values presented are reasonable except for the longitudinal cracking and IRI both of them excessively larger compared to the limits. However, it cannot be concluded that the model performance for these two distresses is inadequate because

these maximums values are the result of just one simulation, which represents a particular combination of the factors analyzed.

Table 3.3 Maximum values of the predicted distresses for 10 million ESAL's.

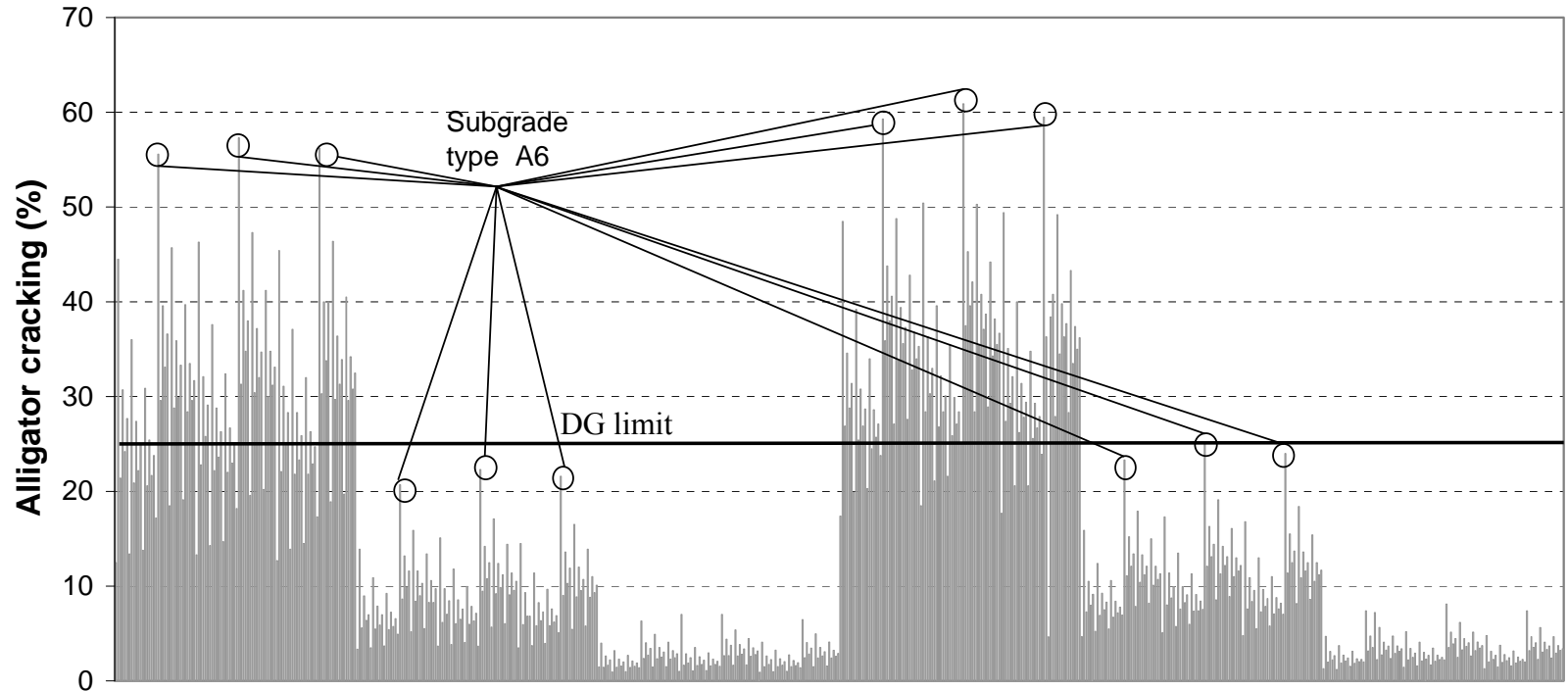
Distress	Max Value	Limit
Alligator cracking (%)	60.9	25
Longitudinal cracking (ft/mi)	10400	1000
Transverse cracking (ft/mi)	2100	1000
Total Rutting (in)	1.047	0.75
AC Rutting (in)	0.775	0.25
IRI (in/mi)	1363.3	172

Table 3.4 shows the maximum values for the predicted distresses for 1 million ESAL's. Rutting is the only distress that does not exceed the limited values recommended in the design guide. The values presented are reasonable except for the prediction of the IRI that is quite large compare to the suggested limits.

Table 3.4 Maximum values of the predicted distresses for 1 million ESAL's.

Distress	Max Value	Limit
Alligator cracking (%)	37.1	25
Longitudinal cracking (ft/mi)	7240	1000
Transverse cracking (ft/mi)	2110	1000
Total Rutting (in)	0.575	0.75
AC Rutting (in)	0.261	0.25
IRI (in/mi)	1473.9	172

Figures 3.1 to 3.6 show the predicted distresses after 20 years for the 10 million ESAL's for all the simulations. Figure 3.1 shows the predicted alligator cracking; it can be seen that alligator cracking is reduced considerably when the thickness of the AC layer is increased. There is no noticeable difference between the predicted alligator cracking in Grand Forks and in Rochester. Nevertheless, there are some spikes in figure 3.1. These sudden changes reflect a change in the subgrade type. Pavements with A6 soils showed considerable more alligator cracking than pavements with A3 soils.



NW - AC = 6 in.			NW - AC = 8 in.			NW - AC = 10 in.			SE - AC = 6 in.			SE - AC = 8 in.			SE - AC = 10 in.		
C1	C2	C3															
F	C	F	C	F	C	F	C	F	C	F	C	F	C	F	C	F	C
B, SB thickness. SG type changed			B, SB thickness. SG type changed			B, SB thickness. SG type changed			B, SB thickness. SG type changed			B, SB thickness. SG type changed			B, SB thickness. SG type changed		

C1 = Top 50% PG 64-34 Bottom PG 58-28
C2 = Top 50% PG 58-34 Bottom PG 58-28 NW= Northwest SE= Southeast
C3 = PG 58-34
F=Fine C=Coarse

Figure 3.1 Alligator cracking after 20 years for 10 million ESAL's..

The predicted longitudinal cracking is presented in figure 3.2. As expected, the longitudinal cracking decreases when the thickness of the AC layer increases. On average, the predicted values for this distress are the same for both climates.

Figure 3.3 presents the predicted transverse cracking after 20 years. The predicted values for C2 (top 50% of the AC layer is PG 58-34 and bottom 50% is PG 58-28) and C3 (all AC layer is PG 58-34) are similar. However, C1 (top 50% of the AC layer is PG 64-34 and bottom 50% is PG 58-28) shows significant thermal cracking although the top layer has the same PG lower limit as C2 and C3. This problem was initially attributed to the large differences in the default material properties between PG 64-34 and PG 58-34. However, it was found later that the problem was caused by a memory allocation bug in the MEPDG software. The problem was reported to the MEPDG team and was fixed in version 1.0. Figure 3.3 also shows that when the thickness of the AC layer increases the predicted transverse cracking decreases slightly. The climate has a pronounced effect in the prediction of the transverse cracking, as expected. The average predicted for Grand Forks is 1500 ft/mi, and for Rochester is 500 ft/mi.

Figures 3.4 and 3.5 show the predicted total rutting and AC rutting, respectively. The PG 64 binder (C1) ruts less than the PG 58 (C2 and C3). The southern location has slightly more rutting. The finer mixtures are less prone to rutting and the thicker asphalt layers show slightly lower AC rutting than the thinner one. No significant changes are observed for changes in the base and subbase factors. Generally the trends observed for these two predictions are reasonable.

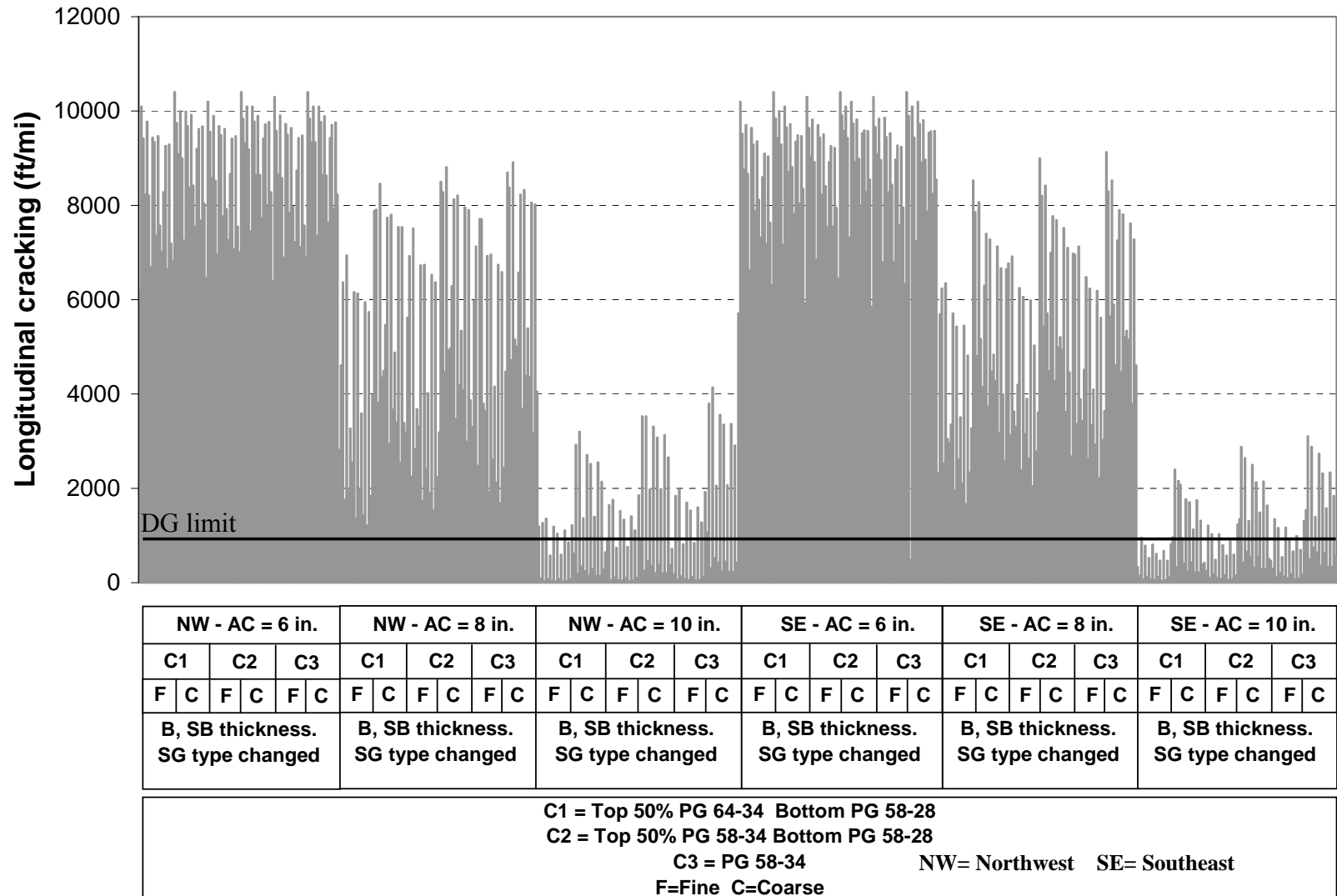


Figure 3.2 Longitudinal cracking after 20 years for 10 million ESAL's.

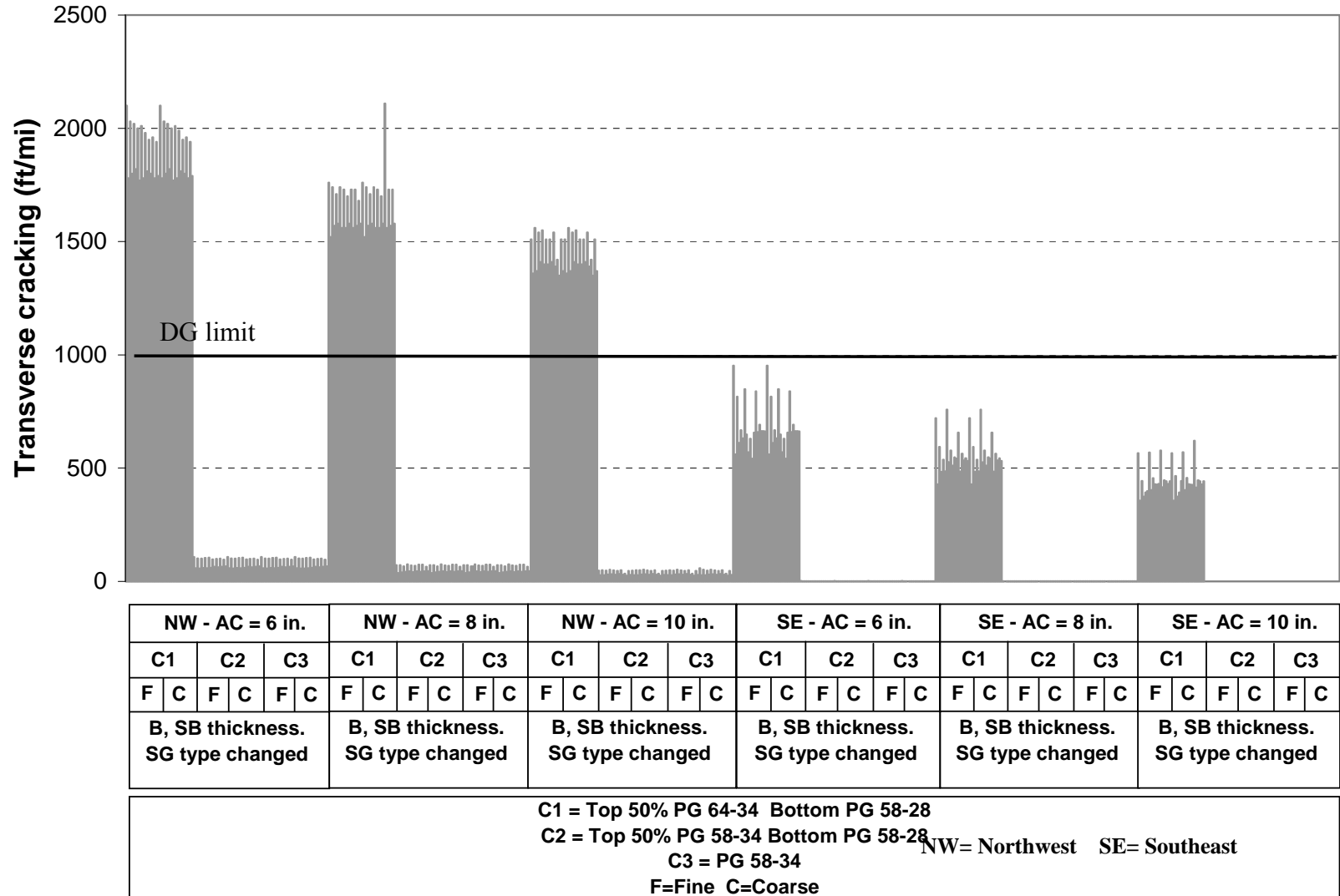
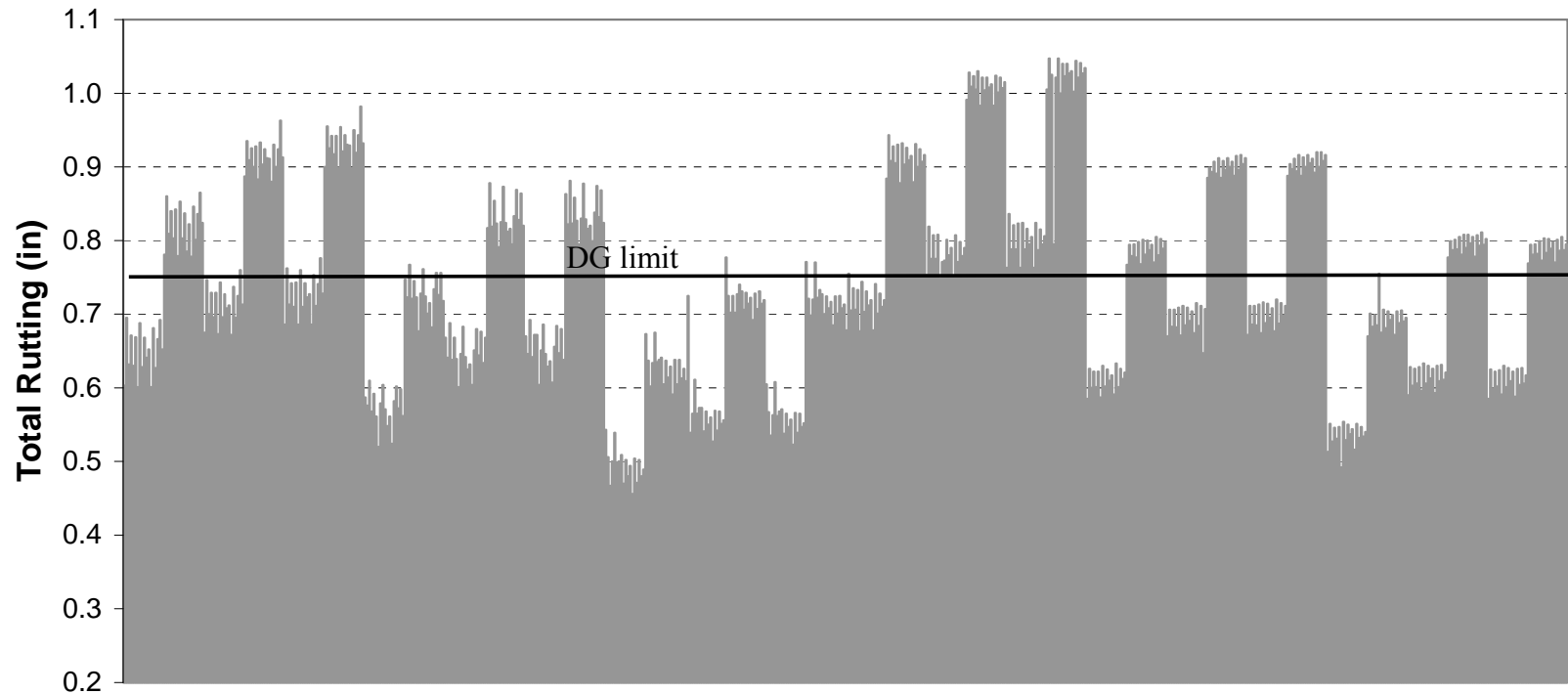


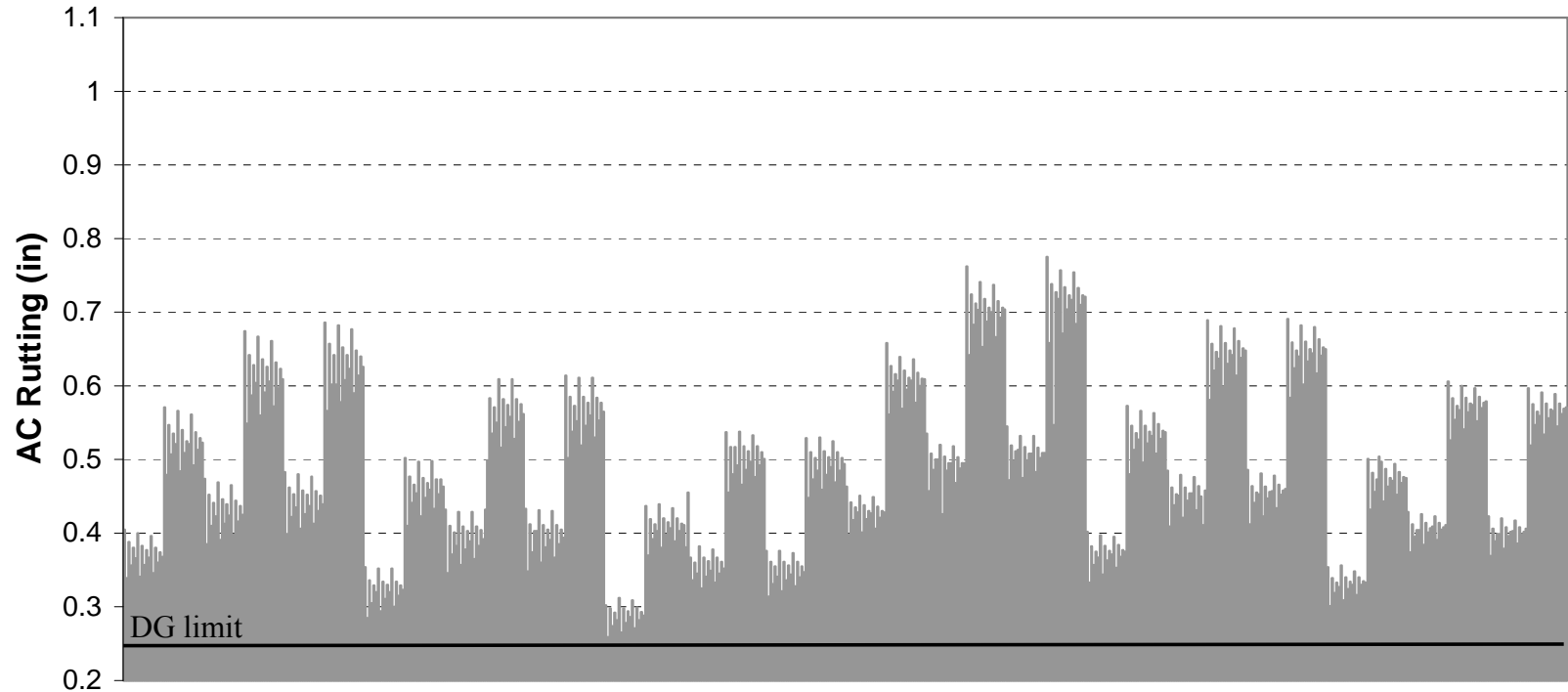
Figure 3.3 Transverse cracking after 20 years for 10 million ESAL's.



NW - AC = 6 in.			NW - AC = 8 in.			NW - AC = 10 in.			SE - AC = 6 in.			SE - AC = 8 in.			SE - AC = 10 in.		
C1	C2	C3															
F	C	F	C	F	C	F	C	F	C	F	C	F	C	F	C	F	C
B, SB thickness. SG type changed			B, SB thickness. SG type changed			B, SB thickness. SG type changed			B, SB thickness. SG type changed			B, SB thickness. SG type changed			B, SB thickness. SG type changed		

C1 = Top 50% PG 64-34 Bottom PG 58-28
C2 = Top 50% PG 58-34 Bottom PG 58-28 NW= Northwest SE= Southeast
C3 = PG 58-34
F=Fine C=Coarse

Figure 3.4 Total rutting after 20 years for 10 million ESAL's.



NW - AC = 6 in.			NW - AC = 8 in.			NW - AC = 10 in.			SE - AC = 6 in.			SE - AC = 8 in.			SE - AC = 10 in.		
C1	C2	C3															
F	C	F	C	F	C	F	C	F	C	F	C	F	C	F	C	F	C
B, SB thickness. SG type changed			B, SB thickness. SG type changed			B, SB thickness. SG type changed			B, SB thickness. SG type changed			B, SB thickness. SG type changed			B, SB thickness. SG type changed		

C1 = Top 50% PG 64-34 Bottom PG 58-28
C2 = Top 50% PG 58-34 Bottom PG 58-28 NW= Northwest SE= Southeast
C3 = PG 58-34
F=Fine C=Coarse

Figure 3.5 AC rutting after 20 years for 10 million ESAL's.

The prediction for the IRI for high volume traffic is presented in figure 3.6. The change in predicted performance with changes in design features is not reasonable; there is not a general trend. The average predicted IRI value for all the simulations is 200 in/mi; IRI values of zero are predicted in some of the simulations. Moreover, two strange peaks are presented for simulations in the Rochester climate. The input parameters for these two simulations are as follows:

- AC thickness of 8 in., C1(top 50% of the AC layer is PG 64-34 and bottom 50% is PG 58-28) binder, fine mix gradation, base thickness of 3 in., subbase thickness of 24 in and A6 subgrade type.
- AC thickness of 10 in., C3 (all PG 58-34) binder, fine mix gradation, base thickness of 9 in., subbase thickness of 24 in. and A6 subgrade type.

Figures 3.7 to 3.12 show the predicted distresses after 20 years for the 1 million ESAL's traffic. Figure 3.7 shows the predicted alligator cracking. This distress is reduced when thickness of the AC layer is increased. There is no difference between the predicted alligator cracking in the simulations from Grand Forks and Rochester climates.

Significant differences between two consecutive simulations are observed in figure 3.7 and 3.8. The factor responsible for the difference in the predictions of the distresses is the subgrade type. Pavements with soil A6 will crack considerable more than pavements with soil A3. The predicted longitudinal cracking is presented in figure 8. Contrary to the case of high volume traffic, predicted longitudinal cracking considerable increases when the thickness of the AC layer increases. The predicted values are almost the same for both climates.

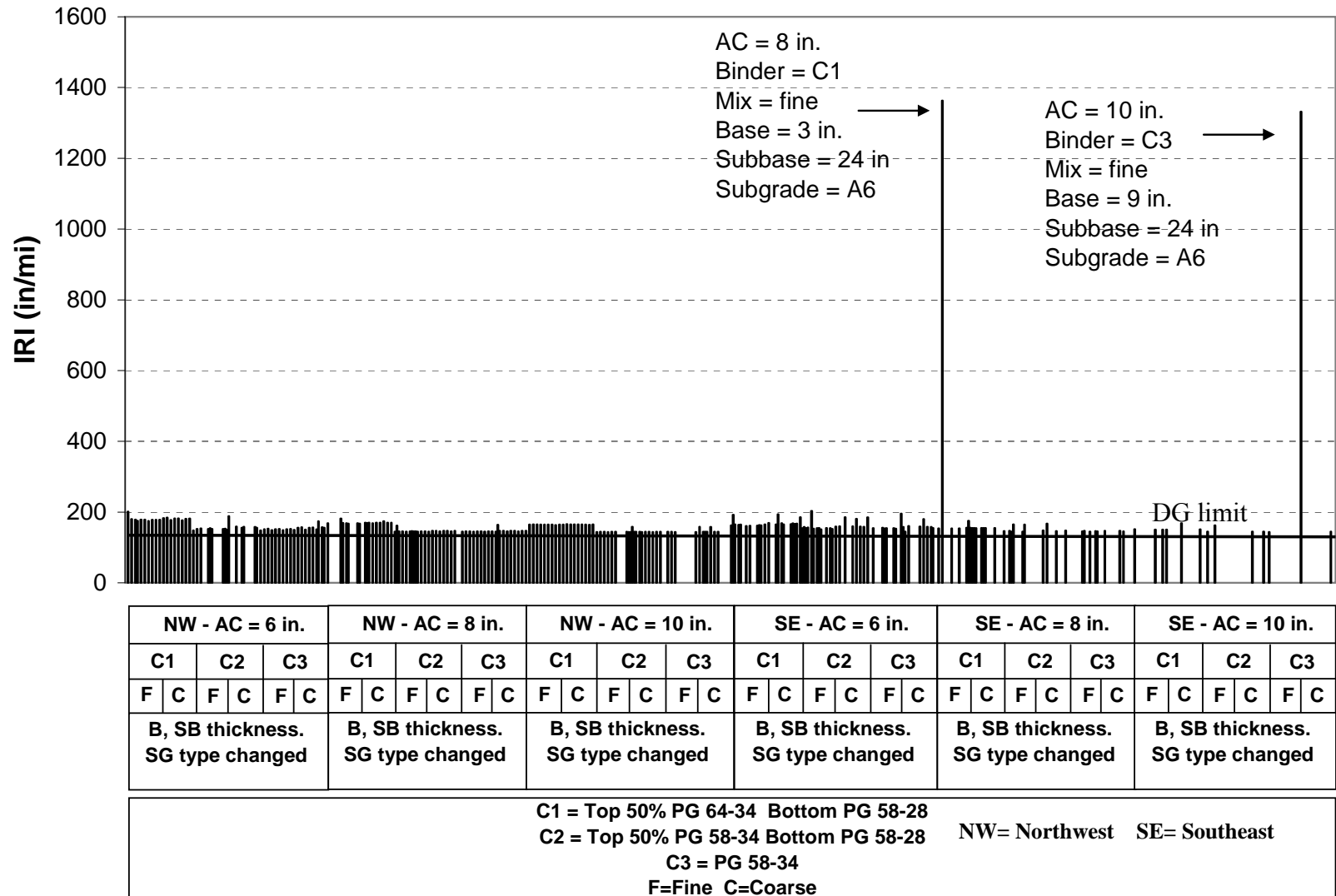
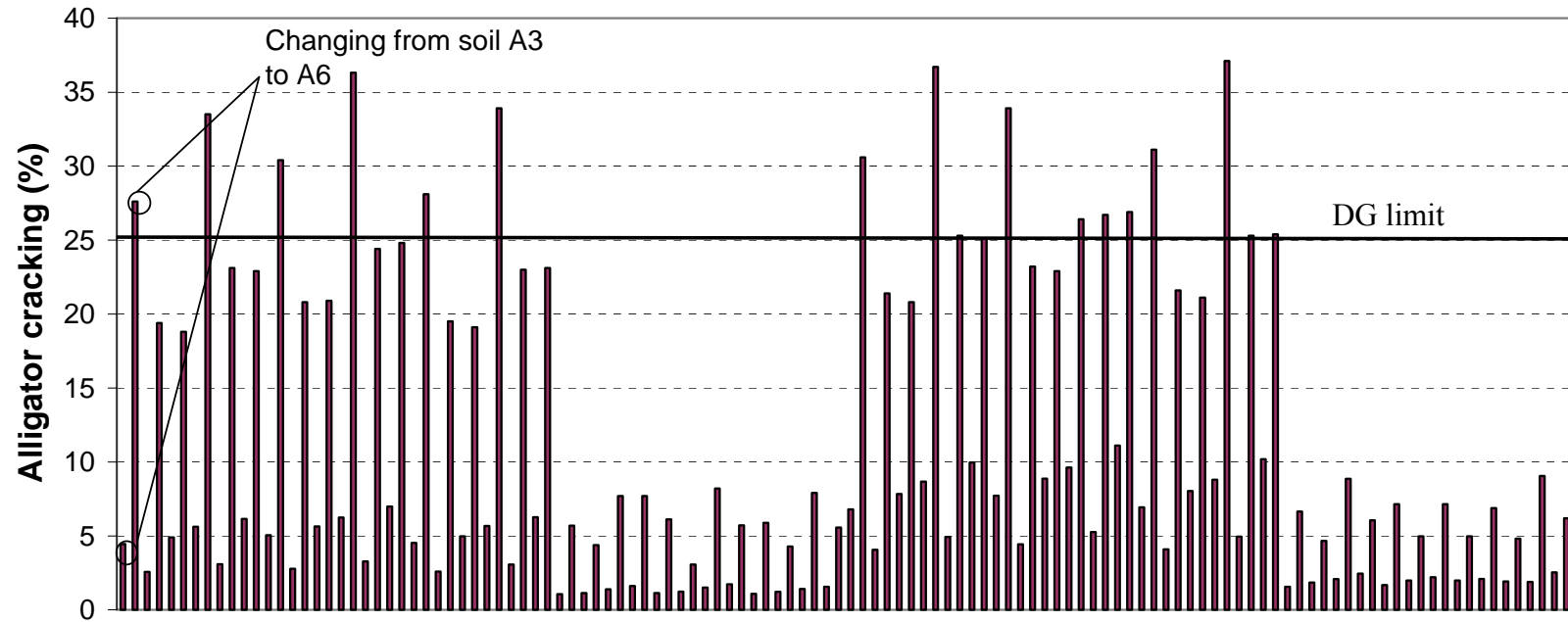
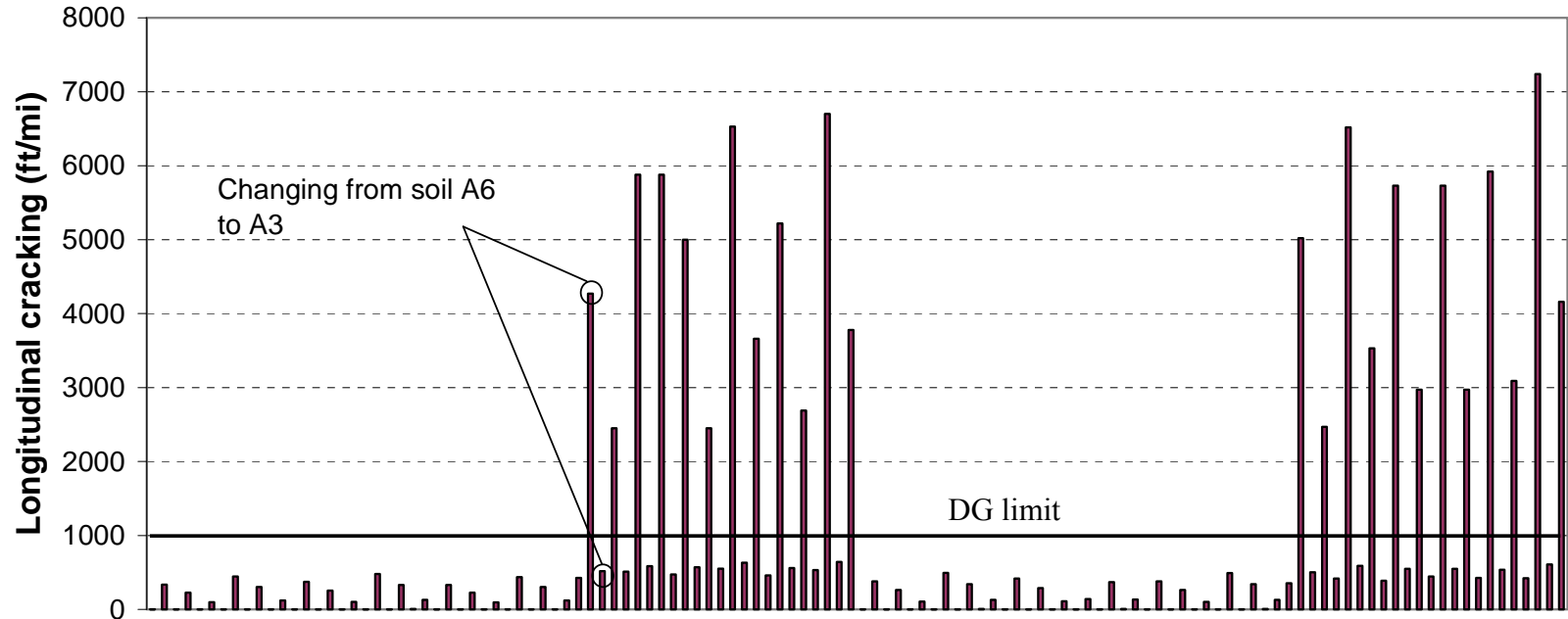


Figure 3.6 IRI after 20 years for 10 million ESAL's.



NW - AC = 4 in.						NW - AC = 6 in.						SE - AC = 4 in.						SE - AC = 6 in.					
C1		C2		C3		C1		C2		C3		C1		C2		C3		C1		C2		C3	
F	C	F	C	F	C	F	C	F	C	F	C	F	C	F	C	F	C	F	C	F	C	F	C
Base, subbase thickness, subgrade type changed						Base, subbase thickness, subgrade type changed						Base, subbase thickness, subgrade type changed						Base, subbase thickness, subgrade type changed					
C1 = PG 64-34 C2 = PG 58-34 C3 = PG 58-28						C1 = Top 50% PG 64-34 Bottom PG 58-28 C2 = Top 50% PG 58-34 Bottom PG 58-28 C3 = PG 58-34						C1 = PG 64-34 C2 = PG 58-34 C3 = PG 58-28						C1 = Top 50% PG 64-34 Bottom PG 58-28 C2 = Top 50% PG 58-34 Bottom PG 58-28 C3 = PG 58-34					

Figure 3.7 Alligator cracking after 20 years for 1 million ESAL's.



NW - AC = 4 in.						NW - AC = 6 in.						SE - AC = 4 in.						SE - AC = 6 in.					
C1		C2		C3		C1		C2		C3		C1		C2		C3		C1		C2		C3	
F	C	F	C	F	C	F	C	F	C	F	C	F	C	F	C	F	C	F	C	F	C	F	C
Base, subbase thickness, subgrade type changed						Base, subbase thickness, subgrade type changed						Base, subbase thickness, subgrade type changed						Base, subbase thickness, subgrade type changed					

C1 = PG 64-34
 C2 = PG 58-34
 C3 = PG 58-28

C1 = Top 50% PG 64-34
 Bottom PG 58-28
 C2 = Top 50% PG 58-34
 Bottom PG 58-28
 C3 = PG 58-34

C1 = PG 64-34
 C2 = PG 58-34
 C3 = PG 58-28

C1 = Top 50% PG 64-34
 Bottom PG 58-28
 C2 = Top 50% PG 58-34
 Bottom PG 58-28
 C3 = PG 58-34

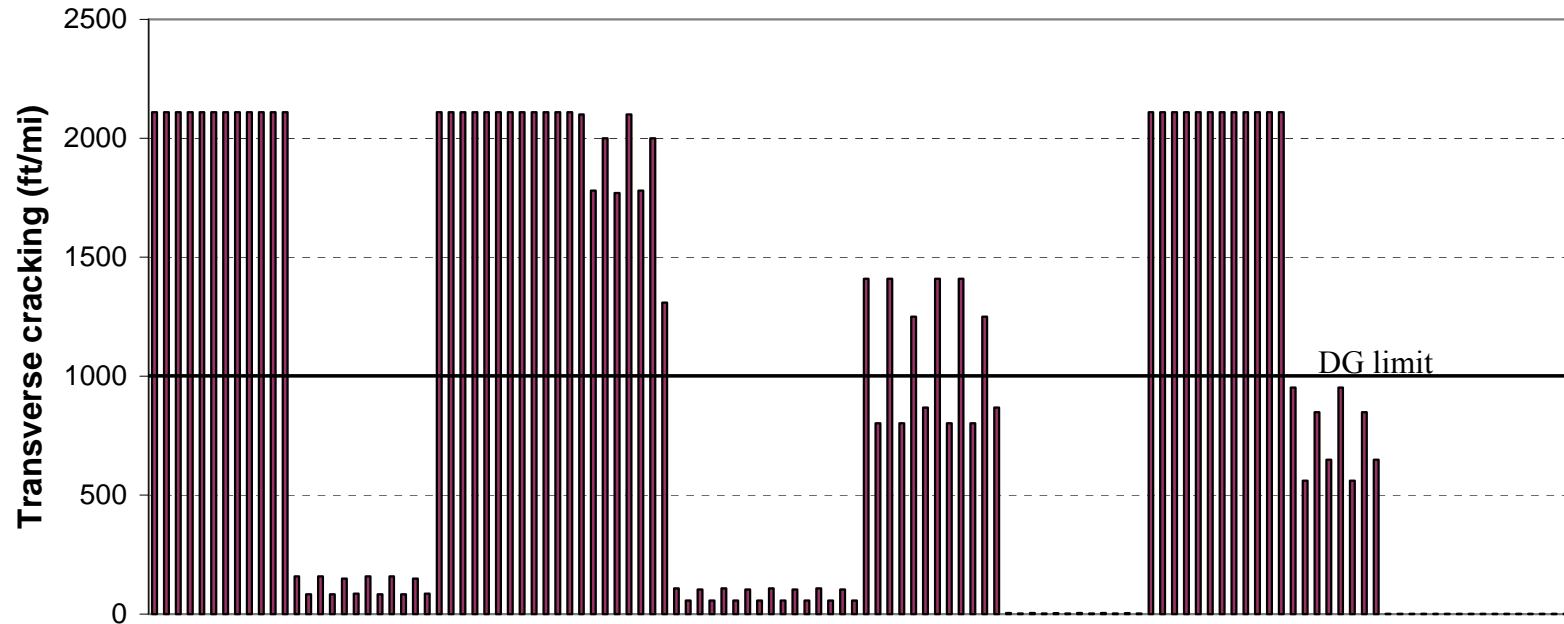
NW= Northwest SE= Southeast

Figure 3.8 Longitudinal cracking after 20 years for 1 million ESAL's.

Figure 3.9 shows the predicted transverse cracking. The climate has an important effect in the prediction of the transverse cracking for low volume traffic. Generally, if north climate regions are used in the simulation, larger predictions of thermal cracking will be obtained.

Figures 3.10 and 3.11 show the predicted total rutting and AC rutting. The predicted distress is reduced when the thickness of the asphalt layer is increased. Coarse gradation of the mix has higher predicted values compared to fine mixes. Moreover, the prediction model does not seem to be susceptible to changes in the climate; the prediction for Rochester climate is slightly higher than the prediction for Grand Forks climate. Generally the trends observed for these two performance models are reasonable.

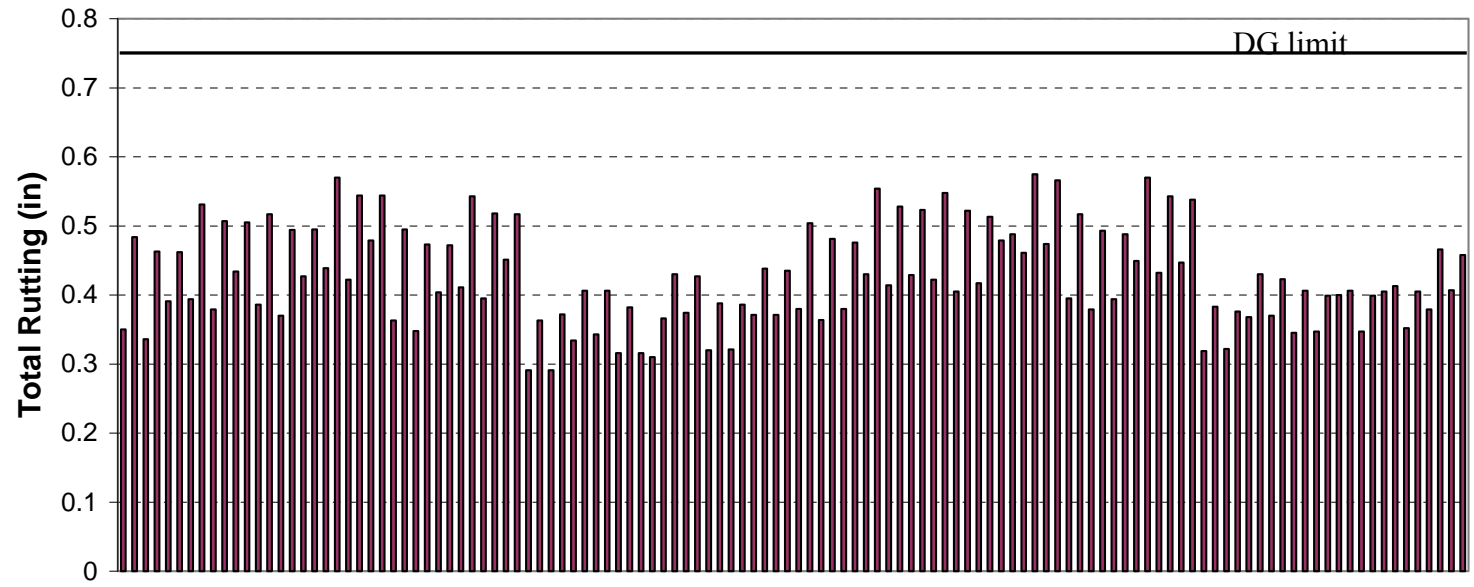
The prediction for the IRI for low volume traffic is presented in figure 3.12. The change in predicted performance with changes in design features is not reasonable; IRI values of zero are predicted in several simulations. Moreover, a jump in the value of the IRI is present in the set of one hundred and twenty simulations. The input parameters for this simulation are AC thickness of 6 in., C1 binder, fine mix gradation, base thickness of 3 in., and A3 subgrade type. The input parameters for this simulation are AC thickness of 6 in., C1 binder (top 50% of the AC layer is PG 64-34 and bottom 50% is PG 58-28), fine mix gradation, base thickness of 3 in., and A3 subgrade type



NW - AC = 4 in.						NW - AC = 6 in.						SE - AC = 4 in.						SE - AC = 6 in.					
C1		C2		C3		C1		C2		C3		C1		C2		C3		C1		C2		C3	
F	C	F	C	F	C	F	C	F	C	F	C	F	C	F	C	F	C	F	C	F	C	F	C
Base, subbase thickness, subgrade type changed						Base, subbase thickness, subgrade type changed						Base, subbase thickness, subgrade type changed						Base, subbase thickness, subgrade type changed					
C1 = PG 64-34 C2 = PG 58-34 C3 = PG 58-28						C1 = Top 50% PG 64-34 Bottom PG 58-28 C2 = Top 50% PG 58-34 Bottom PG 58-28 C3 = PG 58-34						C1 = PG 64-34 C2 = PG 58-34 C3 = PG 58-28						C1 = Top 50% PG 64-34 Bottom PG 58-28 C2 = Top 50% PG 58-34 Bottom PG 58-28 C3 = PG 58-34					

NW= Northwest SE= Southeast

Figure 3.9 Transverse cracking after 20 years for 1 million ESAL's.

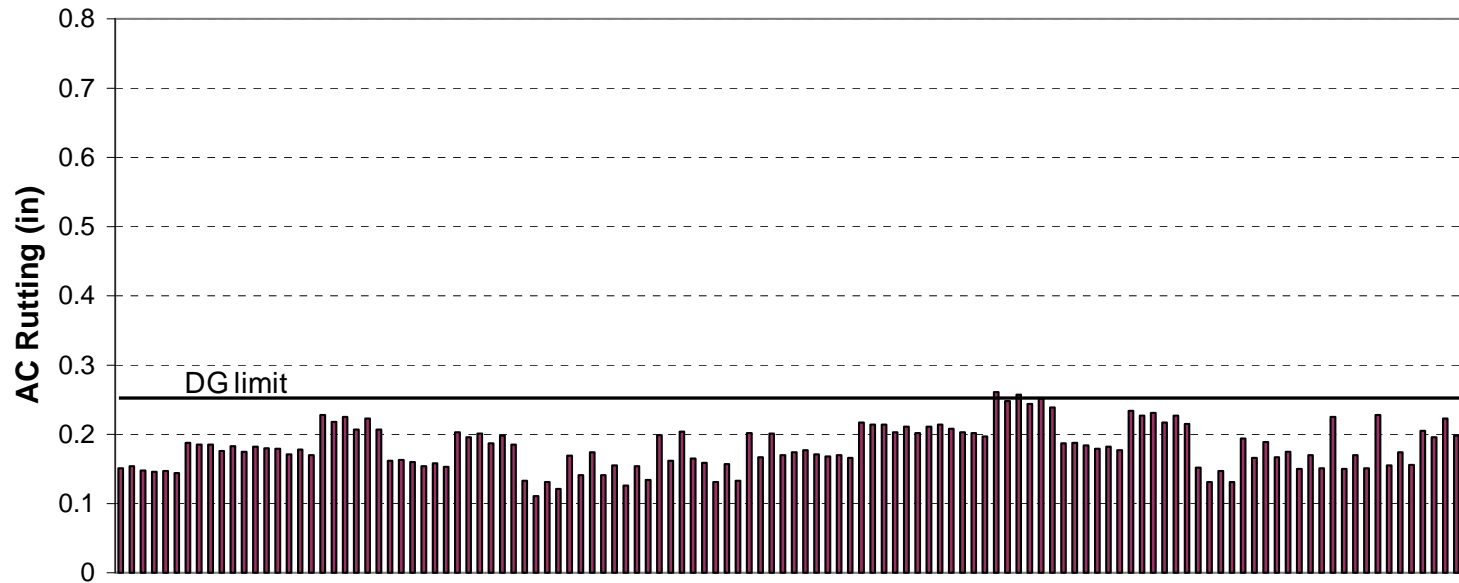


NW - AC = 4 in.						NW - AC = 6 in.						SE - AC = 4 in.						SE - AC = 6 in.					
C1		C2		C3		C1		C2		C3		C1		C2		C3		C1		C2		C3	
F	C	F	C	F	C	F	C	F	C	F	C	F	C	F	C	F	C	F	C	F	C	F	C
Base, subbase thickness, subgrade type changed						Base, subbase thickness, subgrade type changed						Base, subbase thickness, subgrade type changed						Base, subbase thickness, subgrade type changed					

C1 = PG 64-34 C2 = PG 58-34 C3 = PG 58-28	C1 = Top 50% PG 64-34 Bottom PG 58-28 C2 = Top 50% PG 58-34 Bottom PG 58-28 C3 = PG 58-34	C1 = PG 64-34 C2 = PG 58-34 C3 = PG 58-28	C1 = Top 50% PG 64-34 Bottom PG 58-28 C2 = Top 50% PG 58-34 Bottom PG 58-28 C3 = PG 58-34
---	---	---	---

NW= Northwest SE= Southeast

Figure 3.10 Total rutting after 20 years for 1 million ESAL's.



NW - AC = 4 in.						NW - AC = 6 in.						SE - AC = 4 in.						SE - AC = 6 in.					
C1		C2		C3		C1		C2		C3		C1		C2		C3		C1		C2		C3	
F	C	F	C	F	C	F	C	F	C	F	C	F	C	F	C	F	C	F	C	F	C	F	C
Base, subbase thickness, subgrade type changed						Base, subbase thickness, subgrade type changed						Base, subbase thickness, subgrade type changed						Base, subbase thickness, subgrade type changed					

C1 = PG 64-34
C2 = PG 58-34
C3 = PG 58-28

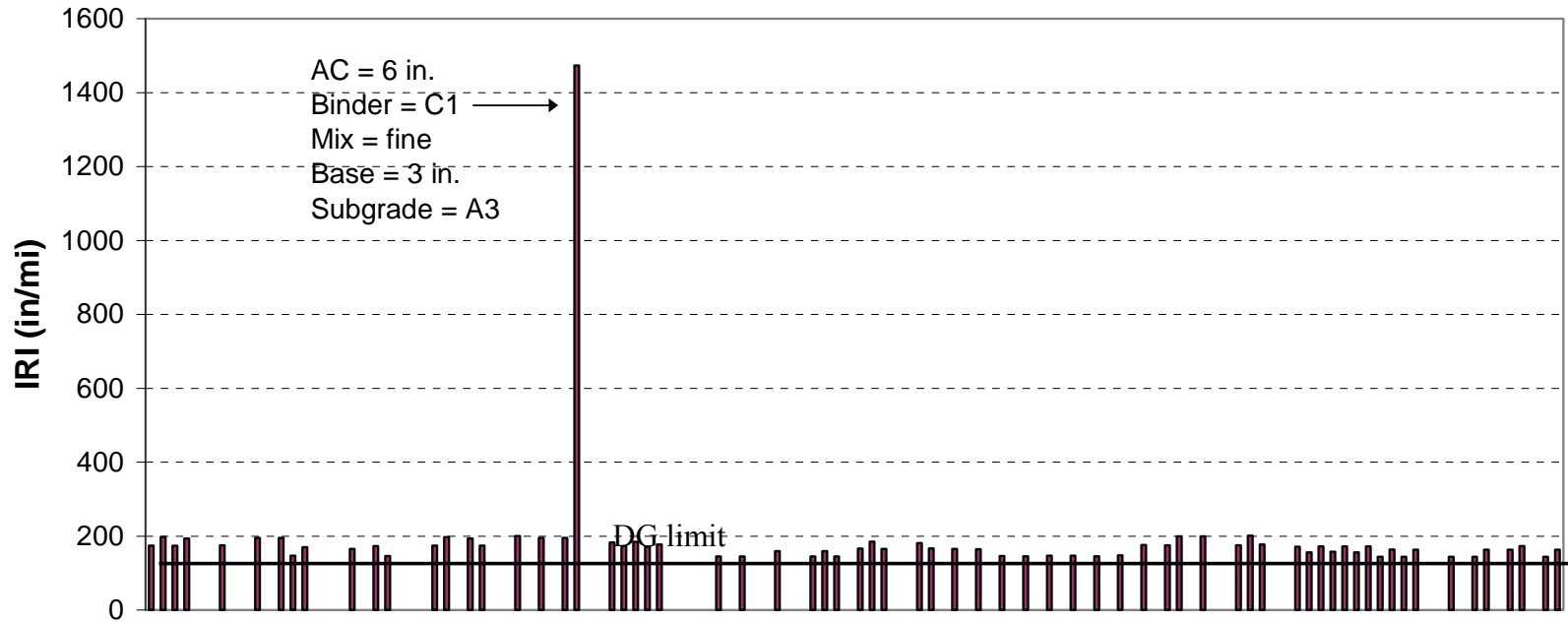
C1 = Top 50% PG 64-34
Bottom PG 58-28
C2 = Top 50% PG 58-34
Bottom PG 58-28
C3 = PG 58-34

C1 = PG 64-34
C2 = PG 58-34
C3 = PG 58-28

C1 = Top 50% PG 64-34
Bottom PG 58-28
C2 = Top 50% PG 58-34
Bottom PG 58-28
C3 = PG 58-34

NW= Northwest SE= Southeast

Figure 3.11 AC rutting after 20 years from 1 million ESAL's.



NW - AC = 4 in.						NW - AC = 6 in.						SE - AC = 4 in.						SE - AC = 6 in.					
C1		C2		C3		C1		C2		C3		C1		C2		C3		C1		C2		C3	
F	C	F	C	F	C	F	C	F	C	F	C	F	C	F	C	F	C	F	C	F	C	F	C
Base, subbase thickness, subgrade type changed						Base, subbase thickness, subgrade type changed						Base, subbase thickness, subgrade type changed						Base, subbase thickness, subgrade type changed					
C1 = PG 64-34 C2 = PG 58-34 C3 = PG 58-28						C1 = Top 50% PG 64-34 Bottom PG 58-28 C2 = Top 50% PG 58-34 Bottom PG 58-28 C3 = PG 58-34						C1 = PG 64-34 C2 = PG 58-34 C3 = PG 58-28						C1 = Top 50% PG 64-34 Bottom PG 58-28 C2 = Top 50% PG 58-34 Bottom PG 58-28 C3 = PG 58-34					

NW= Northwest SE= Southeast

Figure 3.12 IRI after 20 years for 1 million ESAL's.

3.2.2 Statistical Analysis

A formal statistics analysis (ANOVA and p-values calculations) was performed using the predicted distress and the input parameters from the simulations. For the calculation of the P-values all of the input parameters were treated as dummy variables with the following reference level for the 10 million ESAL's:

- Climate: NW-Grand Forks
- AC thickness: 6 in.
- Binder: Case 1
- Mix gradation: Fine
- Base thickness: 3 in.
- Subbase thickness: 0 in.
- Soil: A3

The reference level for 1 million ESAL's is:

- Climate: NW-Grand Forks
- AC thickness: 4 in.
- Binder: Case 1
- Mix gradation: Fine
- Base thickness: 3 in.
- Soil: A3

P-values less than 0.05 are significant or are important for the prediction of the distresses. P-values were used to rank the significance of the input parameters with respect to the different distresses.

Table 3.5 shows the p-values for the input parameters and their interactions for the 10 million ESAL's traffic. The bold values represent the parameters that are significant. The AC thickness is significant for all the distresses. Many interaction terms containing AC thickness are also significant.

Table 3.5 P-values for 10 million ESAL's.

Parameter	Alligator cracking	Longitudinal cracking	Transverse cracking	Total Rutting
AC_THICK	0	0	0	0
BASE_THICK	0.0002	0.8826	0.0539	0.0005
BINDER_CASE	0.3032	0.5887	0	0
CLIMATE	0	0.2278	0	0
MIX_GRADATION	0	0.0099	0.4432	0
SOIL_TYPE	0	0	0	0
SUBBASE_THICK	0	0	0	0.0008
AC_THICK*BASE_THICK	0	0	0.0639	0.0048
AC_THICK*BINDER_CASE	0.4323	0.0023	0	0
AC_THICK*CLIMATE	0	0.0478	0	0
AC_THICK*MIX_GRADATION	0	0	0.8626	0
AC_THICK*SOIL_TYPE	0	0	0.0015	0
AC_THICK*SUBBASE_THICK	0.6262	0.0408	0.812	0
BASE_THICK*CLIMATE	0.8826	0.7382	0.3408	0.0005
BASE_THICK*MIX_GRADATION	0.8666	0.8244	0.7979	0.0855
BASE_THICK*SOIL_TYPE	0	0	0.0022	0.2456
BASE_THICK*SUBBASE_THICK	0.0364	0.3878	0.5803	0.0006
BINDER_CASE*BASE_THICK	0.7209	0.9953	0.9801	0.7295
BINDER_CASE*CLIMATE	0.5844	0.4124	0	0.1135
BINDER_CASE*SOIL_TYPE	0.5932	0.9081	0	0.0913
BINDER_CASE*SUBBASE_THICK	0.8646	0.8136	0	0.8042
CLIMATE*MIX_GRADATION	0.6497	0.6947	0.7251	0
CLIMATE*SOIL_TYPE	0.0226	0	0	0
CLIMATE*SUBBASE_THICK	0.3433	0.7186	0.0076	0.7916
MIX_GRADATION*SOIL_TYPE	0.0437	0.4551	0.5836	0.0076
MIX_GRADATION*SUBBASE_THICK	0.7126	0.8659	0.8401	0.6458
SOIL_TYPE*SUBBASE_THICK	0	0	0	0
BINDER_CASE*MIX_GRADATION	0.6358	0.618	0.7036	0

The binder grade is significant for the prediction of transverse cracking and rutting. The base thickness is important for the prediction of rutting and alligator cracking. Climate is relevant for all the distresses except longitudinal cracking. The subgrade type and subbase thickness are significant for all distresses. The mixture gradation is significant in the prediction of rutting, alligator and longitudinal cracking and not significant for transverse cracking where the important factors are binder type and climate.

Table 3.6 shows the p-values for different input parameters and their interactions for the 1 million ESAL's traffic. Similar trends to the ones discussed above were found.

Table 3.6 P-values for 1 million ESAL's.

Parameter	Alligator cracking	Longitudinal cracking	Transverse cracking	Total Rutting
AC_THICK	0	0.0097	0	0
BASE_MODULUS	0.0015	0.2215	0.8463	0.0059
BASE_THICK	0.1049	0.0013	0.2094	0.098
BINDER_CASE	0.2917	0.5937	0	0
CLIMATE	0.0007	0.6722	0	0.0014
MIX_GRADATION	0.007	0.9566	0.8941	0
SOIL_TYPE	0	0.0047	0	0
AC_THICK*BASE_THICK	0	0	0.5313	0.2675
AC_THICK*BINDER_CASE	0.3753	0.5593	0	0
AC_THICK*CLIMATE	0.0070	0.9623	0.2548	0.1131
AC_THICK*MIX_GRADATION	0.0098	0.0006	0.584	0.7077
AC_THICK*SOIL_TYPE	0	0	0.2994	0
BASE_THICK*CLIMATE	0.6198	0.3879	0.5581	0.1131
BASE_THICK*MIX_GRADATION	0.8032	0.9427	0.5840	0.2265
BASE_THICK*SOIL_TYPE	0	0	0.4787	0.0015
BINDER_CASE*BASE_THICK	0.7769	0.4962	0.3324	0.8870
BINDER_CASE*CLIMATE	0.5792	0.7157	0	0.3845
BINDER_CASE*SOIL_TYPE	0.9992	0.6295	0	0.0844
CLIMATE*MIX_GRADATION	0.4692	0.2324	0.6243	0.0961
CLIMATE*SOIL_TYPE	0.2719	0.7348	0.0331	0.2455
MIX_GRADATION*SOIL_TYPE	0.0008	0.0023	0.6244	0.629
BINDER_CASE*MIX_GRADATION	0.3719	0.4139	0.7847	0.8477
BASE_MODULUS*BINDER_CASE	0.8778	0.9158	0.9461	0.7721
BASE_MODULUS*CLIMATE	0.7938	0.8038	0.7043	0.2250
BASE_MODULUS*MIX_GRADATION	0.5493	0.9081	0.8359	0.3610
BASE_MODULUS*SOIL_TYPE	0	0.0066	0.8716	0.2908

The AC thickness is significant for all four distresses. Climate, binder type and soil type are the parameters that contain almost all the predictive information for transverse cracking. Base thickness is important for the prediction of longitudinal cracking and the modulus of this layer is significant in estimating rutting and alligator cracking.

The correlation factors between each distress and the input parameter for each level of traffic was calculated. For this analysis the input parameters were coded as presented in tables 3.7 and 3.8 (none of the variables were treated as continuous).

Table 3.7 Coding of input parameters for 10 million ESAL's.

Parameter	Description	Code
Climate	NW - Grand Forks, ND SE - Rochester	Case 1 Case 2
AC thickness	6" 8" 10"	Case 2 Case 3 Case 4
Binder PG	Case 1: 64-34 Case 2: 58-34 Case 3: 58-28	Case 1 Case 2 Case 3
Mix gradation	Fine mix Coarse mix	Case 1 Case 2
Base thickness	3" 6" 9"	Case 1 Case 2 Case 3
Subbase thickness	0" 12" 24"	Case 1 Case 2 Case 3
Soil	A3 A6	Case 1 Case 2

Correlation factors more than $\frac{2}{\sqrt{n}}$ (rule of thumb) where n is the number of samples or simulations (Krehbiel, T., 2003) indicates that the parameter contains important information for the prediction of the distress. Correlation factors larger than 0.07(n = 648) and 0.18(n = 120) are significant for 10 million and 1 million ESAL's respectively. The significant parameters for each distress are presented in bold in tables 3.8 through 3.10.

Table 3.8 Coding of input parameters for 1 million ESAL's.

Parameter	Description	Code
Climate	NW - Grand Forks, ND SE - Rochester	Case 1 Case 2
AC thickness	4" 6"	Case 1 Case 2
Binder PG	Case 1: 64-34 Case 2: 58-34 Case 3: 58-28	Case 1 Case 2 Case 3
Mix gradation	Fine mix Coarse mix	Case 1 Case 2
Base thickness	3" 6"	Case 1 Case 2
Soil	A3 A6	Case 1 Case 2

Table 3.9 Correlation matrix for 10 million ESAL's.

Parameter	Alligator cracking	Longitudinal cracking	Transverse cracking	Total Rutting
AC_THICK	-0.8599	-0.9028	-0.0856	-0.5751
BASE_THICK	-0.0674	-0.0738	-0.0007	-0.0095
BINDER_CASE	0.0059	0.0428	-0.7243	0.2804
CLIMATE	0.0805	-0.0057	-0.3327	0.2415
MIX_GRADATION	0.1592	0.1397	0.0013	0.6846
SUBBASE_THICK	-0.0255	0.0766	-0.0106	0.0195
SOIL_TYPE	0.2094	-0.1611	-0.0441	0.0656

Table 3.10 Correlation matrix for 1 million ESAL's.

Parameter	Alligator cracking	Longitudinal cracking	Transverse cracking	Total Rutting
AC_THICK	-0.5701	0.6287	-0.4211	-0.6004
BASE_THICK	-0.1463	-0.0395	-0.0794	-0.0891
BINDER_CASE	0.0036	0.0166	-0.0879	0.1247
CLIMATE	0.0758	0.0016	-0.2140	0.1470
MIX_GRADATION	0.0948	0.0752	-0.0041	0.3220
BASE_MODULUS	0.1040	-0.2533	0.1734	0.1703
SOIL_TYPE	0.6673	0.4755	-0.0609	0.6155

For 10 million ESAL's AC thickness has a negative correlation with alligator cracking meaning that increasing the thickness of the pavement reduces alligator cracking. Soil type has a positive correlation with alligator cracking, thus, changing the subgrade type from A3 to A6 increases alligator cracking. Using coarse mix gradation instead of fine increases alligator cracking. For longitudinal cracking changing the subgrade from A3 to A6 reduces the prediction of this distress. Climate has a negative correlation with transverse cracking.

Thus, pavements in Grand Forks climate are more susceptible to transverse cracking than the Rochester climate. Binder case has a negative correlation with transverse cracking meaning that case 2 (PG 58-34) and case 3 (PG 58-28) present less transverse cracking than 64-34. Total rutting has a negative correlation with AC thickness and a positive correlation with binder case, climate and mix gradation. Thus, total rutting decreases when AC thickness increases and it is larger in the Rochester climate conditions and when coarse mix gradation and case 2 and 3 are used.

For 1 million ESAL's AC thickness has a negative correlation with alligator cracking. Thus increasing the thickness of the pavement reduces alligator cracking. Soil type has a positive correlation with alligator cracking. If subgrade type A6 instead of A3 is used alligator cracking is increased. For longitudinal cracking changing the subgrade from A3 to A6 increases distress. Climate has a negative correlation with transverse cracking. Meaning there is more thermal cracking in Grand Forks than in Rochester. Thermal cracking has a negative correlation with AC thickness thus increasing AC thickness reduces transverse cracking. Total rutting has a negative correlation with AC thickness and a positive correlation with mix gradation and subgrade type. Thus, rutting decreases when AC thickness increases. Total rutting is larger when coarse mix gradation and soil A6 are used.

Table 3.11 presents the summary of a qualitative measure of the sensitivity of the distresses predictions to the principal design input variables for the 10 million ESAL's traffic. To obtain the qualitative measure several simulations of each distress were plotted against time, for each plot one parameter was changed meanwhile the other set of parameters were constant. A significant difference between simulations in each plot was considered as high sensitive and no difference was considered as insensitive.

Table 3.11 Sensitivity summary for 10 million ESAL's.

Parameter	L. Cracking	T. Cracking	A. Cracking	Total Rutting
Climate	IS	HS	LS	LS
AC thickness	HS	HS	HS	HS
Binder	LS	HS	LS	LS
Gradation	LS	IS	LS	LS
Base thickness	IS	IS	IS	IS
Subbase thickness	LS	IS	LS	LS
Soil	HS	LS	LS	LS

* IS-insensitive
 LS-low sensitivity
 HS-high sensitivity

The summary indicates that the most important variable is the AC thickness; all four distresses investigated are highly sensitive to changes in this parameter. The binder type is highly significant for thermal cracking. Longitudinal cracking is insensitive to changes in climate and base thicknesses. Additionally, changing base thickness in the design does not affect significantly any of the four distresses.

Table 3.12 shows the sensitivity analysis summary for 1 million ESAL's traffic. For this case, AC thickness and subgrade type are highly significant parameters in predicting most of the distresses. Transverse cracking is highly sensitive to climate input, binder and subgrade type. For rutting, only AC thickness is a highly significant variable.

Table 3.12 Sensitivity summary for 1 million ESAL's.

Parameter	L. Cracking	T. Cracking	A. Cracking	T. Rutting
Climate	LS	HS	LS	LS
AC thickness	HS	LS	HS	HS
Binder	LS	HS	LS	LS
Gradation	LS	IS	LS	LS
Base thickness	LS	IS	LS	LS
Soil	HS	HS	HS	LS

* IS-insensitive
 LS-low sensitivity
 HS-high sensitivity

Please note that the statistical analysis presented above is based on a limited number of data (simulations runs) and is based on assumptions of normality and independence

3.2.3 Comparison of Various Versions of the MEPDG for Flexible Pavements

3.2.3.1 Comparison of Versions 0.615 and 0.900: The results of the performance prediction presented above were obtained using 0.615 version of the MEPDG software. This version, however, is not the final version of the MPEDG. Recently the MEPDG procedure went through the external review under the NCHRP 1-40A project which results in several recommendations to modify the procedure. In addition, the MEPDG users identified many bugs in the software. To address these comments and bugs, ARA, Inc and the Arizona State University research team under the NCHRP 1-40D developed a newer (0.900) version of the MEPDG software. This, however, did not make the analysis presented above completely obsolete. A database of the results of a large factorial runs can be used for evaluation of the subsequent versions of the software, including a future final version accounting for the local calibration.

Figures 3.13 to 3.16 show a comparison between the predicted distresses for all traffic levels using versions 0.615 and 0.900 of the MEPDG. In these figures, the x-axis represents the predicted distress after 20 years using the old version and the y-axis the predicted distresses after 20 years using the 0.900 version. Figure 3.13 shows that modification on the alligator cracking models on the 0.900 version reduced the magnitude of the predicted distress compared to the previous version. Moreover, the same behavior for longitudinal cracking and AC rutting can be observed (Figures 3.14 and 3.15). It can be observed from Figure 3.16 that the total rutting

prediction did not vary considerably between the two versions. On the other hand, improvements on the prediction of IRI in the 0.900 version are implemented. The 0.900 version models predict reasonable values of IRI compared to the previous version.

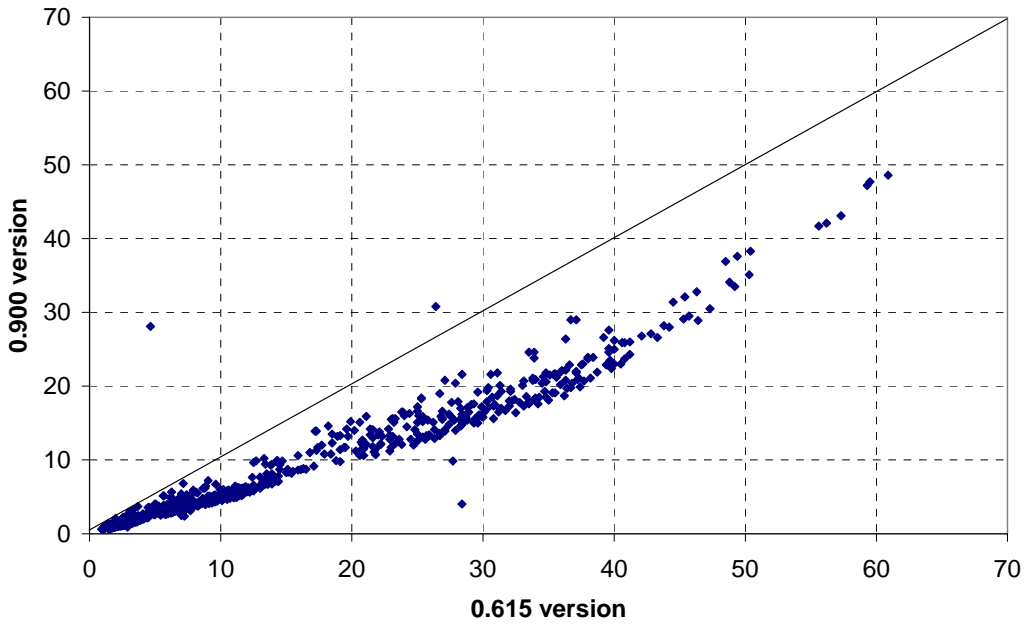


Figure 3.13 Comparison for predicted distresses between 0.615 and 0.900 version for alligator cracking.

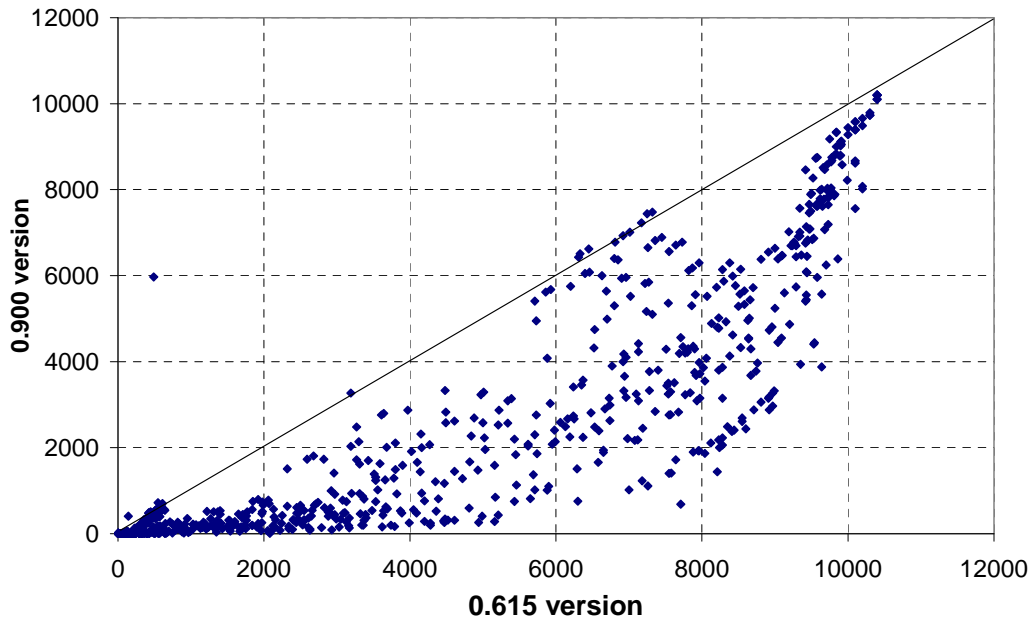


Figure 3.14 Comparison for predicted distresses between 0.615 and 0.900 version for longitudinal cracking.

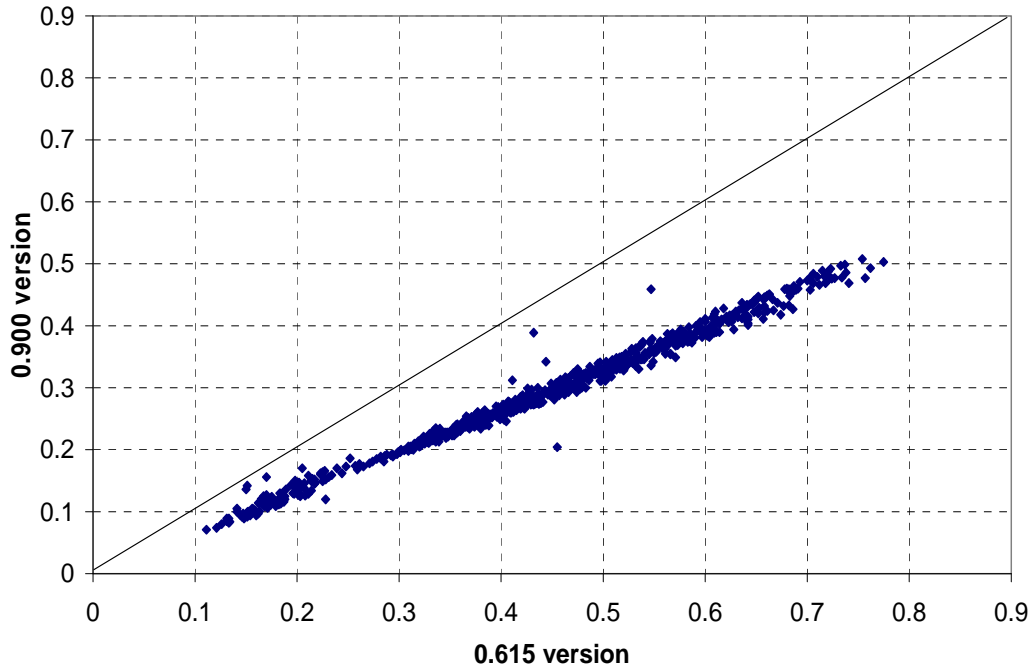


Figure 3.15 Comparison for predicted distresses between 0.615 and 0.900 version for AC rutting.

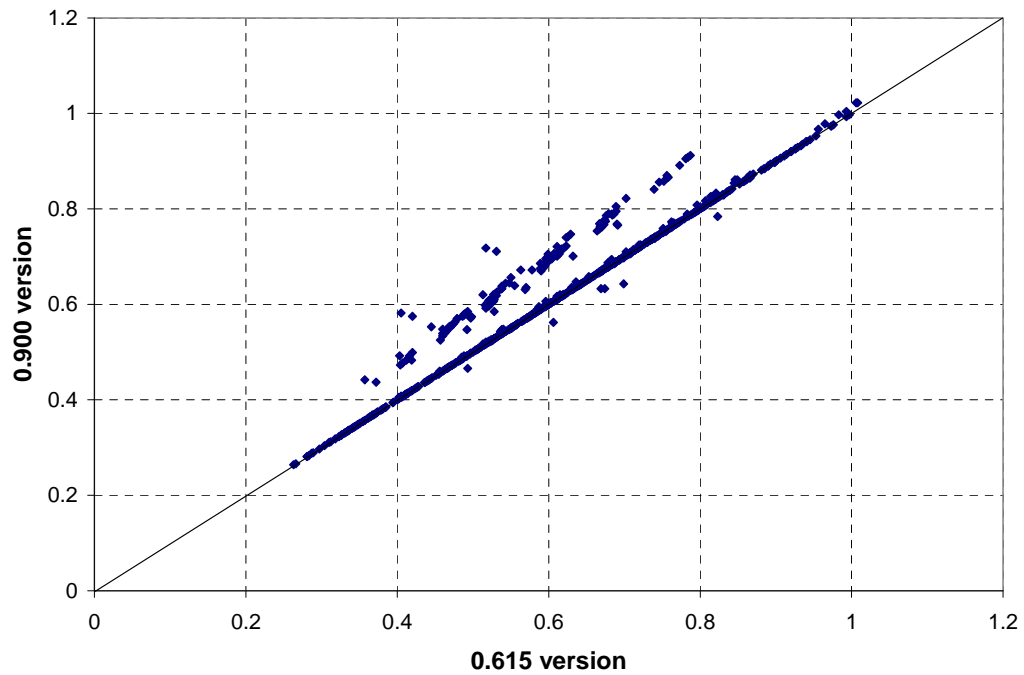


Figure 3.16 Comparison for predicted distresses between 0.615 and 0.900 version for total rutting.

3.2.3.2 *Comparison of Version 0.910 versus 0.900*: A comparison between an updated (0.910) and previous (0.900) version of the MEPDG to study the changes in the performance prediction models. Typical design inputs for Minnesota conditions were used to run a total of 768 simulations. From the comparison between update and previous version improvements on the prediction model for IRI was observed.

The following figures show the predicted distresses after 20 years using the versions 0.900 and 0.910. Figure 3.17 shows that for some projects alligator cracking prediction was reduced in version 0.910. Additionally, for several projects the MEPDG 0.910 predicted zero alligator cracking, specifically projects with subgrade soil A3 and with AC layer having the top 50% with PG 58-34 and the bottom with PG-58-28.

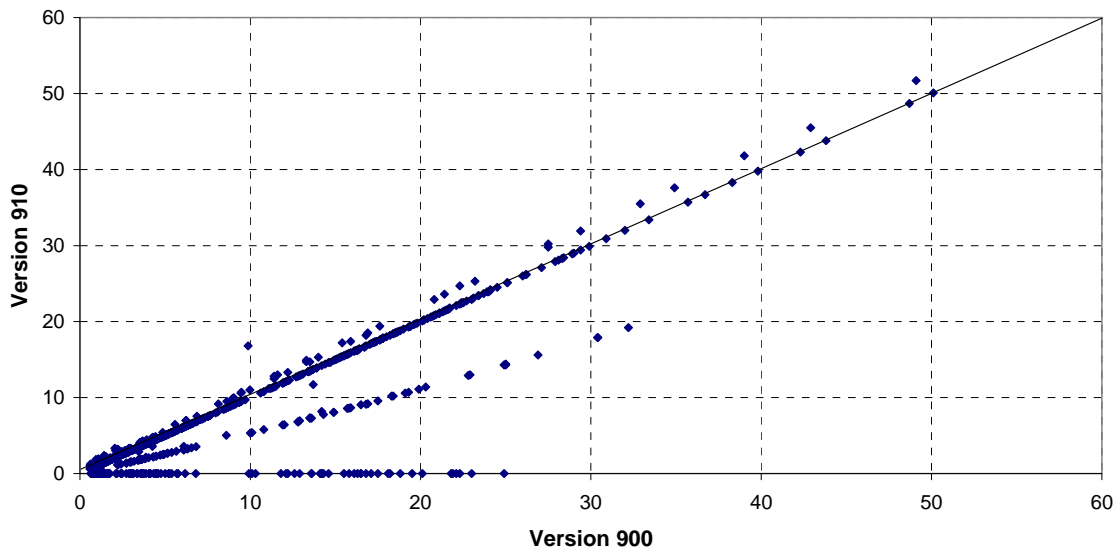


Figure 3.17 Alligator cracking comparison.

Figure 3.18 shows comparison for longitudinal cracking. The new version predicts lower values of longitudinal cracking compared to previous versions. Again, zero values were predicted for projects with subgrade A3 and AC layer having top 50% with PG 58-34 and the bottom with PG-58-28.

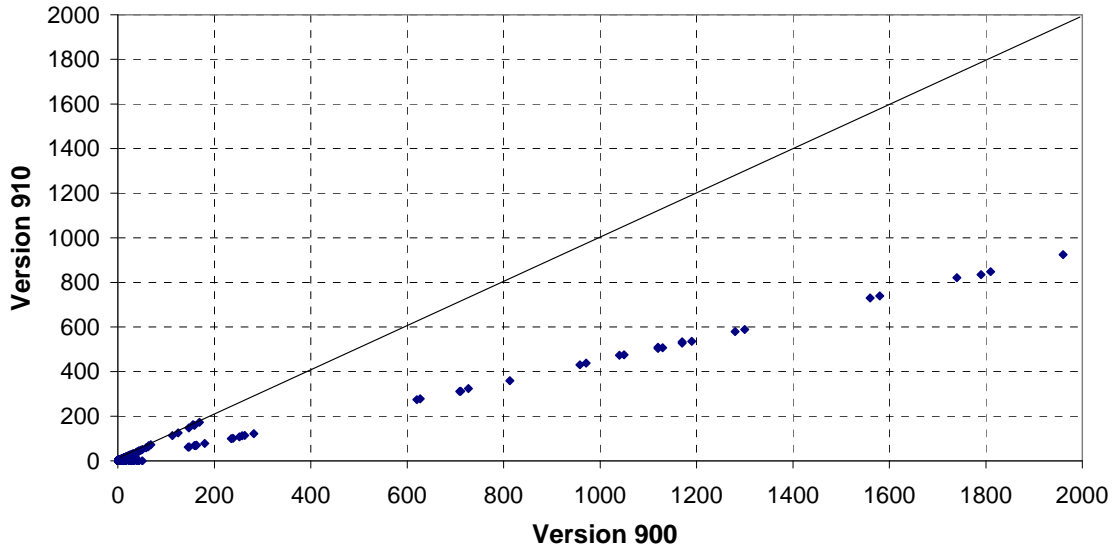


Figure 3.18 Longitudinal cracking comparison

Figure 3.19 shows that total rutting did not vary significantly between the versions 0.900 and 0.910. For rutting, the same sections that predicted zero values for the previous distresses predicted zero for total and AC rutting; indicating that for that combination of input factors the MEPDG is not working properly. The behavior observed for AC rutting predictions was the same as the observed for total rutting.

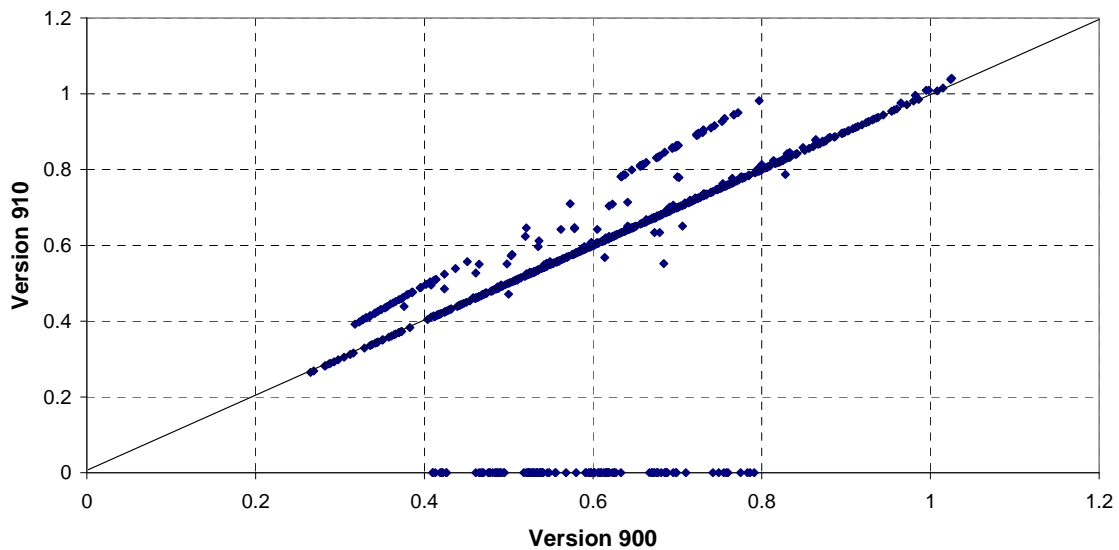


Figure 3.19 Total rutting comparison.

Figure 3.20 shows the comparison for transverse cracking. Almost all the projects predicted zero transverse cracking for the latest version. These values are unreasonable because transverse cracking is one of the most important and common distresses for Minnesota and high values of predicted thermal cracking are expected for this climate. As it was found by the research team,

the zero value predictions were the results of a bug in the MEPDG software. This bug was reported to ARA, Inc. and appropriate corrections were made by ARA, Inc. under the NCHRP 1-40D contract.

Finally, figure 3.21 shows the comparison for IRI. Improvement in the prediction model for IRI was observed. More reasonable values were obtained using version 0.91 of the MEPDG compared to previous versions. One of the reasons for this improvement is that the IRI prediction model depends on performances prediction of the individual distresses. Thus improvements in the prediction models for fatigue cracking, transverse cracking and rutting resulted in more reasonable values of IRI.

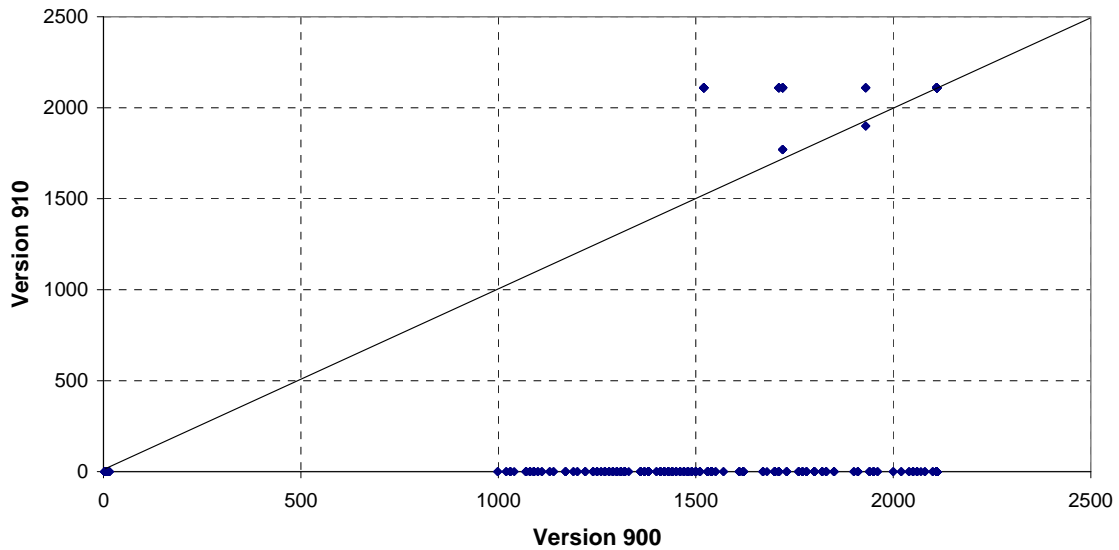


Figure 3.20 Transverse cracking comparison.

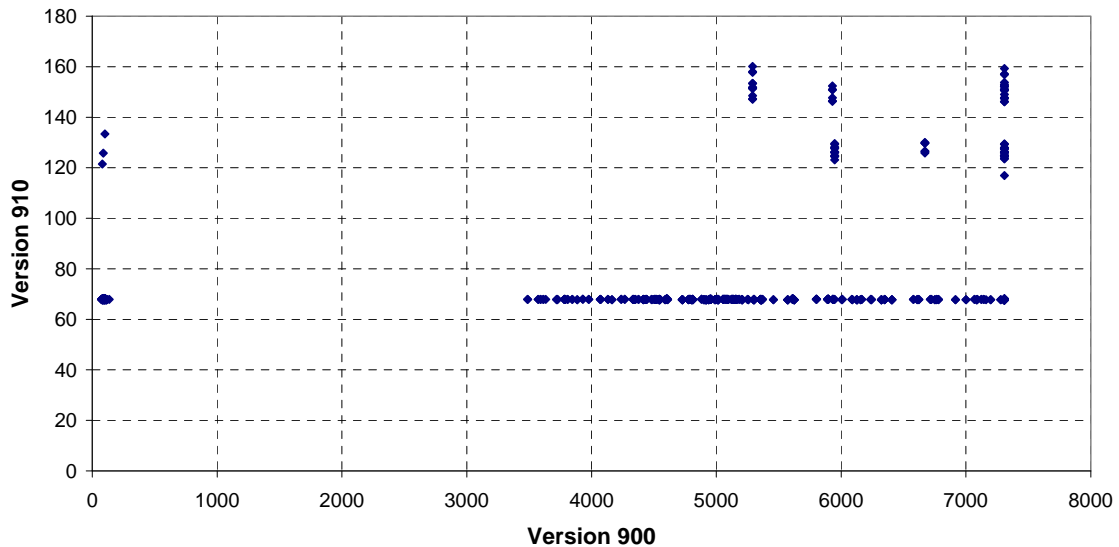


Figure 3.21 IRI comparison.

3.2.3.3 *Comparison of Version 1.003 versus 0.910 (high volume)*: Version 1.003 was released in May/June 2007. A comparison between an updated (1.003) and the previous (0.910) version of the MEPDG was evaluated to study the changes in the performance prediction models. Typical design inputs for Minnesota conditions (see tables 3.1 and 3.2) were used to run a total of 768 simulations.

The following figures show predicted distresses after 20 years using the versions 0.910 and 1.003 for high volume traffic. Figure 3.22 shows that for some projects alligator cracking prediction was increased in version 1.003. Additionally, for several projects the MEPDG 0.910 predicted zero alligator cracking, whereas 1.003 predicted alligator cracking.

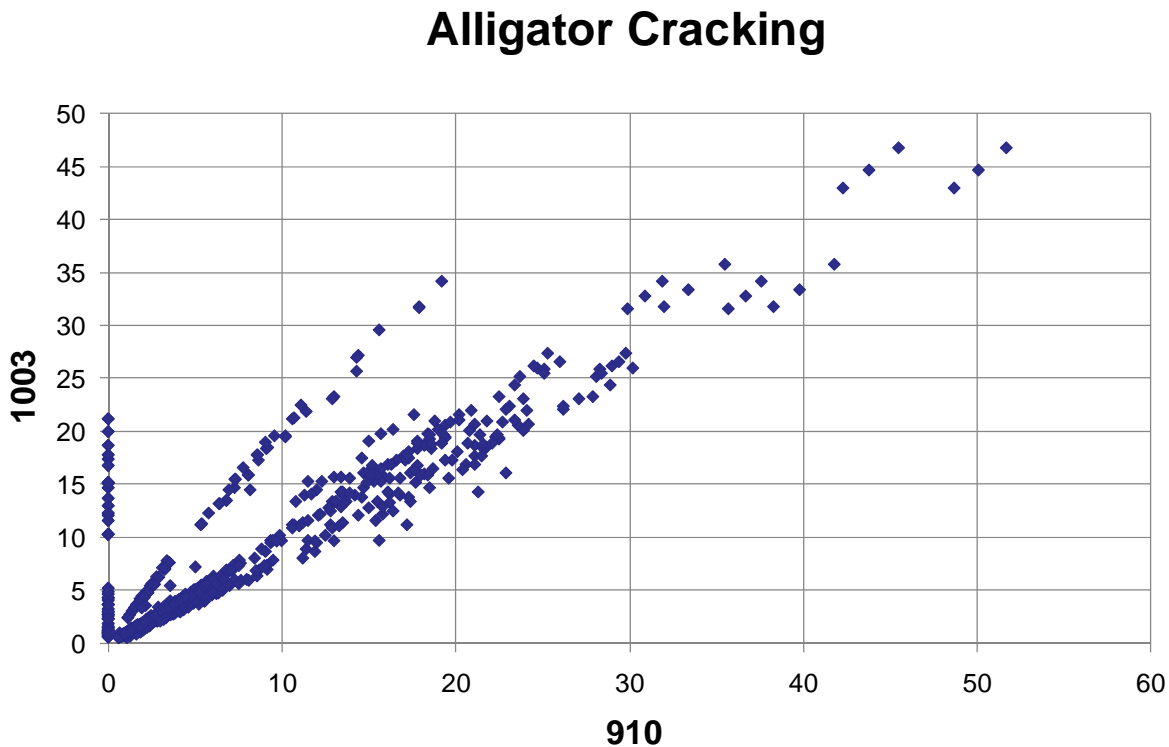


Figure 3.22 Alligator cracking comparison.

Figure 3.23 shows comparison for longitudinal cracking. The new version predicts higher values of longitudinal cracking compared to previous versions. Zero values were predicted for many projects for the MEPDG 0.910, whereas 1.003 predicted non-zero level of longitudinal cracking. However, even for the cases of non-zero values of longitudinal cracking from version 0.910 those values are several orders of magnitude lower than the prediction from version 1.003. This means that the longitudinal cracking model went through a significant overhaul from version 0.91 to version 1.003. Due to time and resources constraints, a comprehensive evaluation of this version of the model was not feasible in this study. Therefore, it was recommended to remove this model from local adaptation and calibration under this project.

Longitudinal Cracking

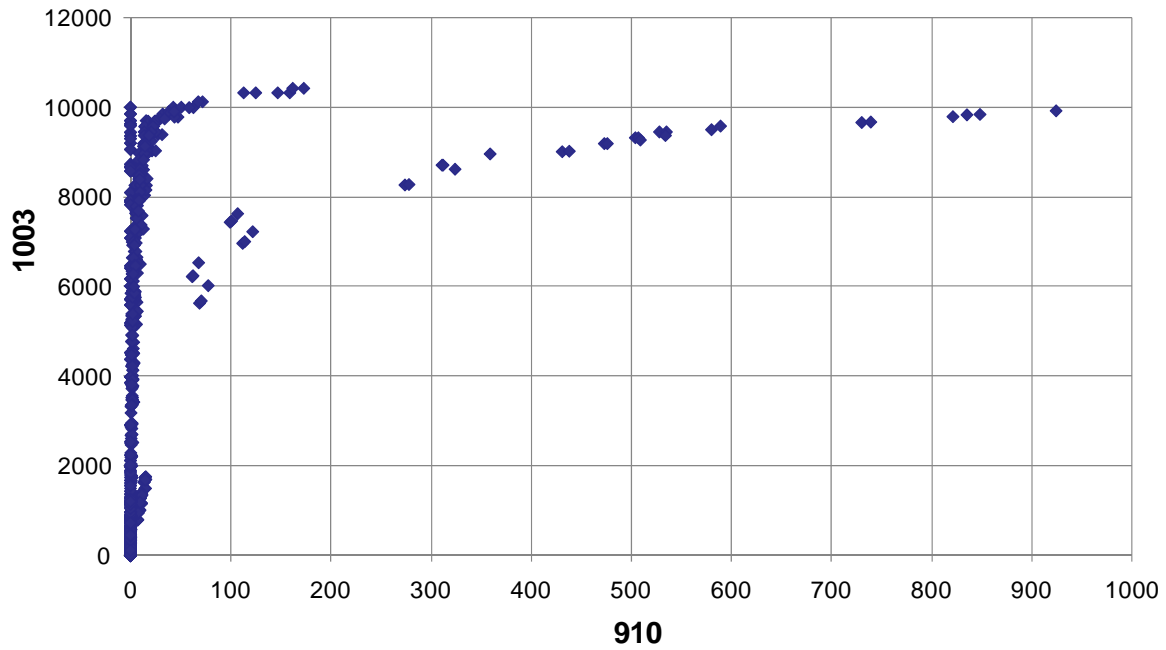


Figure 3.23 Longitudinal cracking comparison.

Figures 3.24 and 3.25 show that total and AC rutting did not vary significantly between the versions 0.900 and 0.910. However, there were some cases in which the version 1.003 version predicted rutting whereas the previous version did not. It can be observed that the behavior observed for AC rutting predictions was the same as the observed for total rutting.

Total Rutting

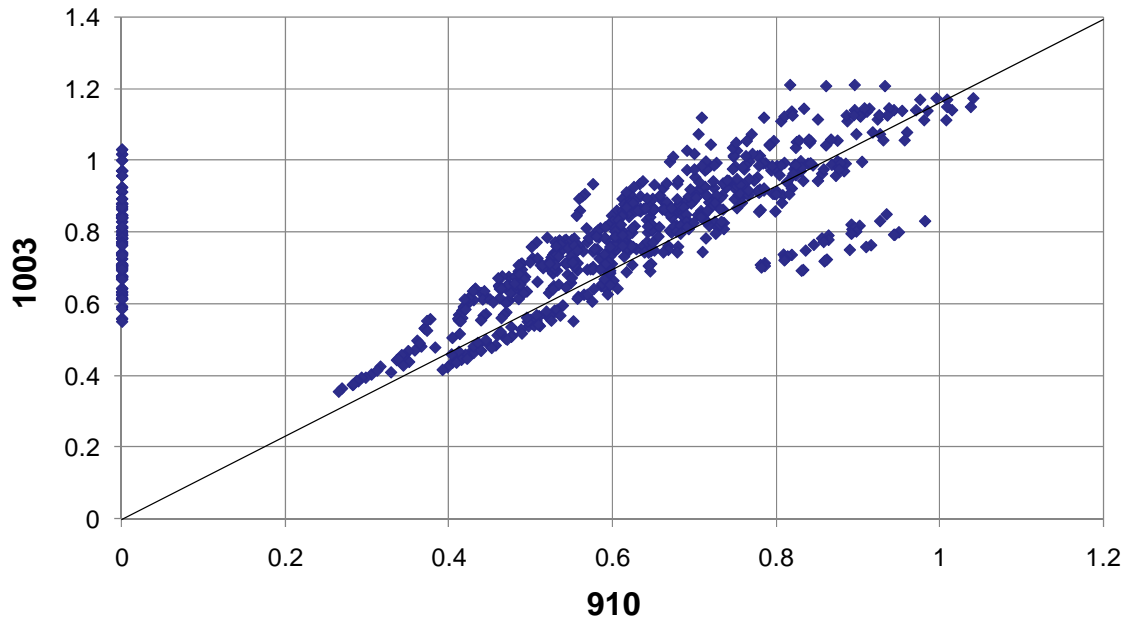


Figure 3.24 Total rutting comparison.

AC Rutting

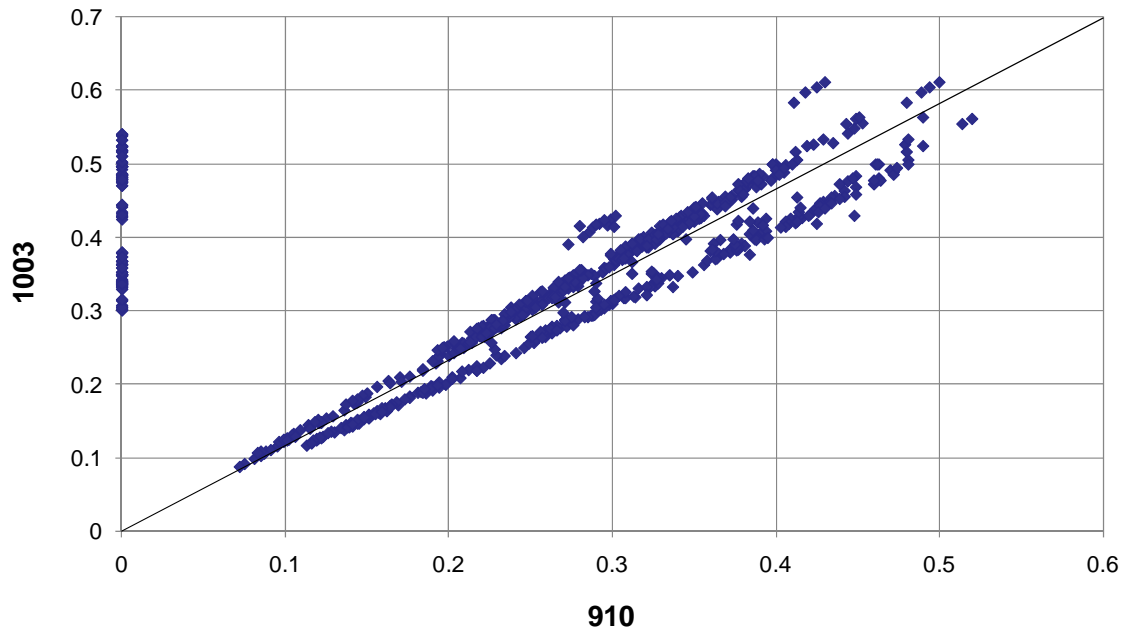


Figure 3.25 AC rutting.

Figure 3.26 shows the comparison for transverse cracking. As discussed earlier, almost all the projects predicted zero transverse cracking for the 0.910 version. These values were unreasonable because transverse cracking is one of the most important and common distresses for Minnesota and high values of predicted thermal cracking are expected for this climate. Communication with the MEPDG software developers helped to identify a memory allocation bug in the MEPDG thermal cracking models in versions 0.910 and older. As Figure 3.26 shows, the newest version seems to be free from this bug, as there is a range of predicted cracking for the values that previously predicted zero cracking.

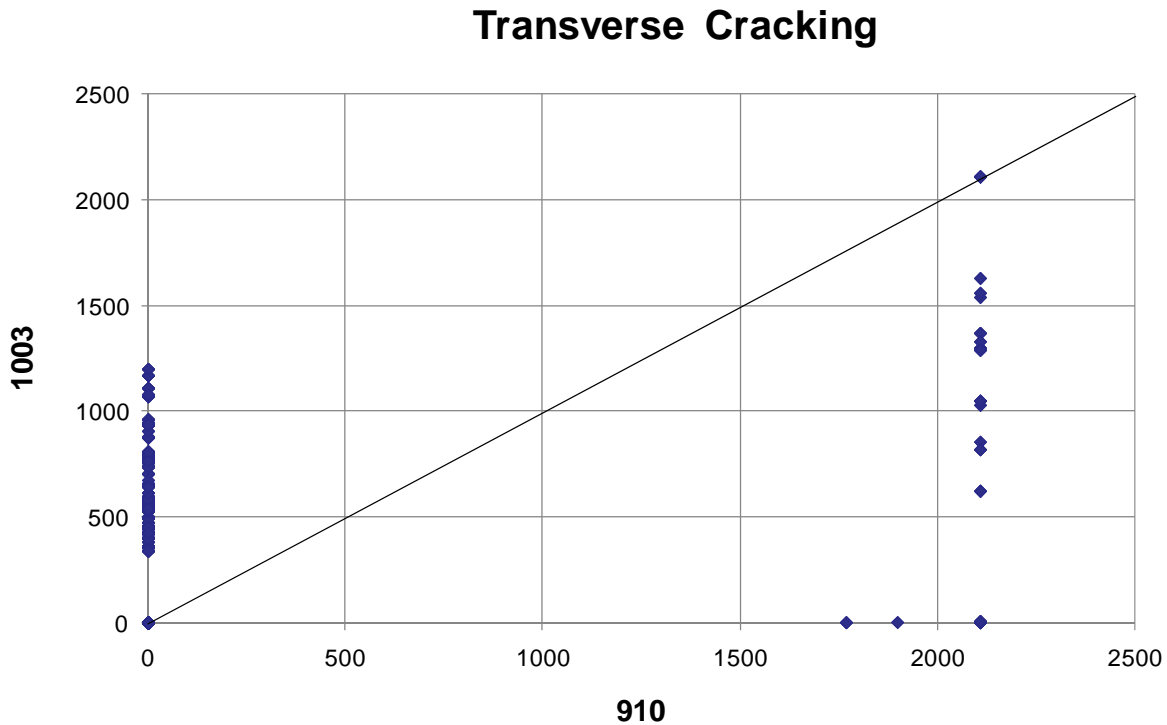


Figure 3.26 Transverse cracking comparison.

Figure 3.27 shows the comparison for IRI. It can be observed that the predicted IRI is higher in the newer version. Since IRI depends on performances prediction of the individual distresses, and the thermal cracking bug causing 0 predicted cracking was eliminated in the newer version, these higher predictions are logically more reasonable.

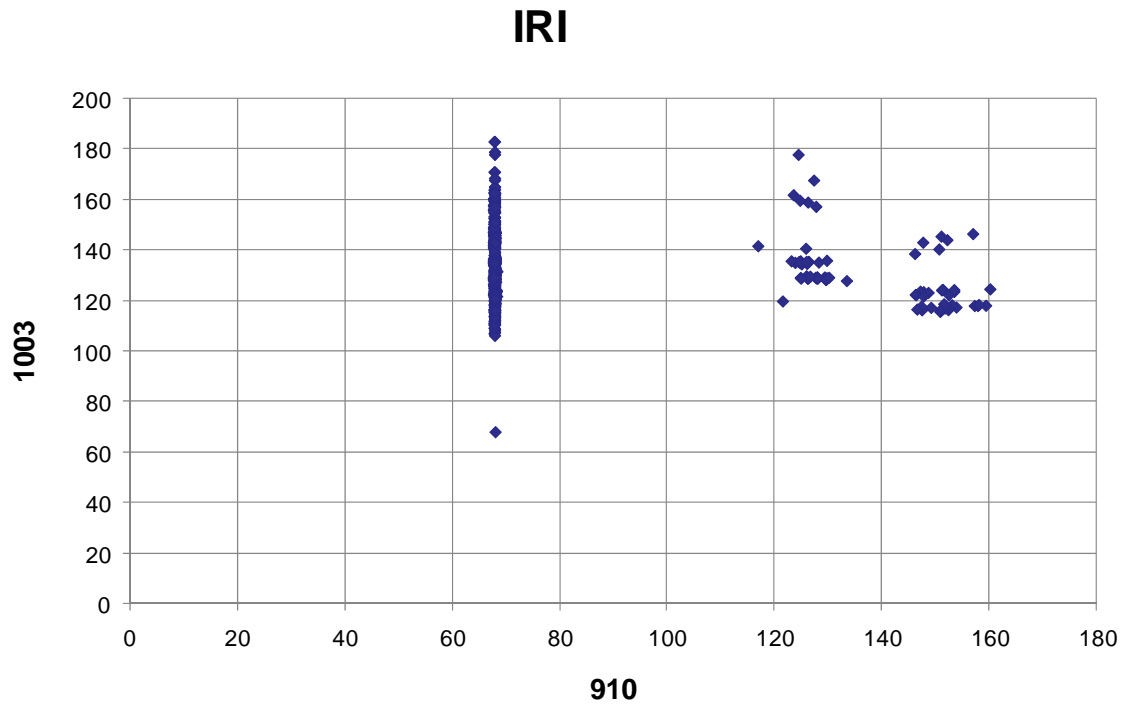


Figure 3.27 IRI comparison.

3.2.3.4 Comparison of Version 1.003 versus 0.910 (low volume): The following figures show the predicted distresses after 20 years using the versions 0.910 and 1.003 for low volume traffic. Figure 3.28 shows that the alligator cracking prediction was similar in both versions. However, the newer version predicted slightly less alligator cracking for some cases.

Alligator Cracking

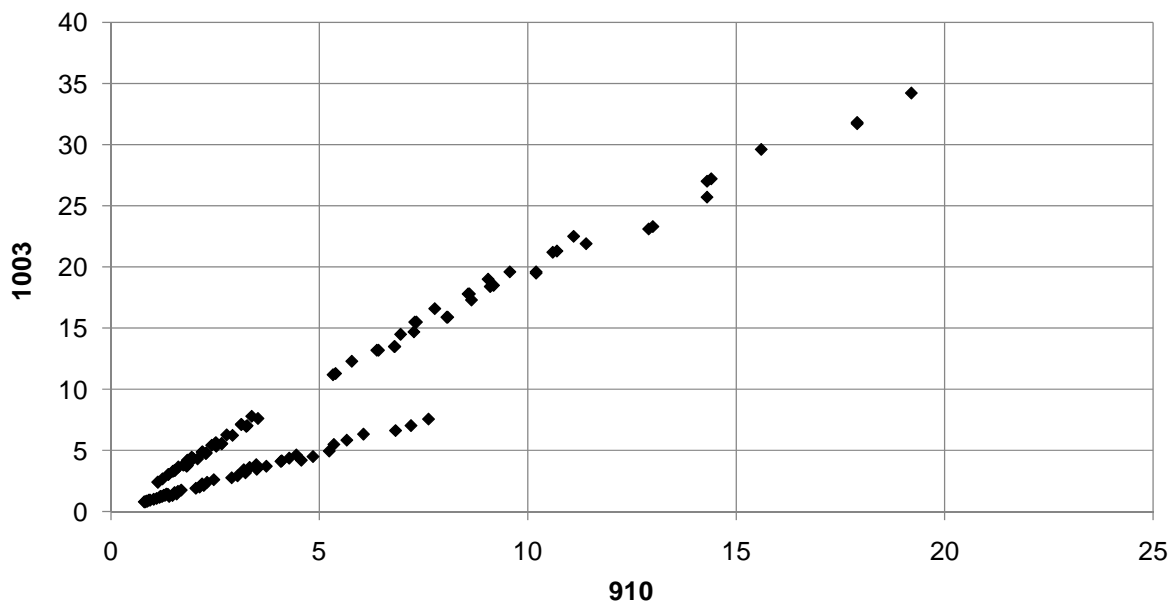


Figure 3.28 Alligator cracking comparison.

Figure 3.29 shows comparison for longitudinal cracking. It can be observed that the low volume comparison between the two versions was similar to the high volume comparison discussed above.

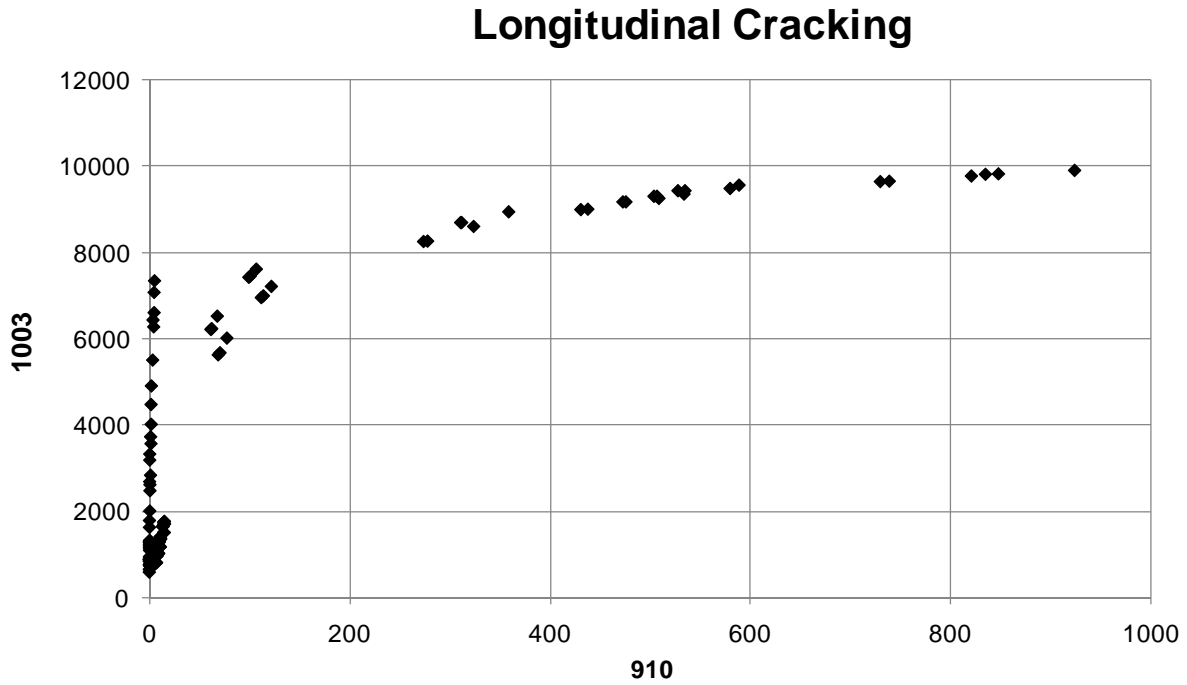


Figure 3.29 Longitudinal cracking comparison.

Figures 3.30 and 3.31 show the total and AC rutting, respectively, for versions 0.910 and 1.003. The total rutting predictions were significantly higher in all cases of the newer version. However, the AC rutting predictions were similar for the two versions in some cases, and were significantly higher in the newer version for some cases.

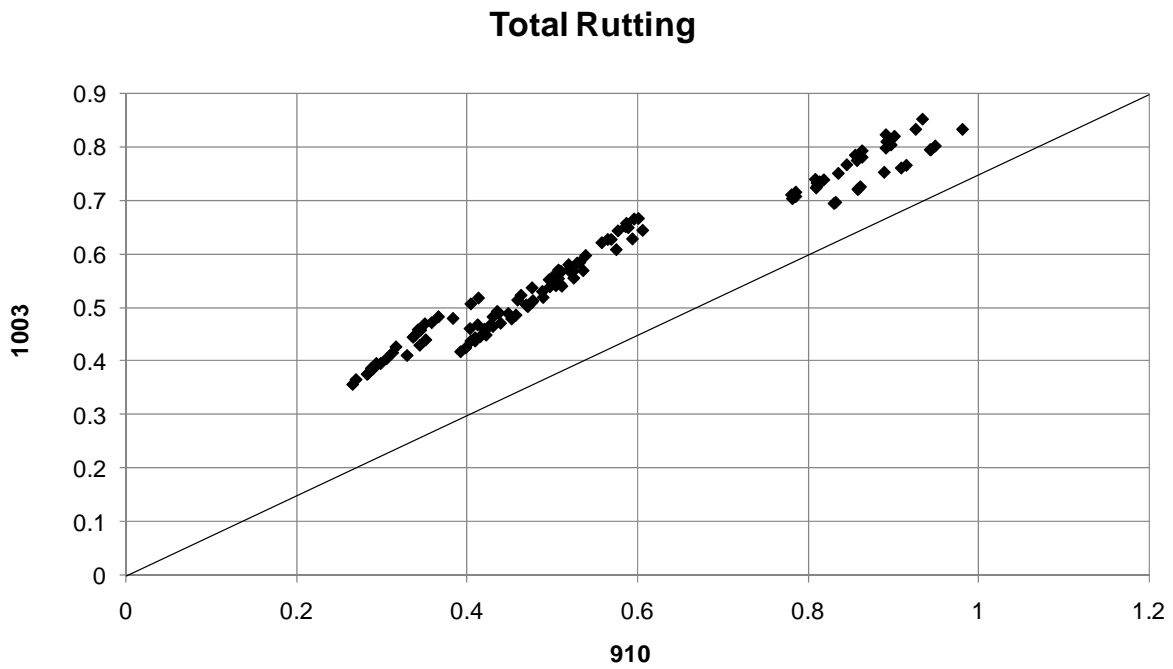


Figure 3.30 Total rutting comparison.

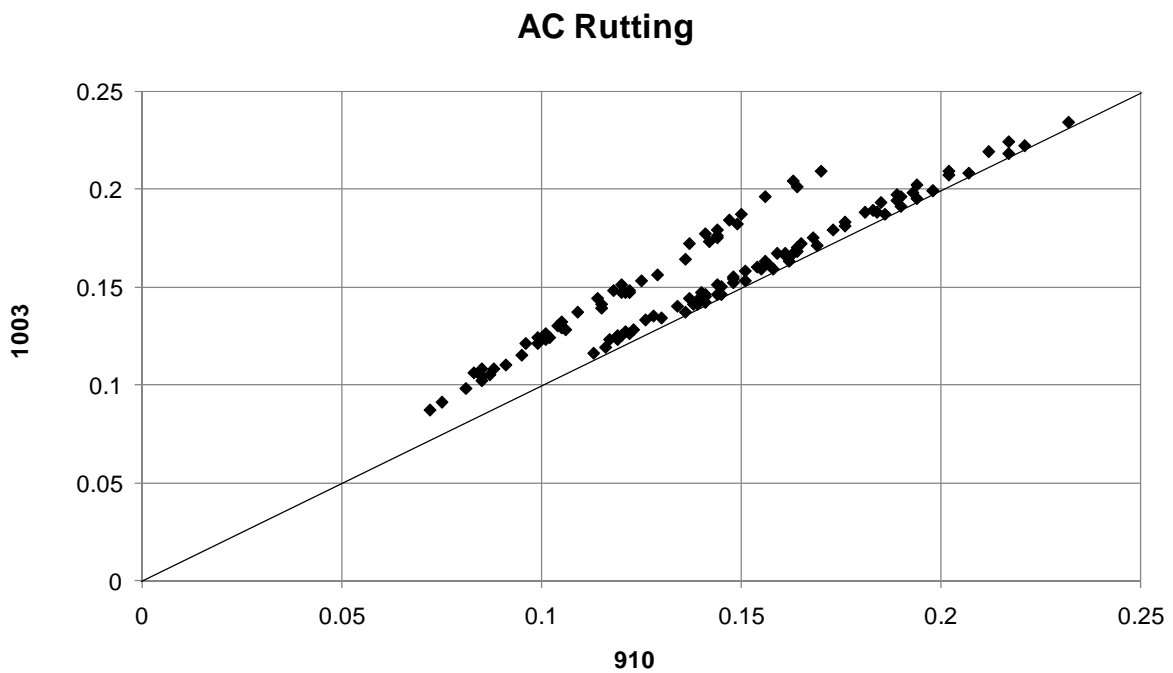


Figure 3.31 AC rutting.

Figure 3.32 shows the comparison for transverse cracking. It can be observed that the same trends observed for the high volume traffic were observed for the low volume.

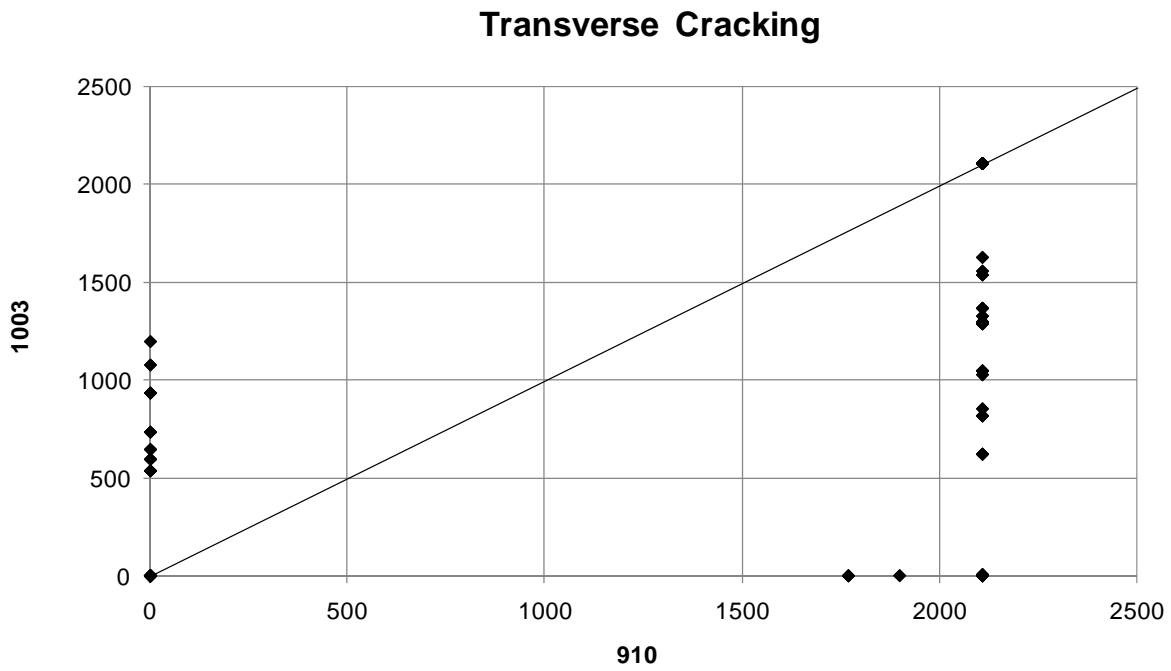


Figure 3.32 Transverse cracking comparison.

Figure 3.33 shows the comparison for IRI. It can be observed that a similar trend was observed for the low volume as was observed for the high volume traffic.

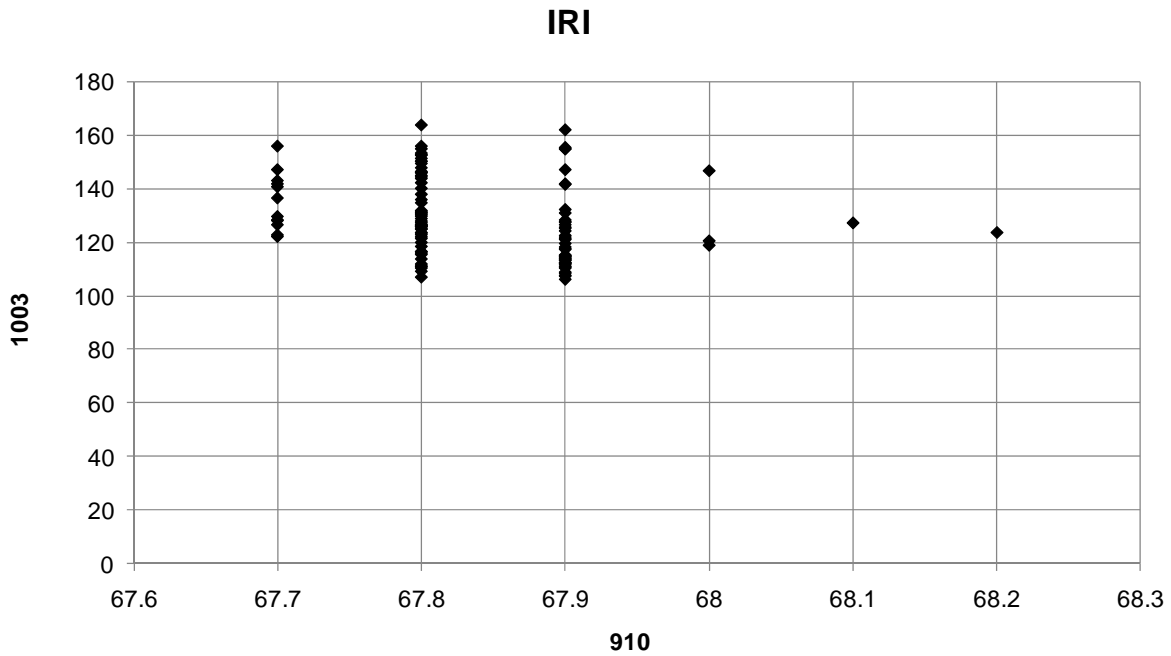


Figure 3.33 IRI comparison.

3.2.4 Analysis of MEPDG Version 1.003

A sensitivity analysis was also performed for a factorial of MEPDG version 1.003 simulations. The same parameters used in the 0.615 version were used in this analysis of version 1.003. Figures 3.34 to 3.38 show the predicted distresses after 20 years for the 10 million ESAL's for all the simulations using version 1.003. Longitudinal cracking after 20 years for 10 million ESAL's is given in figure 3.34. Figure 3.35 gives the transverse cracking after 20 years for 10 million ESAL's. Figures 3.36 and 3.37 give the AC and total rutting respectively after 20 years for 10 million ESAL's. IRI after 20 years for 10 million ESAL's is given in figure 3.38. Similar observations can be made for the distribution of each distress as were discussed for figures 3.1 to 3.6 for version 0.615.

Longitudinal Cracking

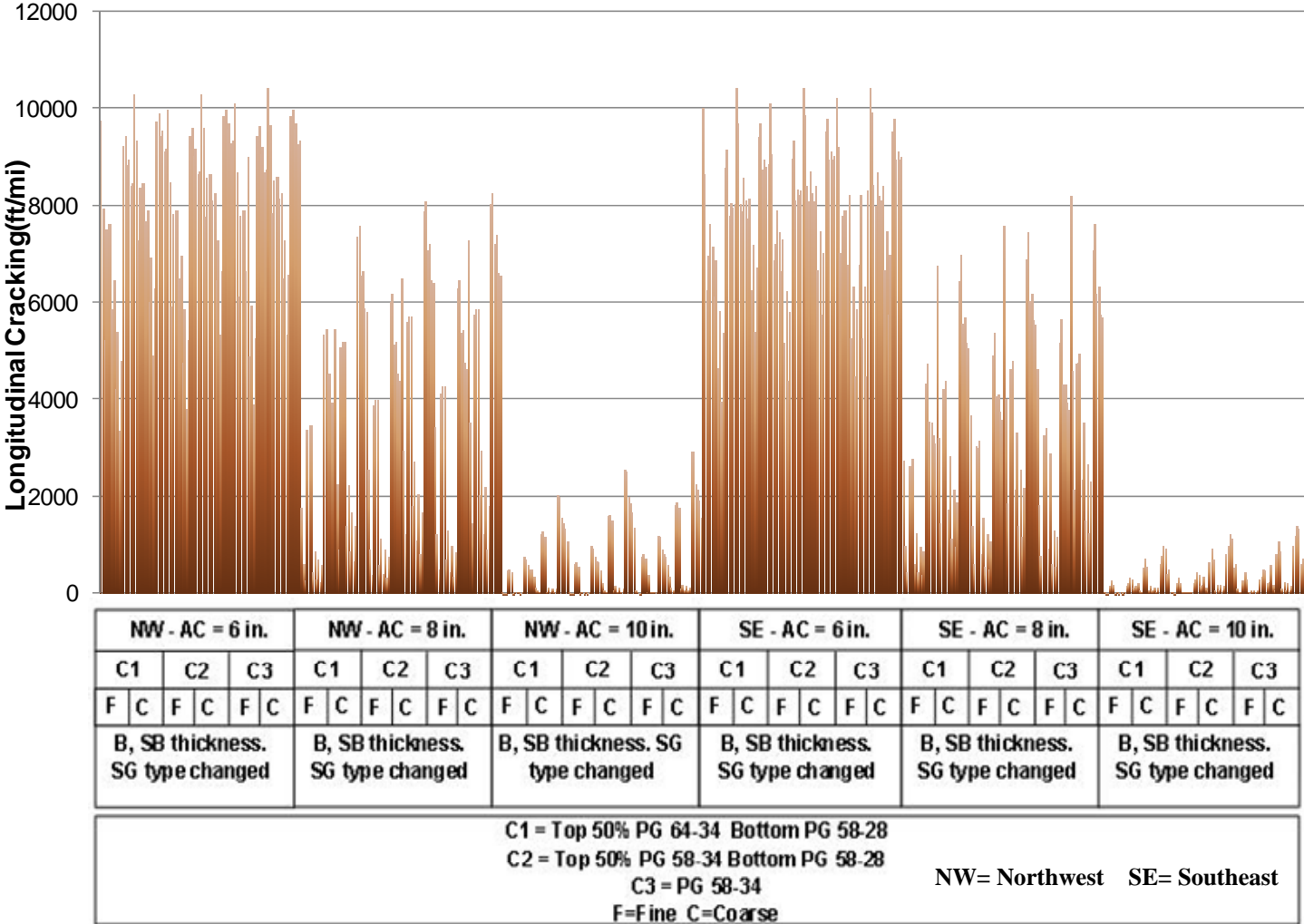


Figure 3.34 Longitudinal cracking after 20 years for 10 million ESAL's.

Transverse Cracking

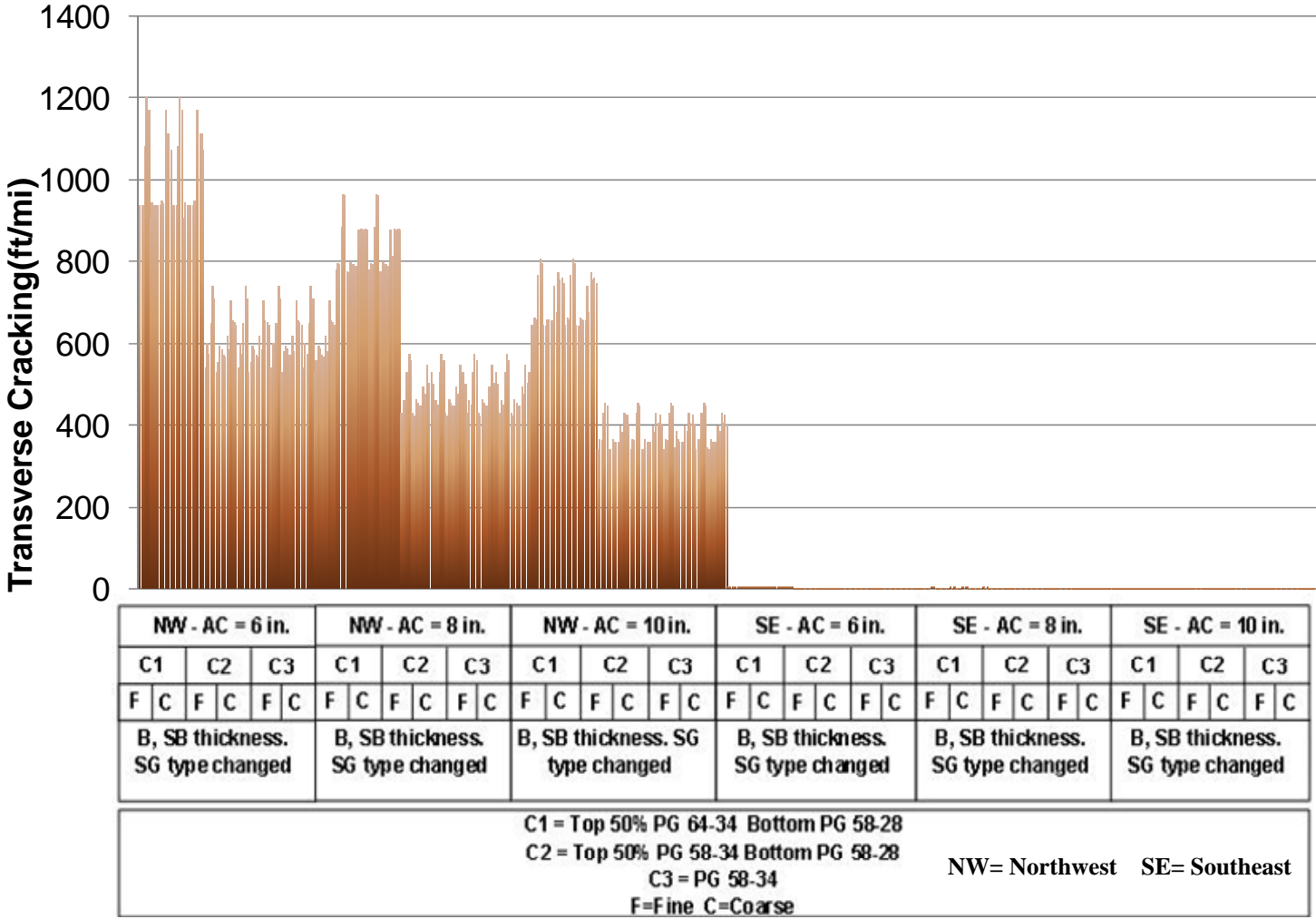


Figure 3.35 Transverse cracking after 20 years for 10 million ESAL's.

AC Rutting

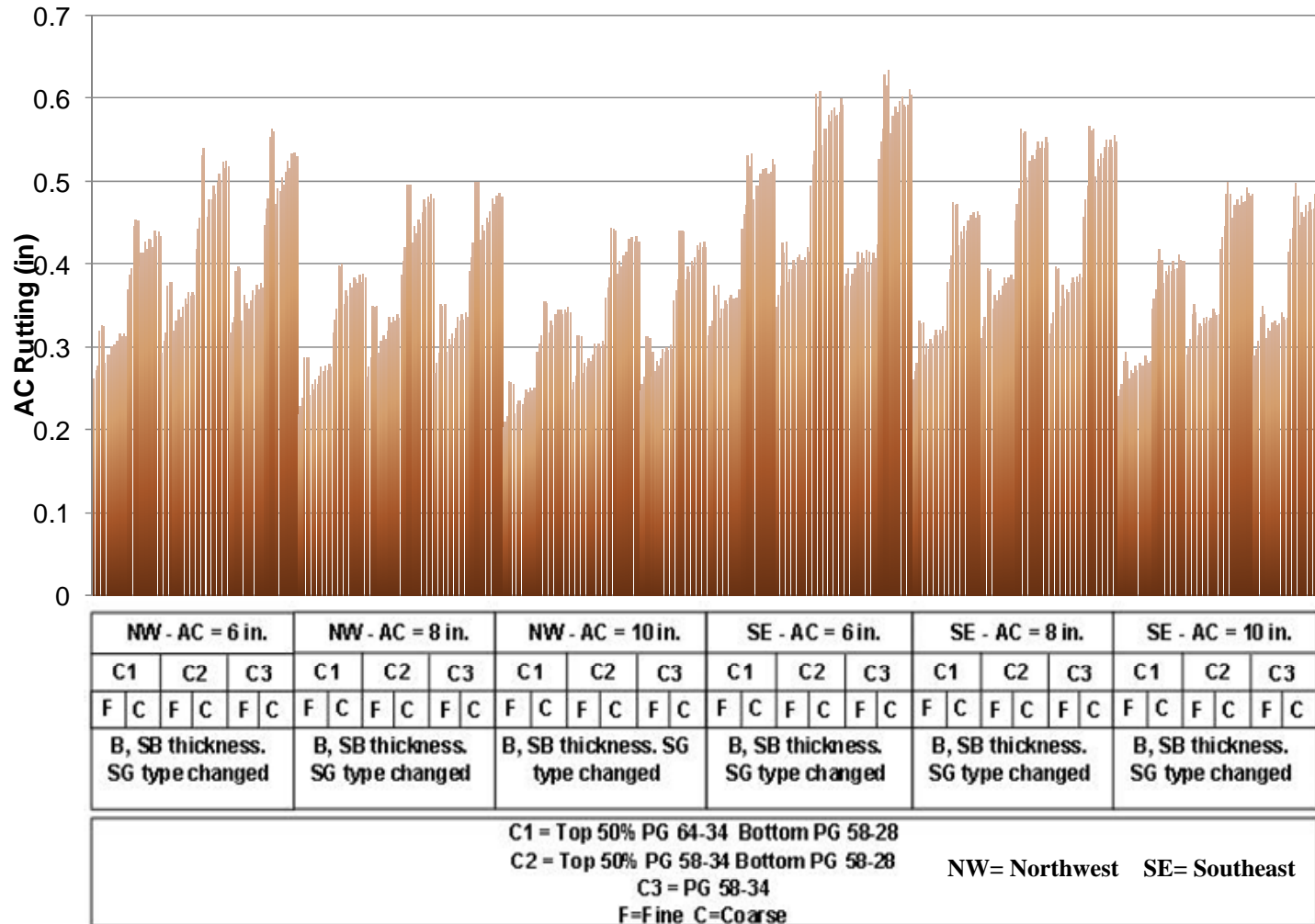


Figure 3.36 AC Rutting after 20 years for 10 million ESAL's.

Total Rutting

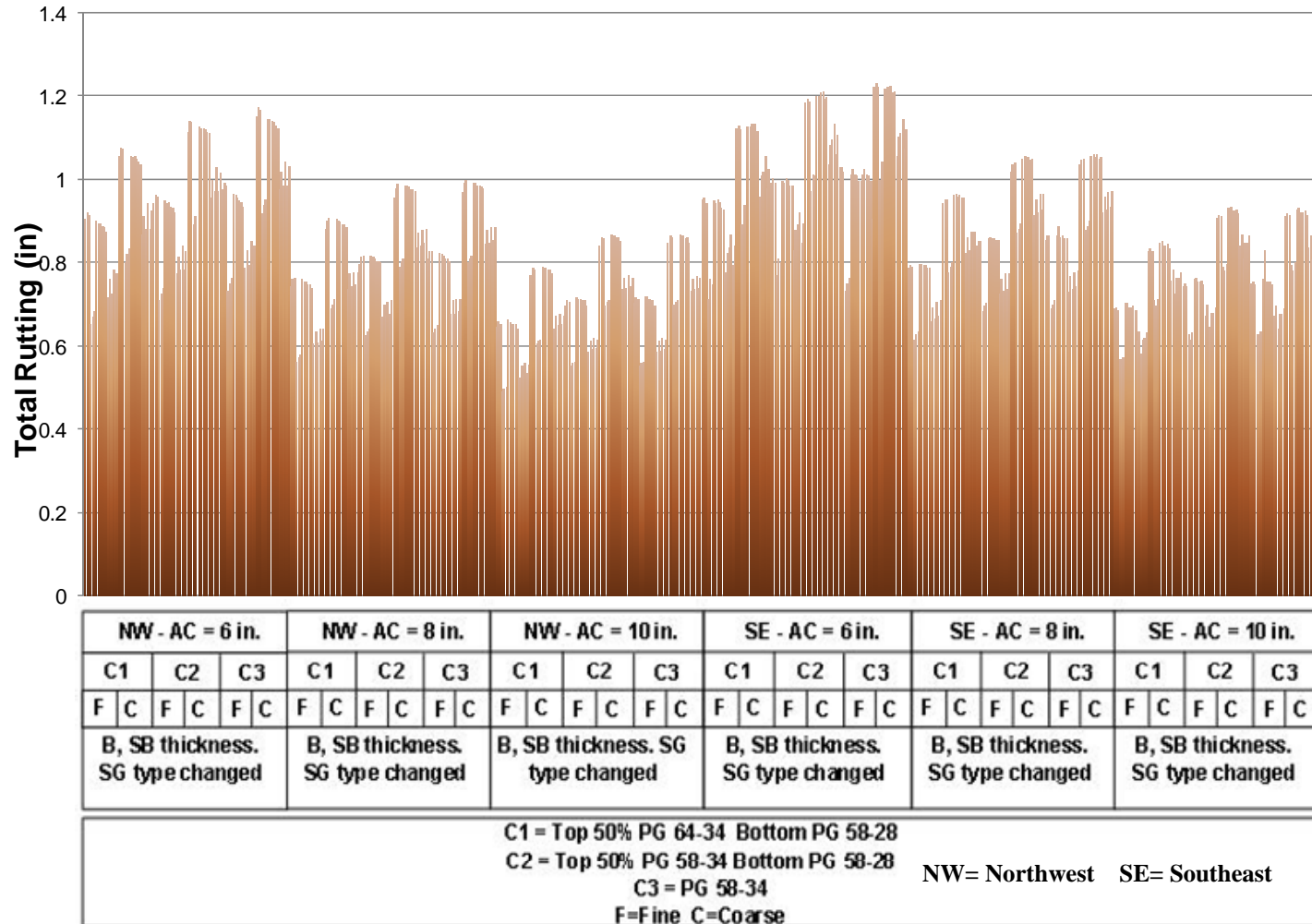


Figure 3.37 Total rutting after 20 years for 10 million ESAL's.

IRI

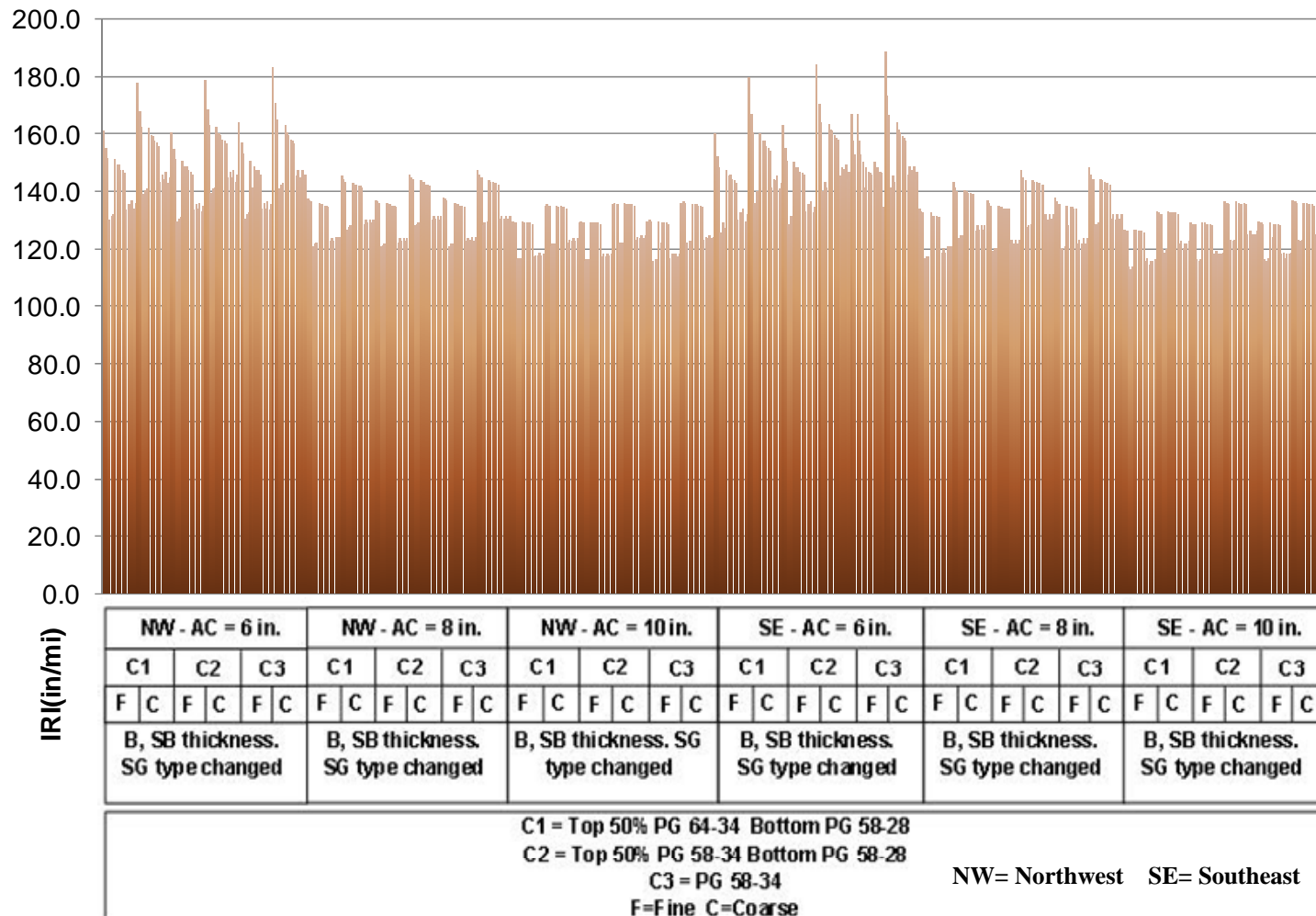


Figure 3.38 IRI after 20 years for 10 million ESAL's.

3.2.5 Conclusions for Flexible Pavement Analysis

The sensitivity analysis of the flexible pavements was conducted over the span of several years where the MEPDG software underwent significant flexible pavement modifications, partially due to feedback from this project. Therefore, along with a detailed analysis of the results from MEPDG version 0.615, a comparison with the updated versions was conducted to be able to understand how the software was improving and how the analysis of version 0.615 can be used. Through the analysis and comparisons, some of the bugs and unreasonable results were identified and reported to ARA, Inc, which was addressed under the NCHRP 1-40D contract. This study also confirmed that the latest (1.0) version of the MEPDG software represents a significant improvement over the previous versions. Nevertheless, the research team does not recommend adaptation of the longitudinal cracking model because of questionable distress level predictions and significant changes in the model from the previous versions of the MEPDG software.

3.3 Rigid Pavements

The following MEPDG design factors and site conditions were included in the sensitivity study of the rigid pavements:

- Traffic volume
- Coefficient of thermal expansion of PCC (COTE)
- Modulus of rupture of PCC (MR)
- Base thickness
- Base type
- Subgrade type
- Joint spacing
- Edge support
- Slab width
- Dowel diameter
- Pavement location

In the first phase of simulation, 360 separate MEPDG version 0.615 projects were created, using the basic factorial of inputs, as shown in Table 3.13.

Table 3.13 Factorial of input parameters – First phase.

Parameter	Cases	Description
Location (Climate)	5	North-East – Grand Forks North – Hibbing Center – Minneapolis South-East – Rochester South-West – Redwood Falls
PCC thickness	6	6” 7” 9” 10” 12” 14”
Base Thickness	3	6” 18” 48”
Base type	2	Class 5 Class 3
Subgrade type	2	A-6 A-3

The threshold criteria for all cases were 15% cracked slabs and 0.12 in faulting for a 20 year design life.

In the second phase, 576 runs for each project were performed using the batch mode. The factorials of design features and input parameters shown in Table 14 were analyzed.

Once all runs were performed, the cracking and faulting output results were screened using Excel Macro-driven Visual Basic Application (VBA). Preliminary sensitivity analysis was performed by comparing the cracking and faulting predictions for the pavement sections with the same design features and site conditions except the variable of interest. Over 1200 cracking charts and 4800 faulting charts were developed based on the results of the MEPDG simulations. 48 charts of predicted cracking and 64 charts of predicted faulting were chosen as representatives for the different groups of parameters. The results of this analysis are presented below.

Table 3.14 Factorial of input parameters – Second phase.

Parameter	Cases	Description
PCC modulus of rupture	2	500 psi 700 psi
PCC coefficient of thermal expansion	3	$4.8 \times 10^{-6} / ^\circ\text{F}$ $5.5 \times 10^{-6} / ^\circ\text{F}$ $6.7 \times 10^{-6} / ^\circ\text{F}$
Joint spacing	2	15 ft 20 ft
Slab width	2	12 ft 13.5 ft
Shoulder type	2	AC PCC
Dowel diameter	4	None 1” 1.25” 1.5”
Traffic AADTT	3	500 200 10000

3.3.1 PCC Cracking

3.3.1.1 Effect of Traffic Volume on Cracking: It was found that traffic volume affects the percentage of cracking differently at various slab thicknesses. Thinner PCC slabs were more sensitive to a lower level of traffic, whereas thicker PCC slabs were more sensitive to a higher level of traffic. This can be explained by the S-shaped form of the fatigue cracking model. When the traffic volume is low then the thicker pavements do not exhibit significant damage and it might be concluded that they are “insensitive” to traffic. Accordingly, when the traffic volume is high then cracking of thin slabs is close to 100 percent, which makes them “insensitive” to traffic as well. The charts for traffic analysis are presented in figures 1 through 6 in Appendix A.

3.3.1.2 Effect of Coefficient of Thermal Expansion of PCC (COTE) on Cracking: Figures 7 through 12 in Appendix A represent the predicted cracking for pavements with the AADTT equal to 500. The same design parameters as in previous figures were used, except for slab thickness and COTE.

As predicted by the MEPDG, an increase in COTE caused a significant increase in the percentage of slabs cracked. It was observed that an increase in COTE from $4.8\text{E-}06/^\circ\text{F}$ to $5.5\text{E-}06/^\circ\text{F}$ affected cracking growth less than an increase from $5.5\text{E-}06/^\circ\text{F}$ to $6.7\text{E-}06/^\circ\text{F}$. The increase in pavement thickness from 6 in to 7, 9, 10, 12, and 14 in respectively significantly decreased the maximum percentage of cracked slabs.

3.3.1.3 Effect of PCC Modulus of Rupture (MR) on Cracking: The charts were plotted for PCC thicknesses of 10, 12, and 14 in and COTE of 4.8E-06/'F, 5.5E-06/'F, and 6.7E-06/'F with the MR equal to 500 or 700 psi. As presented by Figures 13 through 18 in appendix A, the increase in MR from 500 psi to 700 psi decreased the level of cracking significantly, especially in pavements with the highest COTE of 6.7E-06/'F. The joint spacing assigned for this analysis was 20 feet.

3.3.1.4 Effect of Base Thickness on Cracking: In the analysis of the effect of base thickness at different slab thicknesses (6, 7, 9, 10, 12, and 14 inches) the following range of base thickness was chosen: 6, 18 and 48 in. For thin pavements (6, 7, and 9 in) a 15-ft joint spacing was assigned. The thick pavements (10, 12, and 14 in) did not exhibit any cracking at a joint spacing of 15 ft, which made visual analysis of charts difficult. Therefore, 20-ft joint spacing was assigned for these pavements.

Figures 19 through 21 in Appendix A show that the MEPDG predicted a minor difference in cracking percentage from 6 to 9-in thick pavements supported by a 6-in or 18-in thick base layer. However an increase in base thickness up to 48 in diminished the cracking level to zero. Thick pavements (10 to 14 in) exhibited the same trend as thin pavements, as shown in figures 22 through 24 in Appendix A.

3.3.1.5 Effect of Base and Subgrade Materials on Cracking (Foundation Support): Two types of bases (class 5 and class3) and two types of subgrades (A-6 and A-3) were used for the analysis of foundation support. The sensitivity runs were performed for all possible combinations of base and subgrade. Figures 25 through 30 in Appendix A represent the results for different slab thicknesses. Joint spacing was 15 ft for pavements with PCC thickness from 6 to 9 in and 20 ft for pavements with PCC slab thickness from 12 to 14 in.

Analysis of the plotted data indicated a minor difference in cracking between the four possible combinations of supporting layer materials. The maximum percentage of cracked slabs depended mostly on the pavement thickness, when other parameters were fixed. However, the class 5 base performed better than the class 3 base regardless of the subgrade material.

3.3.1.6 Effect of Joint Spacing on Cracking: The effect of joint spacing on cracking was investigated by completing identical runs for joint spacing of 15 and 20 ft. The fixed parameters and changing slab thicknesses were the same as in the earlier analysis.

As presented in figures 31 through 36 (Appendix A), all pavements were predicted to have a higher level of cracking at increased joint spacing. There was a decrease in this effect for thicker pavements (10 to 14 in.).

3.3.1.7 Effect of Edge Support and Slab Width on Cracking: All possible combinations of shoulders (AC, PCC) and slab widths (12 ft and 13.5ft- widened) were used to evaluate the effect of the edge support and slab width on the percentage of cracked slabs in concrete pavements. As in the previous analysis, the sensitivity runs were performed for different slab thicknesses with different joint spacing. The history of cracking for this analysis is presented by figures 37 through 42 in Appendix A.

All thin pavements (6 to 9 in thick) with joint spacing of 15 ft exhibited the worst performance with an absence of the edge support (AC shoulders) at the usual slab width of 12 ft. Although the cracking percentage was lower in pavements with PCC shoulders, the presence of a widened slab diminished the effect of the shoulders material. The same trend was observed in 10 to 14-in thick pavements with 20 ft long slabs.

3.3.1.8 Effect of Location (Climatic zone) on Cracking: The temperature data from climatic stations in Minnesota (Rochester, Minneapolis Hibbing, and Redwood Falls) and North Dakota (Grand Forks) were used to evaluate the effect of climate on cracking. These climatic stations represent the following locations:

- North-West – Grand Forks
- North – Hibbing
- Center – Minneapolis
- South-East – Rochester
- South-West – Redwood Falls

As shown in figures 43 through 48 (Appendix A), there were some unexpected trends in pavement performance. For instance, a lower level of cracking was obtained for Rochester, which is located furthest South, than Grand Forks, which is the furthest North, while Redwood Falls yielded the highest level of cracking. Also, the use of Minneapolis temperature data yielded much lower cracking than other stations. This indicated possible problems with temperature data obtained for this analysis. Therefore, the final conclusions about the effect of location were not drawn in this report.

3.3.2 PCC Faulting Analysis

3.3.2.1 Effect of Traffic Volume on Faulting: As found by many previous studies, the pavement responded to traffic differently at various slab thicknesses and dowel diameters. Therefore, the predicted faulting charts were created separately for each slab thickness (6, 7, 9, 10, 12, and 14 in) and each dowel diameter (none, 1, 1.25, and 1.5 in). As shown in figures 49 through 72 in Appendix A, each chart include three series for different levels of AADTT: 500, 2000, and 10000.

The MEPDG demonstrated an overall increase in faulting with the growth of traffic volume. As can be seen in the charts, there was a proportional effect of AADTT on the level of faulting at 240 months for every slab thickness, given that dowels are present. The absence of dowels increased the effect of traffic volume growth, while an increase in slab thickness weakened such an effect. This implied a possible high level of interaction between the PCC thickness and dowel diameter on faulting.

3.3.2.2 Effect of Dowel Diameter on Faulting: Four dowel diameters were chosen for this analysis: none, 1, 1.25, and 1.5 in. Figures 73 through 78 in Appendix A represent the results of sensitivity runs for different slab thicknesses: 6, 7, 9, 10, 12, and 14 in. There was a large decrease in faulting in doweled pavements compared to undoweled pavements. Additionally, an increase in dowel diameter from 1 in to 1.25 in caused a greater decrease in faulting than a change in diameter from 1.25 to 1.5 in.

3.3.2.3 Effect of Coefficient of Thermal Expansion of PCC (COTE) on Faulting: There was an observed increase in faulting with an increase in COTE (See figures 79 through 84 in Appendix A). However, the level of faulting for each value of COTE (4.8E-06, 5.5E-06, and 6.7E-06 /°F) stayed approximately the same regardless the slab thickness, given the dowel diameter was 1.25 in.

3.3.2.4 Effect of Base Thickness on Faulting: As shown in figures 85 through 89 in Appendix A, a change in base thickness from 6 in to 18 in did not affect the level of faulting as much as an increase from 18 in to 48 in. However the pavements were predicted to exhibit minor faulting regardless of the slab thickness, given 1.25-in dowels were installed. As expected, the trend in faulting for undoweled pavements was similar to that for cracking. Finally, although the effect of base thickness on faulting was found to be significant, this effect was diminished by the presence of dowels.

3.3.2.5 Effect of Base and Subgrade material on Faulting: Sensitivity runs were performed for different combinations of base and subgrade also. The results are presented in figures 90 through 92 in Appendix A.

The charts show that there is no significant difference in faulting between the base-subgrade combinations; however, unlike in cracking analysis, subgrade strength drove faulting more than base strength (subgrade A-3 performed slightly better than A-6 regardless of the base material). Finally, the effect of supporting layer strength appeared to be non-significant.

3.3.2.6 Effect of Joint Spacing on Faulting: Figures 93 through 98 illustrate the predicted faulting for different slab thickness (6 to 14 in) at joint spacings of 15 and 20 ft and dowel diameter of 1.25 in. The other parameters were fixed as in the previous analysis. It can be observed that an increase in joint spacing caused an increase in faulting in all pavements. The effect of an increase in slab length slightly increases with an increase in the slab thickness. This implied a fairly significant interaction between joint spacing and the slab thickness.

3.3.2.7 Effect of Edge Support and Slab Width on Faulting: As shown in figures 99 through 104 in Appendix A, pavements with 1.25-in diameter dowels did not exhibit a significant difference in faulting at any combination of shoulder material (AC, PCC) and slab width (12 or 13.5 ft), although the use of PCC shoulders caused a decrease in faulting compared with AC shoulders. As in the cracking analysis, the presence of a widened slab diminished the effect of PCC shoulders.

3.3.2.8 Effect of Location (Climatic zone) on Faulting: Because of several discrepancies in the temperature data obtained from the different climatic stations, the analysis of location on faulting was not performed in this study.

3.3.2.9 Effect of Modulus of rupture of PCC (MR) on Faulting: Figures 105 and 106 in Appendix A represent the predicted faulting for 7 in thick pavements with MR equal to 500 psi and 700 psi, respectively, and the presence of 1.25-in diameter dowels. Figures 107 and 108 demonstrate predicted faulting for 9 in thick pavement with no dowels and the MR equal to 500 and 700 psi. Based on paired comparison of the charts, it can be concluded that for pavements with no dowels

an increase in the value of MR did not caused any significant change in faulting. A similar trend was observed for doweled pavements.

3.3.3 Summary of the Sensitivity Analysis for Cracking and Faulting

Based on previously discussed observations, the following conclusions were drawn:

- An increase in traffic volume (AADTT) caused an increase in both cracking and faulting
- The presence of dowels does not affect the cracking level, but significantly decreases faulting. An increase in dowel diameter decreases faulting.
- An increase of the coefficient of thermal expansion (COTE) caused an increase both in cracking and faulting
- Use of concrete with a higher flexural strength (Modulus of Rupture) significantly decreased the level of cracking, but caused a non-significant decrease in faulting
- An increase in the base thickness from 6 in to 18 in caused a small decrease both in cracking and faulting. However, a further increase in base thickness from 18 to 48 in diminished the level of both cracking and faulting to zero. This effect was observed in undoweled pavements more than doweled ones.
- A change in base material from class 5 to class 3, and in the subgrade from A-6 to A-3 does not cause a significant difference in the level of both cracking and faulting. However, it was noticed that an increase of base strength decreased the level of cracking, while an increase in subgrade modulus caused a decrease in faulting
- An increase in joint spacing caused an increase both in cracking and faulting, while an increase in slab thickness weakened such an effect
- The presence of PCC shoulders affected both cracking and faulting less than the use of a widened (13.5-ft wide) slab, while both actions caused a decrease in both distress levels

3.3.4 Statistical Analysis

The statistical analysis of the MEPDG prediction models was performed separately for cracking and faulting using a linear regression method. Both analyses involved the data obtained from the sensitivity runs for Rochester climatic station with design life of 240 months (20 years). The maximum values of distress at the end of the design life (CRACK240 and FAULT240) were chosen as response for both analyses, while the following predictors were considered:

- Traffic volume (AADTT)
- Dowel diameter (DD) – for faulting only
- Joint spacing (JS)
- Slab width (LW)
- Shoulder type (LTES)
- Slab thickness (HPCC)
- Coefficient of thermal expansion (COTE)
- Base Thickness (HBASE)
- Base class (EB)
- Subgrade type (ES)

The data set included 5,184 cases for the cracking model and 20,736 cases for the faulting model. Sample correlations of CRACK240 and FAULT240 with other variables were obtained. The square of the sample correlation can be interpreted as a percentage of variability in the observed values of the response explained by the predictor. Thus, a greater the correlation between the response and a predictor indicates a greater effect of the predictor.

Table 3.15 presents the site conditions and design features in order of their contribution toward cracking. It shows that the slab thickness affects the level of cracking the most (correlation = -0.50), and the effect is negative, i.e. an increase in HPCC significantly decreased cracking. The next two significant factors are base thickness (HBASE) with a negative correlation and joint spacing (JS). Since traffic volume (AADTT) was fourth in significance, a change in HPCC, HBASE, and JS reduce the effect of the change in traffic volume. The effect of COTE is approximately as high as the effect of AADTT, while the change in the other factors is much less significant in their association with cracking.

Table 3.15 Cracking correlation matrix.

CRACK240	Order of Sensitivity	Sample Correlation	Sign of Effect
HPCC	1	-0.50	Negative
HBASE	2	-0.36	Negative
JS	3	0.28	Positive
AADTT	4	0.25	Positive
COTE	5	0.23	Positive
LW	6	-0.11	Negative
LTES	7	-0.07	Negative
EB	8	0.04	Positive
ES	9	0.02	Positive
DD	10	0.00	No effect

Table 3.16 presents the site conditions and design features in order of their contribution toward faulting. The greatest level of correlation was observed between FAULT240 and DD, i. e. between dowel diameter and the level of faulting.

Table 3.16 Faulting correlation matrix.

FAULT240	Order of Sensitivity	Sample Correlation	Sign of Effect
DD	1	-0.55	Negative
AADTT	2	0.36	Positive
HBASE	3	-0.28	Negative
COTE	4	0.20	Positive
LW	5	-0.18	Negative
JS	6	0.14	Positive
HPCC	7	-0.11	Negative
ES	8	-0.09	Negative
LTES	9	-0.06	Negative
EB	10	-0.03	Negative

The following conclusions can be drawn from the analysis of Table 3.16:

- Faulting is most sensitive to a change in dowel diameter (DD) and least sensitive to the base material type (EB)
- An increase in truck traffic volume (AADTT) significantly increased faulting.
- A change in base thickness (HBASE) had a greater effect on faulting than a change in PCC thickness (HPCC)
- The effect of the coefficient of thermal expansion (COTE) on faulting is more significant than the effect of the geometry of the pavement slab (width (LW), length(JS), and thickness (HPCC))

3.3.5 Conclusions for Rigid Pavement Analysis

Based on the results of the chart and statistical analyses, the following conclusions were drawn:

- The statistical analysis verified the trends observed in analysis of predicted cracking and faulting charts
- The following parameters were found most important for control of the level of both cracking and faulting:
 - Traffic volume
 - Slab thickness
 - Base thickness
 - Coefficient of thermal expansion
- Some parameters appeared to affect cracking and faulting differently. A change in flexural strength of the concrete (MR) significantly affected the level of cracking, but did not cause significant change in faulting. Dowel diameter largely affected the level of faulting, but did not affect the percentage of cracked slabs.
- The effect of supporting layer strength was identified as having a minor or non-significant effect on both cracking and faulting.

Chapter 4 Special Topics

4.1 Introduction

During the analysis conducted in this study, multiple issues with the MEPDG were encountered. The following topics are discussed in this chapter:

- Subgrade Characterization
- Stabilized Base Characterization
- Asphalt Binder Characterization
- Climate Inputs

4.2 Subgrade Characterization

The MEPDG inputs were evaluated for unbound materials and recommendations for characterization of Minnesota subgrades were provided.

The MEPDG requires the provision of resilient moduli for all unbound layers and subgrade for each design period (month) (NCHRP, 2004a, NCHRP 2004b). The Guide allows the measurement of resilient moduli from the laboratory, obtaining them through the use of correlations with other material properties or estimating them based on soil classification. The hierarchical approach to design inputs provides the designer with flexibility in obtaining the design inputs for a design project based on the importance of the project and the available resources. The resilient moduli should be provided for each design period (month) for the optimum moisture content. The DG software will adjust it for the moisture content using prediction of the Enhanced Integrated Climatic Model.

Three levels of inputs are provided for characterization of resilient properties unbound materials at the optimum moisture content. A brief description of each level is provided below.

4.2.1 Level 1 - Laboratory Testing

Laboratory testing of resilient moduli is required for Level 1 input. The resilient modulus laboratory testing involves cyclic triaxial testing of prepared representative samples of unbound materials of subgrade. The Design Guide recommends the following standard test methods for the laboratory preparation, testing, and computation of the test results:

- NCHRP 1-28—Harmonized Test Methods for Laboratory Determination of Resilient Modulus for Flexible Pavement Design.
- AASHTO T 307—Determining the Resilient Modulus of Soil and Aggregate Materials.

For M-E design, resilient modulus is estimated using the following generalized k_1 - k_2 - k_3 constitutive model:

$$M_{R_{opt}} = k_1 \cdot p_a \cdot \left(\frac{\theta}{p_a} \right)^{k_2} \cdot \left(\frac{\tau_{oct}}{p_a} + 1 \right)^{k_3} \quad (4.1)$$

where

M_{Ropt} = Resilient modulus at optimum moisture content;

k_1, k_2, k_3 = Regression parameters;

p_a = Atmospheric (normalizing) pressure;

$\theta = J_1 = \sigma_1 + \sigma_2 + \sigma_3$ = Bulk stress (first stress invariant);

$\tau_{oct} = \frac{1}{3} \sqrt{(\sigma_1 - \sigma_2)^2 + (\sigma_1 - \sigma_3)^2 + (\sigma_2 - \sigma_3)^2}$ = Octahedral shear stress.

The k_1 - k_2 - k_3 model is directly applicable to design only if a non-linear axis-symmetric finite element program DSC-2D is used for computing structural responses of flexible pavements (Desai, 2000).

Level 1 analysis of unbound materials uses a 2-D finite element analysis program which is not been tested or calibrated and is not recommended for use (by NCHRP) at this time.

4.2.2 Level 2—Correlations with Other Material Properties

Level 2 inputs for unbound layers and subgrade should be used if the multi-layer elastic theory (MLET) program JULEA is used for calculation of stresses, strains, and deflections in flexible pavements (Uzan, 1989). Laboratory testing is still the preferable source of information for this level of testing. However, if no resilient modulus laboratory test data is available, the MEPDG software calculates the resilient modulus using the relationships presented in Table 4.1.

If the laboratory data or parameters of the k_1 - k_2 - k_3 model are available, the DG recommends an iterative procedure, which would result in a single representative value for the resilient modulus. This procedure was advanced in this project. The discussion of conversion of the parameters of the k_1 - k_2 - k_3 model is presented in the next section of this report.

4.2.3 Level 3—Typical Values (Based on Calibration)

For input Level 3, the resilient modulus for the optimum moisture content is selected based on the material classification. Table 4.2 presents typical values recommended by the Guide.

Table 4.1 Summary of correlations to estimate material properties.(4).

Strength/Index Property	Model	Comments	Test Standard
CBR	$M_r = 2555(\text{CBR})^{0.64}$	CBR = California Bearing Ratio, percent	AASHTO T193—The California Bearing Ratio
R-value	$M_r = 1155 + 555R$	R = R-value	AASHTO T190—Resistance R-Value and Expansion Pressure of Compacted Soils
AASHTO layer coefficient	$M_r = 30000 \left(\frac{a_i}{0.14} \right)$	a_i = AASHTO layer coefficient	AASHTO Guide for the Design of Pavement Structures (1993)
PI and gradation*	$\text{CBR} = \frac{75}{1 + 0.728(w - \text{PI})}$	$w * \text{PI} = \text{P200} * \text{PI}$ $\text{P200} =$ percent passing No. 200 sieve size $\text{PI} =$ plasticity index, percent	AASHTO T27—Sieve Analysis of Coarse and Fine Aggregates AASHTO T90—Determining the Plastic Limit and Plasticity Index of Soils
DCP*	$\text{CBR} = \frac{292}{\text{DCP}^{1.12}}$	CBR = California Bearing Ratio, percent DCP =DCP index, in/blow	ASTM D6951—Standard Test Method for Use of the Dynamic Cone Penetrometer in Shallow Pavement Applications

Table 4.2 Resilient moduli recommended by the MEPDG based on the soil classification.

AASHTO Symbol	Typical CBR Range	M_R Range (ksi)	M_R Default (ksi)
A-7-6	1-5	2.5 – 7	4
A-7-5	2 – 8	4 – 9.5	6
A-6	5 – 15	7 – 14	9
A-5	8 – 16	9 – 15	11
A-4	10 – 20	12 – 18	14
A-3	15 – 35	14 – 25	18
A-2-7	10 – 20	12 – 17	14
A-2-6	10 – 25	12 – 20	15
A-2-5	15 – 30	14 – 22	17
A-2-4	20 – 40	17 – 28	21
A-1-b	35 – 60	25 – 35	29
A-1-a	60 – 80	30 – 42	38

4.2.4 Resilient Modulus Moisture Correction

The MEPDG permits accounting for seasonal variation in properties of unbound materials by adjustment of the resilient moduli for each design period (month). The user has two options:

- Provide the resilient modulus for each design period, or
- Provide resilient modulus for the optimum moisture content.

If the second option is selected, the Enhanced Integrated Climatic Model incorporated into the MEPDG software predicts seasonal variation in the moisture content of the unbound layers (Larson, 1997). Then, the MEPDG software adjusts the moduli for the other moisture conditions using the following model (Witzak et. al, 2000a, Witzak et. al, 2000b):

$$M_{R=10} = 10^{a + \frac{b-a}{1 + \text{EXP}(\beta + k_S \cdot (S - S_0))}} M_{Ropt} \quad (4.2)$$

where

- M_R = resilient modulus at any degree of saturation;
- S = degree of saturation while testing the material;
- M_{Ropt} = resilient modulus at optimum water content and maximum dry density;
- S_0 = degree of saturation at optimum water content;
- a = minimum of $\log\left(\frac{M_R}{M_{Ropt}}\right)$;
- b = maximum of $\log\left(\frac{M_R}{M_{Ropt}}\right)$;
- β = location parameter, obtained as a function of a and b ;
- k_S = regression parameter.

For fine-grained materials, the Guide recommends the following model parameters: $a = -0.5934$, $b = 0.4$, $\beta = -0.3944$, $k_S = 6.1324$. Figure 4.1 presents the correction factor for the moisture condition for the various degrees of saturation. One can observe that increase in moisture content decreases resilient modulus.

Substitution of equation 4.2 into equation 4.1 leads to the following predictive model for the resilient model under an arbitrary moisture condition:

$$M_{R=10} = 10^{a + \frac{b-a}{1 + \text{EXP}(\beta + k_S \cdot (S - S_0))}} k_1 \cdot p_a \cdot \left(\frac{\theta}{p_a}\right)^{k_2} \cdot \left(\frac{\tau_{oct}}{p_a} + 1\right)^{k_3} \quad (4.3)$$

Equation 4.3 can be re-written in the following form:

$$M_R = k_1^* \cdot p_a \cdot \left(\frac{\theta}{p_a}\right)^{k_2} \cdot \left(\frac{\tau_{oct}}{p_a} + 1\right)^{k_3} \quad (4.4)$$

Where,

$$k_1^* = 10^{a + \frac{b-a}{1 + \text{EXP}(\beta + k_S \cdot (S - S_0))}} k_1 \quad (4.5)$$

It can be observed that the MEPDG moisture correction model postulates that change in moisture conditions affects only the k_1 parameters but does not affect k_2 and k_3 .

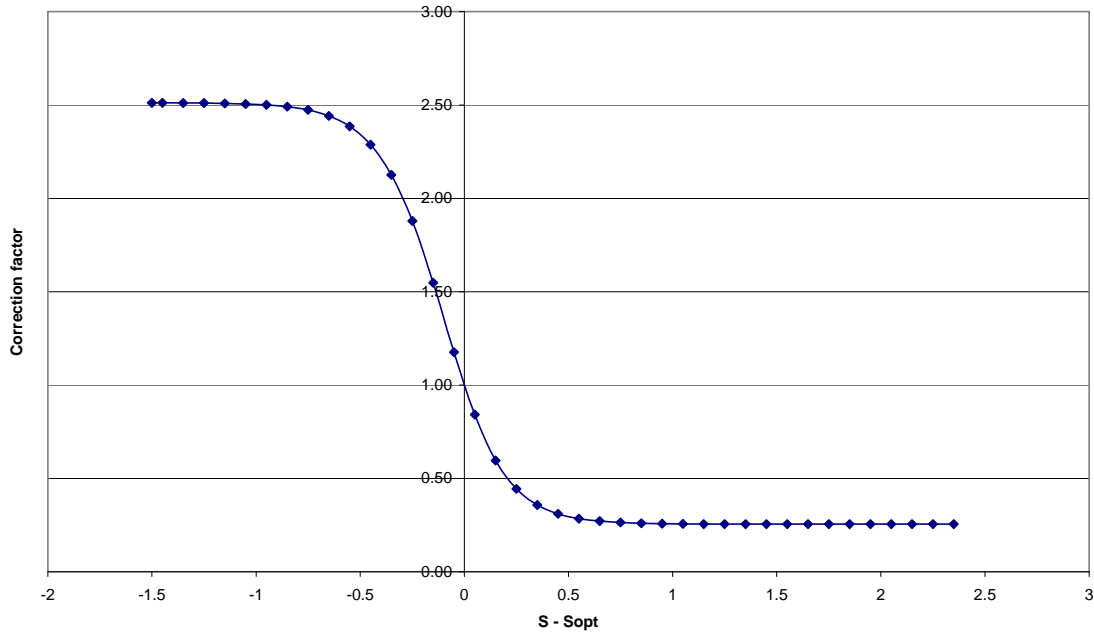


Figure 4.1 Correction factor as a function of the degree of saturation.

4.2.5 Database of $k_1 - k_2 - k_3$ Model Parameters

The first step of implementation of this procedure should be development of a database of k_1 , k_2 , and k_3 parameters for various materials. Past test results, as well as information from the literature were used to initiate development of such a database. Three sources of information were used in this study:

- Test results of the MnROAD materials conducted by CRREL
- Test results of the MnROAD materials conducted by MnDOT
- Arizona DOT database

The test procedures used in these studies were not identical so the modulus values may be different.

4.2.6 CRREL's Test

In early 1990s, the U.S. Army Cold Regions Research and Engineering Laboratory (CRREL) conducted resilient modulus tests (repeated-load triaxial test procedure) on pavement materials from the MnROAD. Several prediction models for the resilient modulus were developed. These models had the following function form:

$$M_R = a_1 \cdot f(S)^{a_2} \cdot f(\gamma)^{a_3} \cdot f(\sigma)^{a_4} \quad (4.6)$$

where

- a_1, a_2, a_3 and a_4 = material constants;
- $f(S) = (S/S_0)$ = function of the moisture level expressed as the degree of saturation S ;
- S_0 = unit reference saturation = 1.0 %;
- $f(\gamma) = (\gamma_d/\gamma_0)$ = function of the dry density, γ_d ;
- γ_0 = unit reference density;
- $f(\sigma)$ = function of the stress state.

For individual materials, it resulted in the following predictive equations:

- Clay Subgrade (1)

$$M_r = 1597000 \cdot f(S)^{-2.63} \cdot f(\gamma)^{14.42} \cdot f_3(\sigma)^{-0.257} \quad (4.7)$$

- Clay Subgrade (2)

$$M_r = 1.518 \times 10^{30} \cdot f(S)^{-13.85} \cdot f_3(\sigma)^{-0.2727} \quad (4.8)$$

- Class 3 “Stockpile”

$$M_r = 283300 \cdot f(S)^{-1.003} \cdot f_2(\sigma)^{0.206} \quad (4.9)$$

- Class 4 (Taxiway A Subbase)

$$M_r = 8.946 \times 10^8 \cdot f(S)^{-3.026} \cdot f_2(\sigma)^{0.292} \quad (4.10)$$

- Class 5 (dense graded stone)

$$M_r = 382400 \cdot f(S)^{-0.8759} \cdot f_2(\sigma)^{0.164} \quad (4.11)$$

- Class 6 “Stockpile”

$$M_r = 1391 \cdot f(S)^{-0.507} \cdot f(\gamma)^{4.04} \cdot f_1(\sigma)^{0.608} \quad (4.12)$$

where

$$f_3 = \frac{\tau_{\text{oct}}}{\sigma_0} \quad (4.13)$$

$$f_2 = \frac{J_2 / \tau_{\text{oct}}}{\sigma_0} \quad (4.14)$$

$$f_1 = \frac{\theta}{\sigma_0} \quad (4.15)$$

and

$$\theta = J_1 = \sigma_1 + \sigma_2 + \sigma_3 = \text{first stress invariant (bulk stress);}$$

$$J_2 = \sigma_1\sigma_2 + \sigma_1\sigma_3 + \sigma_2\sigma_3 = \text{second stress invariant;}$$

$$\tau_{oct} = \frac{1}{3} \sqrt{(\sigma_1 - \sigma_2)^2 + (\sigma_1 - \sigma_3)^2 + (\sigma_2 - \sigma_3)^2} = \text{octahedral shear stress;}$$

σ_0 = unit reference stress.

The CRREL's models were used to generate the test data since the test protocol used in the CRREL study was different from the MEPDG protocols for the resilient moduli testing. The optimum moisture content was assumed and the resilient moduli were calculated using equations 4.4 through 4.9. After that, for each material, the generated data were fitted using the k_1 - k_2 - k_3 model using a non-linear optimization technique. The resulting k_1 , k_2 , and k_3 parameters are presented in table 4.3.

Table 4.3 k_1 , k_2 and k_3 parameters for the materials tested by CRREL.

Material	AASHTO Group	Void ratio e	W_{opt} %	K_1	k_2	k_3
Clay subgrade 1206	A ₆	0.43	18.0	7469.6969	0	-2.32323
Clay subgrade 1232	A ₆	0.36	11.9	100.0000	0.0000	-1.7368
Class 3 "stockpile"	A _{1-b}	0.28	11.0	3666.6667	0.4490	-1.3673
Class 4 taxiway subbase	A _{1-b}	0.3	5.5	1888.8889	0.5306	-1.6531
Class 5 dense graded stone	A _{1-a}	0.4	5.3	2358.8000	0.3223	-1.6497
Class 6 "stockpile"	A _{1-a}	0.3	4.0	2157.5000	0.6080	-4.9234E-08

Figure 4.2 presents comparison of the resilient moduli generated using the CRREL model and the k_1 - k_2 - k_3 model for different levels of the octahedral shear stress τ_{oct} . A very good agreement between two models is observed.

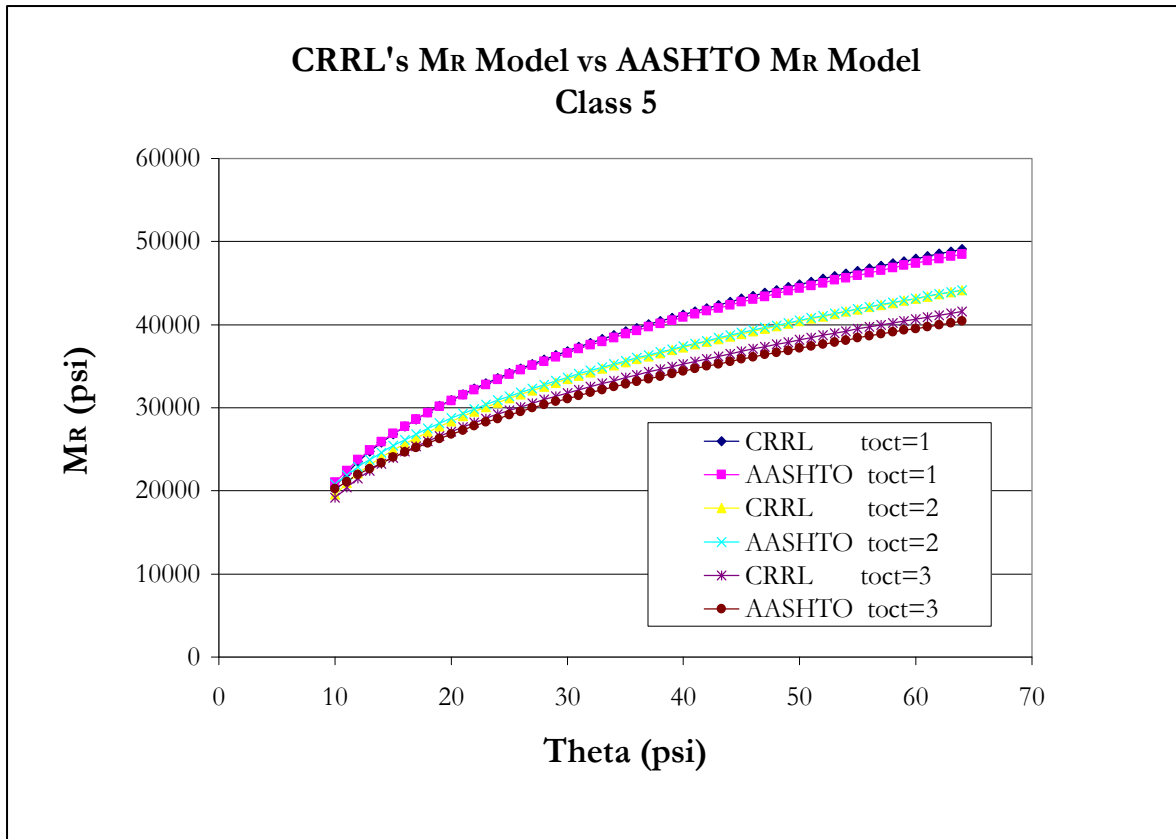


Figure 4.2 Comparison between the CRREL's M_R Model and the k_1 - k_2 - k_3 M_R Model, for different levels of octahedral shear stress.

4.2.7 MnDOT Tests

The results of the resilient modulus test of variety of Minnesota fine subgrades tested by the Office of Materials of MnDOT between October 2000 and February 2002 were evaluated and a database of k_1 , k_2 , and k_3 parameters was created. The majority of the subgrades are A-6 according to AASHTO classification, although several specimens represent A-7-6 and A-7-5 subgrades. The tests were conducted according to the LTPP Protocol 46 for measuring resilient modulus of unbound granular base/subbase materials and subgrade soils. Since not all the tests were carried out at the optimum moisture content, the coefficient k_1 was obtained using equation 4.4. Table 4.4 presents the resulting k_1 , k_1^* , k_2 , and k_3 parameters obtained from the regression analysis along with the moisture content of the subgrade during the test.

Table 4.4 k1-k2-k3 parameters for MnROAD materials obtained from MnDOT test results.

Location	AASHTO Class	Dry Density, Lb/ft ³	Optimum Moisture Content, %	Test Moisture Content, %	K* ₁	K ₁	K ₂	K ₃
CITY OF ROCHESTER	A-7-6	106.27	18	16.2	2554.302	1815.049	0.180793	-4.23504
CITY OF ROCHESTER	A-6	104.22	19.2	17.71	1547.234	1181.946	0.160933	-2.45363
ISANTI COUNTY	A-6	111.46	12.9	11.4	4625.851	3168.056	0.165225	-4.23921
ISANTI COUNTY	A-6	109.81	12.9	13.75	2314.683	2883.263	0.265045	-4.15
ISANTI COUNTY	A-6	110.57	12.9	11.95	2050.835	1596.169	0.18395	-2.35394
ITASCA COUNTY	A-6	111.77	15.1	14.79	2310.489	2149.032	0.113406	-3.29396
KANDIYOHI COUNTY	A-6	114.57	13.1	11.87	2899.871	2072.444	0.249715	-3.09559
KANDIYOHI COUNTY	A-6	115.25	13.1	12.18	2438.324	1906.016	0.204286	-2.95031
LYON COUNTY	A-6	112.65	14.5	14.11	1821.373	1663.879	0.233177	-4.49975
LYON COUNTY	A-6	116.34	12.5	11.74	3636.023	2955.099	0.162358	-3.56106
MEDFORD ROUNDABOUT	A-6	116.55	13.2	12.37	2087.053	1670.209	0.250131	-2.82977
MNROAD CELL 33	A-6	115.44	15	15.42	2989.392	3277.297	0.156599	-5.13509
MNROAD CELL 34	A-6	119.4	15	12.91	2317.111	1532.798	0.156738	-2.64929
MNROAD CELL 35	A-6	118.79	15	13.68	2618.802	2001.015	0.232257	-4.3486
ST LOUIS COUNTY	A-7-6	90.22	25.6	27.63	1266.482	1661.842	0.02788	-3.04364
ST LOUIS COUNTY	A-7-5	89.41	23.7	23.07	1596.688	1437.535	0.012749	-1.91293
STEARNS CO	A-6	104.66	17.8	15.69	1190.627	798.2841	0.323623	-3.42635
STEARNS CO	A-6	110.99	14.3	13.32	2963.512	2296.077	0.321999	-5.8838
WRIGHT COUNTY	A-7-6	97.9	21.3	21.44	1256.837	1285.827	0.207286	-5.05057
WRIGHT COUNTY	A-6	106.75	21	19.05	1109.774	829.0605	0.290016	-5.33975
WRIGHT COUNTY	A-6	103.61	21	19.9	674.3569	563.9285	0.377793	-4.96021
WRIGHT COUNTY	A-7-6	106.86	16.5	17.97	1369.223	1861.696	0.21318	-4.04342
WRIGHT COUNTY	A-7-6	108.82	16.5	15.6	2496.026	2064.54	0.054135	-1.69998

4.2.8 Arizona DOT Tests

Arizona DOT sponsored a series of tests to determine k_1 , k_2 and k_3 parameters for the typical granular materials used by Arizona DOT for construction of granular bases. Table 4.5 summarizes the reported values for k_1 - k_2 - k_3 parameters.

Table 4.5 k_1 - k_2 - k_3 parameters obtained in the Arizona DOT-sponsored study.

Material	AASHTO Group	USCS	w_{opt} %	K_1	k_2	k_3
Phoenix Valley Subgrade	A _{2-a}	SC	11.3	467	0.358	-0.686
Yuma Area Subgrade	A _{1-a}	GP	11.0	1468	0.838	-0.888
Flagstaff Area Subgrade	A ₂₋₆	SC	19.0	634	0.187	-0.855
Sun City Subgrade	A ₂₋₆	SC	11.3	747	0.224	-0.104
Grey Mountain Base	A _{1-a}	GW	6.7	1432	0.758	-0.288
Salt River Base	A _{1-a}	SP	6.9	1170	0.919	-0.572
Globe Area Base	A _{1-a}	SP-SM	6.7	1032	0.830	-0.307
Precott Area Base	A _{1-a}	SP-SM	6.3	1092	0.784	-0.236
ADOT A _{1-a} Base Material	A _{1-a}	SP-SM	6.7	1075	0.841	-0.305

4.2.9 Recommended Ranges for K_1 , K_2 , and K_3 Parameters

Based on the results of the model parameters obtained from the CRREL and MnDOT test data, as well as the parameters reported by the Arizona DOT, the ranges for the k_1 , k_2 , and k_3 parameters were proposed. Table 4.6 presents the recommended ranges. These ranges can be used for initial screening of the test results, as well as for rough estimation of the subgrade properties.

Table 4.6 Typical ranges of values for each of the k parameters for coarse grained and fine grained materials.

Parameter	Coarse Grained Material	Fine Grained Material
k_1	400 - 1500	1000 – 6000
k_2	0.2 - 1	0.01- 0.5
k_3	-0.1 - -0.9	-1.5 - -6

4.2.10 Determination of the MEPDG Level 2 Subgrade Input from the K1-K2-K3 Model

4.2.10.1 *General procedure:* The MEPDG recommends an iterative approach for determination of the resilient modulus input for use with MLET analysis. To determine the resilient modulus, the density and thickness of each pavement layer and soil stratum above the point of resilient modulus determination must be known or assumed. The total lateral and vertical stresses for typical wheel loading and the at-rest earth pressure must be known. On the other hand, the stress distribution in the multi-layered system is affected by the moduli of elasticity of the individual layers. Therefore, an iterative procedure shall be used for the moduli calculation.

The following approach was proposed several decades ago (Smith & Witczak 1980, Moossazadeh & Witczak 1981) and, with minor modifications, recommended by the MEPDG. The recommended procedure involves the following steps:

- Step 1. Assume initial moduli for each unbound layer in the pavement system.
- Step 2. Compute a stress state for critical points within unbound layers from the wheel loading.
- Step 3. Use the stresses obtained in step 2 to compute the total stress state from the wheel loading and the overburden pressure. The vertical component of the stress state should be computed using the following equation:

$$\sigma_z = \sigma_v + p_0 \quad (4.16)$$

where

σ_z = vertical stress from the wheel load as computed with elastic layer theory;
 p_0 = at-rest vertical pressure from the overburden of other layers:

$$p_0 = D_n \cdot \gamma_n + \sum_{i=1}^{n-1} D_i \cdot \gamma_i \quad (4.17)$$

where

D = thickness of the i^{th} layer above the stress calculation point of interest:

γ_i = density of the i^{th} layer.

i = layer above the soil layer, n , for which the resilient modulus is being estimated. It is assumed here that layer 1 is the surface and that i increases with depth.

For computing the contribution of the overburden stresses to the total lateral stress, it is necessary to estimate the at-rest pressure coefficient, K_0 . Such a coefficient for cohesive soils (such as clays) is normally calculated as a function of Poisson's ratio, μ , according to the following equation:

$$K_0 = \frac{\mu}{1 - \mu} \quad (4.18)$$

For non-cohesive soils (such as gravel and sand), the at-rest pressure coefficient is a function of the angle of shearing resistance, ϕ , i.e.:

$$K_0 = 1 - \sin \phi \quad (4.19)$$

with φ measured in radians..

The total lateral stress, σ_3 , for determining the resilient modulus of the soil layer then can be determined from the following equation:

$$\sigma_3 = \sigma_H + K_0 \cdot p_0 \quad (4.20)$$

where

σ_H = horizontal stress from the wheel load applied at the pavement surface and computed with elastic layer theory

- Step 4. Using the stress obtained in step 3 and the constitutive equation 4.2, compute predicted resilient moduli.
- Step 5. Compare the resilient moduli computed in step 4 with the assumed moduli. If these moduli significantly differ from each other, steps 2 through 4 should be repeated using the set of the moduli obtained in the last iteration.

The described above procedure closely follows the guidelines provided in the MEPDG. However, its implementation is not straightforward, since many important details are not specified in the Guide. After consultations with the NCHRP 1-40B team (Harold Van Quintus, ARA, Inc.), the following refinements of the MEPDG procedure were adopted in this study:

1. The wheel load used for computation of the traffic stresses was assumed to be an FWD-type single wheel load.
2. The following locations were specified for computing stresses in the unbound layers:
 - a. Base and subbase – $\frac{1}{4}$ of the depth of each unbound layer
 - b. Subgrade – 18 inches from the top of the subgrade
3. The iteration process was assumed to be converged if the relative errors between assumed and calculated moduli were less than 5 percent each.

4.2.10.2 Procedure Implementation: Although the procedure described above is relatively simple, its implementation is time consuming, because all iterations require performing of a MLET analysis run. To speed up the process, several rapid solutions were developed for predicting critical MLET responses for typical pavement systems for the locations specified used in the procedure described above.

A factorial of the MLET program was performed for a 4-layered system loaded by a two-wheel load as shown in figure 4.3. The top layer simulated an asphalt layer, the second and the third from the top layers simulated a granular base and subbase, respectively, and the semi-infinite layer modeled a subgrade. The stresses were calculated in the second and the third layers at $\frac{1}{4}$ of the depth (positions A and B), and at 18 inches below the top of the subgrade (position C).

Almost 600,000 MLET program runs were performed to create a training database. The Poisson ratios of the layers were kept constant and assumed to be equal to 0.3, 0.35, 0.35, and 0.45 for the asphalt, base, subbase, and subgrade layers. The layer thicknesses and moduli of elasticity varied in wide ranges to cover the typical values of these parameters. The following values for the thickness and the moduli of elasticity were considered:

- AC thickness: 2, 4, 6, 8, 10, and 12 in
- Base thickness: 6, 9, 12, 15, 18, and 21 in
- Subbase thickness: 6, 9, 12, 15, 18, and 21 in
- AC modulus of elasticity: 200, 400, 600, 800, 1000, 1500, and 2000 ksi
- Base modulus of elasticity: 10, 15, 20, 25, 30, and 40 ksi
- Subbase modulus of elasticity: 10, 15, 20, 25, 30, and 40 ksi
- Subgrade modulus of elasticity: 3, 5, 7, 9, 11, 13, 15, 18, 22, 25, and 30 ksi

Based on the results of these runs, several rapid solutions were developed. They permitted computations of the stresses at the critical locations much faster than it would be done using the MLET program. More importantly, these solutions could be called directly from the Excel spreadsheet, in which the procedure for resilient moduli iterations was implemented. This permitted a very efficient analysis of the effect of the unbound layer parameters and asphalt layer thickness on predicted resilient moduli.

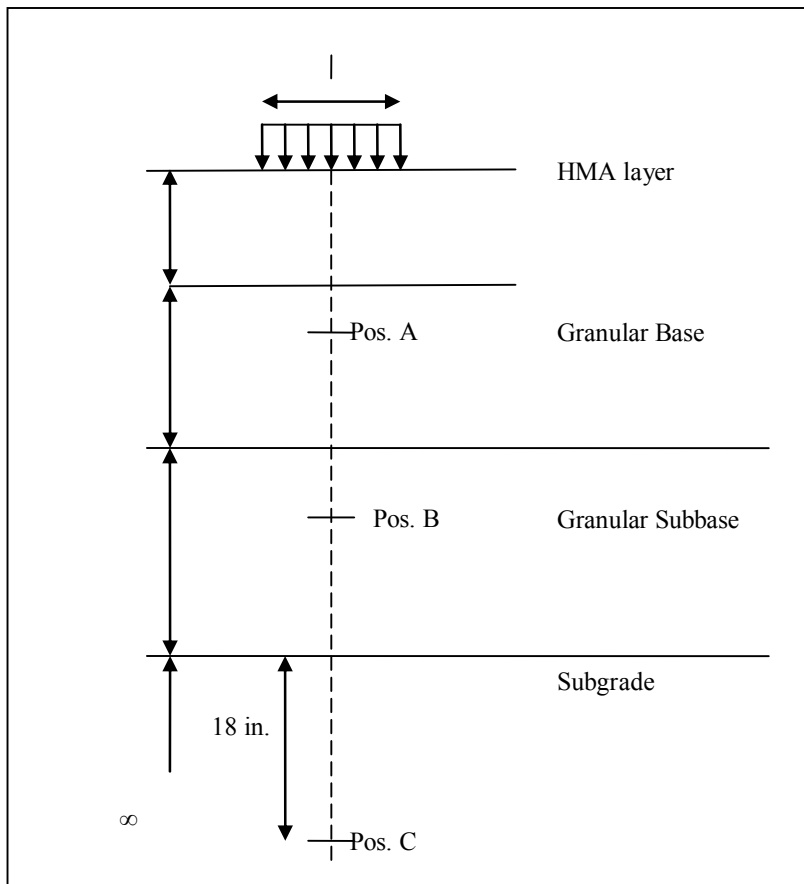


Figure 4.3 A pavement system assumed for calculation with BISAR.

4.2.11 Sensitivity Analysis

Using the rapid solutions described above, several sensitivity studies were conducted to investigate the effect of k_1 , k_2 , and k_3 parameters on the predicted resilient moduli. A set of

baseline parameters was selected (see table 4.7). After that, for selected pavement structures, one parameter was changed and the iterative procedure for predicting the resilient modulus was performed. Several examples of this analysis are presented below.

Table 4.7 Sets of k parameters chosen for the unbound layers and subgrade of the pavement structure examined in the sensitivity analysis.

	Thickness	Modulus of Elasticity, psi	k_1 , psi	k_2	K_3
Asphalt	4	600,000			
Base1	6		1432	0.758	-0.288
Subbase	6		1888.9	0.5306	-1.653
Subgrade	infinite		1468	0.838	-0.888

Figures 4.4, 4.5, and 4.6 present the effect of the AC, base, and subbase layer thicknesses, respectively, on the predicted resilient moduli. Figure 4.4 shows that increase in asphalt thickness significantly reduces predicted base modulus, but has less pronounced effect on the subbase and subgrade moduli. Nevertheless, increase in AC thickness from 2 to 8 inches leads to an increase of the subgrade resilient modulus from 11.9 to 13.7 ksi. A similar effect was observed for the base thickness (see figure 4.5). Although the change in the base resilient modulus was not as significant as it was observed when the AC thickness was changed, the subgrade resilient modulus changes from 12.5 ksi to 14.1 ksi when the base thickness increased from 6 to 21 inches. As can be observed from figure 4.6, an increase in subbase thickness does not substantially change the base and subbase moduli, but increases the subgrade modulus.

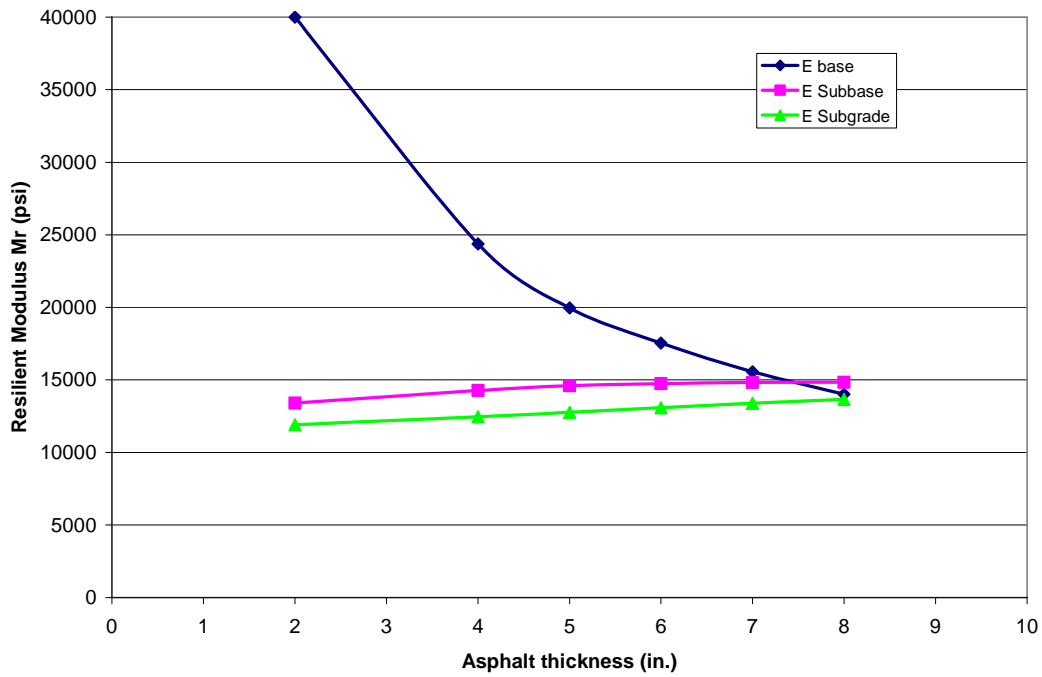


Figure 4.4 Effect of the asphalt layer thickness on predicted resilient moduli.

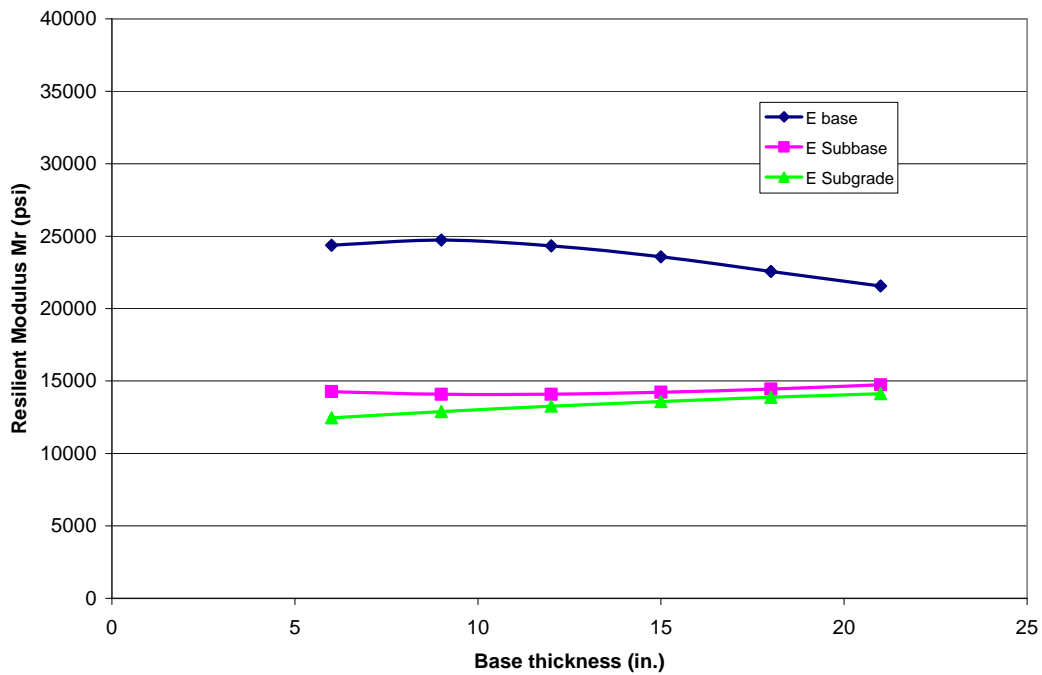


Figure 4.5 Effect of base thickness on predicted resilient moduli.

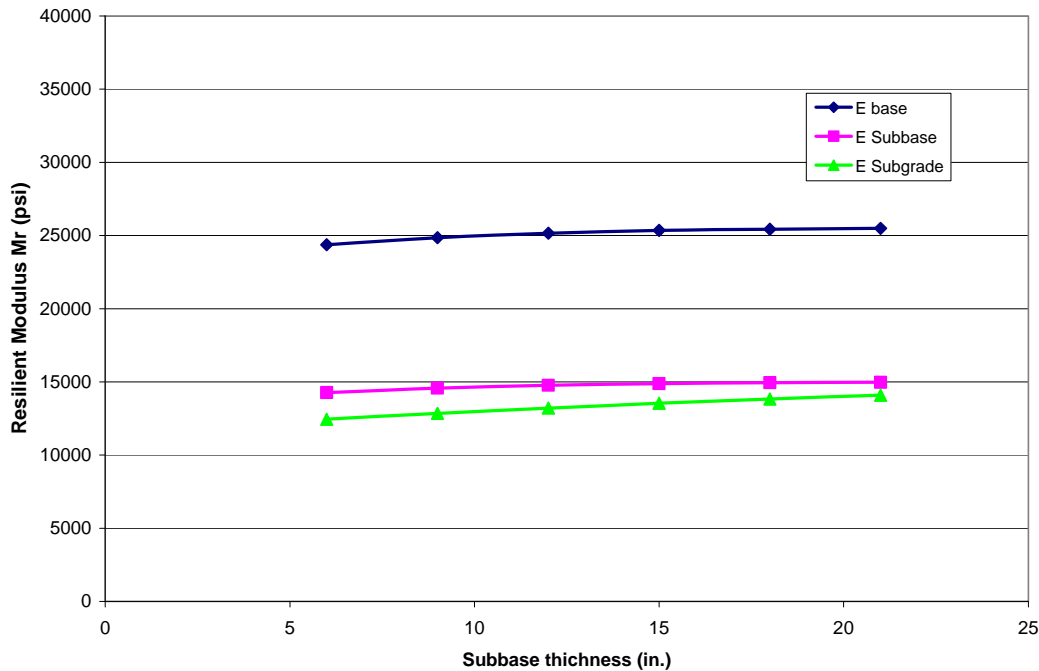


Figure 4.6 Effect of subbase thickness on predicted resilient moduli.

Naturally, the material model parameters (k_1 , k_2 , and k_3) affect the predicted moduli. Figures 4.7, 4.8, and 4.9 present the effect of the parameters k_1 , k_2 , and k_3 , respectively, of the base layer on the predicted resilient moduli in the unbound layers. One can observe that an increase of these parameters increases the predicted resilient modulus of the base layer, but does not significantly change the resilient moduli of the subbase and subgrade.

Figures 4.10, 4.11, and 4.12 show that change in parameters k_1 , k_2 , and k_3 , respectively, of the subbase layer may affect not only the resilient modulus of the subbase, but the resilient modulus of the base layer, as well. At the same time, no appreciable effect of change in subbase k_1 , k_2 , and k_3 on the subgrade resilient modulus was observed.

The effects of the k_1 , k_2 , and k_3 of the subgrade on the pavement system resilient moduli are shown in figures 4.13, 4.14, and 4.15, respectively. It can be observed from figure 4.12 that parameter k_1 significantly affects not only the resilient modulus of the subgrade, but also the resilient moduli of the base and subgrade. The effect of the parameters k_2 and k_3 are much less pronounced.

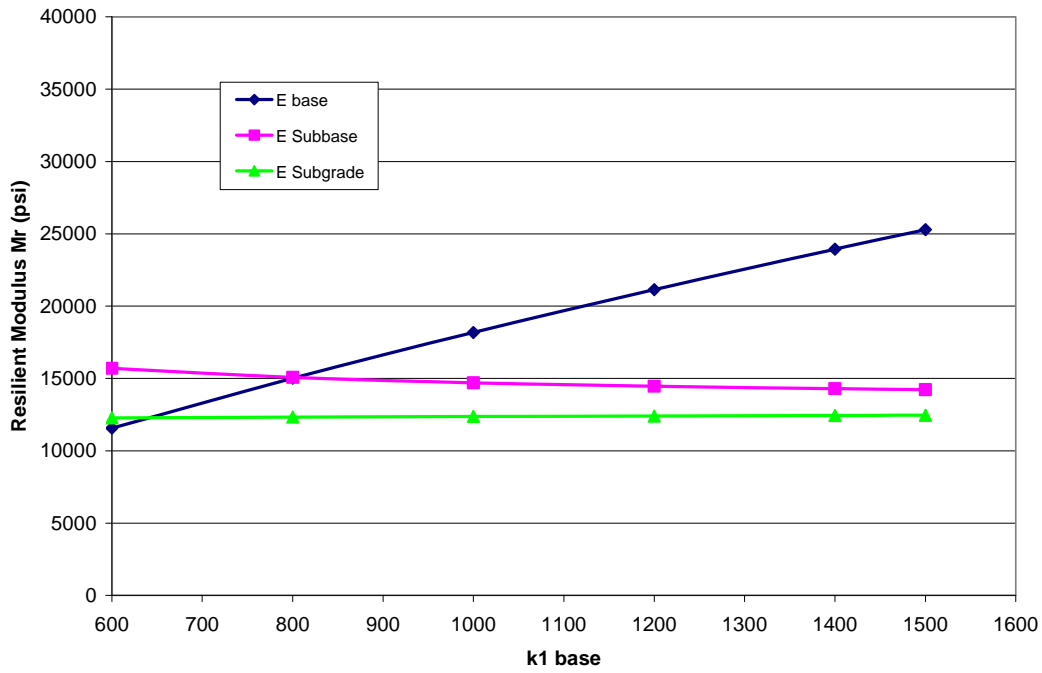


Figure 4.7 Effect of base k1 on predicted resilient moduli.

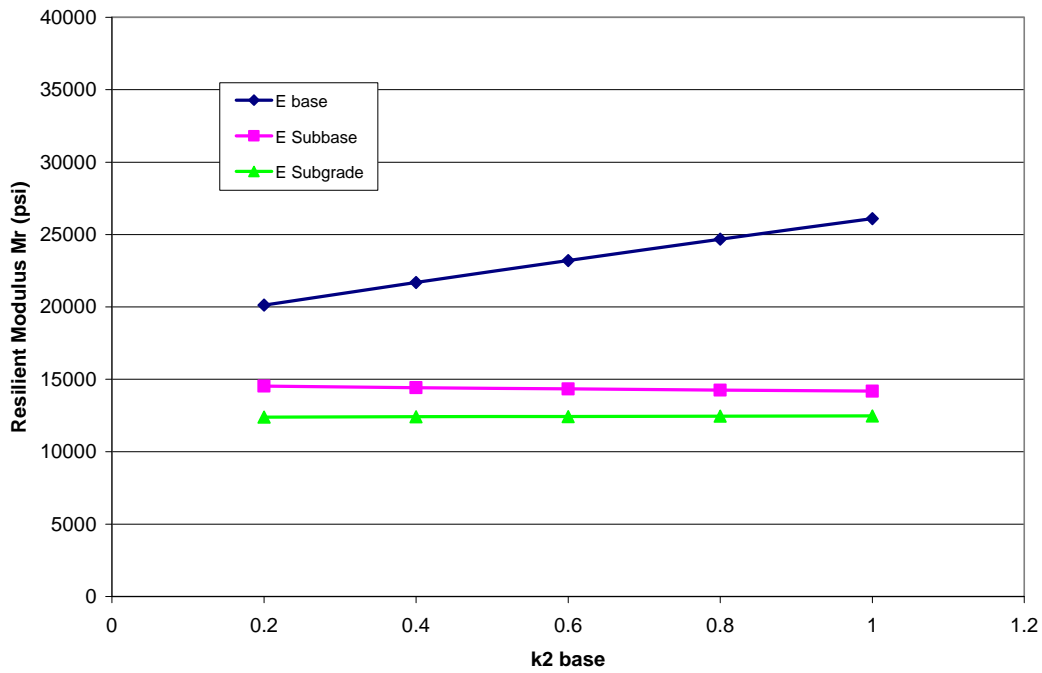


Figure 4.8 Effect of base k2 on predicted resilient moduli.

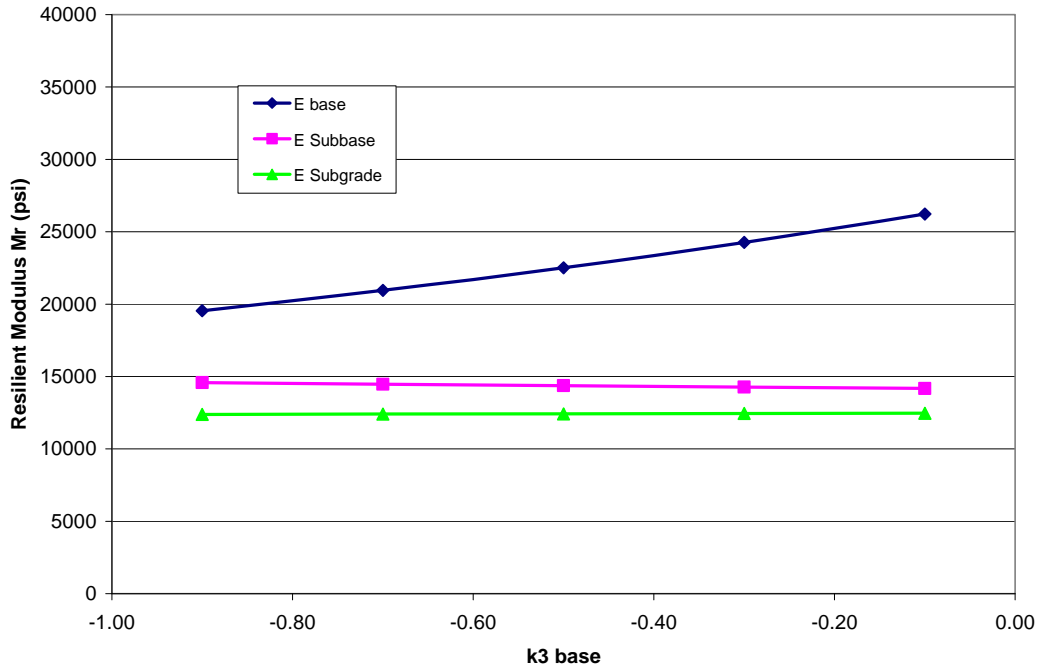


Figure 4.9 Effect of subbase k3 on predicted resilient moduli.

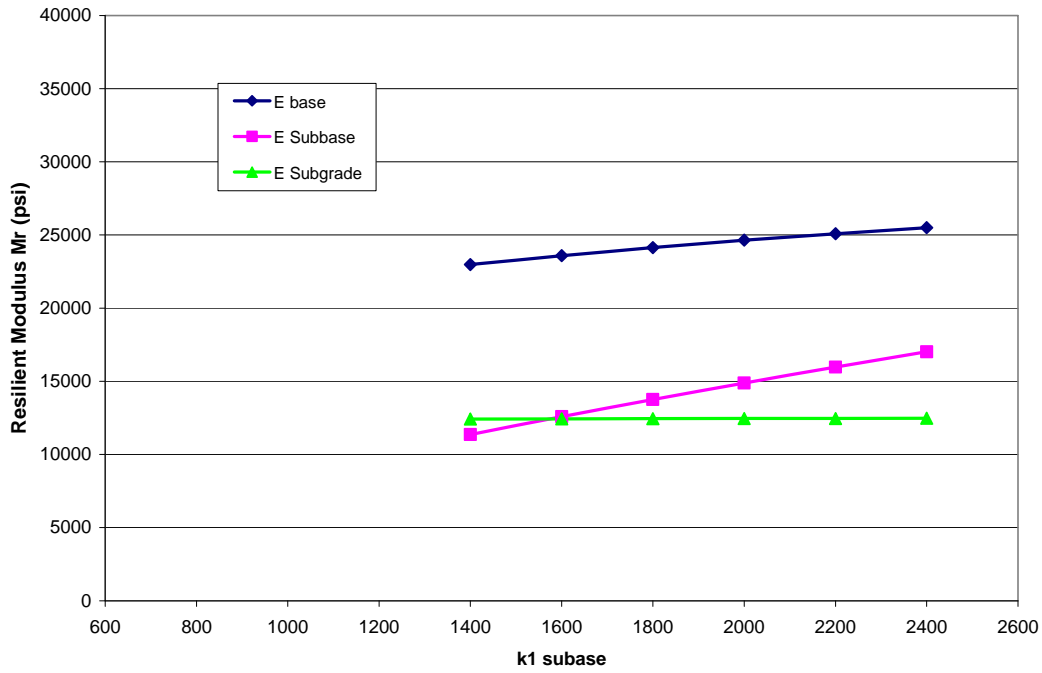


Figure 4.10 Effect of subbase k1 on predicted resilient moduli.

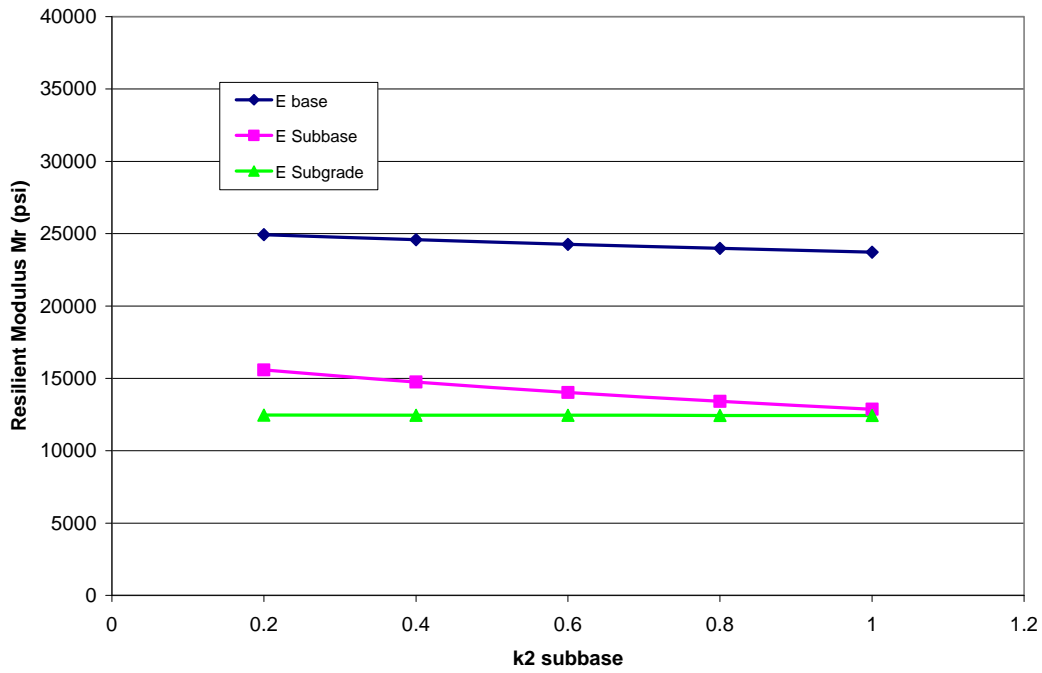


Figure 4.11 Effect of subbase k2 on predicted resilient moduli.

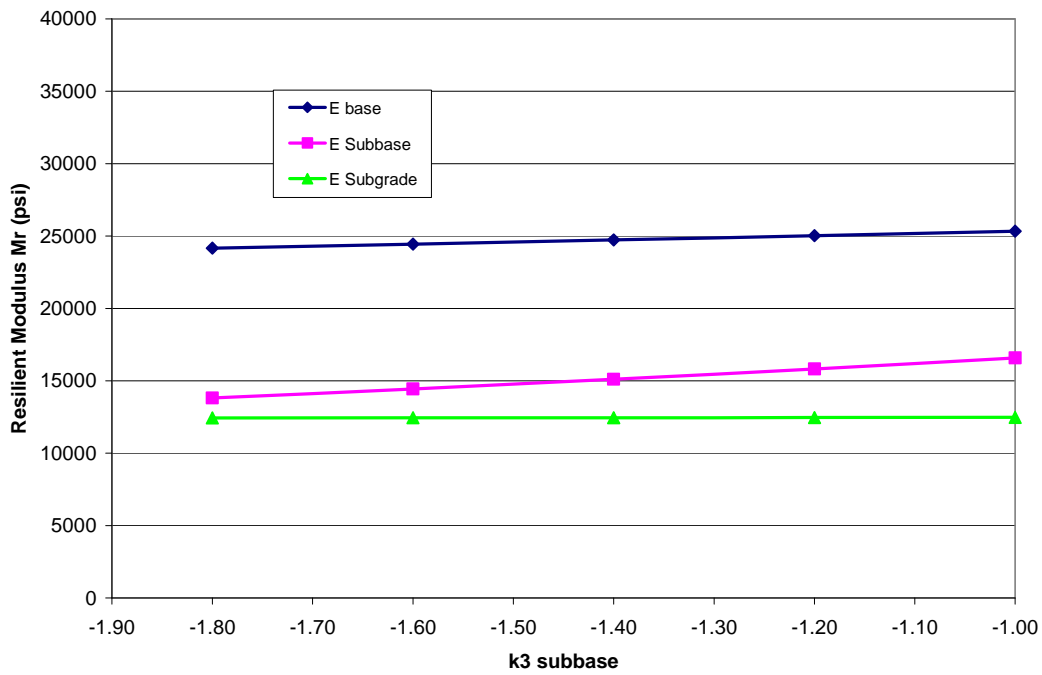


Figure 4.12 Effect of subgrade k3 on predicted resilient moduli.

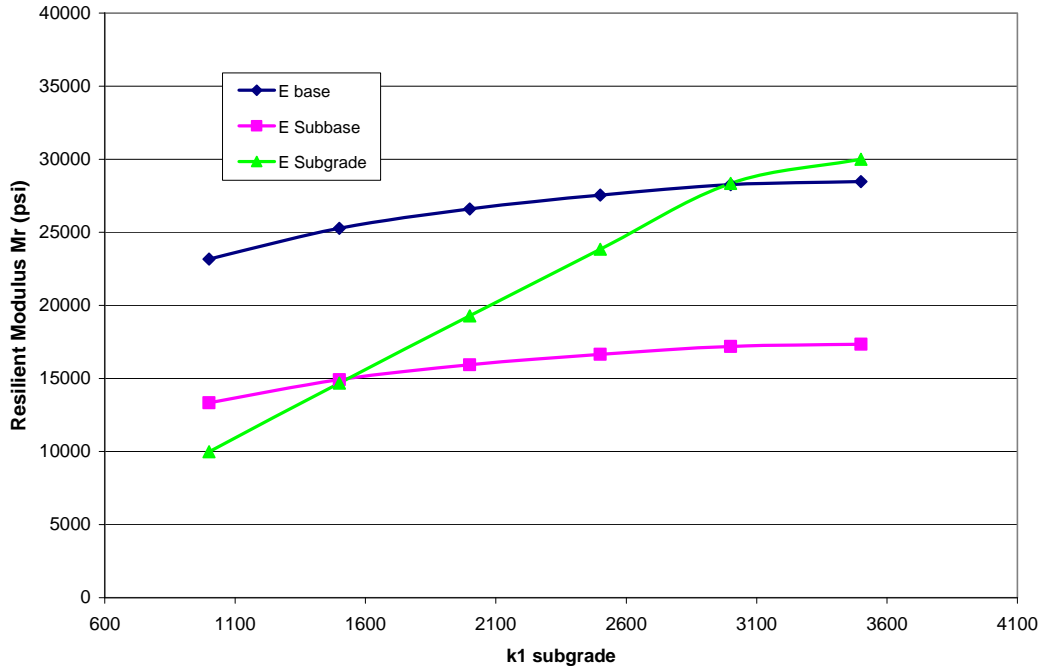


Figure 4.13 Effect of subgrade k_1 on predicted resilient moduli.

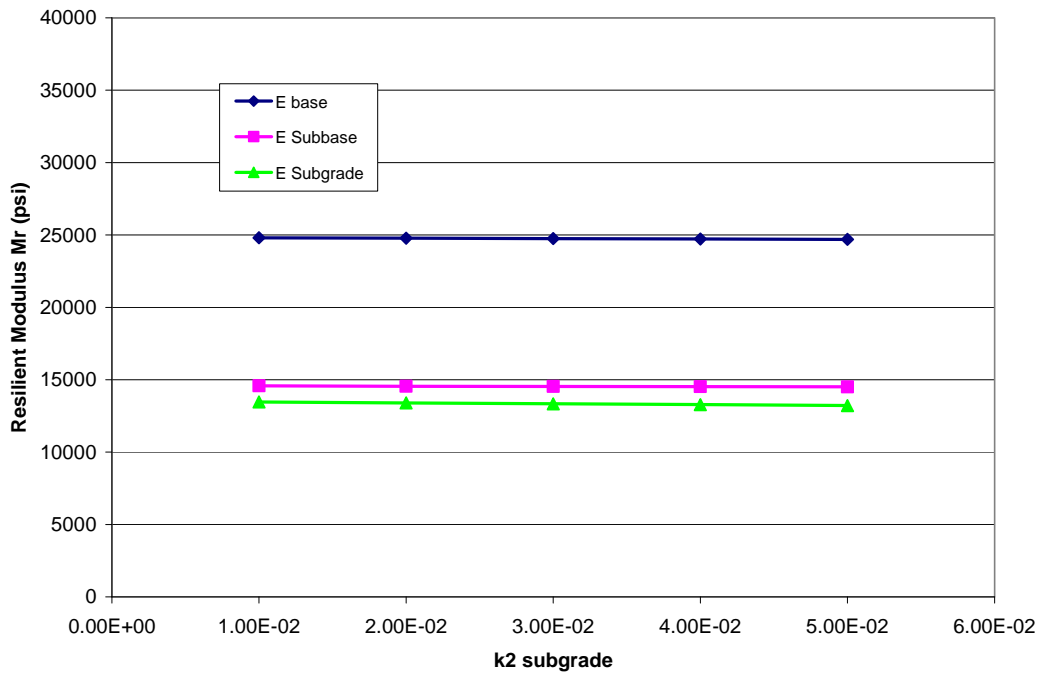


Figure 4.14 Effect of subgrade k_2 on predicted resilient moduli.

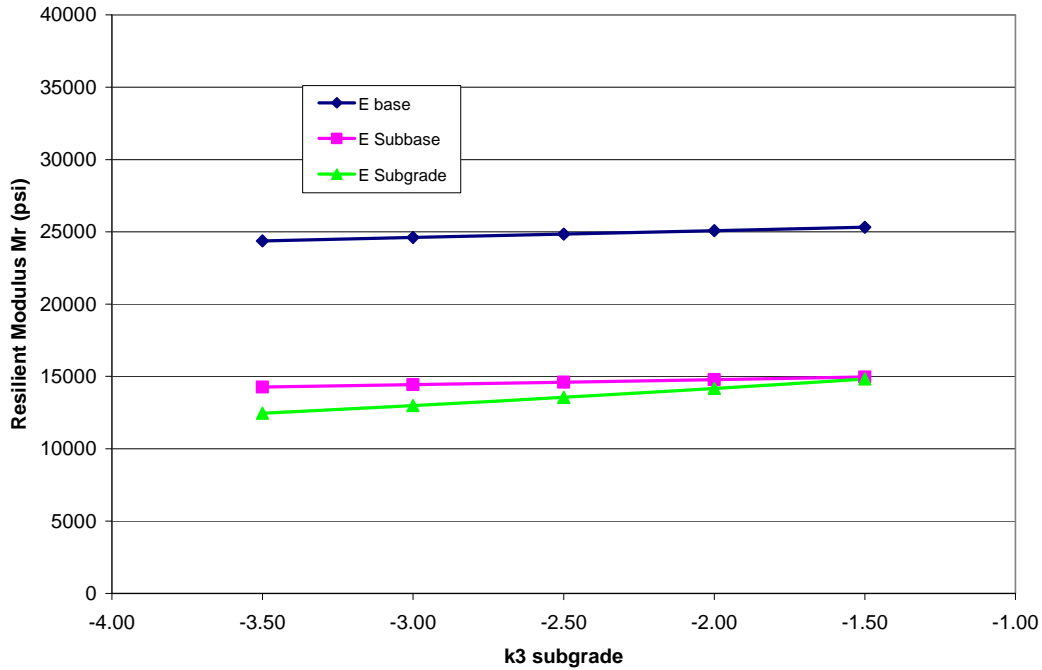


Figure 4.15 Effect of subgrade k3 on predicted resilient moduli.

The MEPDG procedure often results in very low base moduli, especially if a very stiff or thick AC layer is present. Although the focus of this investigation was the evaluation of the subgrade resilient moduli, there was a concern that unrealistically low base moduli may compromise the predicted subgrade moduli. To eliminate this concern, two types of analysis were conducted: the base layer was allowed to take any values and the base resilient modulus was assumed to be not lower than 30,000 psi. Figures 4.16 and 4.17 present the results of the analysis for the St. Louis Clay for a wide range of AC thicknesses for unconstrained and constrained base moduli, respectively. Comparison of these figures shows that constraining of the base moduli does not significantly alter prediction of the subgrade moduli.

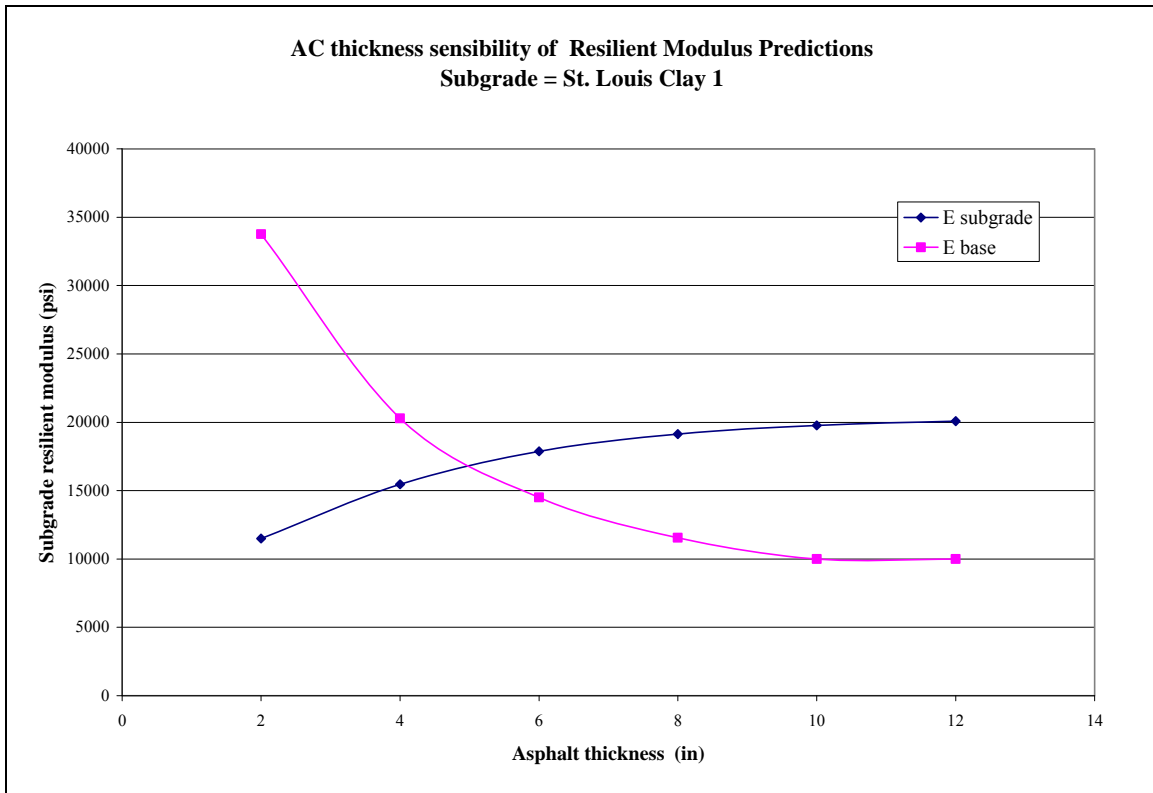


Figure 4.16 Predicted subgrade and base moduli for various AC thicknesses. Base modulus is not constrained.

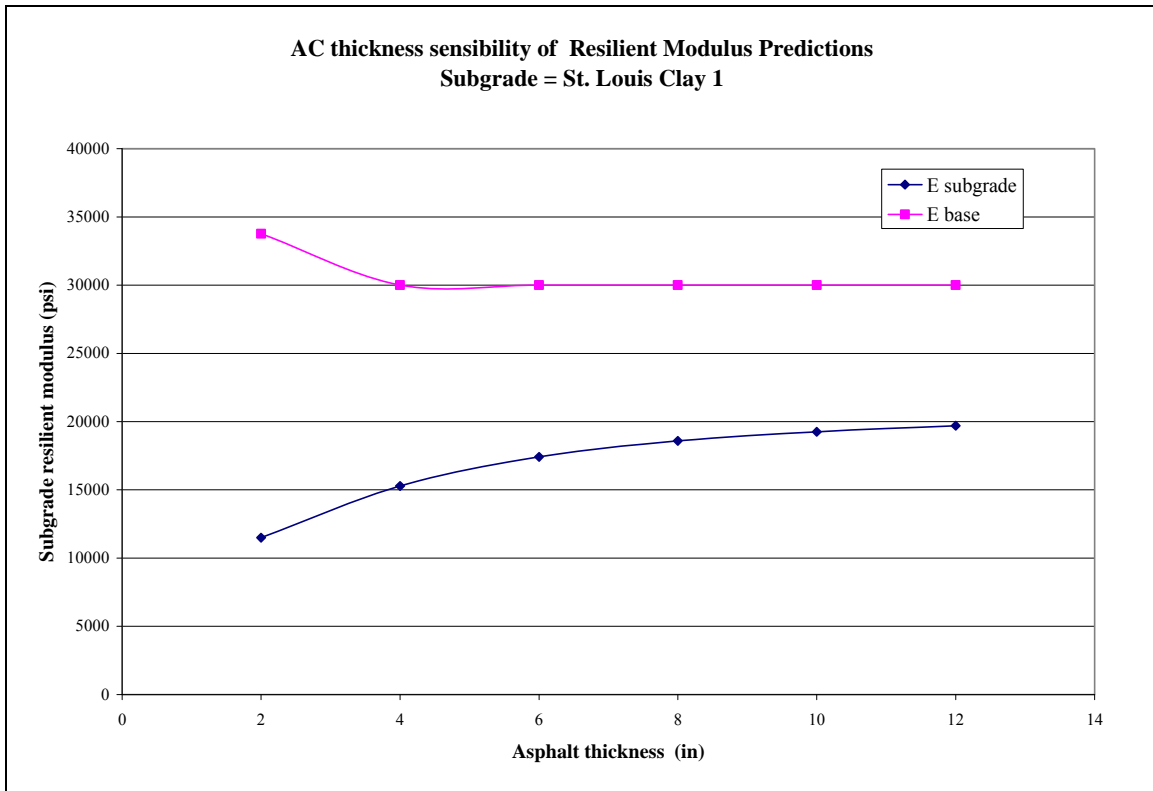


Figure 4.17 Predicted subgrade and base moduli for various AC thicknesses. The minimum allowed value for the base modulus is equal to 30,000 psi.

4.2.12 Evaluation of the Level 2 Resilient Moduli for Minnesota Subgrades.

The MnROAD Low Volume Roadway (LVR) is a 2.5 mile (4.0 km) closed loop where controlled weight and traffic volume simulate conditions on rural roads. It is located 40 miles west of Minneapolis/St. Paul, and runs parallel to Interstate 94 near Otsego, Minnesota. The LVR consists of 26 pavement sections of various lengths. The sections also differ by pavement type (flexible (AC) and rigid (PCC)), and design parameters, such as layers thickness, material properties, edge support

To evaluate robustness of the procedure of conversion of the k_1 - k_2 - k_3 model into a single resilient modules, this procedure was applied for the Minnesota subgrades (see table 4.4) for a variety of hypothetical pavement structures. The following combination of AC and base thicknesses was considered:

- AC thickness: 2, 4, 6, 8, 10, and 12 in.
- AC modulus of elasticity: 200,000 and 2,000,000 psi
- Base thickness: 6, 9, and 12 in.
- Base k_1 , k_2 , and k_3 parameters: 14323, 0.758, and -0.288, respectively
- Subbase thickness: 8 in.

Two levels of AC moduli of elasticity represent very stiff and very soft AC layer. The base layer was assumed to have properties of the Grey Mountain granular base material from the Arizona DOT database (Witczak, 2000a). The subbase layer was assumed to have the same properties as the subgrade, but the minimum resilient modulus was set to be equal to 10,000 psi. The maximum modulus of elasticity was assumed to be equal to 40,000 psi for the base layer and 30,000 psi for the subbase and subgrade.

For each subgrade type and pavement structure (total 36 cases for each subgrade), a resilient modulus was calculated using the modified iterative MEPDG procedure. Table 4.8 present the summaries of the subgrade and subbase resilient moduli in terms of ranges of the observed values and the mean value for each subgrade type. The table also shows recommended ranges based on the AASHTO material classification.

Analysis of table 4.8 shows that, with a few exceptions, the MEPDG level 3 recommendations for the subgrade resilient modulus represent a reasonable estimate of the resilient modulus. At the same time, even for the subgrade of the same AASHTO soil classification class located in the same State, the resilient modulus may vary significantly. Moreover, even for the same material, the ranges of predicted resilient moduli can be quite wide. The subgrade resilient modulus would be much higher for a pavement system with a thick and stiff asphalt layer and much lower for a pavement system with a thin and soft asphalt layer. Therefore, assignment of the resilient modulus based only on the subgrade classification is not completely reliable.

It can also be observed that the subgrade resilient moduli obtained using the iterative procedure, are usually higher than the value recommended in the Design Guide. The reason for this discrepancy is that the stress state at 18 inches below the surface is too low and does not necessarily adequately represent the stress state in the system. The resilient moduli obtained for the subbase are significantly lower because the stress state is calculated 2 inches below the bottom of the base layer.

Determination of the “optimum” location for the stress state calculation is out of the scope of this paper. These recommendations should be developed by comparison of pavement distresses (cracking and rutting) predicted using the responses computing with the non-linear axisymmetric program (level 1 input) and the MLET program (level 2 input). However, the discussion above clearly illustrates importance of defining this location. The current version of the MEPDG lacks specific recommendations for this matter.

Table 4.8 Resilient moduli.

Location	AASHTO Class	2002 DG Recommended Ranges	Subbase MR, psi		Subgrade MR, psi	
			Mean value	Ranges	Mean value	Ranges
CITY OF ROCHESTER	A-7-6	5000-13500	13113	10000 ¹ - 17696	18677	15647 - 21314
CITY OF ROCHESTER	A-6	13500-24000	11167	10000 - 12977	13851	12516 - 14976
ISANTI COUNTY	A-6	13500-24000	20892	10000 - 30000 ²	29659	26540 - 30000
ISANTI COUNTY	A-6	13500-24000	18602	10000 - 26092	28007	23595 - 30000
ISANTI COUNTY	A-6	13500-24000	14338	10000 - 17250	18574	16775 - 20131
ITASCA COUNTY	A-6	13500-24000	17263	10000 - 23475	24018	20804 - 26734
KANDIYOHI COUNTY	A-6	13500-24000	15949	10000 - 20253	22333	19490 - 24889
KANDIYOHI COUNTY	A-6	13500-24000	15428	10000 - 19564	21145	18596 - 23377
LYON COUNTY	A-6	13500-24000	11790	10000 - 15247	16596	13791 - 19077
LYON COUNTY	A-6	13500-24000	21578	10000 - 30000	29664	26872 - 30000
MEDFORD ROUNDABOUT	A-6	13500-24000	13547	10000 - 16534	18428	16301 - 20317
MNROAD CELL 33	A-6	13500-24000	19464	10000 - 30000	29271	24957 - 30000
MNROAD CELL 34	A-6	13500-24000	13536	10000 - 16715	17751	15862 - 19346
MNROAD CELL 35	A-6	13500-24000	13612	10000 - 18492	20030	16656 - 23036
ST LOUIS COUNTY	A-7-6	5000-13500	14938	10000 - 19983	19745	17380 - 21618
ST LOUIS COUNTY	A-7-5	8000-17500	15268	10000 - 18733	18547	17112 - 19624
STEARNS CO	A-6	13500-24000	10000	10000 - 10000	8274	7245 - 9212
STEARNS CO	A-6	13500-24000	12762	10000 - 17945	20035	15652 - 24142
WRIGHT COUNTY	A-7-6	5000-13500	10327	10000 - 11759	12619	10382 - 14583
WRIGHT COUNTY	A-6	13500-24000	10000	10000 - 10000	7887	6535 - 9104
WRIGHT COUNTY	A-6	13500-24000	10000	10000 - 10000	5322	4500 - 6081
WRIGHT COUNTY	A-7-6	5000-13500	13359	10000 - 17808	19136	16128 - 21782
WRIGHT COUNTY	A-7-6	5000-13500	13113	10000 - 17696	26328	24426 - 27868

¹minimum value for subbase MR

²maximum value for subgrade and subbase MR

4.2.12.1 *Effect of Pavement Structure on Resilient Modulus Selection:* As it was stated above, the same k_1 - k_2 - k_3 model can result in different resilient moduli. Depending on the stiffness of the structure above the subgrade (thickness and stiffness of the AC and base layers), it may have a significant effect on the predicted moduli of unbound materials. To evaluate this effect, the resilient moduli were compared with the effective flexural stiffness of the pavement system defined as follows:

$$D_{eff} = E_{AC} \cdot h_{AC}^3 + E_{base} \cdot h_{base}^3 \quad (4.21)$$

where:

- D_{eff} = effective pavement stiffness;
- E_{AC} = elastic modulus of the asphalt layer;
- h_{AC} = thickness of the asphalt layer;
- E_{base} = resilient modulus of the base layer;
- h_{base} = thickness of the base layer.

Figures 4.18 and 4.19 present the resilient moduli versus the effective flexural stiffness for two of Minnesota subgrades. It was found that the effect of the pavement structure on the resilient moduli may be described with a high level of confidence using the following simple predictive model:

$$M_r = A \cdot \ln D_{eff}^{1/3} + B \quad (4.22)$$

where A and B are fitting parameters.

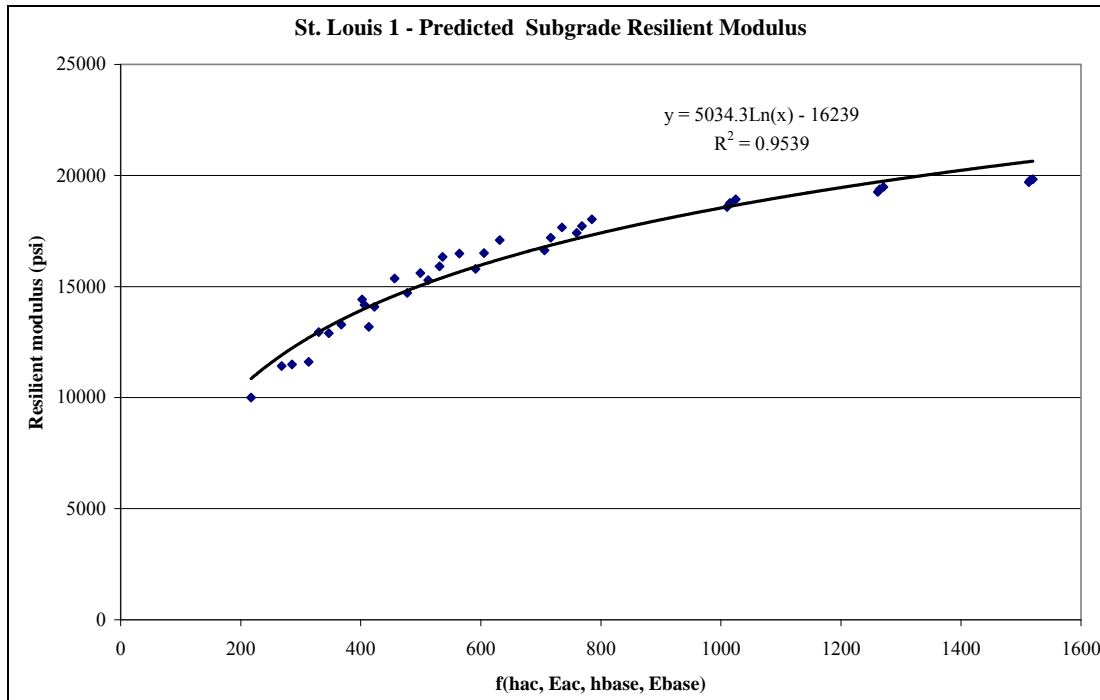


Figure 4.18 Predicted resilient modulus for the A₇₋₆ subgrade material St. Louis 1.

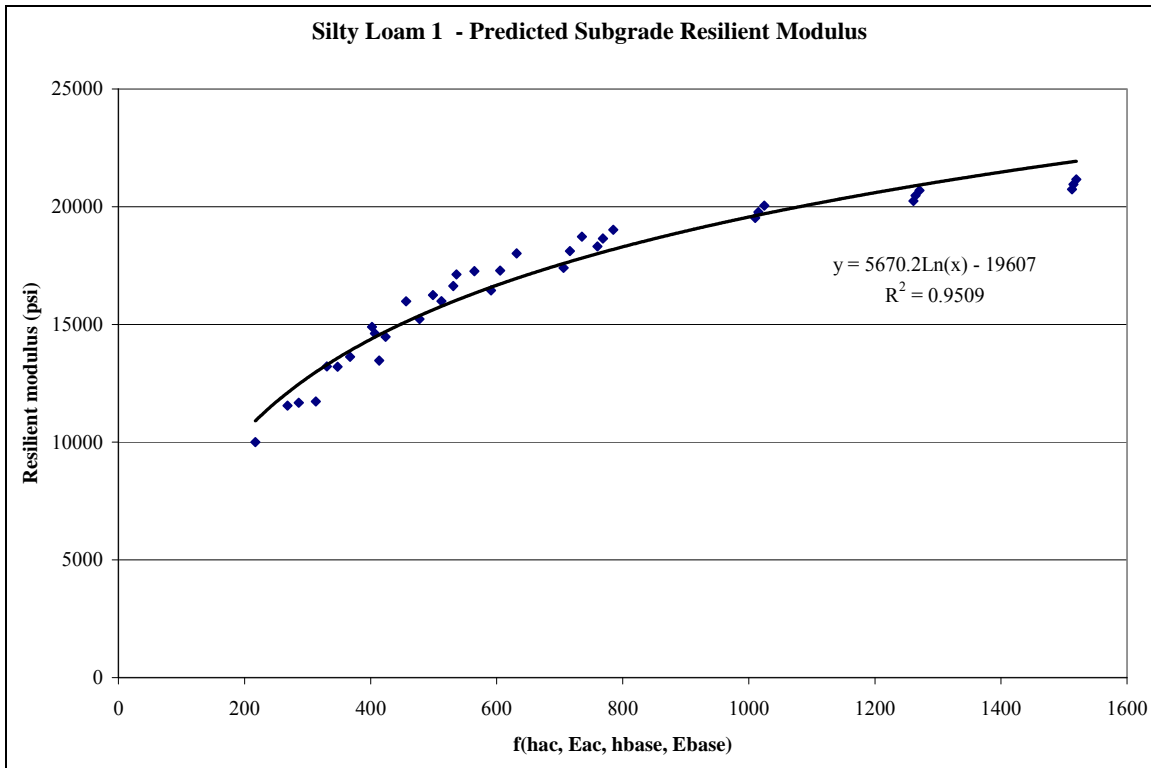


Figure 4.19 Predicted resilient modulus for the A₆ subgrade material Silty Loam 1.

Table 4.9 presents values of the regression parameters and a goodness-of-fit characteristic for the subgrade materials. A very high R^2 (88 percent or higher) was observed for 19 out of 23 subgrades. This means that for the majority of the tested Minnesota subgrades more than 88 percent of variation in the predicted resilient moduli may be attributed to change in the effective flexural stiffness. Therefore, higher subgrade moduli may be used as the Level 2 input for design of thicker and stiffer AC pavements. However, since the resilient modulus – flexural stiffness relationship depends on the subgrade material properties (k_1 - k_2 - k_3 parameters), resilient modulus testing is required to justify increase in subgrade resilient modulus.

It is important to note that in Minnesota the AC modulus of elasticity varies significantly during the year. Therefore, an effective flexural stiffness may vary from month to month. A significant effect of the effective flexural stiffness on the subgrade resilient modulus also means that seasonal adjustment of the subgrade modulus should account not only for seasonal variations in moisture conditions, but also for seasonal variations in AC modulus. The default seasonal adjustment procedure does not account for this effect.

Table 4.9 Coefficients of the effective stiffness – subgrade resilient modulus correlations.

Subgrade Number	Location	A	B	R2
1	CITY OF ROCHESTER	2761.965	1011.461	0.959799
2	CITY OF ROCHESTER	1162.421	6417.754	0.931872
3	ISANTI COUNTY	982.33	23371.95	0.402854
4	ISANTI COUNTY	3302.7	6870.348	0.843207
5	ISANTI COUNTY	1573.928	8504.884	0.921337
6	ITASCA COUNTY	2896.655	5482.509	0.964598
7	KANDIYOHI COUNTY	2539.942	6080.855	0.923769
8	KANDIYOHI COUNTY	2268.813	6628.459	0.93482
9	LYON COUNTY	2560.032	223.0965	0.953461
10	LYON COUNTY	938.4947	23656.56	0.428909
11	MEDFORD ROUNDABOUT	1871.449	6456.11	0.913378
12	MNROAD CELL 33	1819.023	17630.19	0.542029
13	MNROAD CELL 34	1662.978	7113.909	0.943121
14	MNROAD CELL 35	3081.767	317.0227	0.952096
15	ST LOUIS COUNTY	2123.267	6161.618	0.977855
16	ST LOUIS COUNTY	1248.64	10558.66	0.97669
17	STEARNS CO	897.2161	2538.019	0.88286
18	STEARNS CO	4114.52	-6282.26	0.953069
19	WRIGHT COUNTY	2060.483	-556.573	0.96136
20	WRIGHT COUNTY	1231.764	12.9514	0.943927
21	WRIGHT COUNTY	727.4203	673.1695	0.899084
22	WRIGHT COUNTY	2727.254	1691.147	0.951131
23	WRIGHT COUNTY	1672.368	15621.62	0.963422

4.2.13 Resilient Modulus Conclusions

Characterization of unbound materials in the MEPDG was reviewed in this portion of the project and applied it to Minnesota subgrades. The main emphasis was made on collection of k_1 , k_2 , and k_3 parameters for Minnesota fine-grained soil and the procedure for interpretation of the resilient modulus test to provide an input to the MLET analysis (Level 2 input). This is an important aspect of adaptation of the MEPDG, because the Guide recommends measurement of resilient moduli from the laboratory testing, but the procedure of interpreting the test data to obtain an input for an MLET analysis lacks specifics.

The procedure for conversion of the k_1 - k_2 - k_3 model into a modulus of elasticity for the level 2 input was refined. Rapid solutions were developed to eliminate direct use of the MLET program and make execution of the procedure less tedious. This allowed conducting a comprehensive sensitivity analysis of the effect of base, subbase, and subgrade k_1 - k_2 - k_3 parameters on resulting moduli of elasticity. It was found that for the same pavement structure, and asphalt modulus, the subgrade modulus is mostly affected by the subgrade k_1 parameter, followed by subgrade k_3 parameter. Although base and subbase material properties affected subgrade modulus of elasticity, the effect was less significant than from these two parameters.

Analysis of the test results for 23 samples collected from several Minnesota locations indicated that the k_1 , k_2 , and k_3 parameters may vary in wide ranges. These 23 combinations of the k_1 , k_2 ,

and k_3 parameters were converted into to subgrade moduli of elasticity for a wide range of pavement structures. The obtained elastic moduli were compared with the MEPDG recommended ranges for subgrade moduli of elasticity based on the soil classification (Level 3 inputs). The MEPDG Level 3 ranges – recommended moduli of elasticity based on the soil classification – were found to be reasonable.

It was found that the effective pavement stiffness may significantly affect the subgrade resilient modulus. Since the AC modulus may vary significantly, especially in a climate such as that of Minnesota, it is important to adjust the subgrade modulus not only for the change in moisture conditions, but also for the change in the effective pavement stiffness. Currently, the default seasonal adjustment procedure accounts only for seasonal variation in moisture conditions.

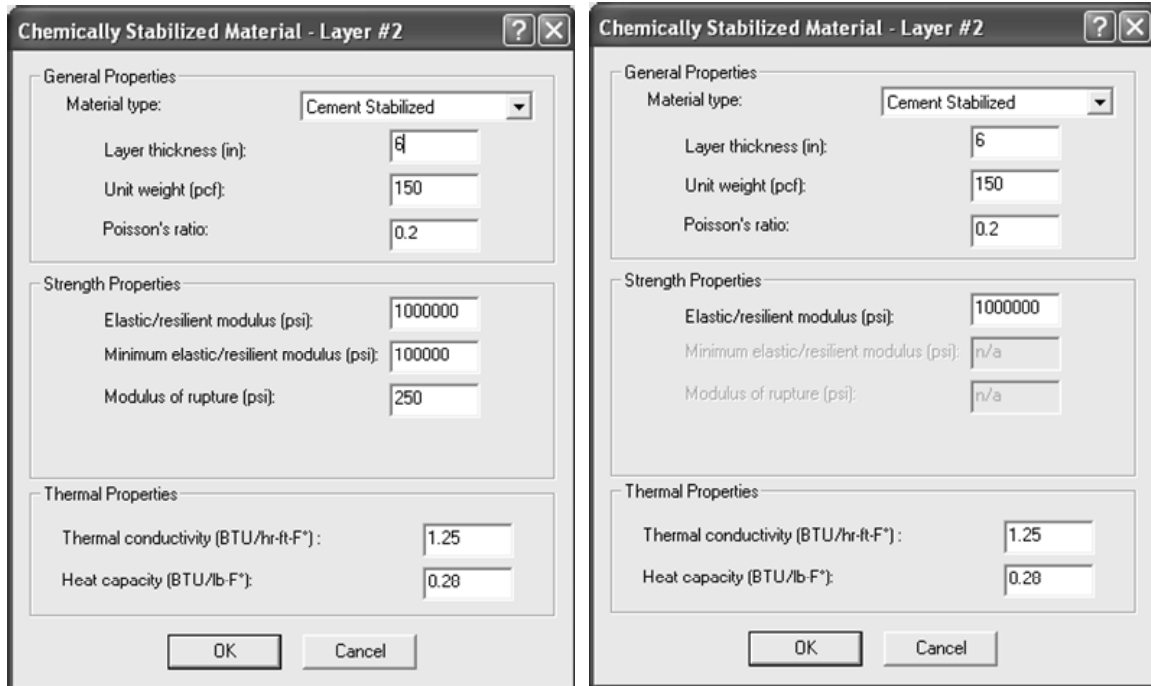
4.3 Stabilized Base Characterization

4.3.1 Design Guide Inputs

The MEPDG version 1.00 recognizes the following materials in the chemically stabilized group:

- Lean concrete,
- Cement stabilized,
- Open graded cement stabilized,
- Soil cement,
- Lime-cement-fly ash, and
- Lime treated materials.

Cementitiously stabilized layers can be used for design with both flexible and rigid pavements. Figure 4.20 shows the current MEPDG user interface for a cement stabilized layer. Other stabilizers can be selected from the “Material type” drop box. The user interface requires the same input options for all types of stabilized materials, but this requirement varies slightly with the type of pavement in consideration. The flexible design considers a reduction in the stiffness of a stabilized layer over time under loading, whereas rigid design assumes that the stiffness is constant. The effect of moisture or temperature (freeze-thaw) on layer stiffness is not considered in rigid nor flexible design in MEPDG analysis. This may be a significant drawback in characterizing stabilized soil layers.



(a)

(b)

Figure 4.20 MEPDG user interface of cement stabilized layer for (a) flexible pavement and (b) rigid pavement.

The MEPDG requires the input of the material, strength and thermal properties of cementitious materials for the design procedure. The properties required are as follows:

- Layer thickness
- Unit weight
- Initial 28-day elastic modulus (E) or resilient modulus (Mr)
- Poisson's ratio
- Minimum elastic modulus or resilient modulus after damage from traffic – For flexible pavements deterioration of cement stabilized materials is highly correlated to repeated traffic loading. However, MEPDG currently assumes values to be used in the design as rational procedure exists to determine these values.
- Initial 28-day flexural strength – This value is an input requirement for flexible pavements only.
- Thermal conductivity and specific heat capacity – These parameters are used by the Enhanced Integrated Climatic Model (EICM) for temperature prediction.

4.3.2 Design Guide Concerns

MEPDG accounts for the effects of stabilization through the effect of higher layer stiffness on critical structural responses (stresses, strains, deflections), thus influencing pavement damage due to axle loading and predicted pavement distresses. In addition, the MEPDG framework accounts for fatigue damage and cracking in the CTB layer for flexible pavements and a

reduction in base erodibility for rigid pavements. The MEPDG does not consider environmental degradation (e.g. freeze-thaw damage or thermal and hygral shrinkage) of stabilized layers.

There are some concerns regarding MEPDG viability in designing pavements with cementitious stabilized layers. The research team has identified several issues with the software, supporting documentation, and the distress model used for predicting semi-rigid performance that raises concern.

4.3.2.1 Issue 1. Calibration: The performance prediction models for semi-rigid pavement have never been calibrated. This is a problem, as any proposed modification to the layer properties in the semi-rigid models or other revisions to the model may be jeopardized by model calibration and the introduction of new, or dramatically changed existing, calibration parameters. The lack of calibration is noted in the MEPDG supporting documentation and in MEPDG software warning screens (Figure 4.21).

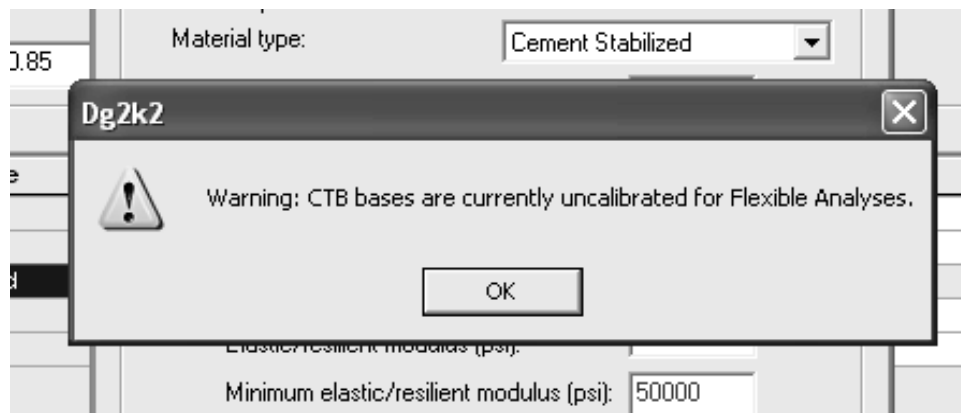


Figure 4.21 Warning screen for CTB layer in flexible pavement.

4.3.2.2 Issue 2. Saving Changes: According to the supporting documentation for MEPDG software version 1.0, for analysis involving semi-rigid pavements, “any changes made to the default values are not saved by the MEPDG software. The values entered always divert back to the default value when the software is run.”

The MEPDG semi-rigid analysis may be handicapped by the inability to work with the software using non-default values.

4.3.2.3 Issue 3. Modulus of Rupture Input: The typical modulus of rupture values suggested in the MEPDG online documentation for various stabilized layers is as shown in table 4.10. However, upon using these values in the user interface warning messages popped up stating that these values are outside of the typical range as shown in figure 4.22.

Table 4.10 Typical values for modulus of rupture (AASHTO 2008).

CSM	Typical MR value, psi
LCB	450
CTB	200
open graded CTB	200
soil cement	100
lime-cement-fly ash	150
lime stabilized soils	25

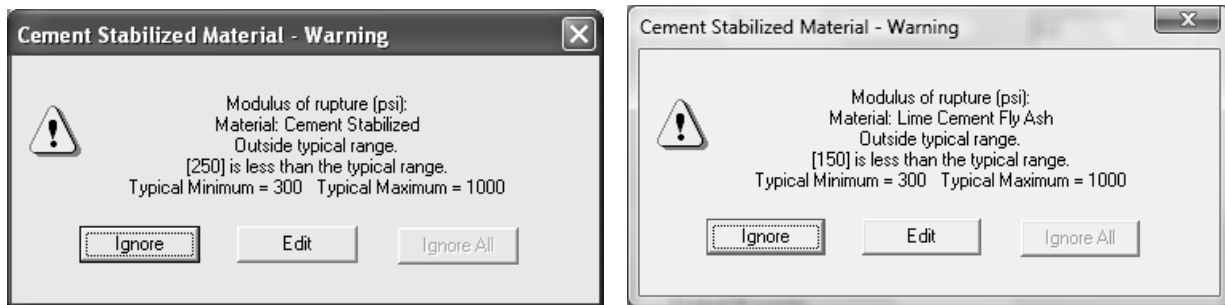


Figure 4.22 Warning messages for modulus of rupture values.

4.3.2.4 Issue 4. Model Implementation: The semi-rigid models for distress and performance do not appear to have been completely implemented. If they have been partially implemented, as claimed in the MEPDG supporting documentation, there is evidence to suggest this implementation was not successful.

The documentation states that “MEPDG predicts reflection cracks in HMA overlays or HMA surfaces on semi-rigid pavements using an empirical equation.” However, while it is true that reflective cracking results are provided for AC overlay analysis (illustrated in Figure 4.23), reflective cracking is not implemented for semi-rigid analysis (illustrated in Figure 4.24).

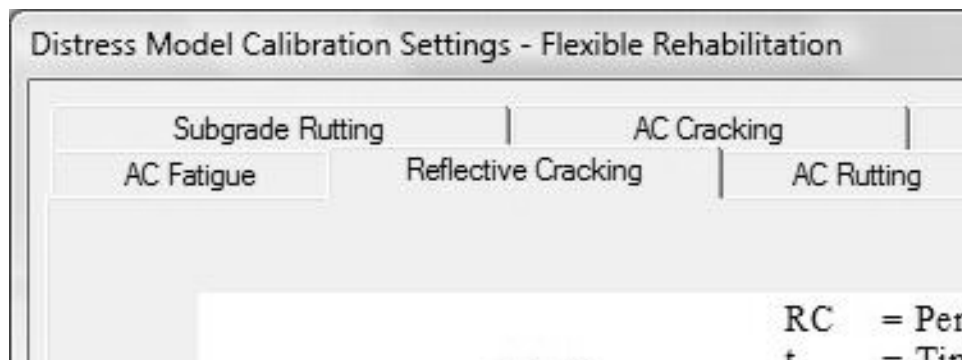


Figure 4.23 MEPDG screenshot illustrating presence of reflective cracking models in AC overlay analysis.

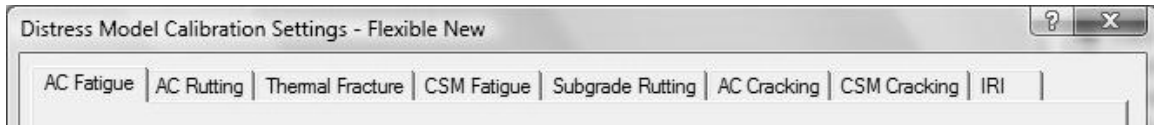


Figure 4.24 MEPDG screenshot suggesting absence of reflective cracking models in flexible analysis.

A comparison of Figures 4.22 and 4.23 reveals that while the Reflective Cracking tab (and corresponding content) is present for AC overlay analysis, it is not present for the analysis of a new flexible pavement. Also, the project output files for new flexible projects do not contain information on the extent of reflective cracking. Hence, the semi-rigid models may be only partially implemented in that performance models for reflective cracking are excluded for new flexible pavements.

4.3.2.5 Issue 5. Model Implementation: The robustness of the implementation of the CTB distress model also is the subject of concern. This can be illustrated using the following arbitrary example for flexible pavements shown in Table 4.11. A new flexible pavement project can be created in MEPDG with the following structure and features.

Table 4.11 Example of new flexible pavement designed in MEPDG for analysis.

Design	Flexible (New)	Structure	
Design life	10 years	Surface	AC, 6 inches, PG 58-38
Climate	O'Hare, Chicago, IL	Base	CTB, 3 inches, Initial modulus = 100,000; Modulus after damage = 50,000; Modulus of Rupture = 250; Poisson's ratio = 0.2, unit weight = 150 pcf
AADTT	25000	Subbase	A-6, 4"
Flexible ESALs	58,600,591	Subgrade	A-6, semi-infinite
<i>All else</i>	MEPDG defaults	<i>All else</i>	MEPDG defaults

After running this example for nearly 60 million flexible ESALs, an examination of the results produced by MEPDG for this new flexible system—incorporating a stabilized layer and thus semi-rigid—is very compelling. Most notable in these results is the lack of degradation in the modulus of elasticity of the CTB layer, as evidenced by Figure 4.25.

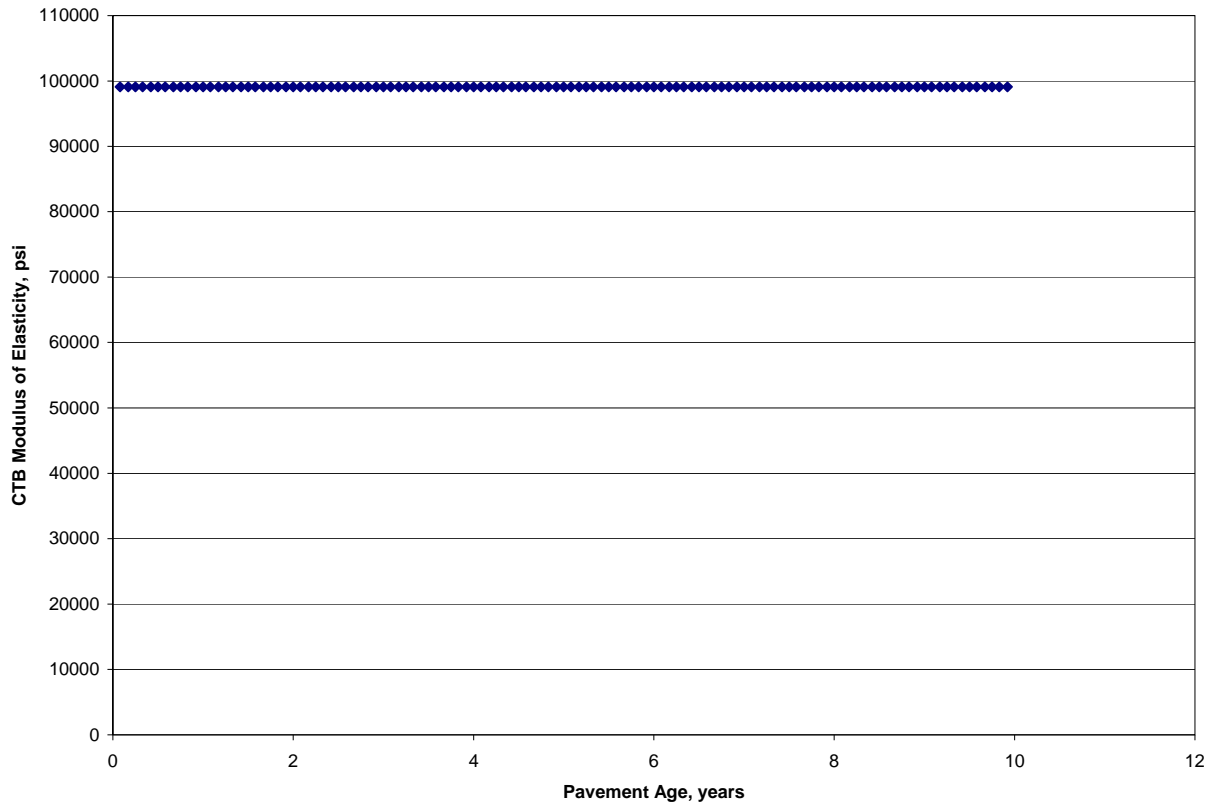


Figure 4.25 Absence of any degradation of the modulus of elasticity of a CTB layer in a new flexible system after 10 years and 60 million flexible ESALs from MEPDG version 1.00.

The concept of the equivalent damaged elastic modulus is one that is proposed in a distress model for CTB in the semi-rigid models. This model is discussed only in the presentation of an equation and is not supported with any citation or further comments in the MEPDG supporting documentation. However, its presence suggests that it should have a noticeable influence on the modulus of elasticity in the MEPDG results: if this is so, then this key distress model is not incorporated into the MEPDG as Figure 4.25 clearly indicates no effect is reported. If the model is implemented, then Figure 4.25 suggests that it may be implemented incorrectly if the long-term degradation concept is sound.

4.3.3 Stabilized Base Conclusions

As discussed above, there are issues with the MEPDG with regards to stabilized base. Therefore, it is not recommended to use the current version of the MEPDG for design of flexible pavements with stabilized layers.

4.4 Asphalt Binder Characterization

The MEPDG provides several alternative input levels as described in Chapter 2. To evaluate the consistency between level 2 and level 3 inputs for asphalt binders, two MEPDG projects were run for the same flexible pavement and site conditions. The asphalt pavement was located in

Columbus, Ohio with an AADTT of 4000. The pavement structure was as follows: 12 in. of AC layer with PG 58-28 binder, 6 in. of A-1-a base, and A-6 subgrade.

First, the structure previously described was analyzed using level 3 input for the asphalt binder. After the analysis was performed, the binder rheological constants from equation 2.1 in Chapter 2, A and VTS, default values for PG 58-28 binder were used to generate complex shear modulus $|G^*|$ and phase angle δ at 10 rad/s. To accomplish this task, equation 2.1 with $A = 11.01$ and $VTS = -3.701$ was used to obtain binder viscosities, η , at various temperatures. Then, the following equation was used to obtain at complex shear modulus for each temperature:

$$\eta = \frac{|G^*|}{10} \left(\frac{1}{\sin \delta} \right)^{4.8628} \quad (4.24)$$

Table 4.12 shows the values of the complex modulus and phase angle for different temperatures for a typical PG 58-28 binder.

Table 4.12 $|G^*|$ and δ at $\omega = 10$ rad/sec for PG 58-28 binder.

Temp (°F)	G^* (Pa)	δ (°)	η (cP)
40	50000000	9.42	3.3228E+10
70	45000000	24.91	3.0158E+08
100	3000000	30.40	8.2300E+06
130	2000000	55.87	5.0148E+05

The binder data presented in Table 4.12 was used as input for level 2 analysis. The MEPDG performance predictions for the asphalt pavement using level 2 and 3 are presented in Figures 4.26 to 4.29. Significant differences between the predicted distresses are observed although the same material, load and environmental conditions were used. A more detailed analysis identified that the binder behavior predictions from level 2 input was not consistent with the input information.

Based on this analysis it was recommended to limit asphalt mix characterization to level 3 inputs.

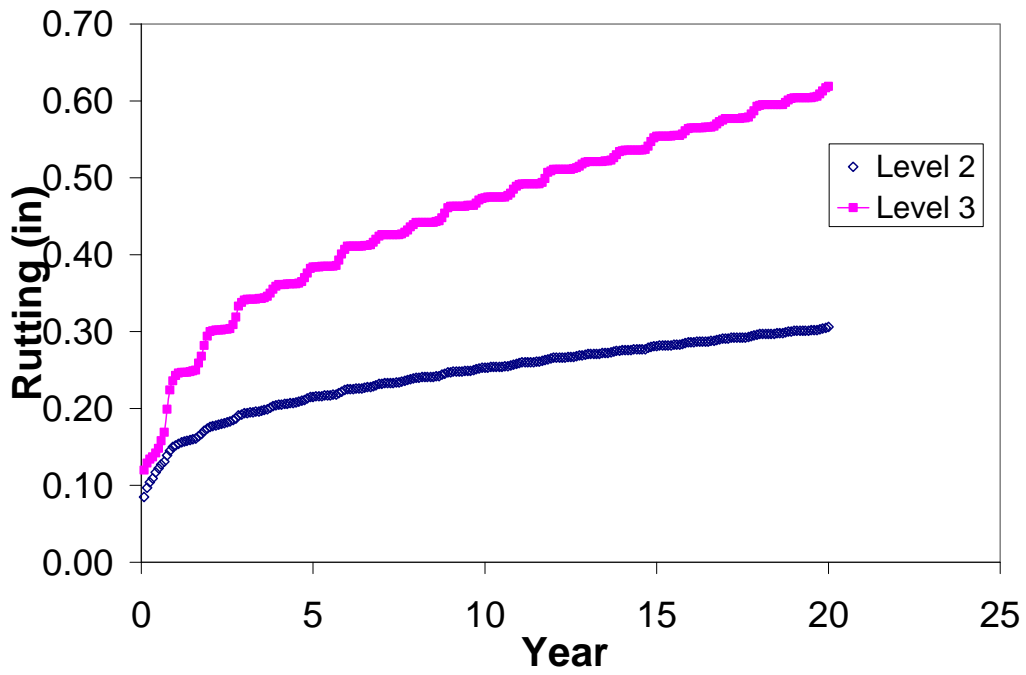


Figure 4.26 Rutting vs. time for AC pavement located in Columbus, Ohio.

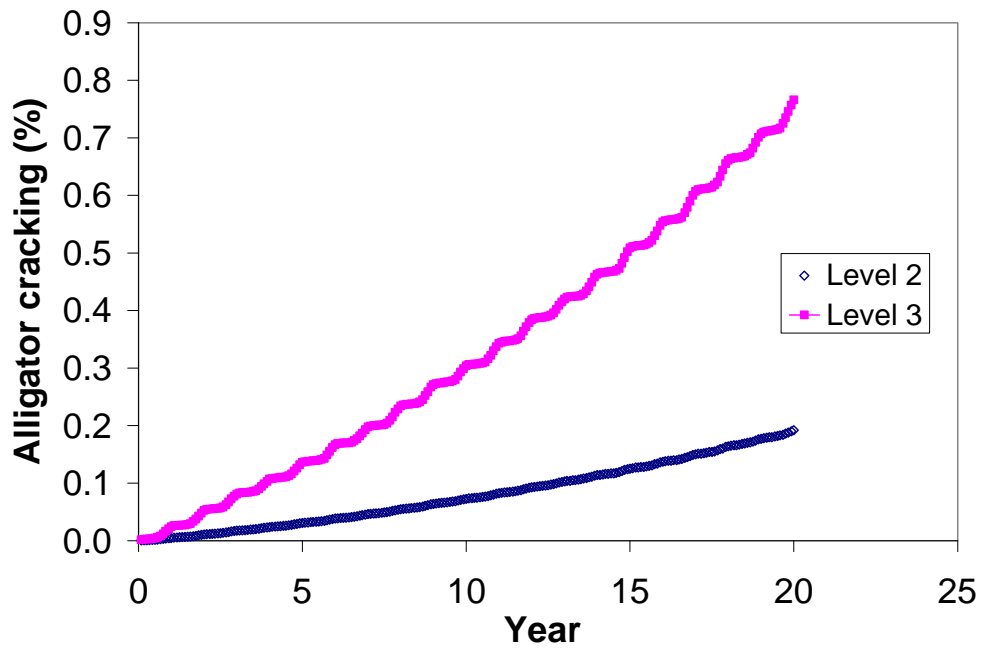


Figure 4.27 Alligator cracking vs. time for AC pavement located in Columbus, Ohio.

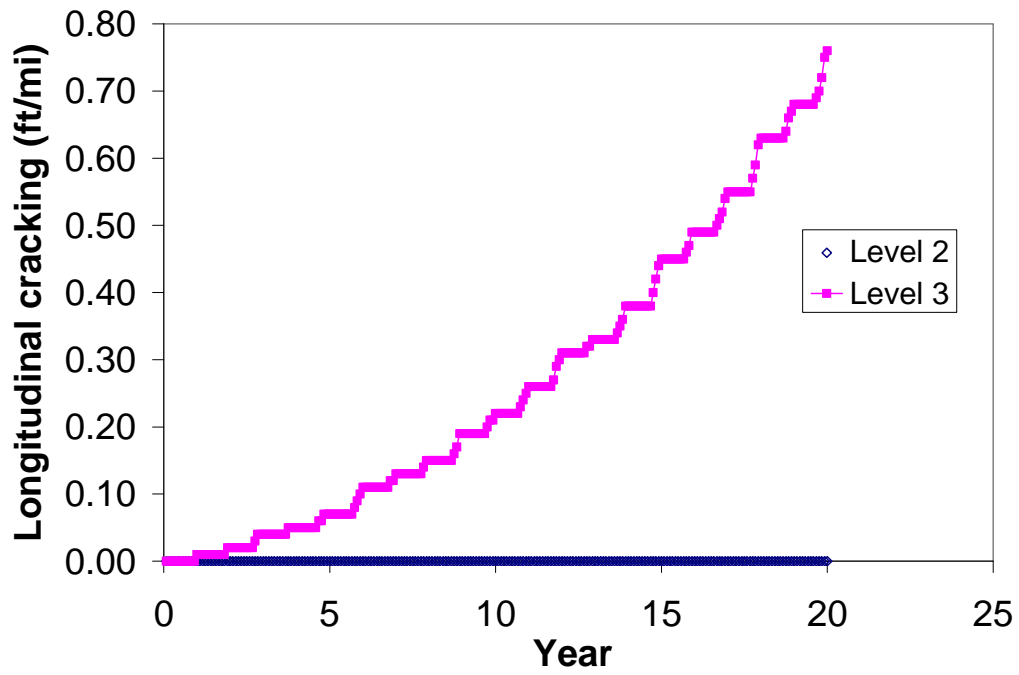


Figure 4.28 Longitudinal cracking vs. time for AC pavement located in Columbus, Ohio.

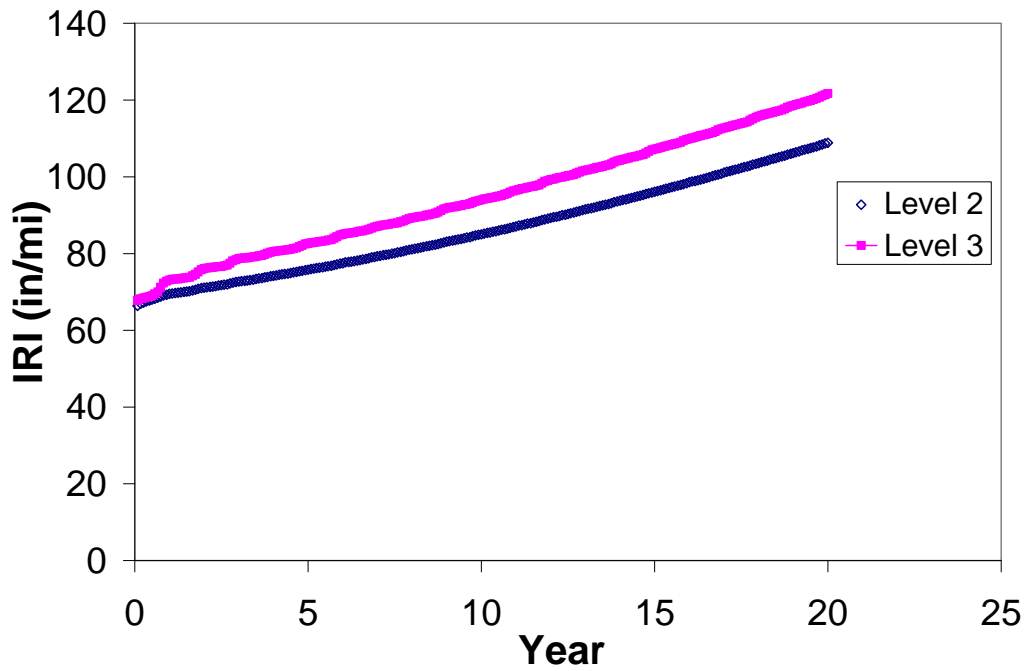


Figure 4.29 IRI vs. time for AC pavement located in Columbus, Ohio.

4.5 Asphalt Binder Characterization

Climatic data significantly affects MEPDG pavement performance prediction. However, until recently, all climate sensitivity studies only include data from a limited number of locations. The MEPDG uses pavement location to determine climate inputs. For a specific location, the MEPDG software permit the user to create a virtual weather station using up to the 6 nearest weather stations, selected from a database containing 851 weather stations. In this study, a comparison of pavement performance predictions for locations in close proximity was made. The same pavement structure and site conditions were considered. Inputs other than that listed in Table 4.13 were equal to the MEPDG default values.

Table 4.13 Input Summary for pavement structure.

Design	JPCP		PCC	JPCP, 9 in
Design Life	20 years		Granular Base	A-1-a, 8 in
AADTT	10775		Subgrade	A-6, semi-infinite
Water Table Depth	5ft		<i>All Else</i>	MEPDG defaults

First the MEPDG analysis was performed for two different locations in Minnesota (Minneapolis and St. Cloud) with these inputs. The climatic files were generated using the nearest weather station (MSP airport for Minneapolis and St. Cloud Regional Airport for St. Cloud). Although these locations are within 50 miles, a significant difference was observed in the transverse cracking obtained for these two locations as only 19.9% slabs cracked in Minneapolis while 75.3% slabs cracked for St. Cloud.

To study the effect further, three additional locations were selected between Minneapolis and St. Cloud as shown in figure 4.30. Several climatic files were generated. These files consisted of three categories, namely:

1. Group 1 – Only the first weather station (out of the six listed) used to generate the climatic file for a specified location. This station was always closest to the location (latitude, longitude, and elevation) entered.
2. Group 2 – All six weather stations were selected.

The weather stations listed by MEPDG were out of the eight (8) different locations shown in figure 4.31. A total of 8 cases were generated for 5 locations. For two locations, the group 1 climatic files could not be generated. The error message that was obtained for the St. Cloud location is shown in figure 4.32. A similar message was obtained for location 4. Some of the hourly climatic data (hcd) files do not contain complete information. As shown in figure 4.33, the St. Cloud weather station has missing information and is marked by the MEPDG interface with symbol (M). It should be noted that the Minneapolis International Airport weather station and several other stations in the state are denoted by the MEPDG software with the symbol (C), which means that the stations do not have missing data.

Table 4.14 documents the percent of cracked slabs predicted by the MEPDG after 20 years of opening to traffic. The outputs varied significantly between locations 1 through 3 in comparison to locations 4 and 5. Predictions for locations 1 through 3 are similar for both ways of generating the climatic files. Considering that the predictions for locations 4 and 5 are dominated by the questionable weather station, it can be concluded that the use of weather stations with missing data should be avoided in the generation of climatic files.

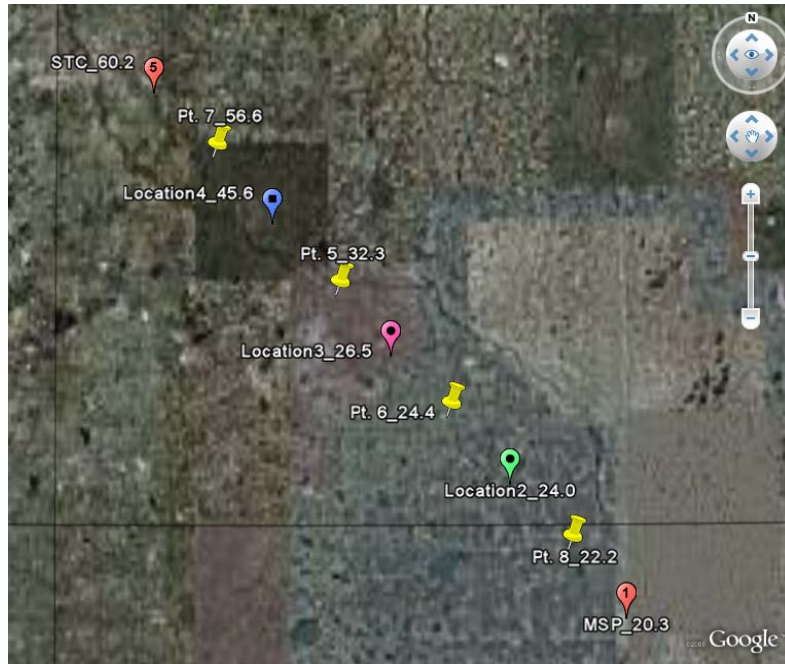


Figure 4.30 Additional locations selected between MSP and STC. (Source: Google Earth)

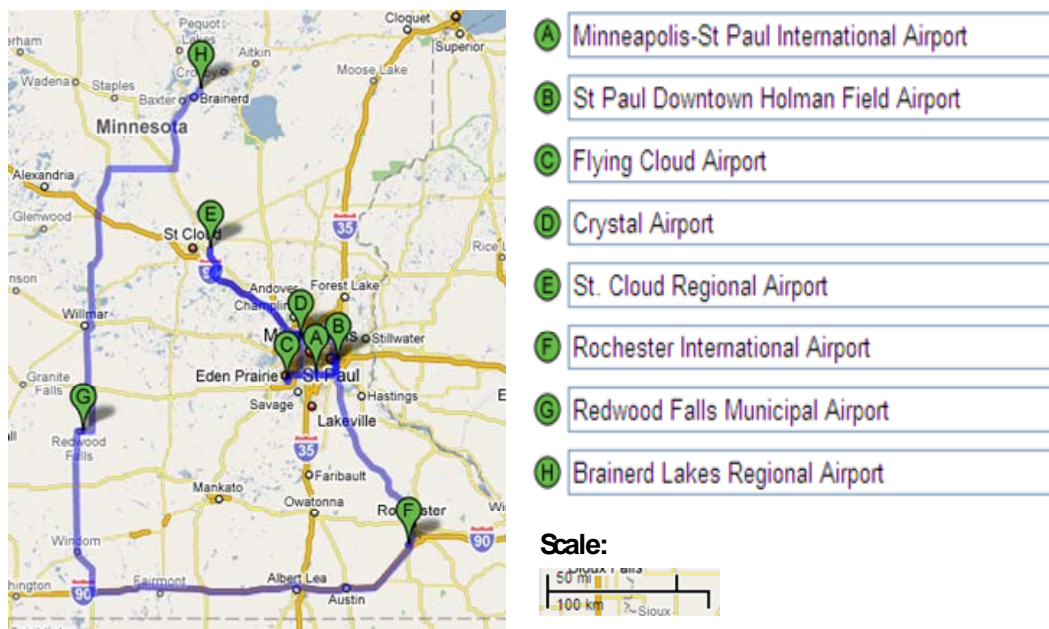


Figure 4.31 Location of weather stations listed by MEPDG for Minnesota. (Source: Google Maps)

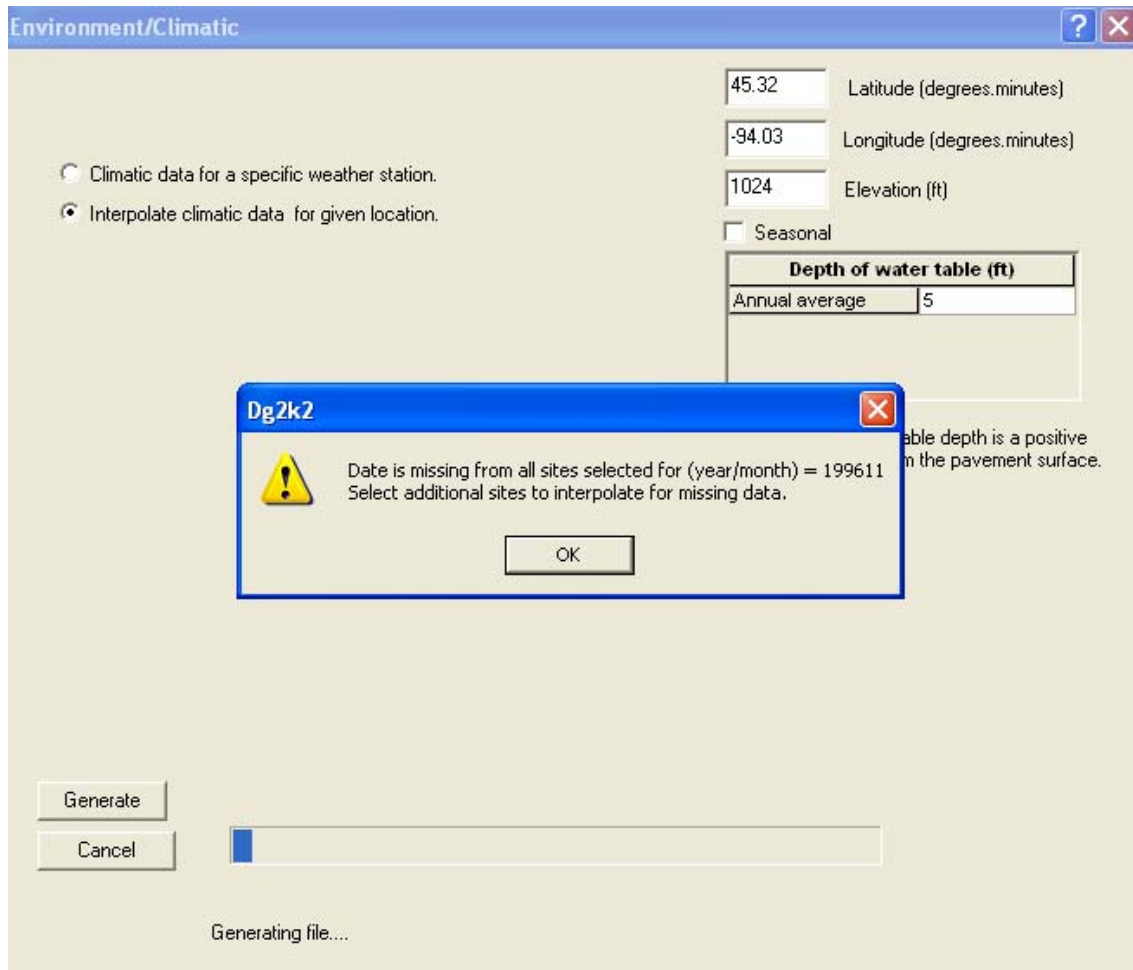


Figure 4.32 MEPDG interface showing error for missing data.

Table 4.14 Percent slabs cracked for locations in Minnesota.

Locations	Lat	Long	Elev	% Cracking after 20 years for weather station	
				Nearest Only	All
Location 1 (Minneapolis)	44.53	-93.14	874	19.9	19.9
Location 2	45.027	-93.261	918	22.3	21.2
Location 3	45.125	-93.383	869	22.6	23.1
Location 4	45.223	-93.506	961	NA*	52.4
Location 5 (St. Cloud)	45.32	-94.03	1024	NA*	75.3

NA*: See section on “Missing Months”

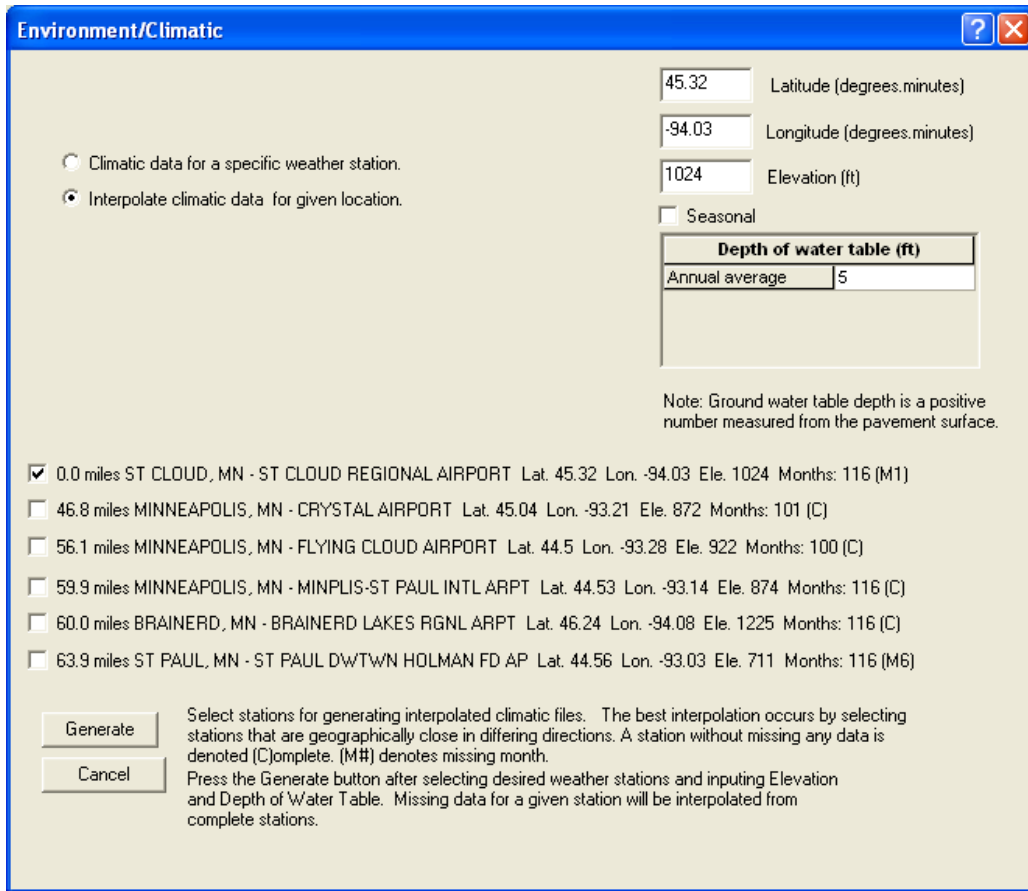


Figure 4.33 MEPDG interface showing number of missing months.

Chapter 5 Recalibration of MEPDG Prediction Models

5.1 Introduction

A recalibration of the Mechanistic-Empirical Pavement Design Guide (MEPDG) version 1.0 distress prediction models was performed for both asphalt and concrete pavements to reduce bias and error of the design procedure. For flexible pavements the following performance models were investigated: rutting, alligator cracking, transverse cracking and IRI. For rigid pavements the faulting, cracking, and IRI models were considered.

The research approach for this task involved the following steps:

- Identify pavement sections with known performance data.
- Obtain the MEPDG inputs that closely represent the asphalt and concrete MnROAD sections.
- Run the MEPDG software for flexible and rigid test cells to obtain predicted distresses.
- Compare predicted and measured distresses for both asphalt and concrete test sections.
- Recalibrate distress models of the MEPDG by adjusting current models to reduce error between predicted and measured performance.

Details and results of the recalibration process for each pavement performance model are presented below.

5.2 Flexible Pavements

The MEPDG for flexible pavements includes the following performance prediction models:

- Rutting
- Alligator cracking
- Transverse cracking
- Longitudinal cracking
- International Roughness Index (IRI)

The information for the MnROAD mainline sections was used for the model recalibration. The mainline is a 3 ½ mile part of westbound Interstate Highway 94 that contains 31 test cells and carries an average of 26,400 vehicles daily. All of the collected data is entered into the MnROAD database for the Minnesota Department of Transportation (MnDOT).

The rutting data used in the recalibration was collected from asphalt cells 1 through 4 and 14 through 22 as shown in Figure 5.1.

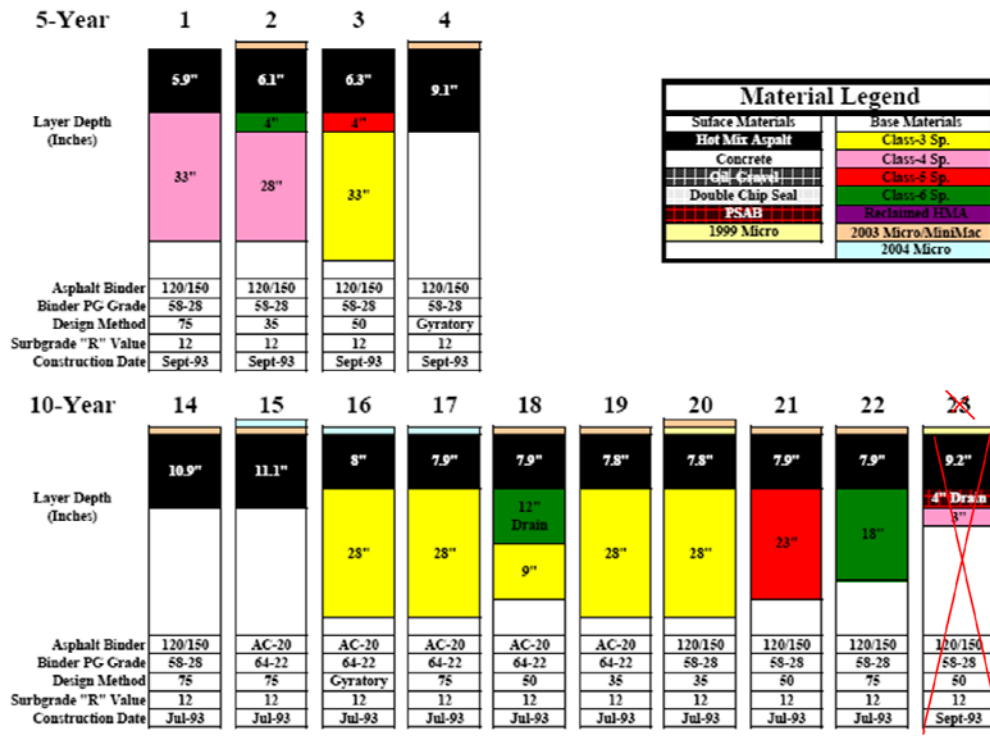


Figure 5.1 MnROAD test sections with design details of the asphalt sections, updated August 2005 (MnROAD 2008).

The sections with various design variables are subjected to the same environmental and traffic loading. Design variables include asphalt binder grades, mix designs, air void content, drainable layers, crown location, hot mix asphalt (HMA) thickness, base type, and base thickness (see Table 5.1). The aggregate sources for the HMA mix were consistent for each cell and the mix design was also held consistent throughout the lifts for each cell (no difference in base and wear courses). The subgrade is clay with an R-value of 12.

The details of the recalibration process for each model are provided below.

Table 5.1 Design parameters of the measured and predicted rutting cells (MnROAD 2008).

Cell	Design Life	Asphalt PG Grade/Type	Asphalt Mix Design/(Blows)	Thickness (inch)	Base Inch / Class	SubBase Inch / Class	Edge Drains	Subgrade R-Value	1993-94 Mean Air Void Percent	2001 Mean Air Void Percent	Change in Air Void %	Paving Crown
1	5 Year	PG 58-28 (120/150)	Marshall (75)	5.9	33" Class-4	--	--	Clay R-12	6.8%	5.7%	-1.1%	Quarter
2			Marshall (35)	6.2	4" Class-6	28" Class-4	--		4.5%	4.0%	-0.5%	Quarter
3			Marshall (50)	6.2	4" Class-5	33" Class-3	--		7.2%	4.6%	-2.6%	Quarter
4			Marshall (75)	9.1	--	--	--		7.2%	6.0%	-1.2%	Quarter
14	10 Year	PG 64-22 (20)	Marshall (75)	11.4	--	--	--		6.0%	6.1%	0.1%	Quarter
15			Marshall (75)	11.4	--	--	--		7.3%	7.1%	-0.2%	Quarter
16			Gyratory	8.2	28" Class-3	--	--		7.8%	7.6%	-0.2%	Centerline
17			Marshall (75)	8.2	28" Class-3	--	--		7.7%	6.4%	-1.3%	Centerline
18			Marshall (50)	8.1	10" Class-6	9" Class-3	Yes	5.8%	5.3%	-0.5%	Centerline	

Cell	Design Life	Asphalt PG Grade/Type	Asphalt Mix Design/(Blows)	Thickness (inch)	Base Inch / Class	SubBase Inch / Class	Edge Drains	Subgrade R-Value	1993-94 Mean Air Void Percent	2001 Mean Air Void Percent	Change in Air Void %	Paving Crown
19			Marshall (35)	8.1	28" Class-3	--	--		6.5%	4.6%	-1.8%	Centerline
20		PG 58-28 (120/150)	Marshall (35)	7.9	28" Class-3	--	--		--	--	--	Centerline
21			Marshall (50)	7.9	23" Class-5	--	--		5.4%	4.4%	-1.0%	Centerline
22			Marshall (75)	7.8	18" Class-6	--	--		6.4%	6.1%	-0.3%	Centerline

5.2.1 Rutting

5.2.1.1 Definition: Rutting is an important distress to limit. It is often measured to determine rehabilitation and reconstruction needs in hot mix asphalt (HMA) pavements (Shalaby et al. 2006). A rut is a depression in the wheel path of an HMA pavement, caused by consolidation of the pavement layers and/or uplift in the pavement adjacent to the rut in the form of shoving. HMA pavements tend to rut when exposed to hot summer days due to a decrease in asphalt binder stiffness. Minimizing HMA pavement rutting is important in preventing accidents caused by hydroplaning (Huang 2004). The Minnesota Department of Transportation considers 0.5 in of rutting a level that can cause potential problems (Mulvaney and Worel 2002). The MnROAD database contains comprehensive performance data for rutting.

5.2.1.2 MnROAD Database: This section presents the evaluation of a specific set of MnROAD rutting data for hot mix asphalt pavement test sections with different pavement design parameters in comparison to the predicted rutting using design guide simulations for those cells. The MnROAD database contains information on 13 asphalt mainline sections (Cell numbers 1, 2, 3, 4, 14, 15, 16, 17, 18, 19, 20, 21, 22) that have been subjected to westbound traffic on I-94 from 1994 to 2003. The traffic that the truck and passing lanes have been exposed to in the time frame of this study is approximately 5 million and 1 million ESALs, respectively.

MnROAD rutting measurements were made approximately 3 times per year in the right and left wheel path in both the truck and passing lanes for each cell throughout the period MnROAD has been open to traffic. Over 1300 truck and passing lane rutting measurements from the MnROAD database are analyzed. An average of the right and left wheel path rutting was used for the analysis. It is important to note that Cell 20 failed and was rehabilitated with MicroSurfacing (1 Layer - 6 foot rut box filling) in both lanes, July 1999, and was thus excluded from the analysis.

Measurements of the total rutting do not reveal the level of rutting in the individual layers of the pavement system. To address this limitation, MnROAD personnel performed several forensic studies, which involved trenching of the flexible MnROAD sections. Trenches were cut for two thirds of the asphalt pavement sections in the mainline in 1998 while the remaining 6 sections were trenched in 2001. Detailed information on these studies can be found elsewhere (Mulvaney and Worel 2002). Both studies indicated that the majority of rutting only occurred in the upper lifts of the hot mix asphalt, with the granular base and subgrade mostly unaffected for the sections evaluated in this study.

Recalibration of the MEPDG rutting model was performed based on measured rutting values from those cells. There are many different ways to measure rut depth. MnROAD used 4 different methods to measure rutting over the life of the project. These methods include measuring manually with a straightedge, using a PaveTech van equipped with ultrasonic sensors, using a Pathway's vehicle with laser sensors and 3-point analysis, and using a newer Pathway's vehicle with laser sensors and 5-point analysis. Since the straightedge method was the only method used for the entire period from 1994-2003, this method was chosen to keep the collection method consistent from year to year. In this method the rutting was measured by MnROAD staff manually using a 6-foot straightedge with drill bits inserted underneath. By placing the six-foot straightedge on the rut, the maximum rut depth at the specific location can be found. Figure 5.2

demonstrates this type of rut depth measurement. It is important, though not easy, to have a consistent zero point when comparing rutting between wheel paths and sections. The database used for this study was gathered by taking the average of multiple rut depth measurements in the section. Two measurements were taken for each section from 1994 to 1996, then 10 measurements were taken for each section from 1997 to 2003 (Mulvaney and Worel 2002).

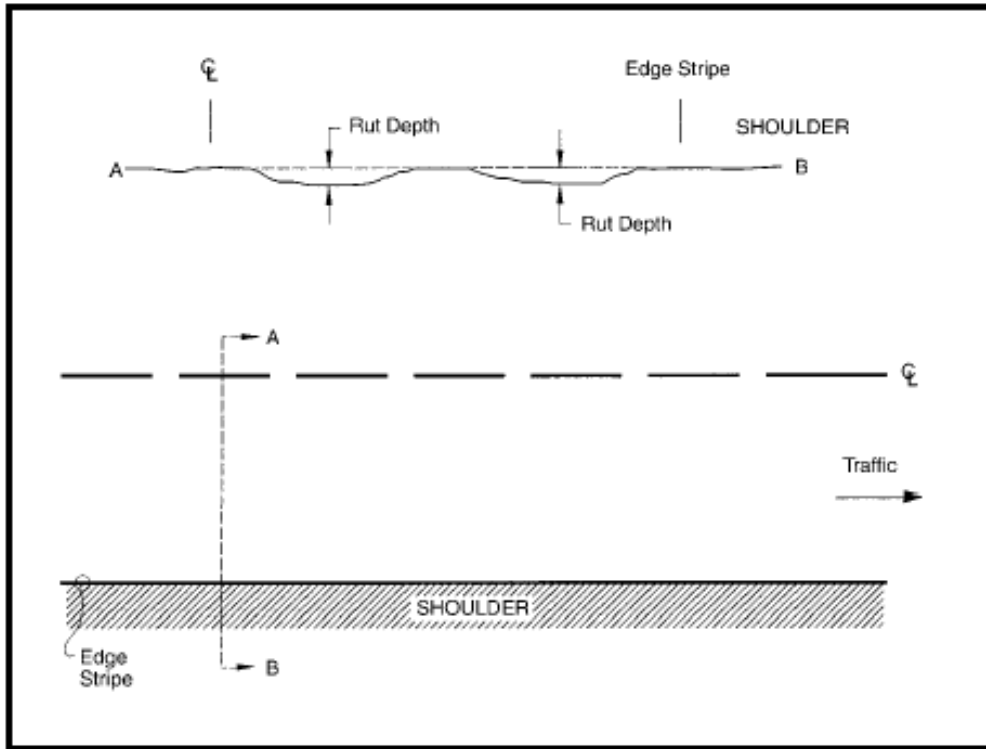


Figure 5.2 Straightedge method for measuring rut depth (Mulvaney and Worel 2002).

In this study, the performance of those cells was also simulated using the MEPDG software version 1.0. The design and traffic parameters of each cell were input when simulating the rutting. The measured material properties were used when available also, as shown by tables 5.2 through 5.4.

Table 5.2 Seasonal FHWA vehicle class distribution.

Month	FHWA Vehicle Class									
	Class 4	Class 5	Class 6	Class 7	Class 8	Class 9	Class 10	Class 11	Class 12	Class 13
January	0.50	0.75	0.59	0.59	0.46	0.88	0.88	0.88	0.88	0.88
February	0.59	0.79	0.71	0.71	0.50	0.93	0.93	0.92	0.92	0.92
March	0.61	0.87	0.87	0.87	0.61	1.00	1.00	0.97	0.97	0.97
April	0.86	0.93	0.92	0.92	0.73	1.03	1.03	1.10	1.10	1.10
May	1.00	0.99	0.86	0.86	0.83	1.01	1.01	0.98	0.98	0.98
June	1.16	1.06	1.15	1.15	0.98	1.12	1.12	1.00	1.00	1.00
July	1.14	1.14	1.18	1.18	1.23	1.05	1.05	1.06	1.06	1.06
August	1.22	1.37	1.15	1.15	1.47	1.08	1.08	0.94	0.94	0.94
September	1.42	1.23	1.41	1.41	1.68	1.11	1.11	1.10	1.10	1.10
October	1.26	1.05	1.29	1.29	1.11	0.99	0.99	1.08	1.08	1.08
November	0.88	0.92	0.80	0.80	0.60	0.88	0.88	0.94	0.94	0.94
December	0.53	0.86	0.73	0.73	0.49	0.94	0.94	1.07	1.07	1.07

Table 5.3 Base material properties.

<u>Gradation and Plasticity Index</u>	
Plasticity Index, PI:	1
Liquid Limit (LL)	6
Compacted Layer	No
Passing #200 sieve (%):	7.5
Passing #40	22.5
Passing #4 sieve (%):	77.5
D10(mm)	0.09118
D20(mm)	0.1992
D30(mm)	0.5682
D60(mm)	1.815
D90(mm)	10.9

Table 5.4 Subgrade material properties.

Subgrade Resilient Modulus at optimum moisture content	13,000 psi
Sieve	Percent Passing
#200	7.5
#80	20.8
#40	22.5
#10	62.5
#4	77.5
3/8"	87.5
1/2"	92.5
3/4"	95
1"	97.5
1 1/2"	100

The design guide predicts the rutting due to the subgrade, base, and AC layer. The total rutting is calculated by summing the rutting in the AC layer, base, and subgrade as shown in equation 5.1:

$$Total_Rutting = Rutting_AC + Rutting_base + Rutting_subgrade \quad (5.1)$$

where *Total_Rutting* is the predicted surface rutting, *Rutting_AC* is the predicted rutting in the asphalt layer only, *Rutting_base* is the predicted rutting in the base layer only, and *Rutting_subgrade* is the predicted rutting in the subgrade only.

The measured total rutting values could then be compared to the predicted rutting values for design guide simulations of those MnROAD cells with various cross-sections and material properties, subjected to the same traffic composition (number, type, and weight of vehicle). The development of rutting with time for both predicted and measured values was then evaluated in this manner in the truck lane for each cell individually.

When comparing the designed and predicted rutting values over the life of the pavement, the relationship could be separated into two groups:

- Group A: Cells where predicted AC rutting is similar to measured rutting: 1, 2, 3, 15, 17, and 22.
- Group B: Cells where predicted AC rutting is lower than measured rutting: 4, 14, 15, 19, 21 and low volume loop cells.

Figures 5.3 and 5.4 show examples of a measured and predicted rutting in the HMA, base, and subgrade for typical group A and group B cells, respectively.

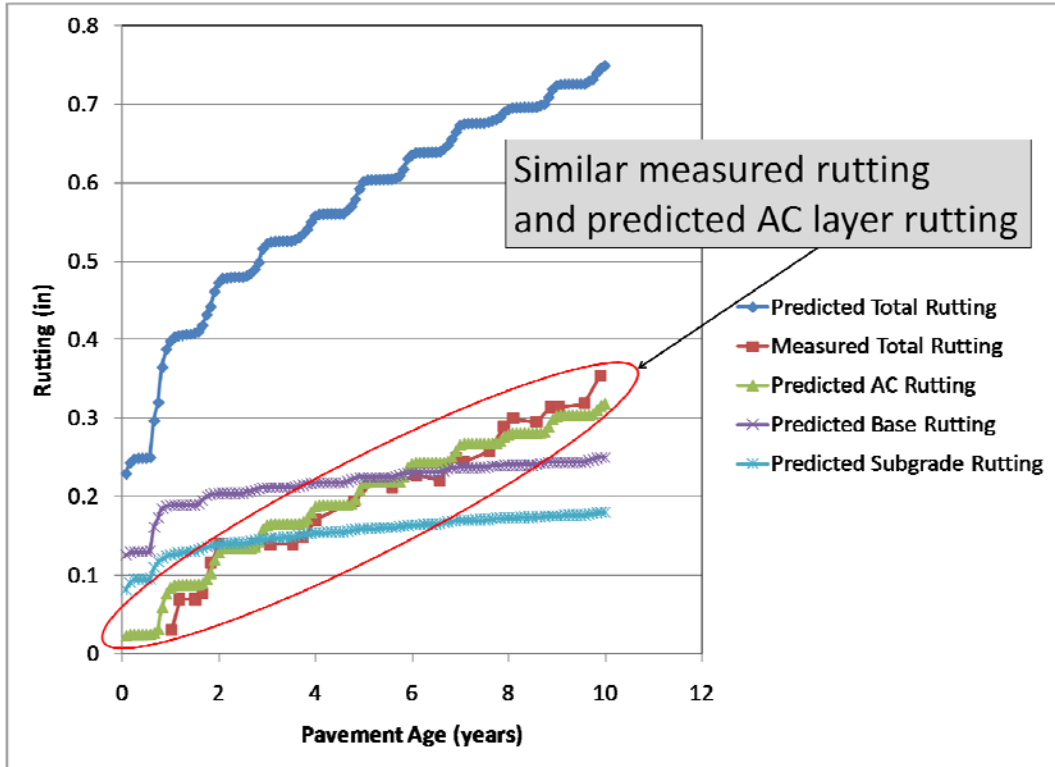


Figure 5.3 Group A measured and predicted rutting over the pavement age (Cell 1).

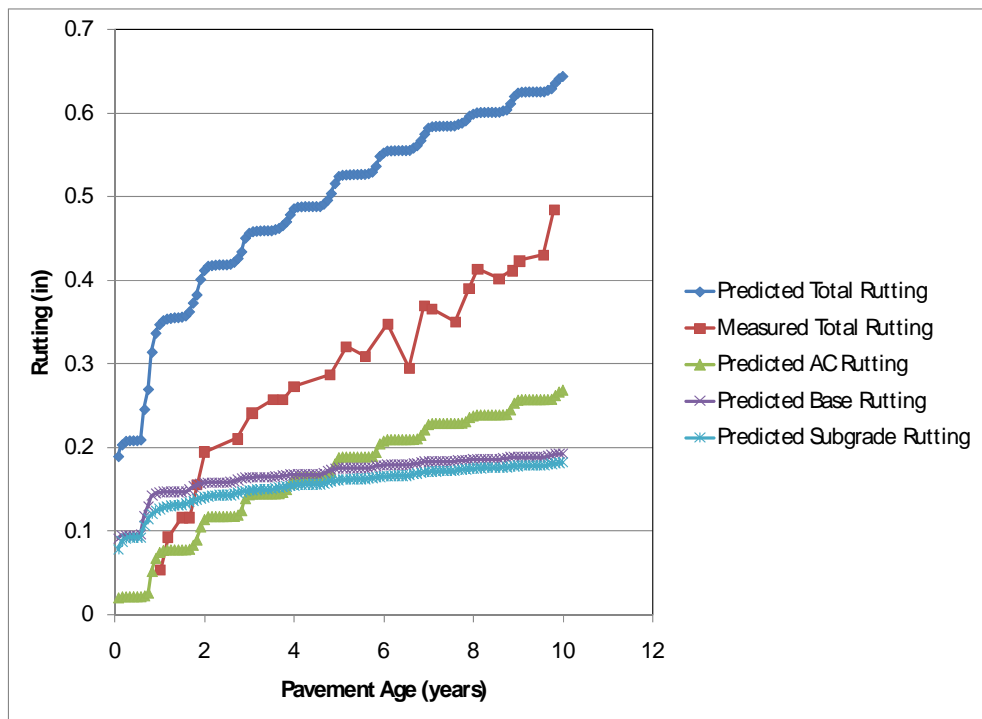


Figure 5.4 Group B measured and predicted rutting over the pavement age (Cell 2).

It can be observed in Figure 5.3 that the predicted HMA rutting is similar to the total measured rutting for the group A cells, represented by Cell 1, for the entire 10 year period. Since the MnROAD forensic studies showed that most of the measured rutting occurred in the HMA layer, analysis of group A cells leads to the conclusion that the MEPDG rutting model is fairly accurate in predicting rutting in the HMA layer, but the MEPDG subgrade and base rutting models grossly overestimate rutting. Therefore, the base and subgrade rutting model for the group A designs should be excluded from rutting prediction.

The observations presented above for group A, however, do not hold true for the cells in group B. For these cells, use of only the predicted rutting in the asphalt layer would greatly under-predict the rutting as shown in figure 5.4. However, use of the MEPDG total rutting model described in equation 5.1 would cause gross over-prediction, especially at early age. Therefore, to avoid under-prediction of the rutting model it is important to account for the base and subgrade. At the same time, the base and subgrade rutting model should be modified to avoid over-prediction of rutting, especially during early pavement ages.

Unfortunately, there are no distinguishable design characteristics between group A or group B cells. Some cells with very similar design parameters are placed in different groups when looking at the predicted versus measured rutting. Further investigation of the base and subgrade rutting prediction at early pavement age identified a consistently unrealistically high rutting prediction for the first month of pavement life. As can be observed from Figure 5.4 after the first month of a pavement life, cell 2 exhibited subgrade rutting of 0.08 inches. However, the predicted rutting after 10 years of pavement life in the subgrade was 0.18 inches. The cumulative number of heavy trucks after one month and ten years was 31,000 and 4.7 million, respectively. In the simulation, it was assumed that the pavement was opened to traffic in August. Although the pavement received less than 1% of heavy truck traffic in the first month of the life of the pavement, it accumulated almost 50% of the subgrade rutting, making it the highest monthly rutting accumulation during the pavement life. Furthermore, all subsequent rutting accumulation in August was negligible. Similar observations were made in the base layer predictions. Therefore it can be concluded that the first month subgrade and base rutting predictions are unrealistic and should be excluded during analysis.

The following modification of the MEPDG rutting model is proposed in this study:

$$\begin{aligned}
 Total_Rutting &= Rutting_AC + Rutting_base^* + Rutting_subgrade^* \\
 Rutting_base^* &= Rutting_base - Rutting_base_1 \\
 Rutting_subgrade^* &= Rutting_subgrade - Rutting_subgrade_1
 \end{aligned}
 \tag{5.2}$$

where *Total_Rutting* is the predicted surface rutting, *Rutting_AC* is the predicted rutting in the asphalt layer only, *Rutting_base** is the modified predicted rutting in the base layer only, *Rutting_subgrade** is the modified predicted rutting in the subgrade only, *Rutting_base* is the predicted rutting in the base layer only using the original MEPDG predictions, *Rutting_subgrade* is the predicted rutting in the subgrade only using the MEPDG original predictions. *Rutting_base_1* is the predicted rutting in the base layer only after one month, and *Rutting_subgrade_1* is the predicted rutting in the subgrade only after one month.

Figure 5.5 presents the predicted rutting for individual layers and total rutting using equation 5.2, as well as measured rutting for cell 2. Comparison of figures 4 and 5 shows that the modified equation 5.2 improves the prediction of the total rutting for the entire range of pavement age (especially early age). A similar trend was observed for all cells in group B. At the same time the modified equations reduces the discrepancy between predicted total rutting and measured rutting for the cells in group A. Figure 5.6 shows the predicted rutting using equation 5.2 for cell 1. As could be expected the total rutting is still greater than the measured rutting, but comparison with figure 5.4 shows that the difference between predicted total rutting and measured rutting from equation 5.2 is much less than from equation 5.1.

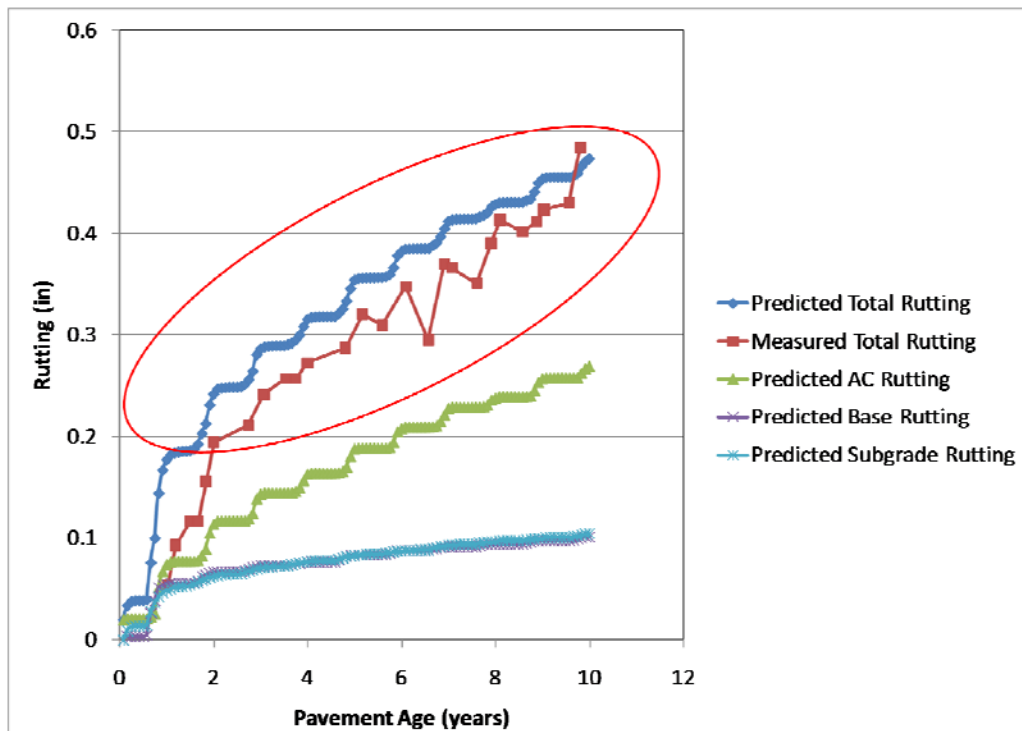


Figure 5.5 Cell 2 predicted and measured rutting versus pavement age using equation 2.

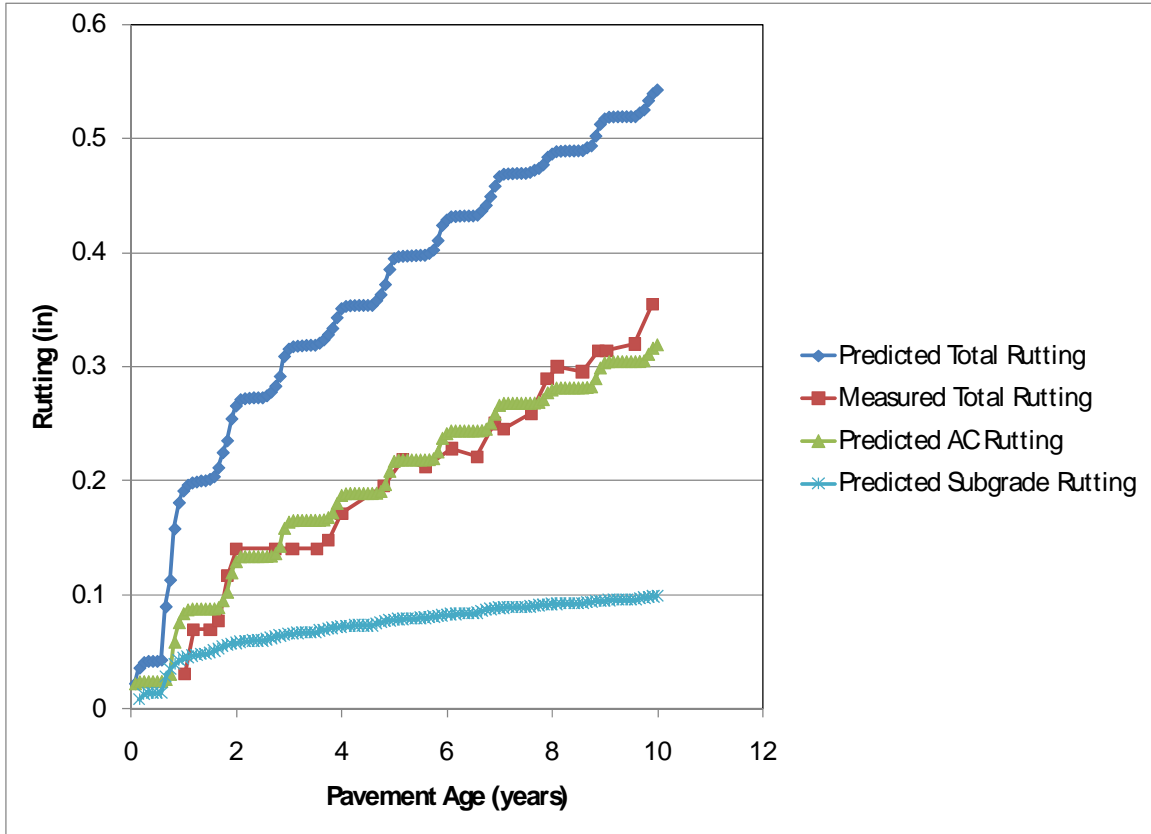


Figure 5.6 Cell 1 predicted rutting using equation 2.

To further illustrate the improvement of the predictive equation 2 versus equation 1, consider measured and predicted total rutting after 10 years of pavement life. Figures 5.7 and 5.8 show the comparison of measured versus predicted rutting after 10 years of pavement exposure using equations 5.1 and 5.2, respectively. It can be observed that the rutting predictions using equation 2 are less biased than the predictions using equation 5.1. Moreover, equation 5.1 fairly accurately predicted the rutting for two cells (cells 19 and 21), and over-predicted rutting for all other cells. Equation 5.2 only slightly under-predicts rutting for cells 19 and 21, fairly accurately predicts rutting for group the remaining cells in group B, and slightly over-predicts the rutting in group A. The advantages of the modified equation are even more obvious for prediction after five year (see figure 5.9). Equation 5.1 significantly over-predicted rutting for all of the cells, while equation 5.2 provided much better correspondence with the measured values. Figure 5.10 shows that equation 5.2 provides a reasonable estimate of the total rutting for the MnROAD cells (truck lane) after 5 and 10 years of traffic

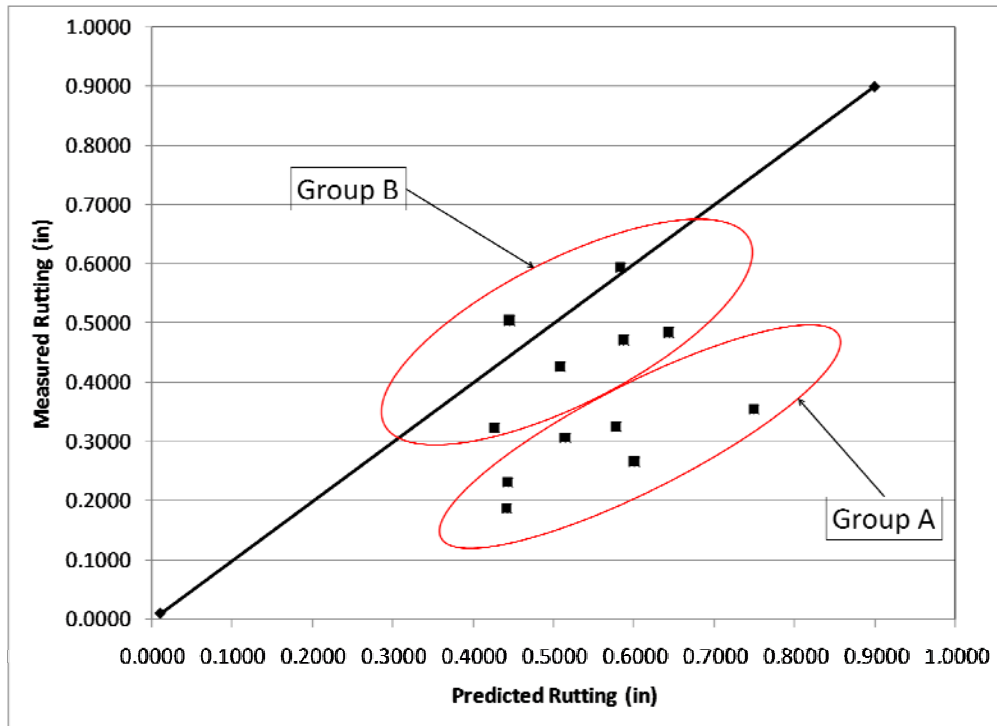


Figure 5.7 Measured versus predicted rutting after 10 years without subtraction of the initial base and subgrade rutting jump.

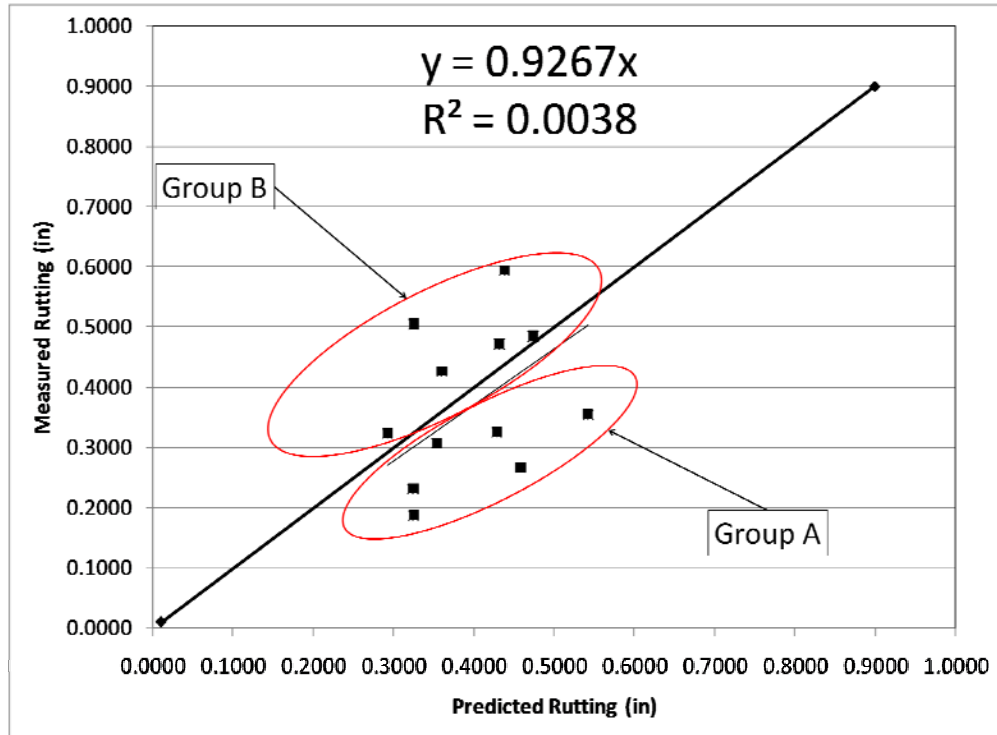


Figure 5.8 10 year total rutting after the correction for the initial subgrade and base rutting.

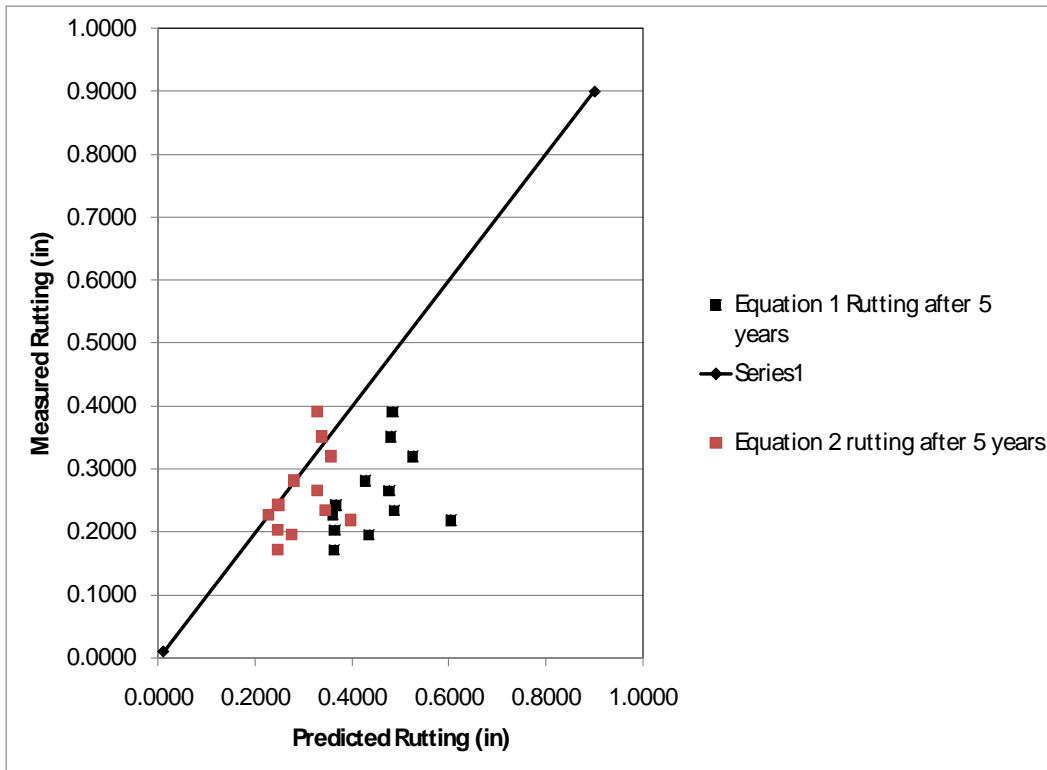


Figure 5.9 Total rutting predictions from 5.1 and 5.2 vs measured rutting after five years.

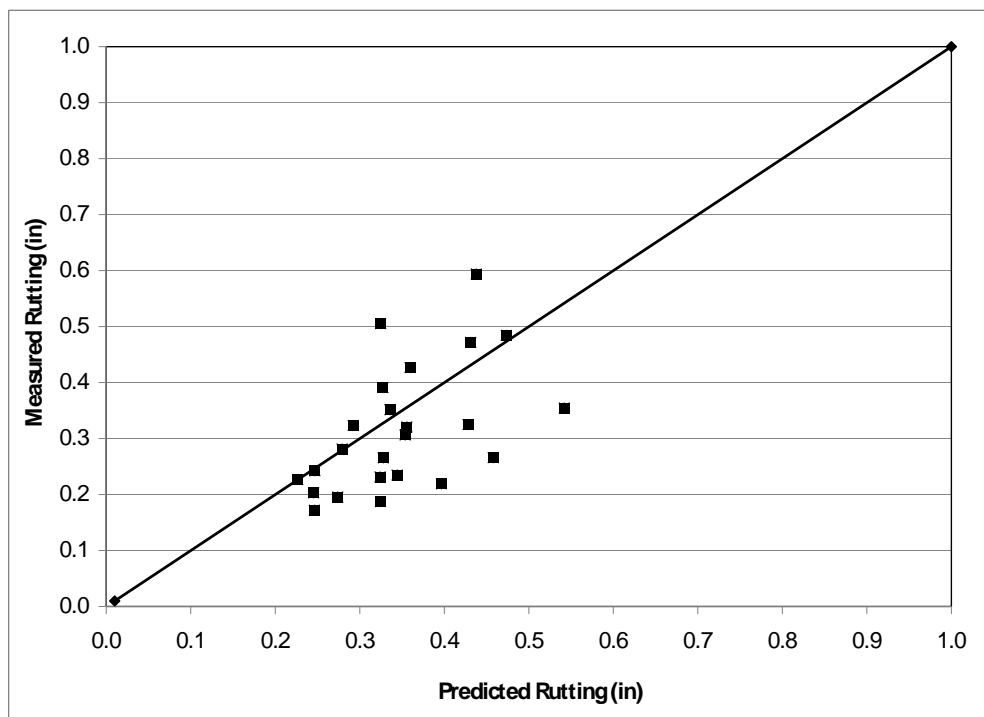


Figure 5.10 Predicted versus measured total rutting after five and ten years.

As discussed earlier, the rutting was measured in the passing lane as well as the truck lane. This gives information about the effect of a different traffic mixes on rutting during the same time period and the same climate. Figure 5.11 presents the comparison between measured and predicted rutting using equation 5.2 for both passing lane and truck lanes after 5 and 10 years in service. It can be observed that a reasonably good correspondence is achieved between measured and predicted rutting despite a wide range of design features, different traffic mixes, and different pavement ages. This suggests that the modified rutting model provided by equation 5.2 is an improvement over the original rutting model for Minnesota conditions.

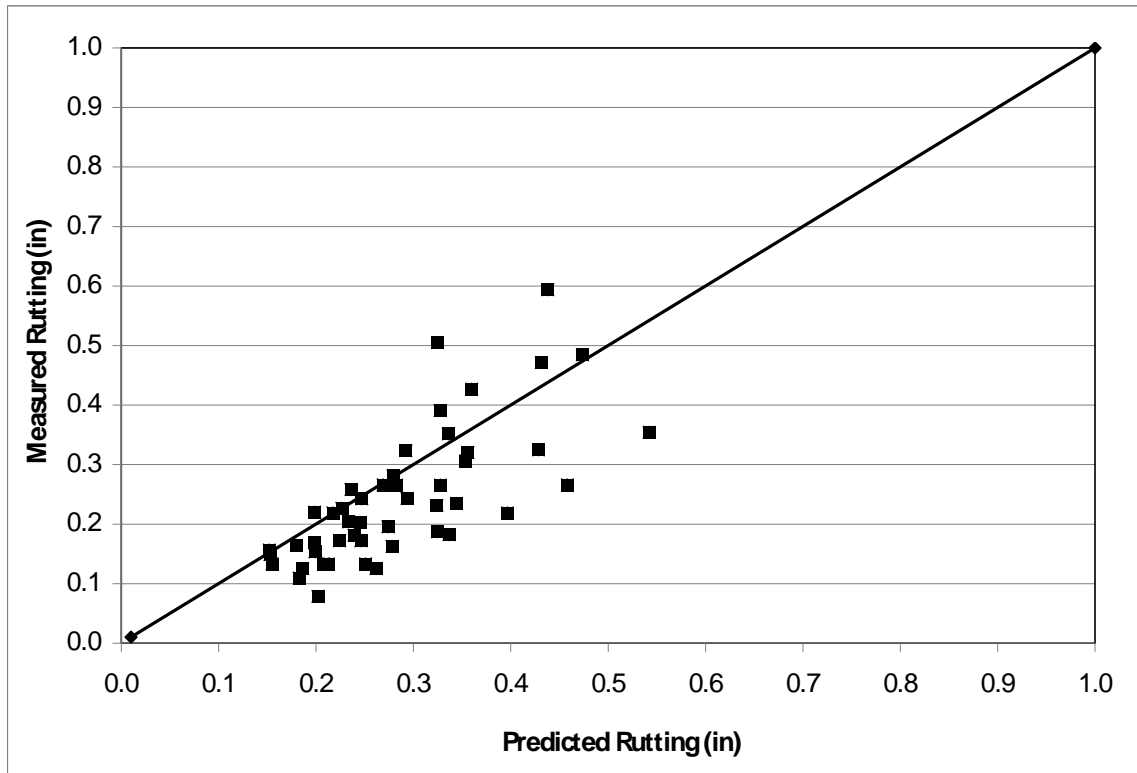


Figure 5.11 Truck and passing lane predicted and measured rutting after five and 10 years.

Based on the results of this analysis, the following procedure is recommended for rutting prediction:

1. Run the MEPDG version 1.0 software. Determine the rutting in each layer at the end of the design period, and rutting in the base and subgrade layers for the first month for the 50% reliability level.

Figure 12 shows the predicted rutting for cell 4 with passing lane traffic using equation 5.1. It can be observed that the initial predicted subgrade rutting is unreasonably high, resulting in a predicted total rutting of 0.587 in.

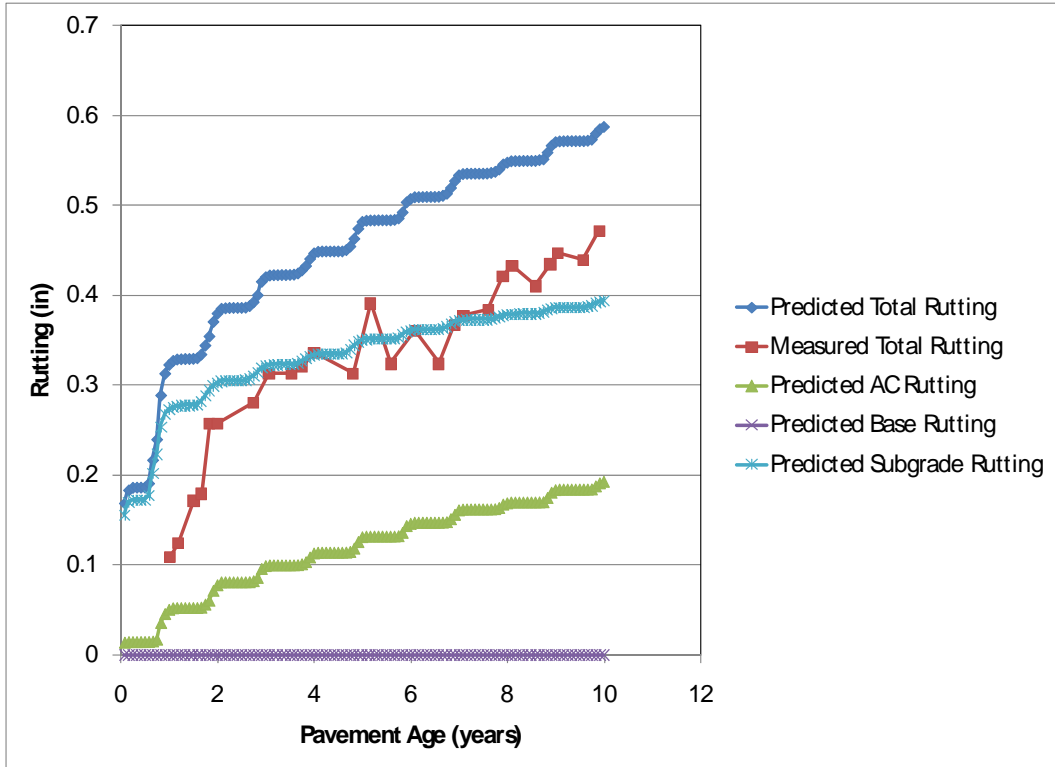


Figure 5.12 Predicted rutting for cell 4 with 50% reliability using equation 5.1.

- Using equation 5.2, determine the total rutting at the end of the design period at the 50% reliability level.

Figure 5.13 shows the predicted total rutting using equation 5.2 at the 50 percent reliability rate for cell 4. It can be observed that the predicted total rutting at ten years is then reduced to 0.431 in.

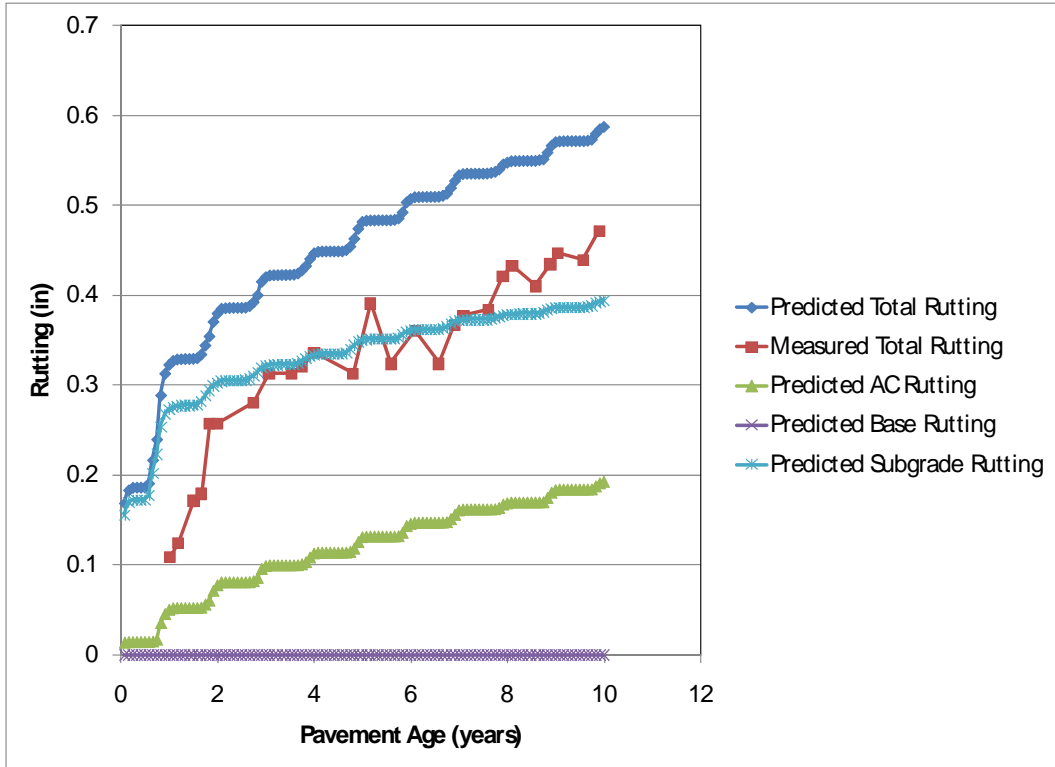


Figure 5.13 Predicted rutting for cell 4 at 50% reliability using equation 5.2.

- Using the output from the design guide, find the rutting corresponding to the specified reliability.

Figure 5.14 shows the predicted total rutting at 90% reliability, using equation 5.2. This results in predicted rutting after 10 years at 0.5619 in.

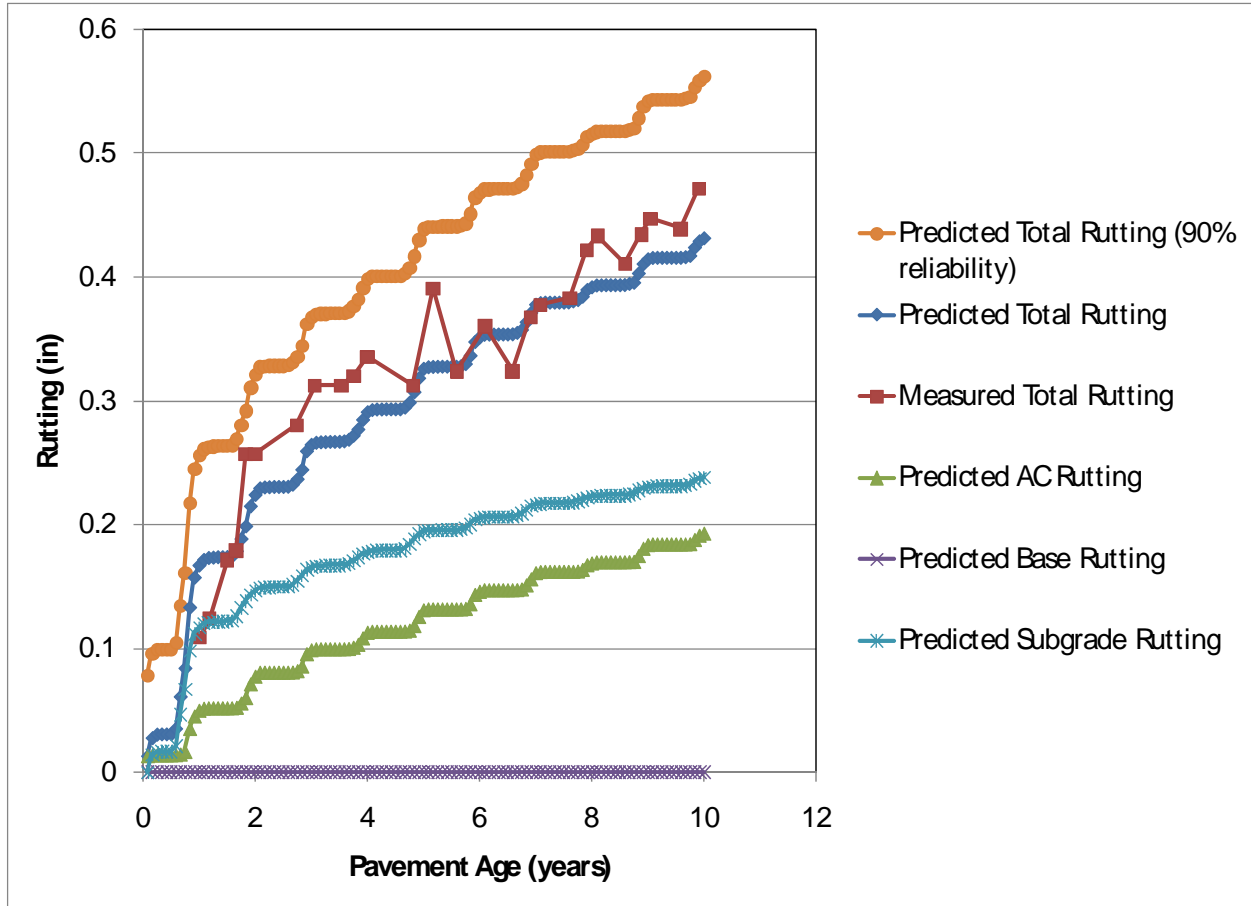


Figure 5.14 Predicted rutting for cell 4 at 90% reliability using equation 5.2.

5.2.2 Alligator Cracking

Alligator cracking is a form of fatigue or wheel load related cracking. It is defined as a series of interconnected cracks. In the MEPDG alligator cracking is calculated as a percent of total lane area. The MEPDG assumes that alligator cracking initiates at the bottom of the HMA layers and propagates to the surface with continued truck traffic. The allowable number of axle load applications needed for the incremental damage index approach to predict alligator cracking is defined as follows:

$$N_f = k_{f1}(C)(C_H)\beta_{f1}(\epsilon_t)^{k_{f2}\beta_{f2}}(E_{HMA})^{k_{f3}\beta_{f3}} \quad (5.4a)$$

Where:

- N_f = Allowable number of axle load applications.
- ϵ_t = Tensile strain at critical locations and calculated by the structural response model, in./in.
- E_{HMA} = Dynamic modulus of the HMA measured in compression, psi.
- k_{f1}, k_{f2}, k_{f3} = Global field calibration parameters (from the NCHRP 1-40D re-calibration; $k_{f1} = 0.007566$, $k_{f2} = -3.9492$, and $k_{f3} = -1.281$).
- $\beta_{f1}, \beta_{f2}, \beta_{f3}$ = Local or mixture specific field calibration constants; for the global calibration effort, these constants were set to 1.0.

$$C = 10^M \quad (5.4.b)$$

$$M = 4.84 \left(\frac{V_{be}}{V_a + V_{be}} - 0.69 \right) \quad (5.4.c)$$

V_{be} = Effective asphalt content by volume, percent.
 V_a = Percent air voids in the HMA mixture.
 C_H = Thickness correction term, dependent on type of cracking.

$$C_H = \frac{1}{0.000398 + \frac{0.003602}{1 + e^{(11.02 - 3.49H_{HMA})}}} \quad (5.4.d)$$

The cumulative damage index (DI) for each critical location is determined by summing the incremental damage indices over time, as shown in equation 5.5.

$$DI = \sum (\Delta DI)_{j,m,l,p,T} = \sum \left(\frac{n}{N_f} \right)_{j,m,l,p,T} \quad (5.5)$$

Where:

n = Actual number of axle load applications within a specific time period.
 j = Axle load interval.
 m = Axle load type (single, tandem, tridem, quad, or special axle configuration).
 l = Truck type using the truck classification groups included in the MEPDG.
 p = Month.
 T = Median temperature for the five temperature intervals or quintiles used to subdivide each month.

The area of alligator cracking, FC_{Bottom} , is calculated from the total damage accumulated over time (equation 5.6) using the following transfer function:

$$FC_{Bottom} = \left(\frac{1}{60} \right) \left(\frac{C_4}{1 + e^{(C_1 C_1^* + C_2 C_2^* \text{Log}(DI_{Bottom} * 100))}} \right) \quad (5.6)$$

Where:

FC_{Bottom} = Area of alligator cracking that initiates at the bottom of the HMA layers, percent of total lane area.

$C_{1,2,4}$ = Transfer function regression constants; $C_4=6,000$; $C_1=1.00$; and $C_2=1.00$

$$C_1^* = -2C_2^* \quad (5.6.b)$$

$$C_2^* = -2.40874 - 39.748(1 + H_{HMA})^{-2.856} \quad (5.6.c)$$

Alligator cracking was not observed in MnROAD mainline HMA cells and was only detected in about half of the cells in the low volume loop. Figure 5.15 shows a comparison between predicted and measured alligator cracking for all MnROAD cells. One outlier with 78% measured cracking and 0.21 predicted cracking in cell 26 of the low volume is not shown on this plot for scaling purposes. It can be observed from Figure 5.15 that although the MEPDG predicts some level of cracking for all mainline cells, there is no measured alligator cracking.

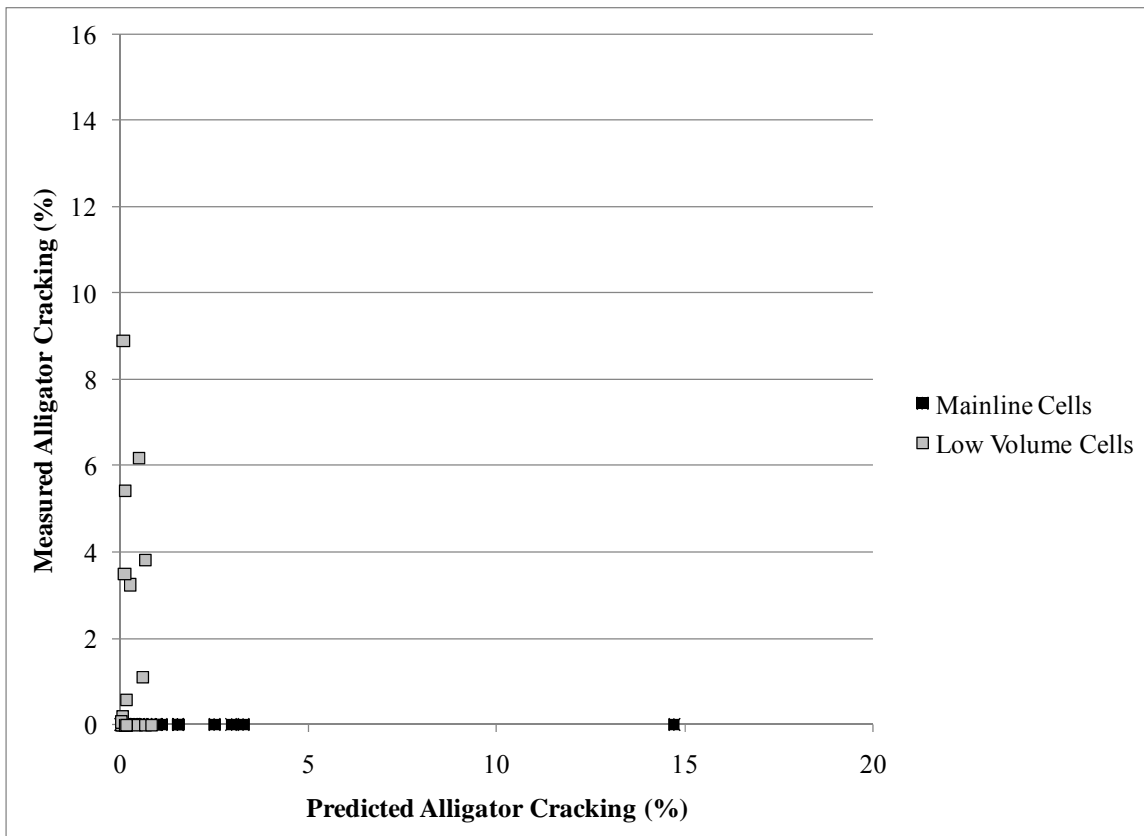


Figure 5.15 Measured and predicted alligator cracking for HMA MnROAD cells.

Recalibration of the alligator cracking performance model was not conducted due to the fact that all of the mainline HMA cells have zero alligator cracking and thus there is no data to perform regression analysis.

To overcome this obstacle, the MEPDG fatigue damage accumulation model was calibrated against MnPAVE. MnPAVE is a mechanistic-empirical design software developed by MnDOT and the University of Minnesota; based on layered elastic theory and calibrated using data from MnROAD test sections, and other Minnesota pavements. The fatigue models in MnPAVE were validated using data from Minnesota trunk highways.

Although both programs use Miner’s concept of damage accumulation, damages that are predicted using MEPDG and MnPAVE cannot be compared directly. This is due to the fact that these two programs use different scales. In MnPAVE, damage equal to 1 indicates that 20% of the pavement area is covered by alligator cracking. In the MEPDG, the equality of damage to 1

corresponds to pavement exhibiting 50% by area of alligator cracking. To make these two damages compatible, the fatigue damage from MnPAVE was multiplied by a factor of 0.31.

Figure 5.16 presents the comparison between the corrected fatigue cracking damage from MnPAVE and the predicted damage from the MEPDG. It can be observed that the damage in the MEPDG is highly correlated with the damage predicted in MnPAVE. It can also be observed that the magnitude of damage due to alligator cracking predicted by the MEPDG is approximately 5 times greater than that predicted by MnPAVE. Therefore, the recalibrated model has the following form, where k_{f1} is multiplied by the slope from figure 5.16 (0.1903).

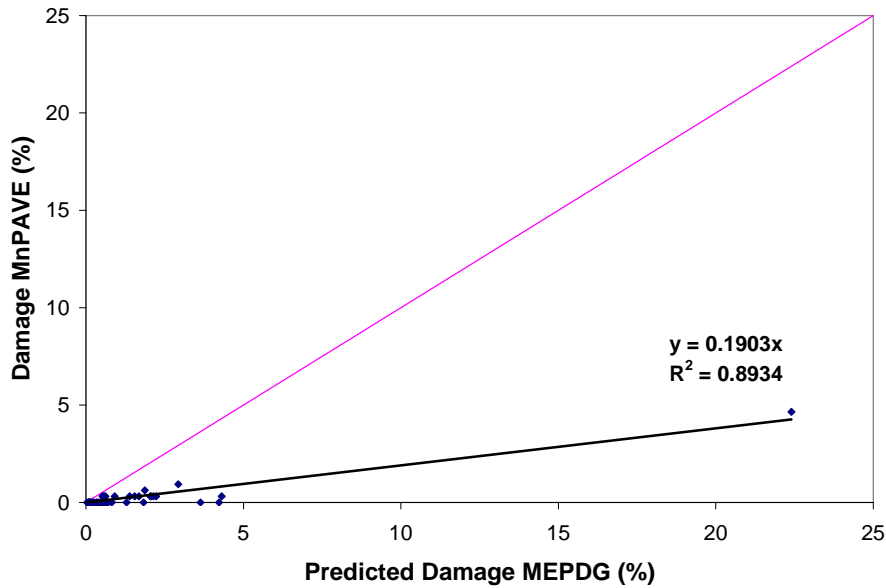


Figure 5.16 Fatigue damage comparison of MnPAVE and MEPDG.

$$N_f = 0.1903 \times k_{f1}(C)(C_H)(\epsilon_t)^{k_{f2}}(E_{HMA})^{k_{f3}} \quad (5.7)$$

This modification can be implemented using the standard MEPDG software features for local calibration. This requires the user to select the State/Regional calibration option, and to set the coefficient Bf1 equal to 0.1903 as shown in figure 5.17.

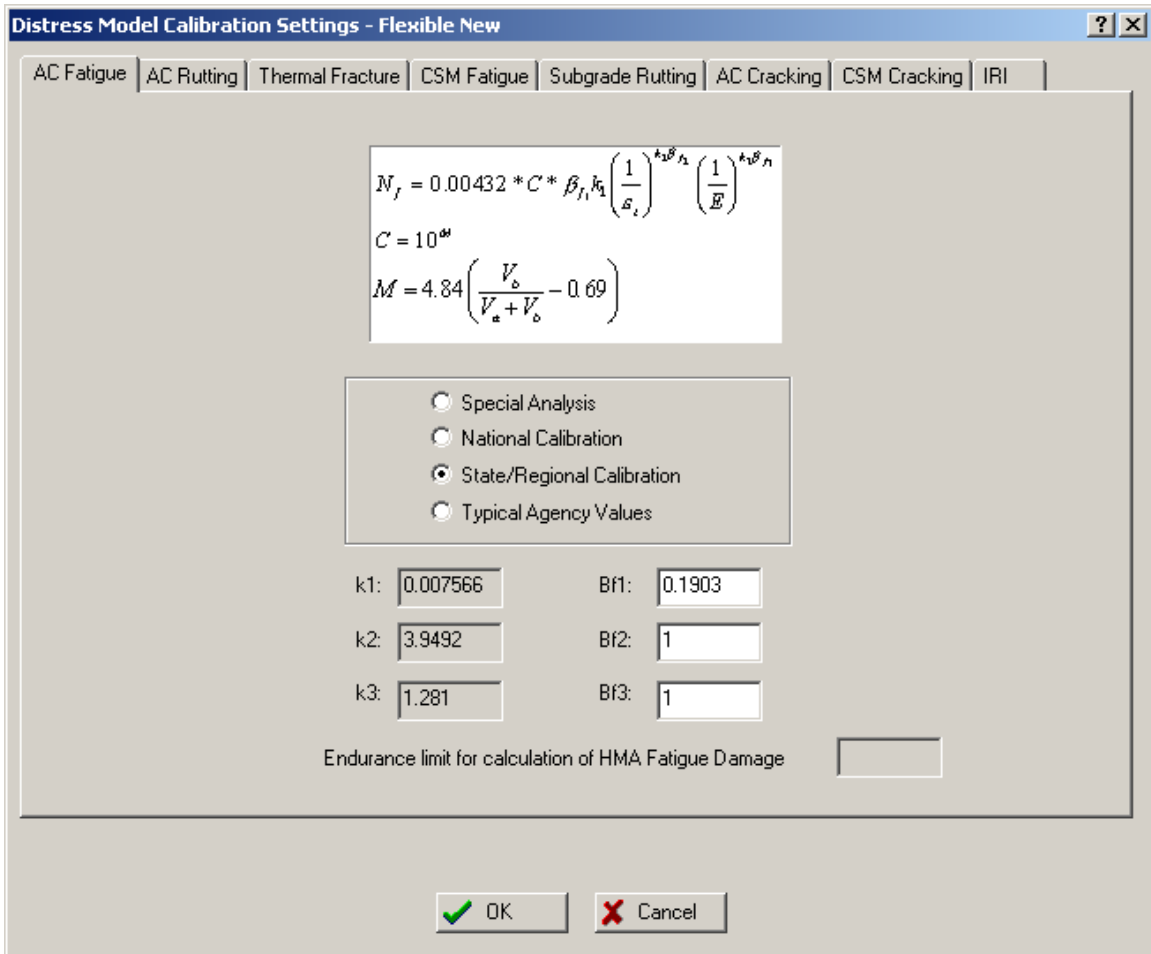


Figure 5.17 Adjustment of local calibration settings in the MEPDG software.

5.2.3 Transverse Cracking

Thermal (transverse) cracking measurements from 14 HMA MnROAD cells (1 - 4, 14 - 19, 21, 22, 33, and 34) were used to estimate a correction factor to account for local conditions in the prediction of transverse cracking. Figure 5.18 shows a comparison between measured and predicted thermal cracking. It is observed that transverse cracking is underpredicted for almost all MnROAD cells. It can be observed that a recalibration factor of 1.85 is suggested after using linear regression. It should be noted that an ongoing pooled-fund study will significantly improve the transverse cracking model and potentially replace the MEPDG low temperature cracking analysis. Therefore, the modification proposed in this study is intended to only be an interim solution.

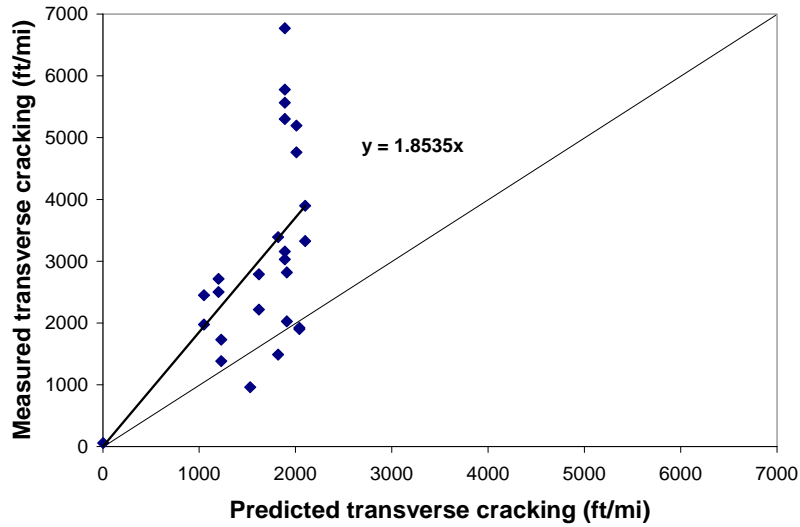


Figure 5.18 Measured and predicted transverse cracking.

5.2.4 Longitudinal Cracking

Field performance of 12 MnROAD cells (1 - 4, 14 – 19, 21, and 22) were used to evaluate the prediction model for longitudinal cracking in the MEPDG. It can be seen from Figure 5.19 that the performance model for top-down cracking poorly represents field observations. Also, the MEPDG cracking model has went through significant modifications from software version 0.91 to version 1.0, and therefore, there is no guarantee that this model is bug free. Moreover, this model most likely will be modified under the ongoing project sponsored by a National Cooperative Highway Research Program (NCHRP) project. Therefore, it is recommended by the research team to exclude the longitudinal cracking prediction model from the local calibration.

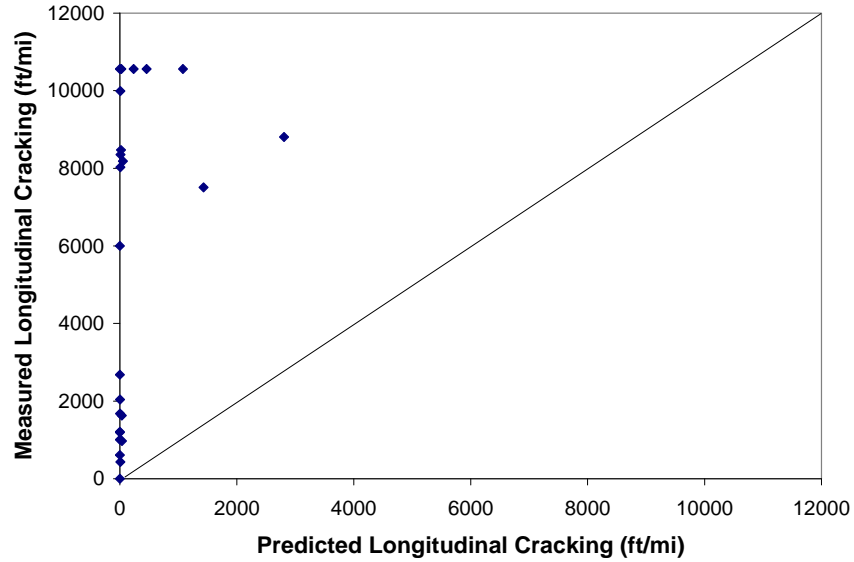


Figure 5.19 Measured and predicted longitudinal cracking.

5.2.5 Roughness (IRI)

The current version of the MEPDG uses the following equation to estimate the International Roughness Index (IRI) for new asphalt pavements:

$$IRI = IRI_o + 0.0150(SF) + 0.400(FC_{Total}) + 0.0080(TC) + 40.0(RD) \quad (5.8)$$

where:

IRI_o = Initial IRI after construction (in/mi).

SF = Site factor that includes pavement age, plasticity index of the soil, average annual freezing index and average annual rainfall.

FC_{Total} = Area of fatigue cracking (%) which combines alligator and longitudinal cracking in the wheel path.

TC = Length of transverse cracking (ft/mi).

RD = Average rut depth (in).

Since the longitudinal cracking model was not calibrated in this study, it was not feasible to calibrate the IRI model as well.

5.3 Rigid Pavements

The mechanistic-empirical performance prediction models for PCC pavements were calibrated using nationwide pavement performance databases, such as LTPP GPS-3, LTPP SPS-2, and FHWA RPPR databases. This section summarizes the verification and calibration process for Minnesota conditions.

The MEPDG for jointed plain concrete pavements (JPCP) includes the following performance prediction models:

- Transverse cracking
- Joint faulting
- IRI

5.3.1 Transverse Cracking

Calibration of the MEPDG cracking model for Minnesota conditions was performed based on the design and performance data for 65 sections located in Minnesota, Iowa, Wisconsin, and Illinois. The calibration coefficients of the cracking model were modified using an iterative optimization procedure. The goal of this procedure was to minimize the discrepancy between predicted and actual values of cracking for the 181 observations in the database. The details of the calibration process are presented below.

5.3.1.1 Step 1 – Collection of the Calibration Dataset: To calibrate the MEPDG cracking model for Minnesota conditions, a subset of 65 sections were selected from the database compiled by Applied Research Associates, Inc. under the NCHRP 1-40D project for the national calibration of the MEPDG (ARA, Inc. personal communication). The selected sections are located in Minnesota, Iowa, Wisconsin, and Illinois. Pavement design and performance information for these sections was obtained from the LTPP database, AASHTO road test, and MnROAD database. A summary of the site conditions and the design features for the pavement sections selected for the local calibration can be found elsewhere (Yut et al. 2007). The final data set consisted of a total of 181 observations, since many sections had time series cracking data. The calibration process that was used in this study is similar that which was used by Yut et al (2007), but MEPDG software version 1.0 was used in this study whereas Yut et al, utilized MEPDG software version 0.868.

5.3.1.2 Step 2 – Compute Corresponding Predicted Values: The second step in the process of recalibrating the MEPDG cracking model involved computing fatigue damage and prediction of the cracking for each pavement section in the calibration dataset using MEPDG software version 1.0. The MEPDG JPCP cracking model has the following form:

$$TOTCRACK = 100 * (BUCRACK + TDCRACK - BUCRACK * TDCRACK) \quad (5.9)$$

where *TOTCRACK* is the total percentage of cracked slabs, *BUCRACK* is the percentage of cracked slabs with the cracking propagated from bottom up, and *TDCRACK* is the percentage of cracked slabs with the cracking propagated from top down.

Bottom-up cracking and top-down cracking are determined from the cumulative fatigue damage at the bottom and at the top of the PCC slab, respectively. The relationships between cracking and the corresponding damage have the following form:

$$BUCRACK = \frac{1}{1 + C4 * BU^{C2}} \quad (5.10)$$

$$TDCRACK = \frac{1}{1 + C4 * TD^{C2}} \quad (5.11)$$

where:

BU is fatigue damage associated with bottom-up cracking

TD is fatigue damage associated with top-down cracking

C1 and *C2* = regression coefficients

In the original model the values of the regression coefficients were as follows:

$$C4=1 \quad (5.12)$$

$$C5= -1.68 \quad (5.13)$$

5.3.1.3 Step 3 – Compare predicted vs. measured cracking: The predicted cracking values were compared with the corresponding measured cracking for each observation in the calibration data base. A plot of predicted versus actual data (see figure 5.20) was prepared to compare the general location of the data points to a one-to-one line (representing predicted = actual). In addition, this plot allowed for evaluating the data by identifying any potential bias, lack of precision, and trends associated with the original model. Thus, the trend line equation presented in the plot suggested that although the model has a reasonably high overall correlation $R^2 = 0.62$, the actual cracking values, on average, corresponded to 80.7 percent of the values predicted by the MEPDG original cracking model. This called for the modification of the regression coefficients in the original model described by equations 12 and 13.

5.3.1.4 Step 4 – Modify regression coefficients: The objective of this step was to find a set of the coefficients *C1* and *C2* that will minimize the discrepancy between the predicted and measured cracking. The predicted value of cracking can be calculated using the equations (9) through (11) and can be expressed in the following way:

$$CALCCRACK = 100 * \left[\frac{1}{1 + C1 * BU^{C2}} + \frac{1}{1 + C1 * TD^{C2}} - \frac{1}{(1 + C1 * BU^{C2}) * (1 + C1 * TD^{C2})} \right] \quad (5.14)$$

The norm of the discrepancy between the predicted and measured cracking, *ERROR*, can be defined as the sum of squares of differences between the predicted and measured cracked slabs for each observation, i.e.

$$ERROR = \sum_i (MEASCRACK_i - CALCCRACK_i)^2 \quad (5.15)$$

where MEASCRACK is the observed percentage of cracked slabs.

Therefore, the objective of re-calibration is find coefficients *C1* and *C2* to minimize *ERROR* defined by equation 15. To achieve this goal, the iterative optimization procedure was executed automatically using the macro-driven MS Excel. It included the following subroutines:

1. Store the coefficients *C4* and *C5* into variables *A* and *B*, respectively.

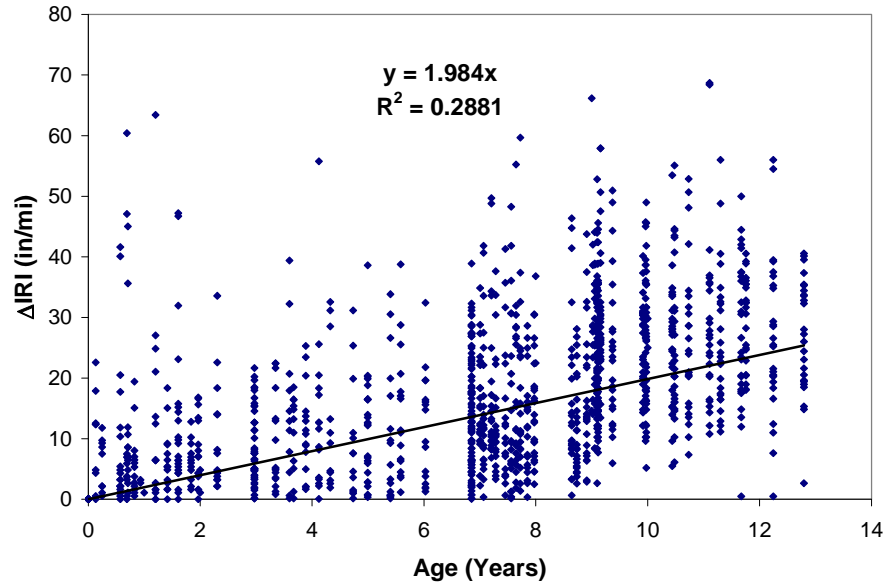


Figure 5.22 IRI as function of the age of PCC pavement.

5.4 Calibration Conclusions

Local calibration of the MEPDG has been conducted for Minnesota conditions. This calibration required modification of the MEPDG rutting model for base and subgrade, and modification of the coefficients for the MEPDG cracking models for rigid and flexible pavements. The MEPDG longitudinal cracking model was not recalibrated due to significant changes of the model from version to version and unclear prospects that the current version won't be changed in the near future by NCHRP or AASHTO sponsored studies.

Chapter 6 Conclusions

The MEPDG and related software provide capabilities for the analysis and performance prediction of different types of flexible and rigid pavements by utilizing information including traffic (full load spectra for single, tandem, tridem, and quad axles), material and subgrade characterization, climatic factors, performance criteria and others. In this study, the following activities were conducted: an evaluation of default inputs, identification of deficiencies in the software, sensitivity analysis, evaluation of the prediction capabilities of the MEPDG, and recalibration of performance prediction models for Minnesota conditions.

Flexible pavements - A sensitivity analysis and comparison of results to the expected limits were performed for typical Minnesota site conditions and a wide range of pavement design features (e.g. layer thickness, material properties, etc), and the effects of different parameters on predicted flexible pavement distresses were analyzed. Since the sensitivity analysis was conducted over a span of several years and the MEPDG software underwent significant modifications, especially for flexible pavements, various versions of the MEPDG software were run. Through the analysis and comparisons, several major bugs were identified and reported to the MEPDG software developers. The analysis of the latest MEPDG software (version 1.003) showed that many of the bugs were fixed.

During the analysis conducted in this study, multiple issues with the MEPDG were encountered. These included:

- Longitudinal cracking prediction
 - Very poor correlations were found between the MEPDG predictions of longitudinal cracking for MnROAD flexible pavements and the observed distresses. In addition, the MEPDG cracking model went through significant modifications from software version 0.91 to version 1.003, and therefore, there is no guarantee that this model is bug free. Considering that the longitudinal cracking model most likely will be modified under the ongoing project sponsored by a National Cooperative Highway Research Program (NCHRP) it is not recommended to use this model for performance prediction of flexible pavements.
- Stabilized base and subgrade characterization
 - Issues with the software, supporting documentation, and the distress model used for predicting semi-rigid performance raised concern. Thus, using the current version of the MEPDG for design of flexible pavements with stabilized base or subgrade is not recommended.
- Asphalt binder characterization
 - Performance predictions using level 2 inputs were not consistent with the input information, and thus it is recommended to limit asphalt binder characterization to level 3 inputs.
- Subgrade characterization
 - Currently, the default seasonal adjustment procedure accounts only for seasonal variation in moisture conditions.

- In some cases, it might be important to adjust the subgrade modulus not only for changes in moisture conditions, but also for changes in the effective pavement stiffness.

Local adaptation of the MEPDG for Minnesota conditions required modification of the MEPDG rutting model for base and subgrade, as well as modification of the coefficients for the MEPDG fatigue cracking model and thermal cracking for flexible pavements. Since the use of the longitudinal cracking model was not recommended for adaptation, the IRI model could not be locally calibrated.

Rigid pavements - Over 200,000 MEPDG simulations were performed for rigid pavements. The analysis of the simulation results concluded that the performance prediction trends for rigid pavements are quite reasonable. No adjustment of the faulting model was recommended, but a recalibration of the cracking model was needed. This recalibration was conducted using the performance data from MnROAD pavement cells as well as the Long Term Pavement Performance (LTPP) test sections from the neighboring states.

MEPDG implementation Modification and re-calibration of the Mechanistic-Empirical Pavement Design Guide (MEPDG) distress prediction models for both asphalt and concrete pavements resulted in a reduction of bias and error in the design predictions for Minnesota conditions. The research team recommends implementation of the MEPDG for rigid pavements with the modified cracking model coefficients. For flexible pavements, the research team recommends use of the modified rutting model and the modified coefficients for the alligator cracking and thermal cracking models developed in this study. At this stage, it is not recommended to use the MEPDG longitudinal cracking and IRI predictions for flexible pavements.

A substantial portion of the efforts on this project were devoted to evaluation of various versions of the MEPDG software and model re-calibration, which reduced the resources previously allocated to verification and validation of the final version of the software and the re-calibrated models. These activities should be performed in future studies. However, it is anticipated that AASHTO will sponsor a significant upgrade of the software in the near future. It is recommended to repeat the calibration process and conduct verification and validation with the professional grade quality software. Meanwhile, the current version of the software, with the proposed model adjustments, should be used for pilot evaluation of the MEPDG along with the current design procedure.

References

AASHTO. *Mechanistic-Empirical Pavement Design Guide, Interim Edition: A Manual of Practice*. American Association of State Highway and Transportation Officials (AASHTO), Washington, DC., 2008.

Darter, M., Khazanovich, L., Snyder, M., Rao, S., Hallin, J. "Development and calibration of a Mechanistic Design Procedure for Jointed Plain Concrete Pavements". Proceedings of the 7th International Conference on Concrete Pavements. Orlando, Florida, 2001.

Desai, C.S. *User's Manual for the DSC-2D Code for the MEPDG*, Arizona State University, 2000.

El-Basyouny, M., and Witczak, M.W. "Verification of the Calibrated Fatigue Cracking Models for the MEPDG." Association of Asphalt Paving Technologists, 2005 Annual Meeting, Long Beach, CA, 2005a.

El-Basyouny, M., and Witczak, M.W. "Development of the Fatigue Cracking Models for the MEPDG." Presented at the Transportation Research Board 84th Annual Meeting, Washington, D.C., January, 2005b.

El-Basyouny, M., and Witczak, M.W. "Calibration of the Alligator Fatigue Cracking Model for the MEPDG." Presented at the Transportation Research Board 84th Annual Meeting, Washington, D.C., 2005c.

El-Basyouny, M., and Witczak, M.W. "Calibration of the Longitudinal Fatigue Cracking Model for the MEPDG." Presented at the Transportation Research Board 84th Annual Meeting, Washington, D.C., 2005d.

Khazanovich, L., Yu, T., and Darter, M. "Mechanistic-Empirical Model for Transverse Joint Faulting Prediction," *Transportation Research Record*, no 1896, pp 34-45, 2004.

Krehbiel, T. "Correlation Coefficient Rule of Thumb", *The Decision Science Journal of Innovative Education*, June 3, 2003.

Larson, G., and Dempsey, B. J. *Integrated Climatic Model. Version 2.0*. Contract DTFA MN/DOT 72114, Department of Civil Engineering, University of Illinois at Urbana-Champaign, Urbana, IL, 1997.

Lytton, R.L., Uzan, J., Fernando, E.G., Roque, R., Hiltunen, D. and Stoffels, S.M. *Development and Validation of Performance Prediction Models and Specifications for Asphalt Binders and Paving Mixes*. Strategic Highway Research Program Report SHRP-A-357, Washington, D.C., 1993.

NCHRP 2004a. *Guide for Mechanistic-Empirical Design of new and rehabilitated pavement structures*. National Cooperative Highway Research Program, Project 1-37A, Final Report. Part 2. *Design Inputs*. Washington, D.C., 2004a.

NCHRP 2004b. *Guide for Mechanistic-Empirical Design of new and rehabilitated pavement structures*. Project 1-37A Final Report. Part 3. *Design Analysis*. Washington, D.C., 2004b.

Roque, R., Hiltunen, D. R., Buttlar, W. G. “Thermal Cracking Performance and Design of Mixtures Using Superpave™.” *Journal of the Association of Asphalt Paving Technologists*, Vol. 64., pp. 718-735, 1995.

Selezneva, O., Rao, C., Darter, M., Zollinger, D., Khazanovich, L. “Development of a Mechanistic-Empirical Structural Design Procedure for Continuously Reinforced Concrete Pavements”. *Proceedings of the 83th Annual Meeting of the Transportation Research Board*, Washington, D.C., 2004.

Smith, B.E. and Witzak, M.W. “Prediction of equivalent granular base moduli incorporating stress dependent behavior in flexible pavement.” *ASCE Journal of Transportation Engineering*, vol. 107, no. 6, pp. 635-652., 1981.

Uzan, J. *JULEA linear elastic analysis computer program*, US Army Waterways Experiment Station, Vicksburg, MS, 1989.

Velasquez, R., Marasteanu, M., Khazanovich, L., and Jensen, M. “Comprehensive Evaluation Approach of Flexible MEPDG for Minnesota Conditions,” *Proceedings of the International Conference on Advanced Characterization of Pavement and Soil Engineering Materials*, 2:1709–1722, Taylor and Francis Group, Edited by Andreas Loizos, Tom Scarpas, and Imad Al-Qadi. Athens, Greece, 2007.

Witzak, M. W., Andrei, D., and Houston, W. N. *Resilient Modulus as Function of Soil Moisture – Summary of Predictive Models. Development of the 2002 Guide for the Development of New and Rehabilitated Pavement Structures*, NCHRP 1-37 A, Inter Team Technical Report (Seasonal 1), TRB, National Research Council, Washington, D.C., 2000.

Witzak, M. W., Houston, W. N., Zapata, C. E., Richter, C., Larson, G., and Walsh, K. *Improvement of the Integrated Climatic Model for Moisture Content Predictions. Development of the 2002 Guide for the Development of New and Rehabilitated Pavement Structures*, NCHRP 1-37 A, Inter Team Technical Report (Seasonal 4), TRB, National Research Council, Washington, D.C., 2000.

Witzak, M. W., and Mirza, M. W. *AC Fatigue Analysis for MEPDG*. Research Report for NCHRP 1-37A Project. Arizona State University, Tempe, AZ., 2000.

Appendix A

Examples of Predicted Distresses for Rigid Pavements

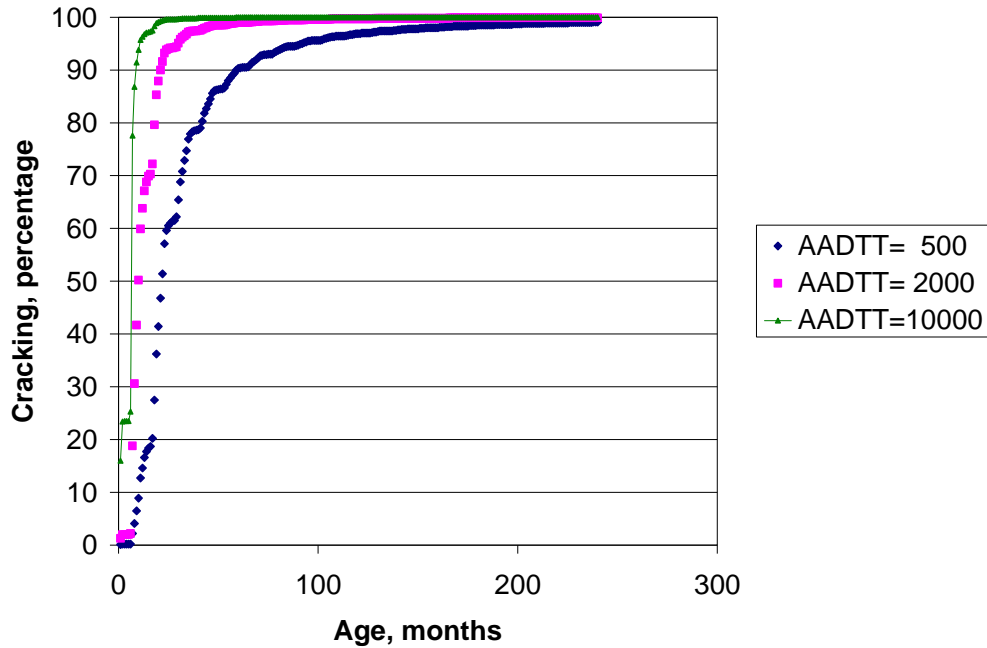


Figure 1 Effect of Traffic on cracking. Location -Rochester, HPCC =6, COTE =0.0000048, MR=500, HBase=6, Base -Class 5, Lane Width =12, Joint Spacing =15, Dowel D = none, Shoulders - AC, Subgrade - A-6

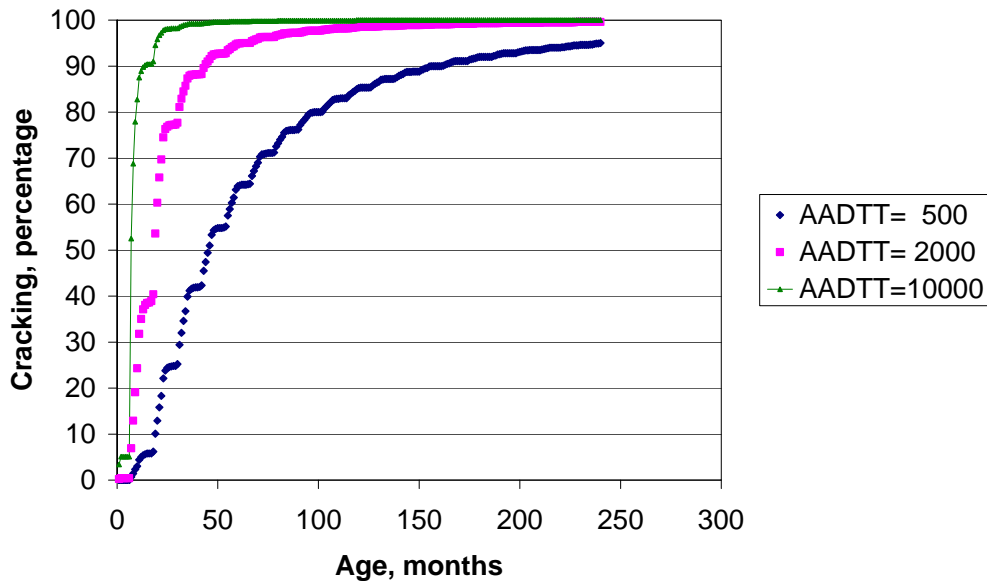


Figure 2 Effect of Traffic on cracking. Location -Rochester, HPCC =7, COTE =0.0000048, MR=500, HBase=6, Base -Class 5, Lane Width =12, Joint Spacing =15, Dowel D = none, Shoulders - AC, Subgrade - A-6

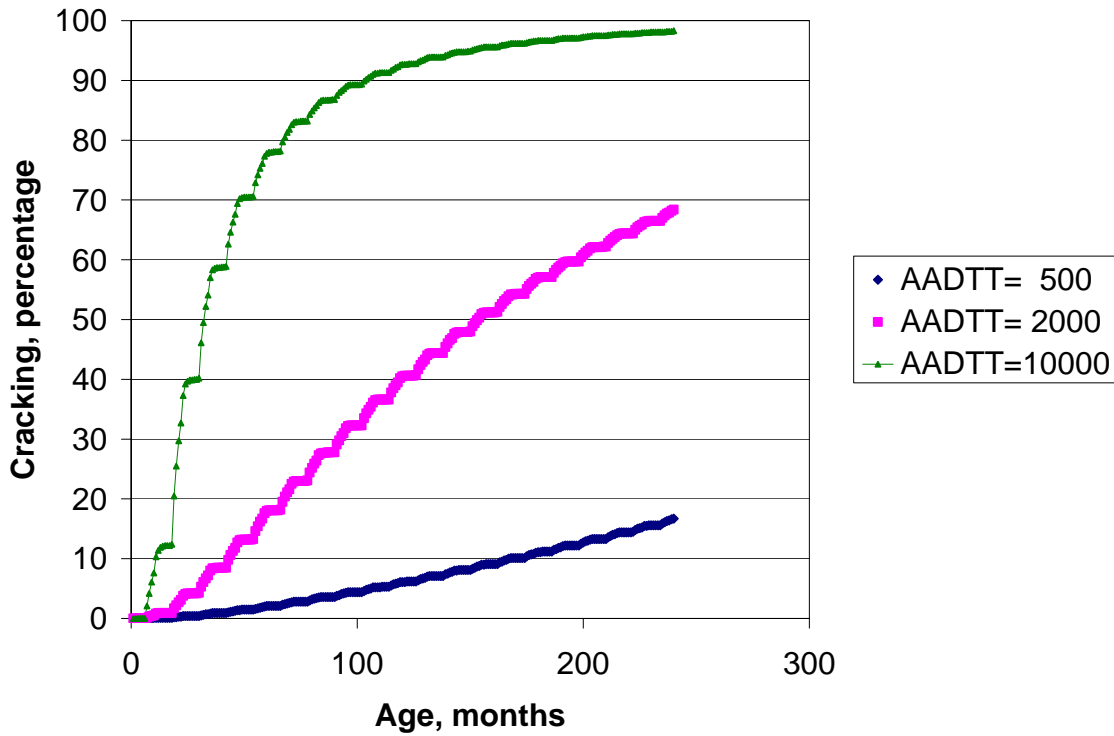


Figure 3 Effect of Traffic on cracking. Location -Rochester, HPCC =9, COTE =0.0000048, MR=500, HBase=6, Base -Class 5, Lane Width =12, Joint Spacing =15, Dowel D = none, Shoulders - AC, Subgrade - A-6

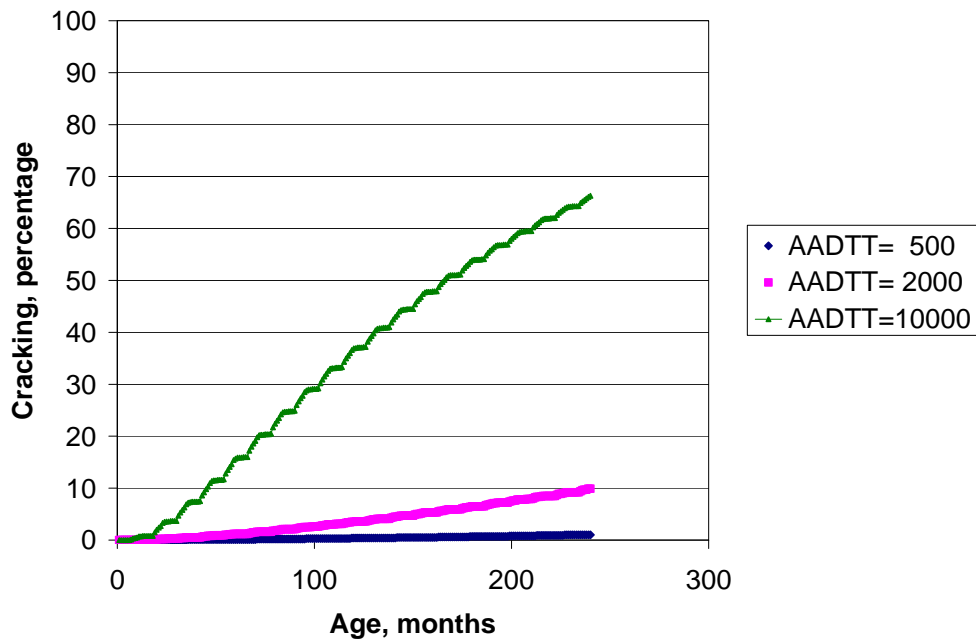


Figure 4 Effect of Traffic on cracking. Location -Rochester, HPCC =10, COTE =0.0000048, MR=500, HBase=6, Base -Class 5, Lane Width =12, Joint Spacing =15, Dowel D = none, Shoulders - AC, Subgrade - A-6

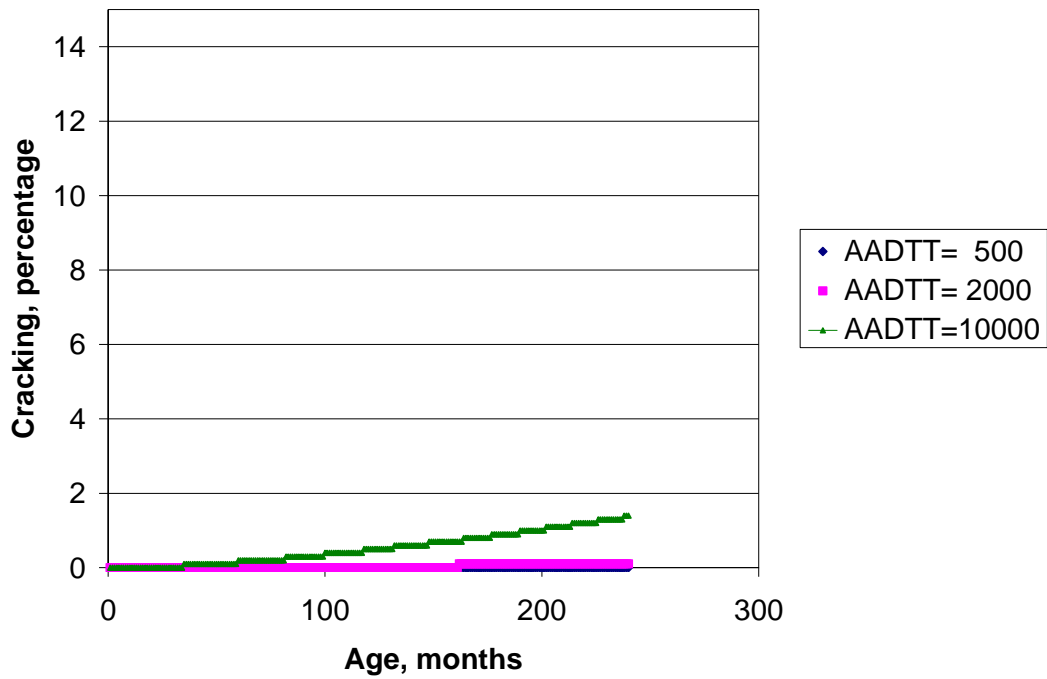


Figure 5 Effect of Traffic on cracking. Location -Rochester, HPCC =12, COTE =0.0000048, MR=500, HBase=6, Base -Class 5, Lane Width =12, Joint Spacing =15, Dowel D = none, Shoulders - AC, Subgrade - A-6

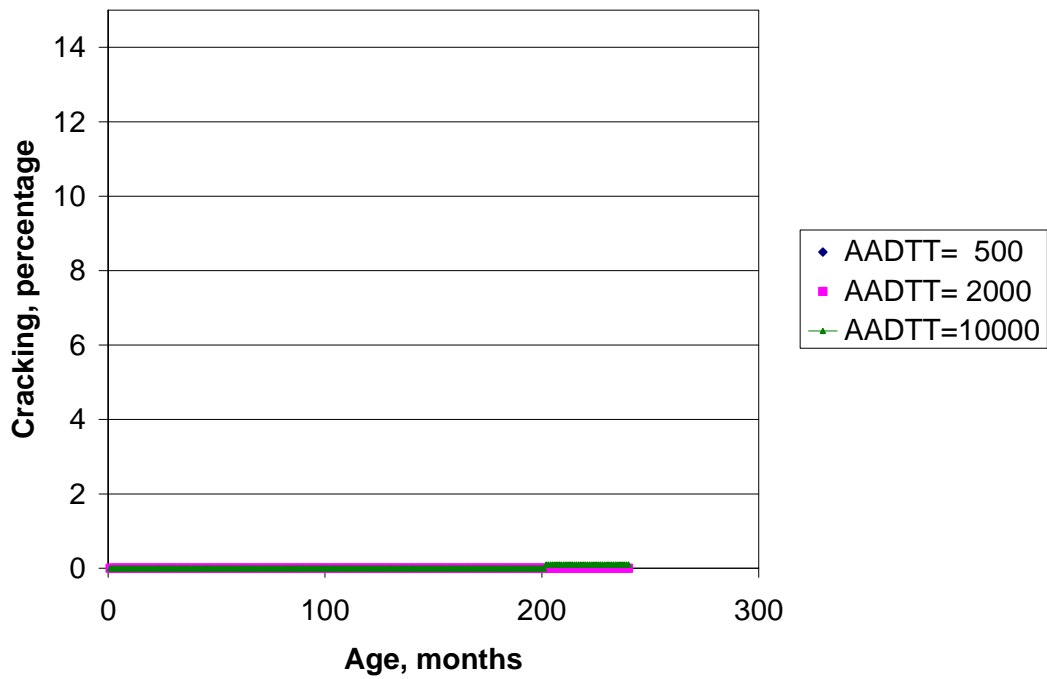


Figure 6 Effect of Traffic on cracking. Location -Rochester, HPCC =14, COTE =0.0000048, MR=500, HBase=6, Base -Class 5, Lane Width =12, Joint Spacing =15, Dowel D = none, Shoulders - AC, Subgrade - A-6
A-3

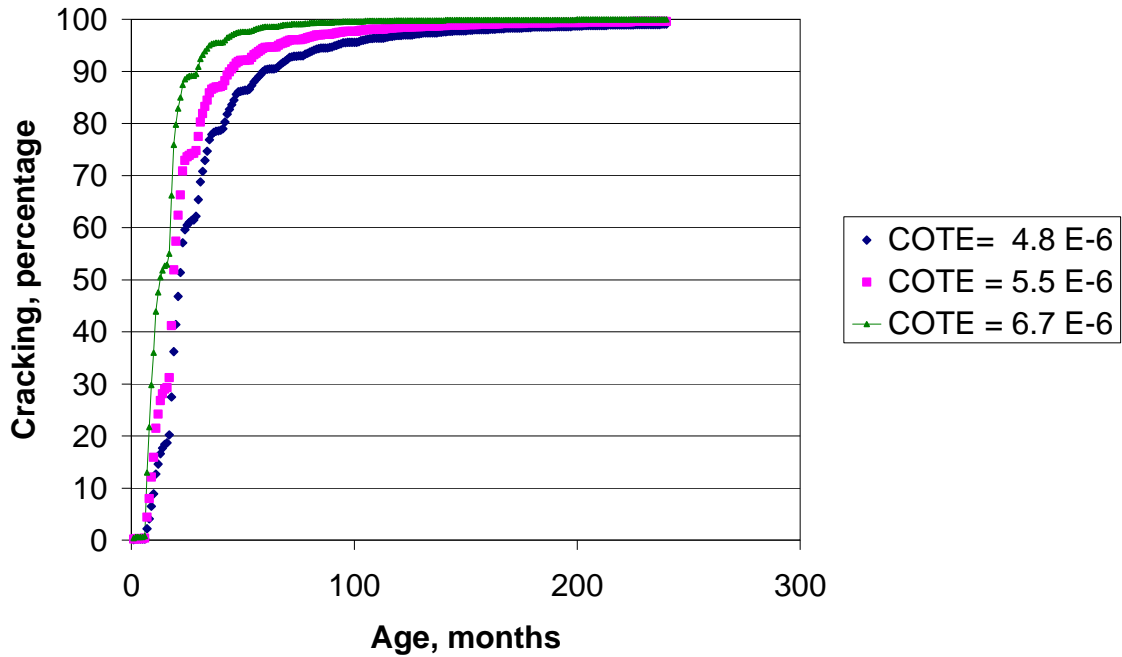


Figure 7 Effect of COTE on cracking. Location -Rochester, AADTT=500, HPCC =6, MR=500, HBase=6, Base -Class 5, Lane Width =12, Joint Spacing =15, Dowel D = none, Shoulders - AC, Subgrade - A-6

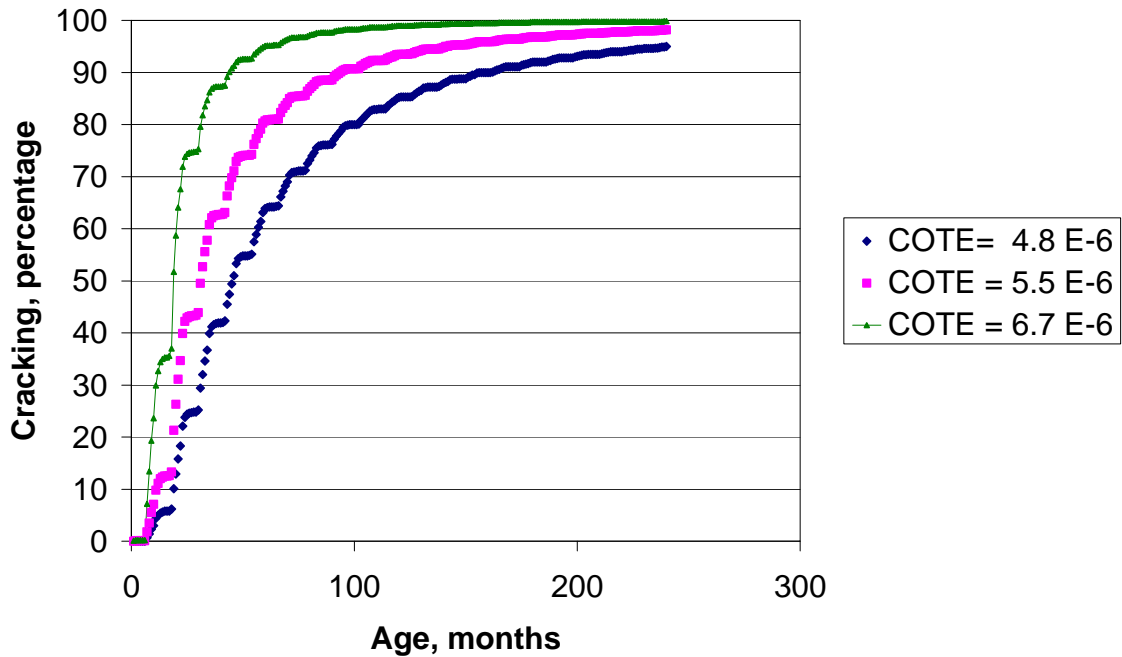


Figure 8 Effect of COTE on cracking. Location -Rochester, AADTT=500, HPCC =7, MR=500, HBase=6, Base -Class 5, Lane Width =12, Joint Spacing =15, Dowel D = none, Shoulders - AC, Subgrade - A-6

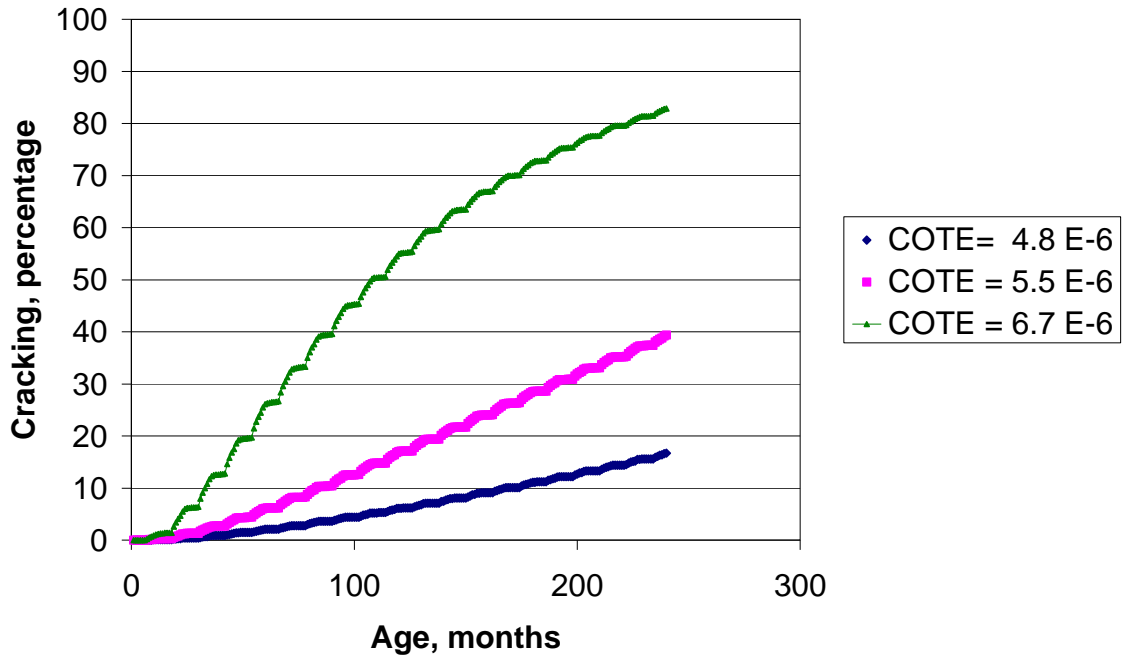


Figure 9 Effect of COTE on cracking. Location -Rochester, AADTT=500, HPCC =9, MR=500, HBase=6, Base -Class 5, Lane Width =12, Joint Spacing =15, Dowel D = none, Shoulders - AC, Subgrade - A-6

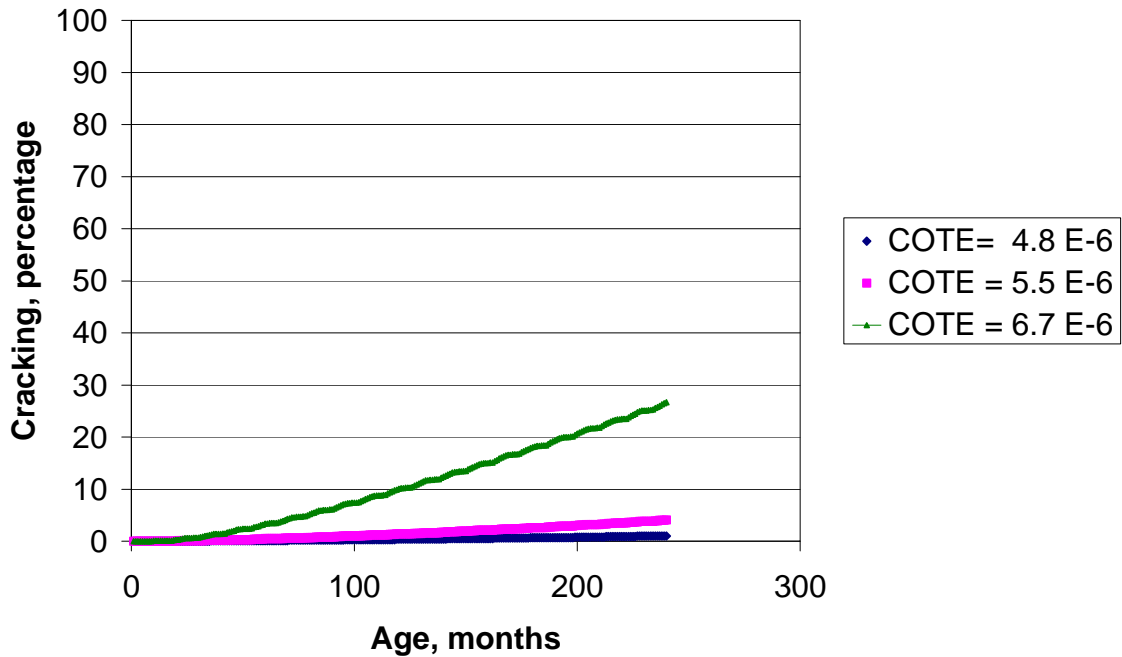


Figure 10 Effect of COTE on cracking. Location -Rochester, AADTT=500, HPCC =10, MR=500, HBase=6, Base -Class 5, Lane Width =12, Joint Spacing =15, Dowel D = none, Shoulders - AC, Subgrade - A-6

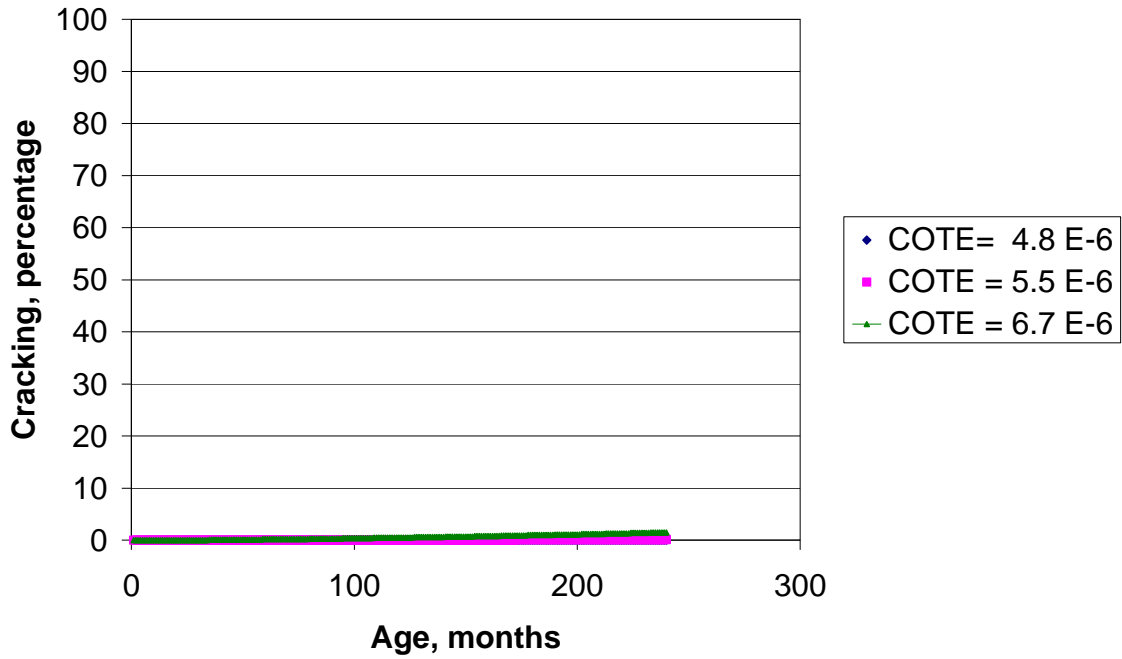


Figure 11 Effect of COTE on cracking. Location -Rochester, AADTT=500, HPCC =12, MR=500, HBase=6, Base -Class 5, Lane Width =12, Joint Spacing =15, Dowel D = none, Shoulders - AC, Subgrade - A-6

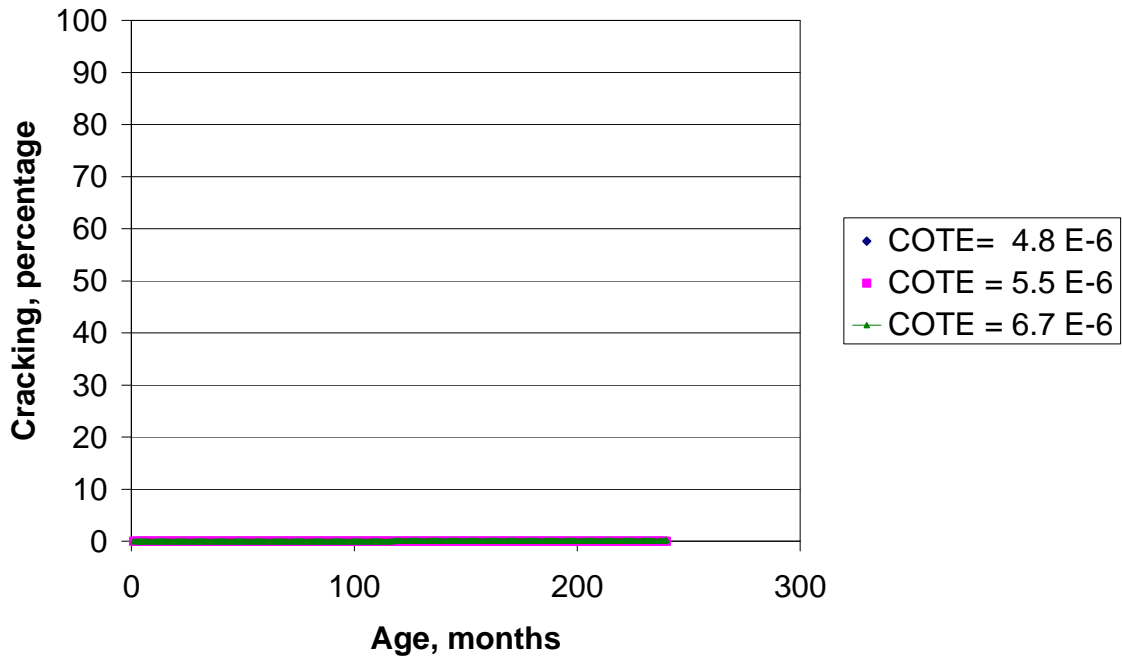


Figure 12 Effect of COTE on cracking. Location -Rochester, AADTT=500, HPCC =14, MR=500, HBase=6, Base -Class 5, Lane Width =12, Joint Spacing =15, Dowel D = none, Shoulders - AC, Subgrade - A-6

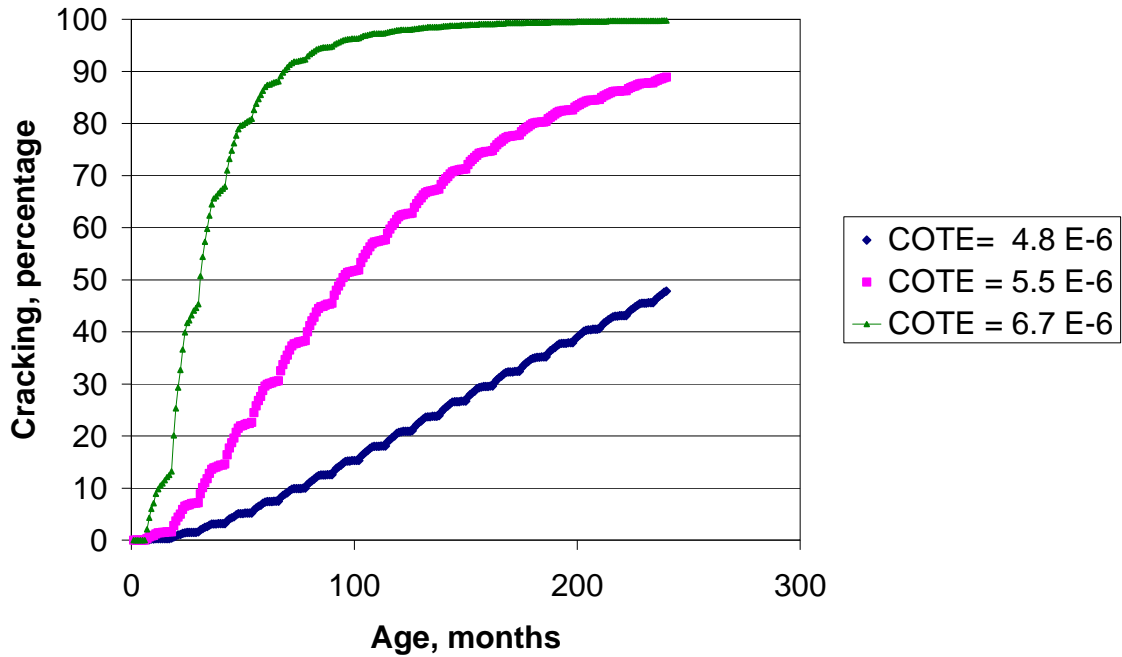


Figure 13 Effect of MR on cracking. Location -Rochester, AADTT=500, HPCC =10, MR=500, HBase=6, Base -Class 5, Lane Width =12, Joint Spacing =20, Dowel D = none, Shoulders - AC, Subgrade - A-6

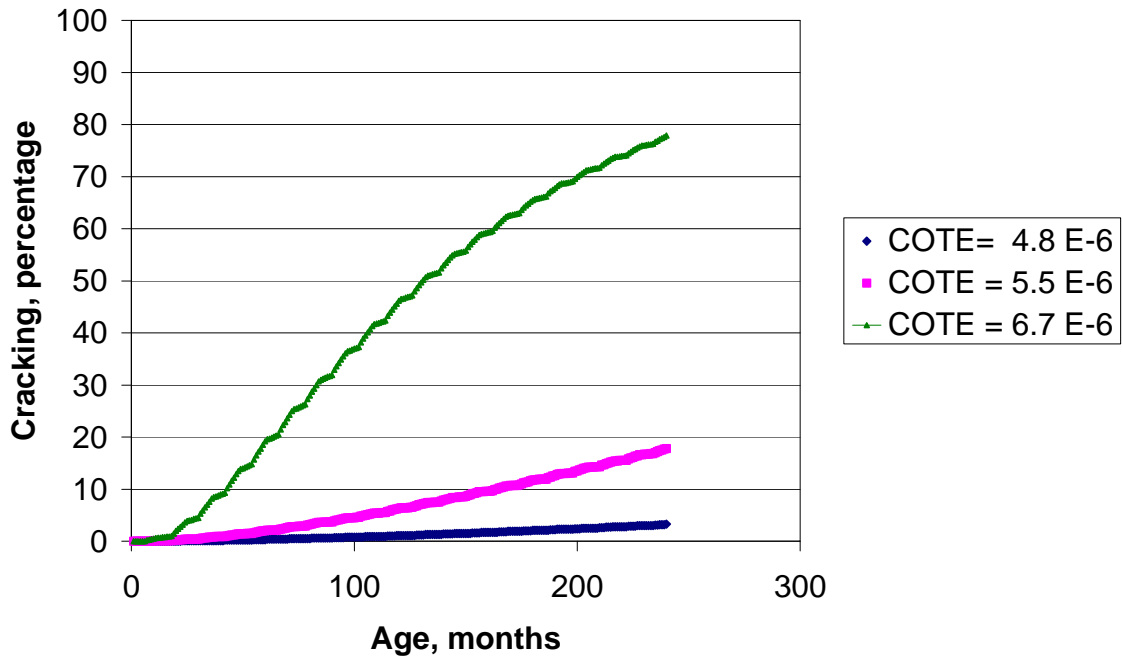


Figure 14 Effect of MR on cracking. Location -Rochester, AADTT=500, HPCC =10, MR=700, HBase=6, Base -Class 5, Lane Width =12, Joint Spacing =20, Dowel D = none, Shoulders - AC, Subgrade - A-6

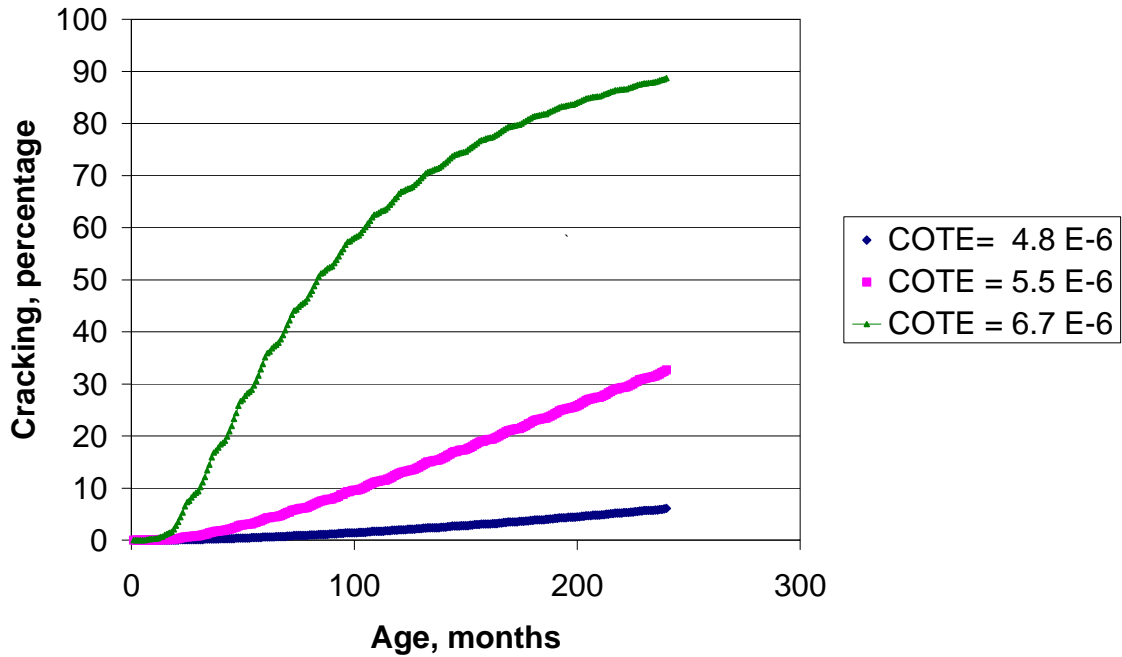


Figure 15 Effect of MR on cracking. Location -Rochester, AADTT=500, HPCC =12, MR=500, HBase=6, Base -Class 5, Lane Width =12, Joint Spacing =20, Dowel D = none, Shoulders - AC, Subgrade - A-6

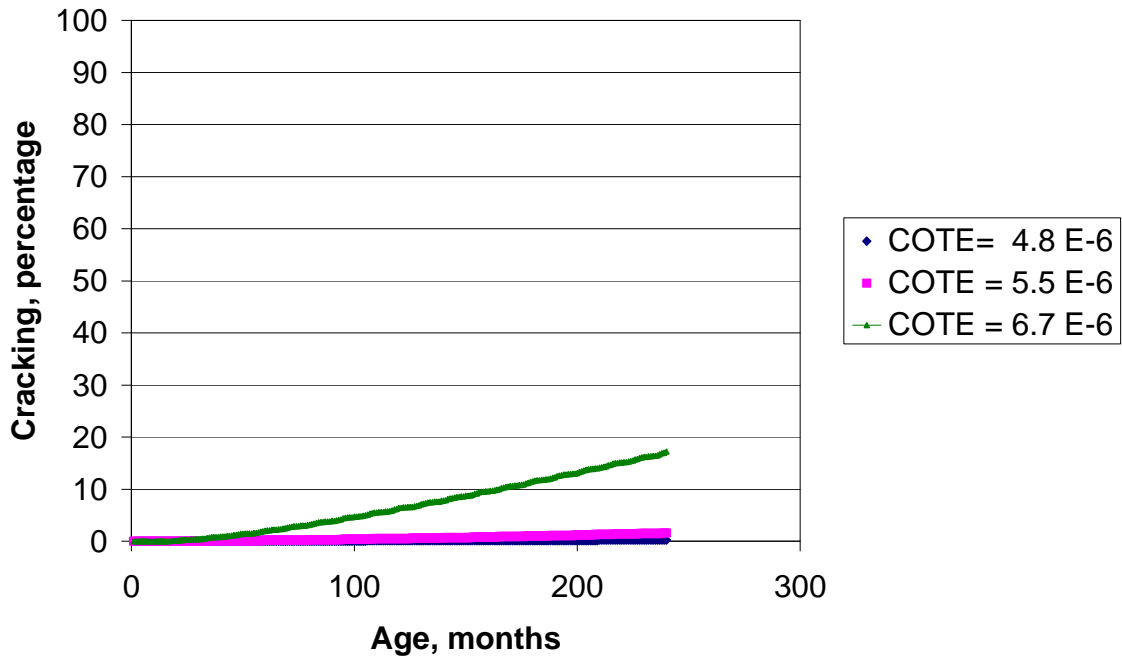


Figure 16 Effect of MR on cracking. Location -Rochester, AADTT=500, HPCC =12, MR=700, HBase=6, Base -Class 5, Lane Width =12, Joint Spacing =20, Dowel D = none, Shoulders - AC, Subgrade - A-6

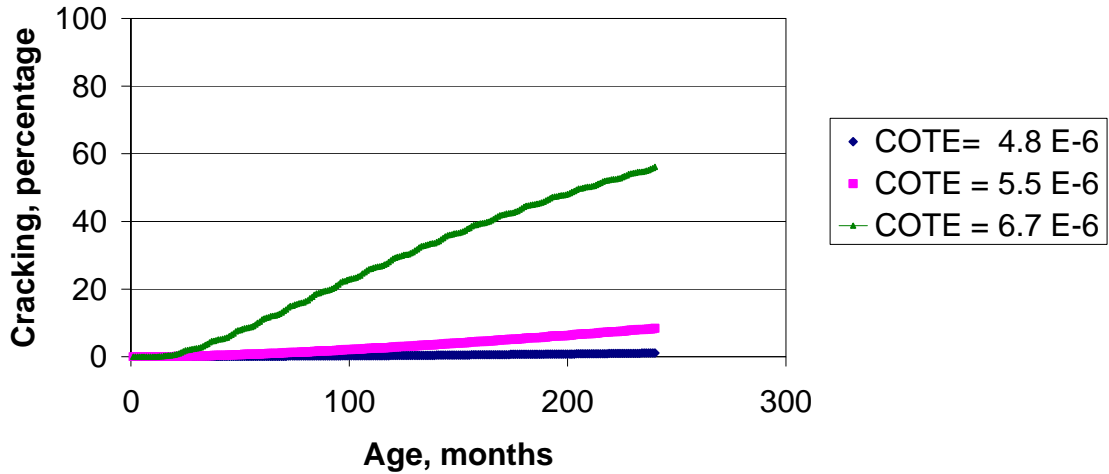


Figure 17 Effect of MR on cracking. Location -Rochester, AADTT=500, HPCC =14, MR=500, HBase=6, Base -Class 5, Lane Width =12, Joint Spacing =20, Dowel D = none, Shoulders - AC, Subgrade - A-6

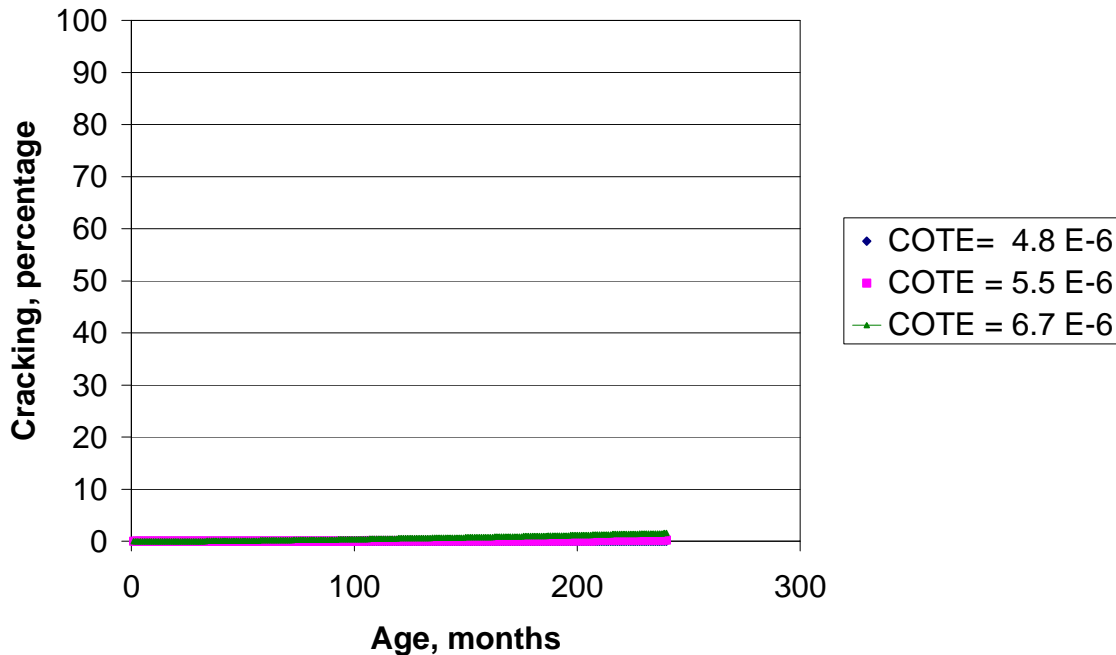


Figure 18 Effect of MR on cracking. Location -Rochester, AADTT=500, HPCC =14, MR=700, HBase=6, Base -Class 5, Lane Width =12, Joint Spacing =20, Dowel D = none, Shoulders - AC, Subgrade - A-6

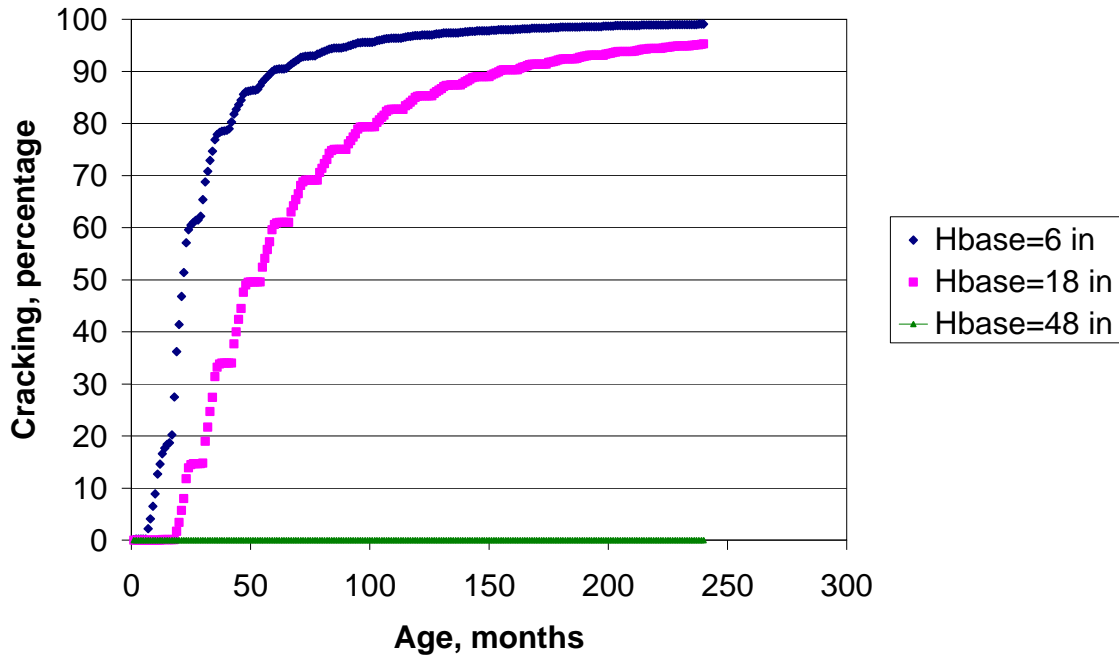


Figure 19 Effect of Base Thickness on cracking. Location -Rochester, AADTT=500, HPCC =6, COTE =0.0000048, MR=500, Base -Class 5, Lane Width =12, Joint Spacing =15, Dowel D = none, Shoulders - AC, Subgrade - A-6

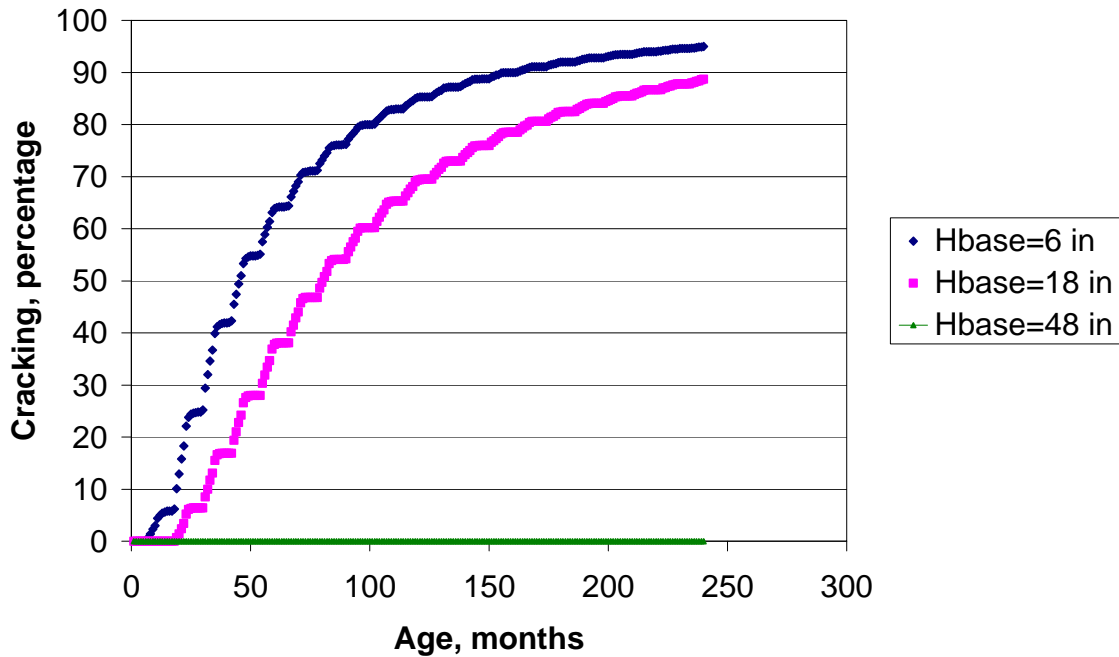


Figure 20 Effect of Base Thickness on cracking. Location -Rochester, AADTT=500, HPCC =7, COTE =0.0000048, MR=500, Base -Class 5, Lane Width =12, Joint Spacing =15, Dowel D = none, Shoulders - AC, Subgrade - A-6

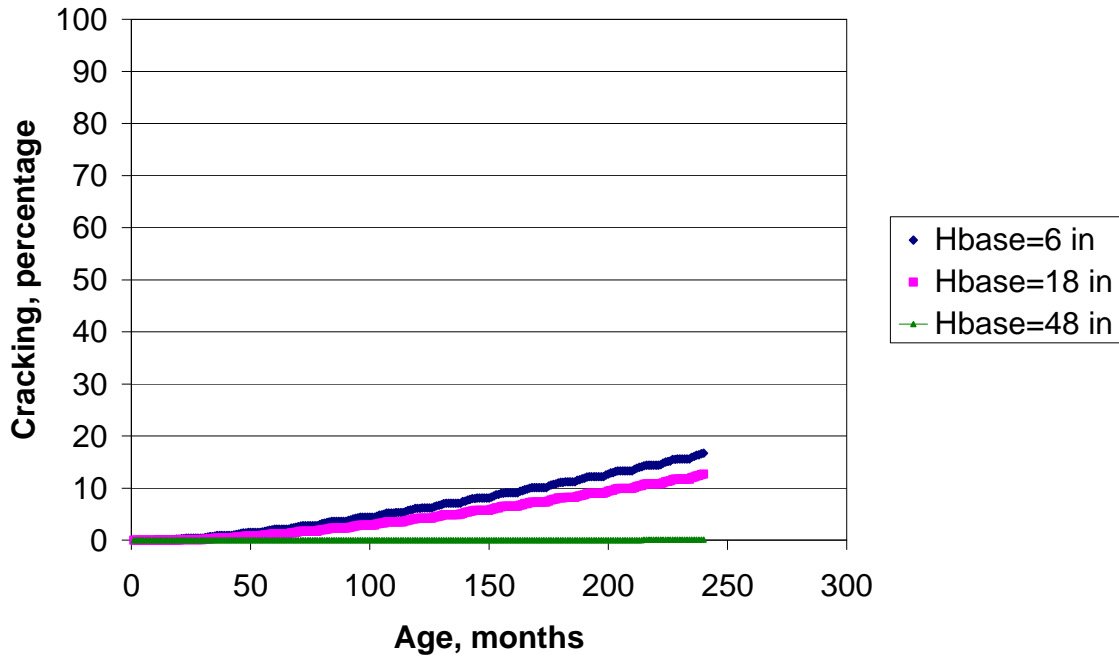


Figure 21 Effect of Base Thickness on cracking. Location -Rochester, AADTT=500, HPCC =9, COTE =0.0000048, MR=500, Base -Class 5, Lane Width =12, Joint Spacing =15, Dowel D = none, Shoulders - AC, Subgrade - A-6

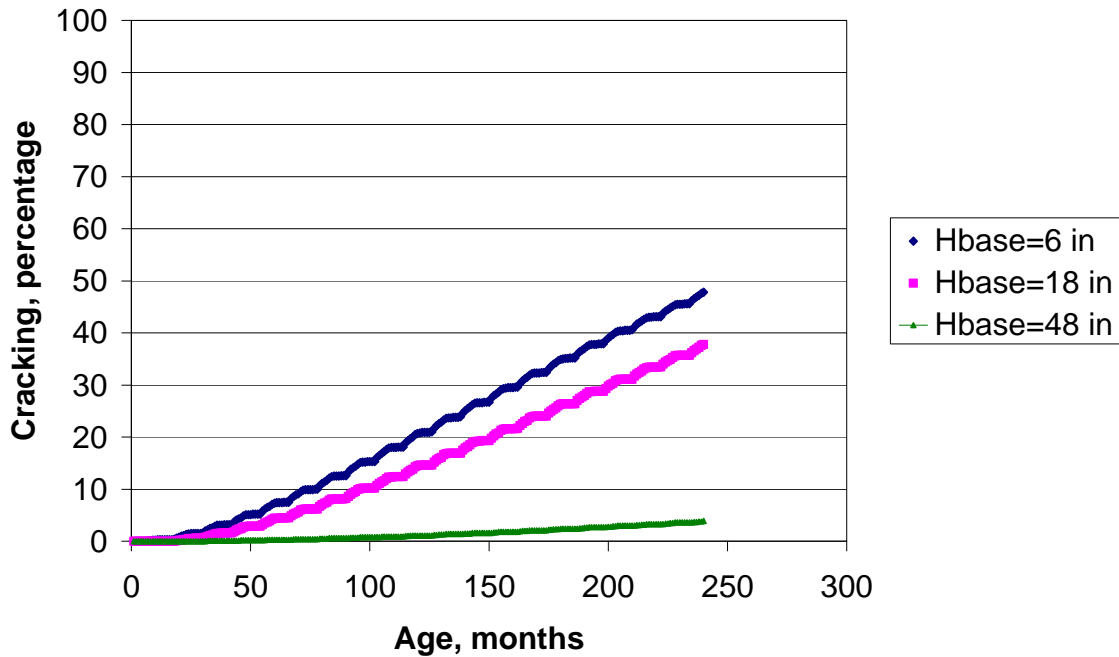


Figure 22 Effect of Base Thickness on cracking. Location -Rochester, AADTT=500, HPCC =10, COTE =0.0000048, MR=500, Base -Class 5, Lane Width =12, Joint Spacing =20, Dowel D = none, Shoulders - AC, Subgrade - A-6

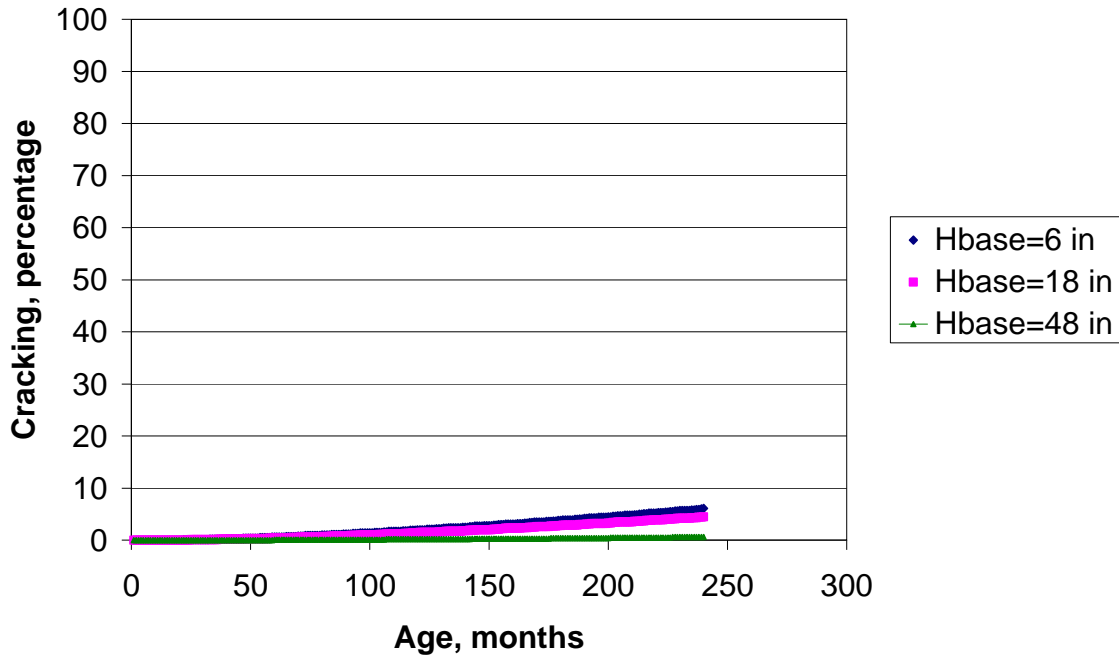


Figure 23 Effect of Base Thickness on cracking. Location -Rochester, AADTT=500, HPCC =12, COTE =0.0000048, MR=500, Base -Class 5, Lane Width =12, Joint Spacing =20, Dowel D = none, Shoulders - AC, Subgrade - A-6

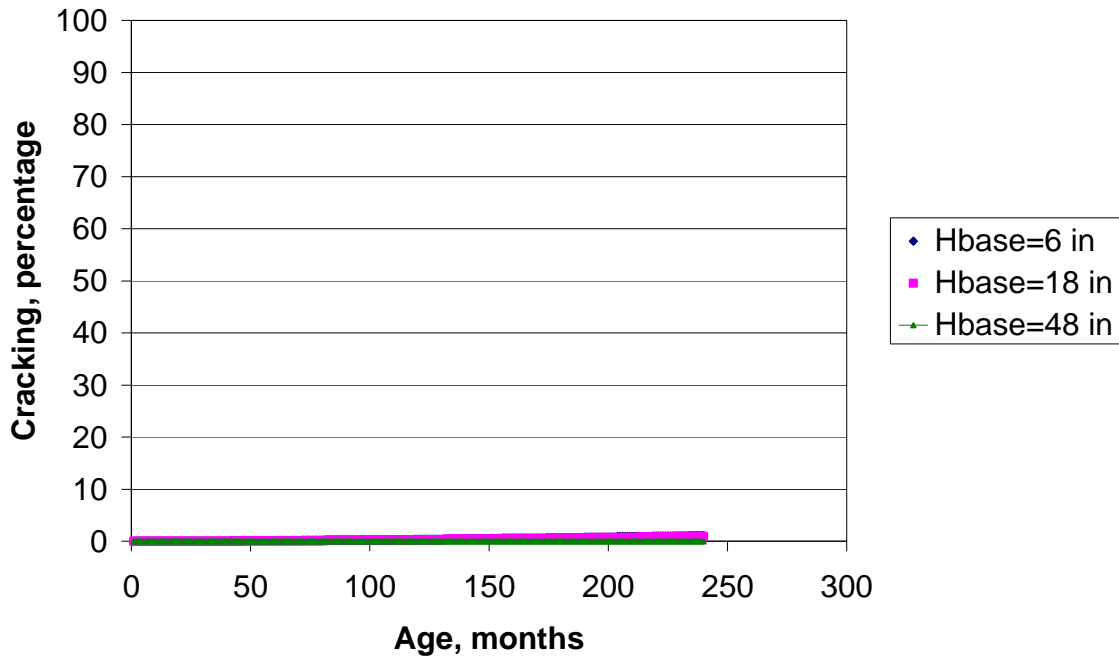


Figure 24 Effect of Base Thickness on cracking. Location -Rochester, AADTT=500, HPCC =14, COTE =0.0000048, MR=500, Base -Class 5, Lane Width =12, Joint Spacing =20, Dowel D = none, Shoulders - AC, Subgrade - A-6

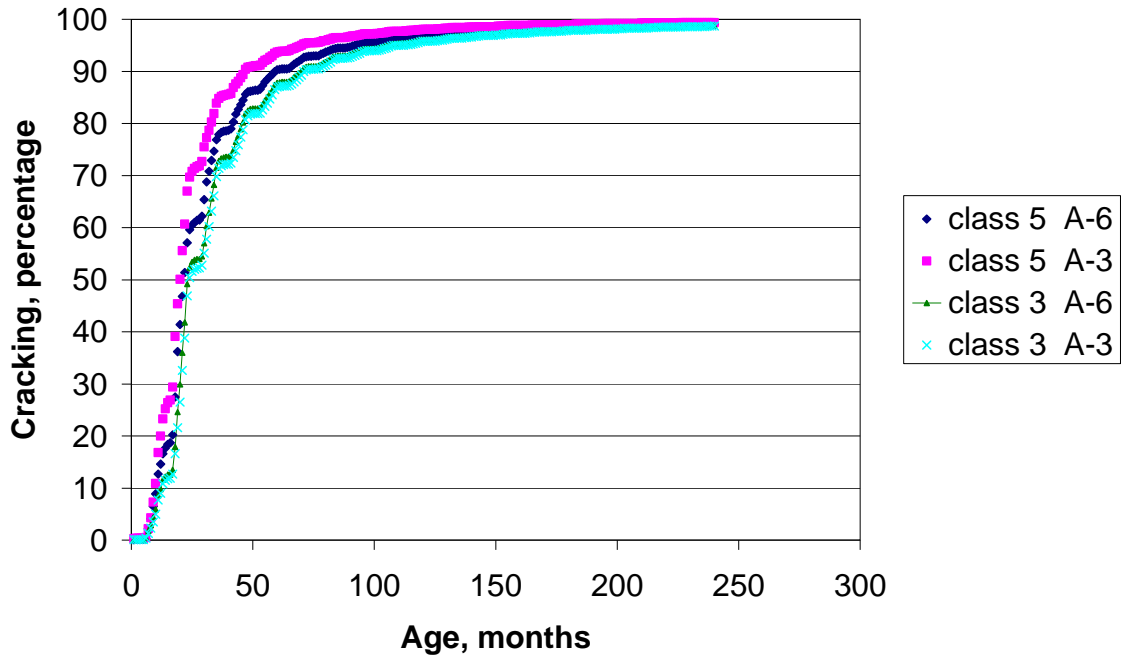


Figure 25 Effect of Base and Subgrade Material on cracking. Location -Rochester, AADTT=500, HPCC =6, COTE =0.0000048, MR=500, HBase=6, Lane Width =12, Joint Spacing =15, Dowel D = none, Shoulders – AC

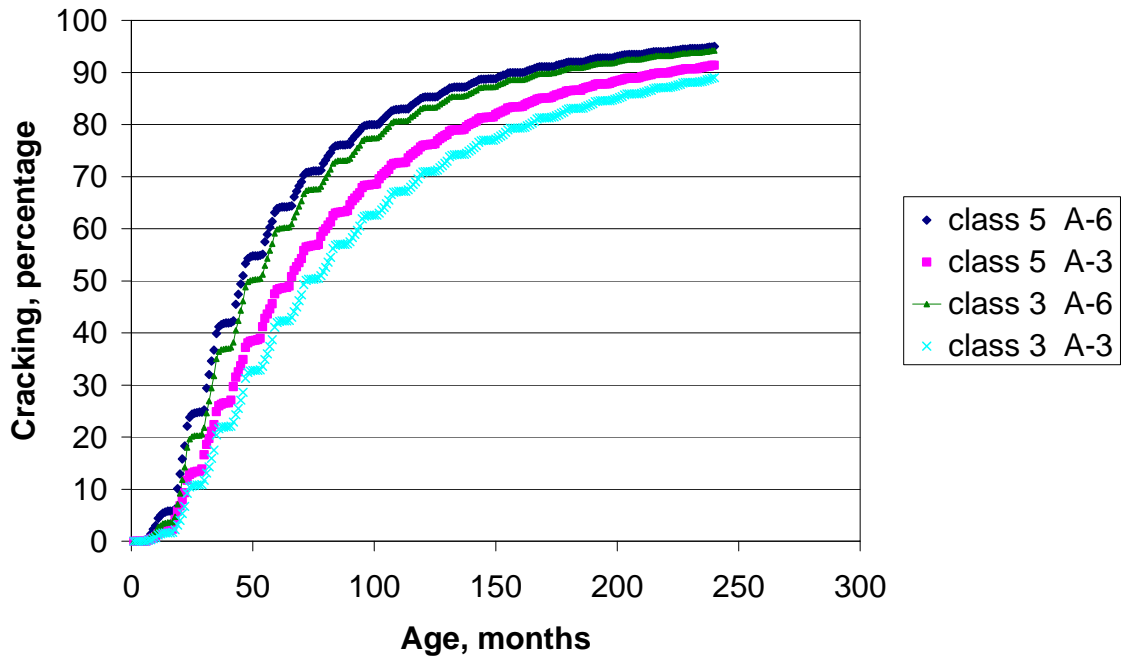


Figure 26 Effect of Base and Subgrade Material on cracking. Location -Rochester, AADTT=500, HPCC =7, COTE =0.0000048, MR=500, HBase=6, Lane Width =12, Joint Spacing =15, Dowel D = none, Shoulders - AC

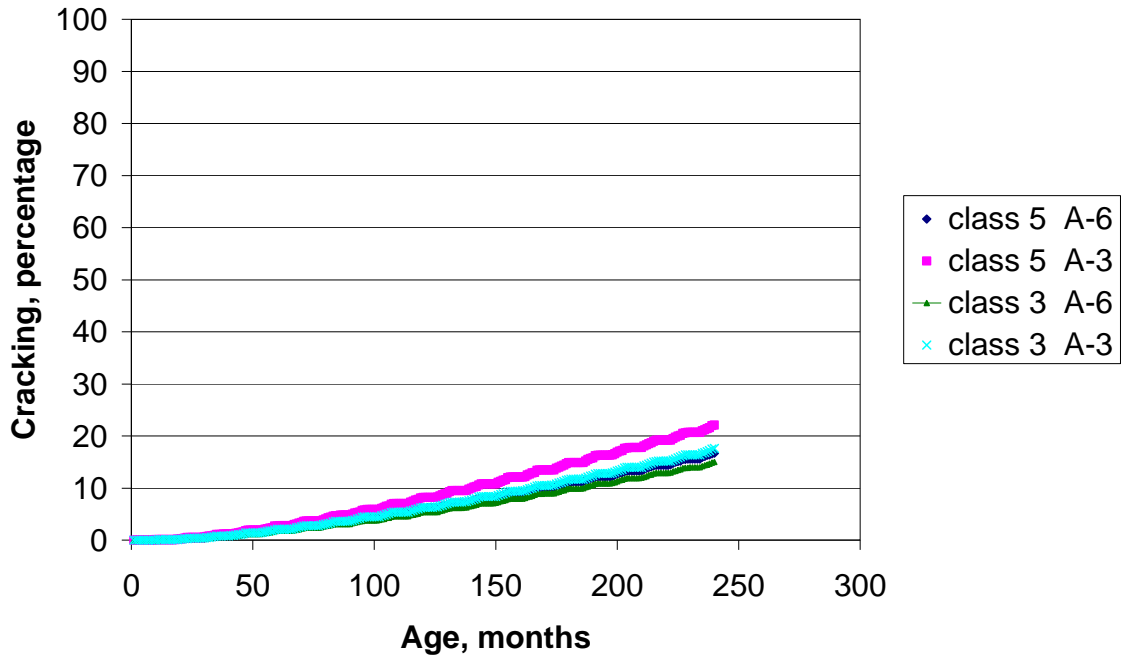


Figure 27 Effect of Base and Subgrade Material on cracking. Location -Rochester, AADTT=500, HPCC =9, COTE =0.0000048, MR=500, HBase=6, Lane Width =12, Joint Spacing =15, Dowel D = none, Shoulders – AC

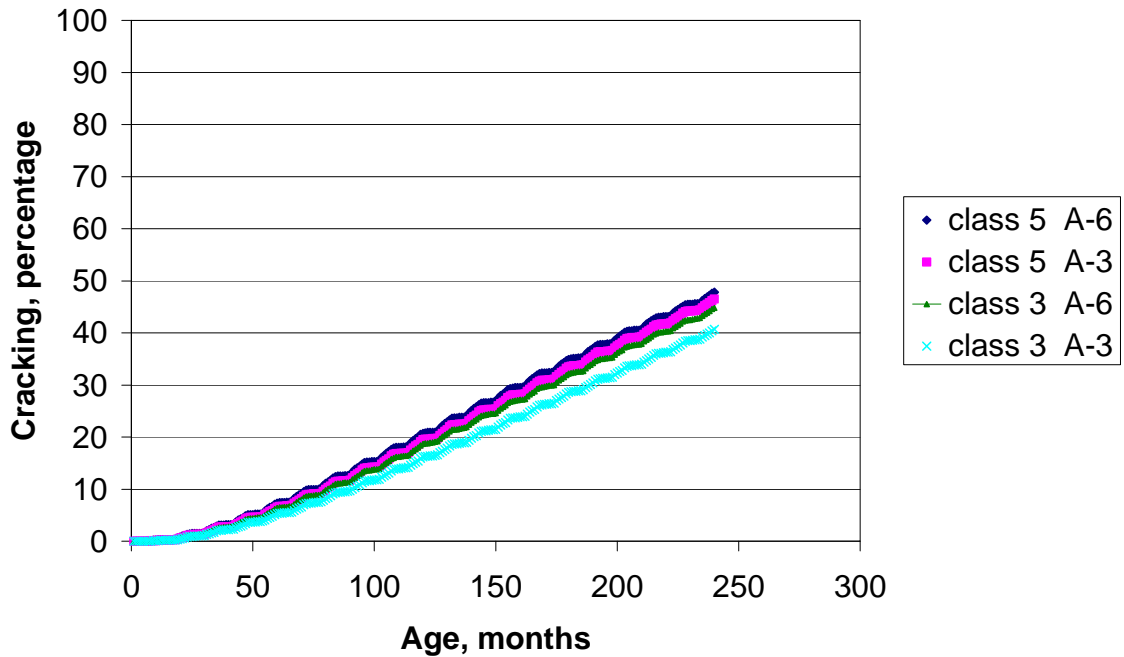


Figure 28 Effect of Base and Subgrade Material on cracking. Location -Rochester, AADTT=500, HPCC =10, COTE =0.0000048, MR=500, HBase=6, Lane Width =12, Joint Spacing =20, Dowel D = none, Shoulders - AC

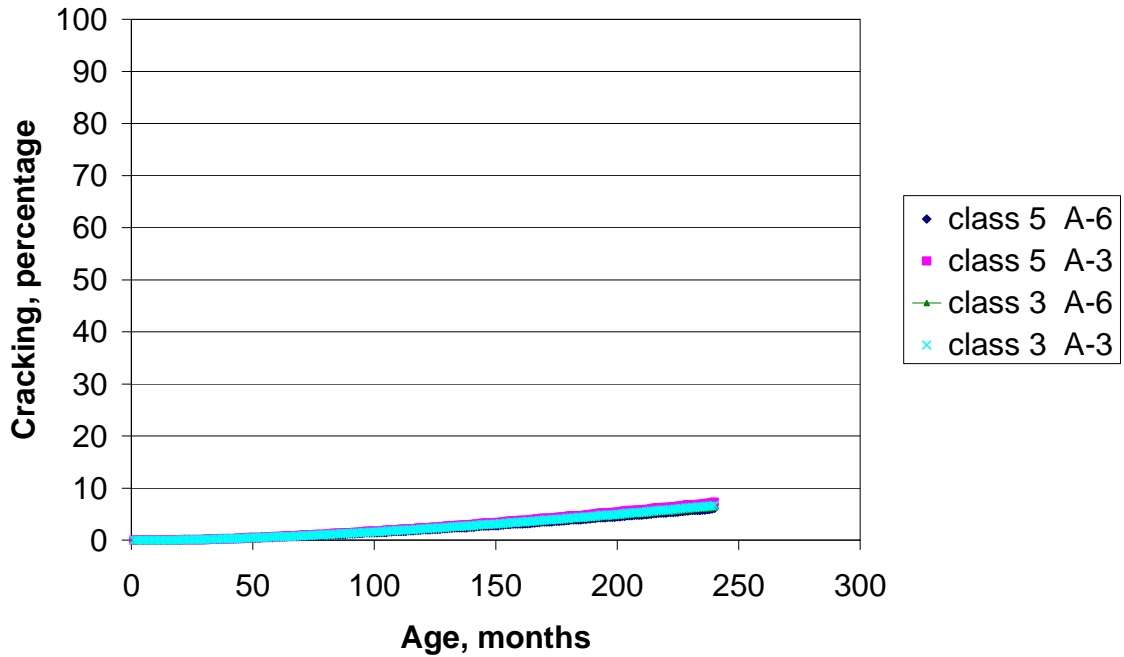


Figure 29 Effect of Base and Subgrade Material on cracking. Location -Rochester, AADTT=500, HPCC =12, COTE =0.0000048, MR=500, HBase=6, Lane Width =12, Joint Spacing =20, Dowel D = none, Shoulders – AC

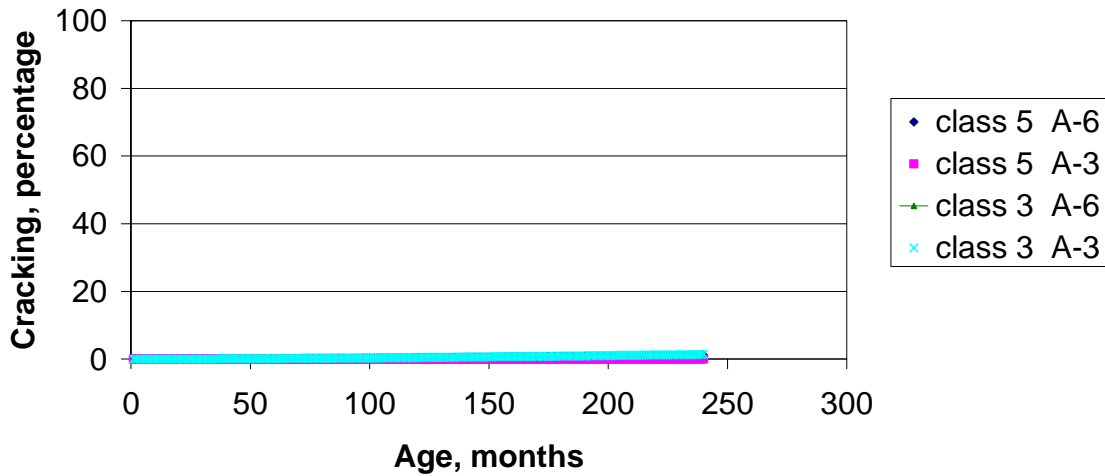


Figure 30 Effect of Base and Subgrade Material on cracking. Location -Rochester, AADTT=500, HPCC =14, COTE =0.0000048, MR=500, HBase=6, Lane Width =12, Joint Spacing =20, Dowel D = none, Shoulders - AC

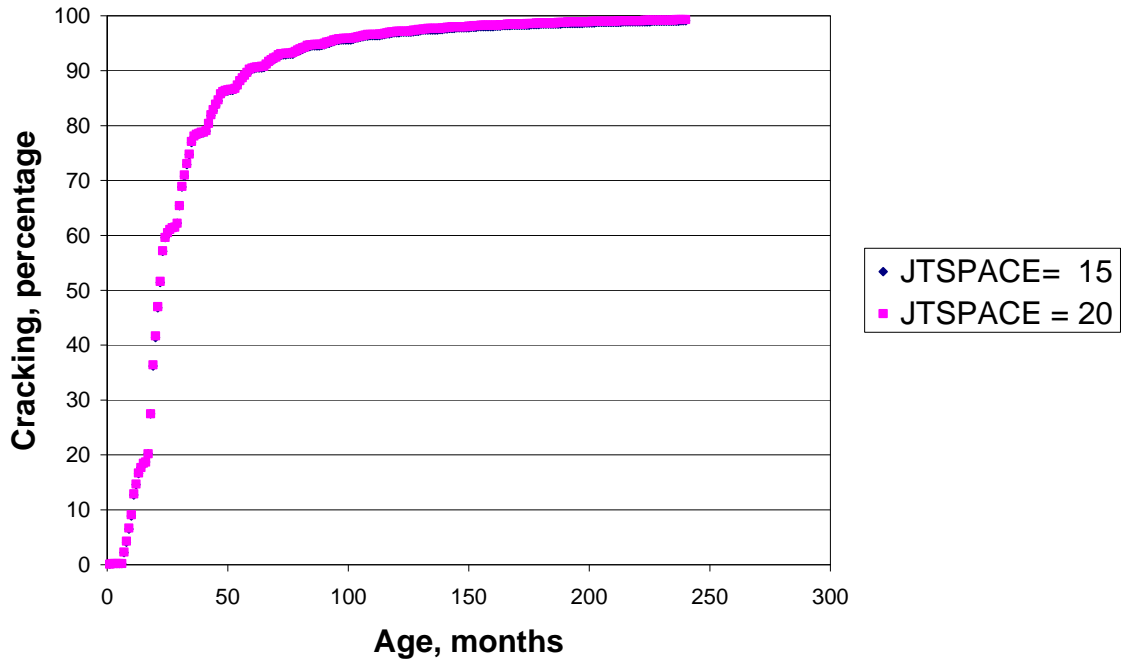


Figure 31 Effect of Joint Spacing on cracking. Location -Rochester, AADTT=500, HPCC =6, COTE =0.0000048, MR=500, HBase=6, Base -Class 5, Lane Width =12, Dowel D = none, Shoulders - AC, Subgrade - A-6

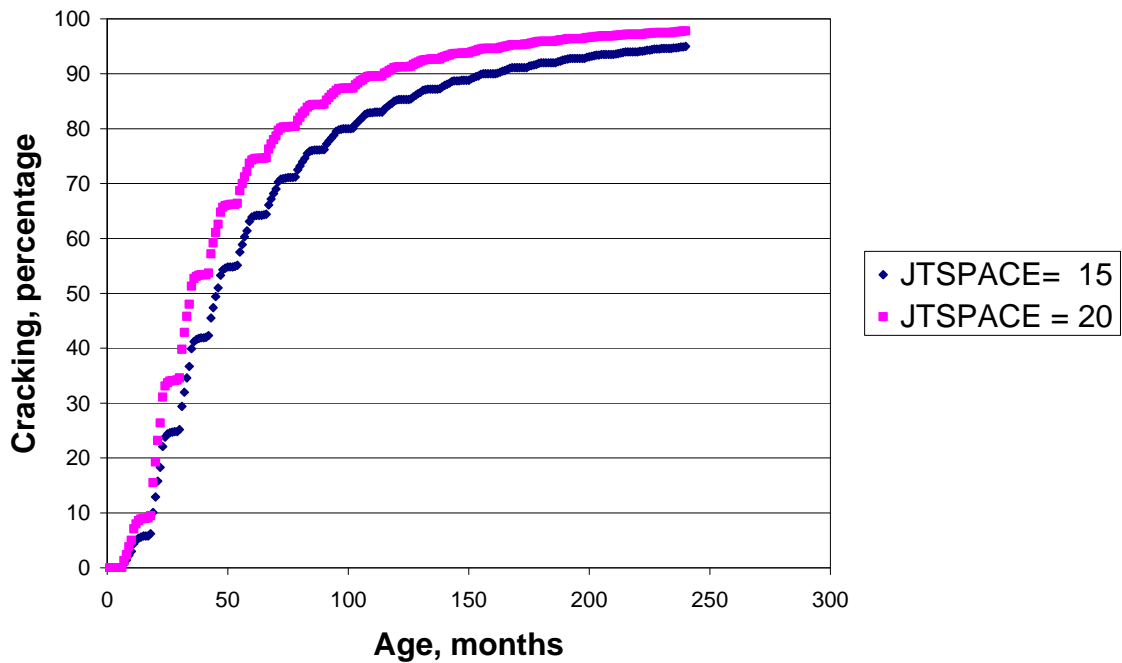


Figure 32 Effect of Joint Spacing on cracking. Location -Rochester, AADTT=500, HPCC =7, COTE =0.0000048, MR=500, HBase=6, Base -Class 5, Lane Width =12, Dowel D = none, Shoulders - AC, Subgrade - A-6

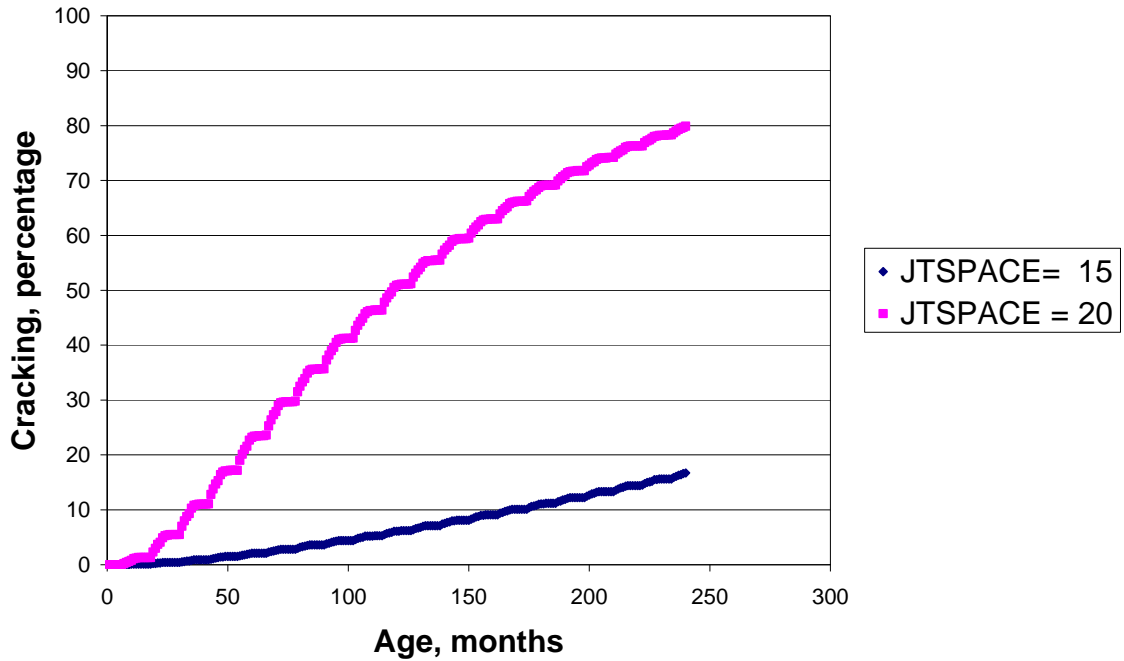


Figure 33 Effect of Joint Spacing on cracking. Location -Rochester, AADTT=500, HPCC =9, COTE =0.0000048, MR=500, HBase=6, Base -Class 5, Lane Width =12, Dowel D = none, Shoulders - AC, Subgrade - A-6

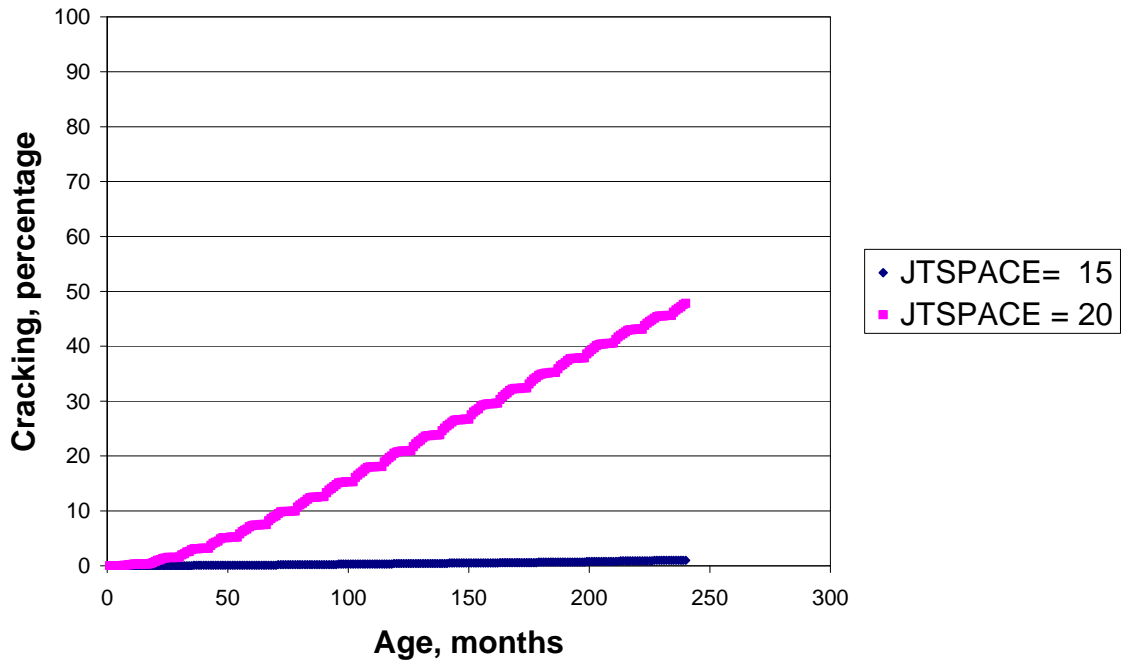


Figure 34 Effect of Joint Spacing on cracking. Location -Rochester, AADTT=500, HPCC =10, COTE =0.0000048, MR=500, HBase=6, Base -Class 5, Lane Width =12, Dowel D = none, Shoulders - AC, Subgrade - A-6

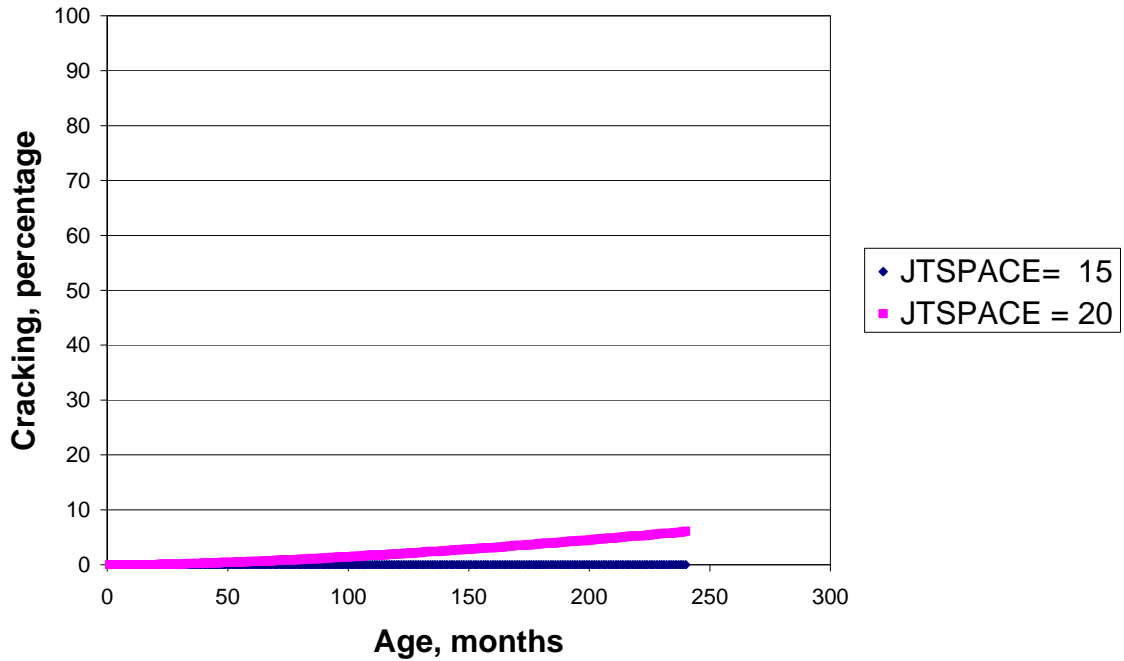


Figure 35 Effect of Joint Spacing on cracking. Location -Rochester, AADTT=500, HPCC =12, COTE =0.0000048, MR=500, HBase=6, Base -Class 5, Lane Width =12, Dowel D = none, Shoulders - AC, Subgrade - A-6

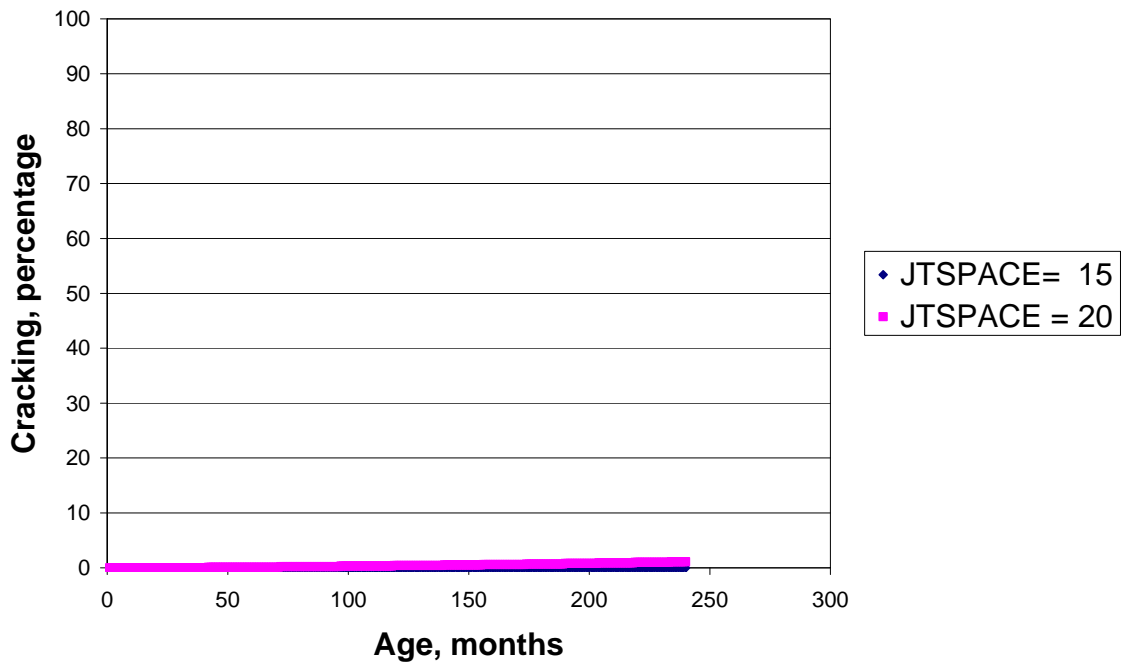


Figure 36 Effect of Joint Spacing on cracking. Location -Rochester, AADTT=500, HPCC =14, COTE =0.0000048, MR=500, HBase=6, Base -Class 5, Lane Width =12, Dowel D = none, Shoulders - AC, Subgrade - A-6

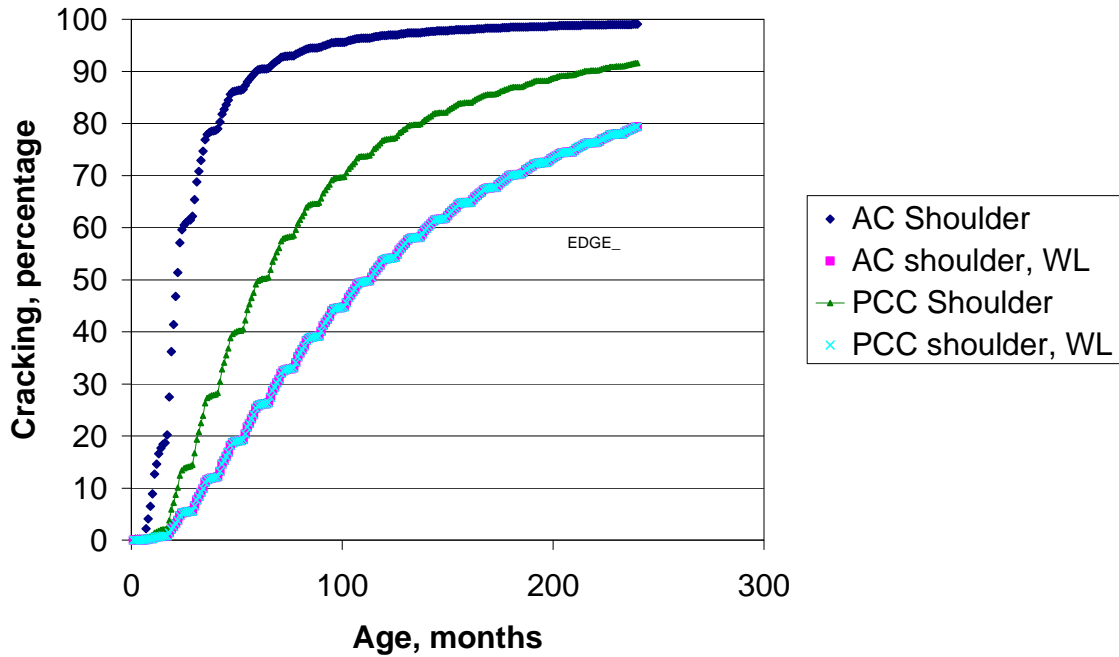


Figure 37 Effect of Edge Support on cracking. Location -Rochester, AADTT=500, HPCC =6, COTE =0.0000048, MR=500, HBase=6, Base -Class 5, Joint Spacing =15, Dowel D = none, Subgrade - A-6

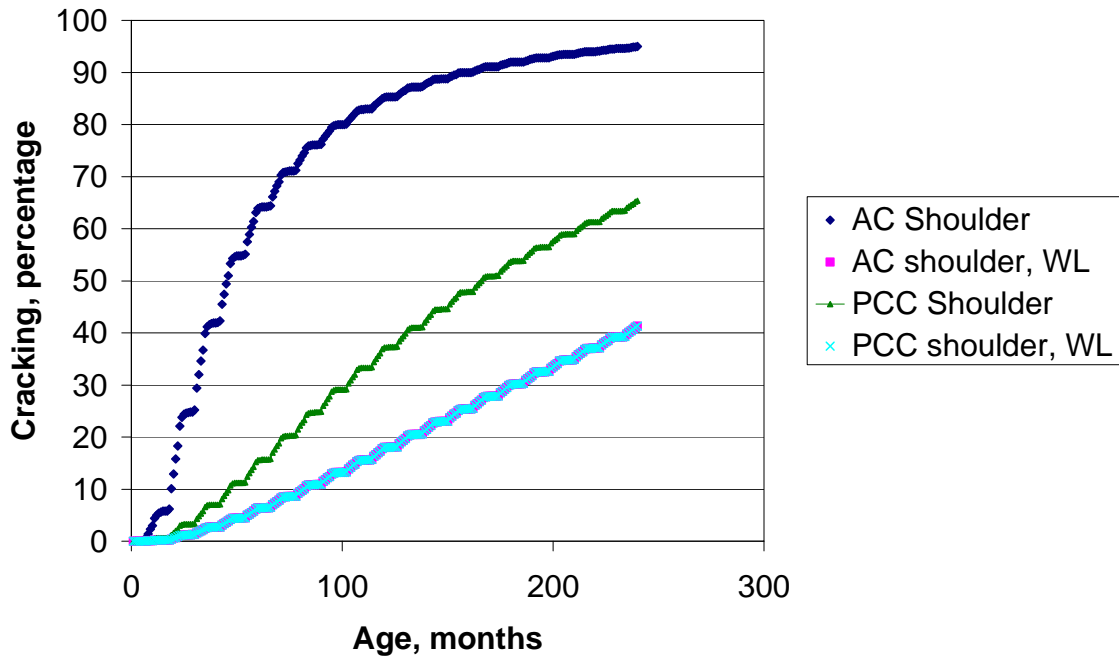


Figure 38 Effect of Edge Support on cracking. Location -Rochester, AADTT=500, HPCC =7, COTE =0.0000048, MR=500, HBase=6, Base -Class 5, Joint Spacing =15, Dowel D = none, Subgrade - A-6

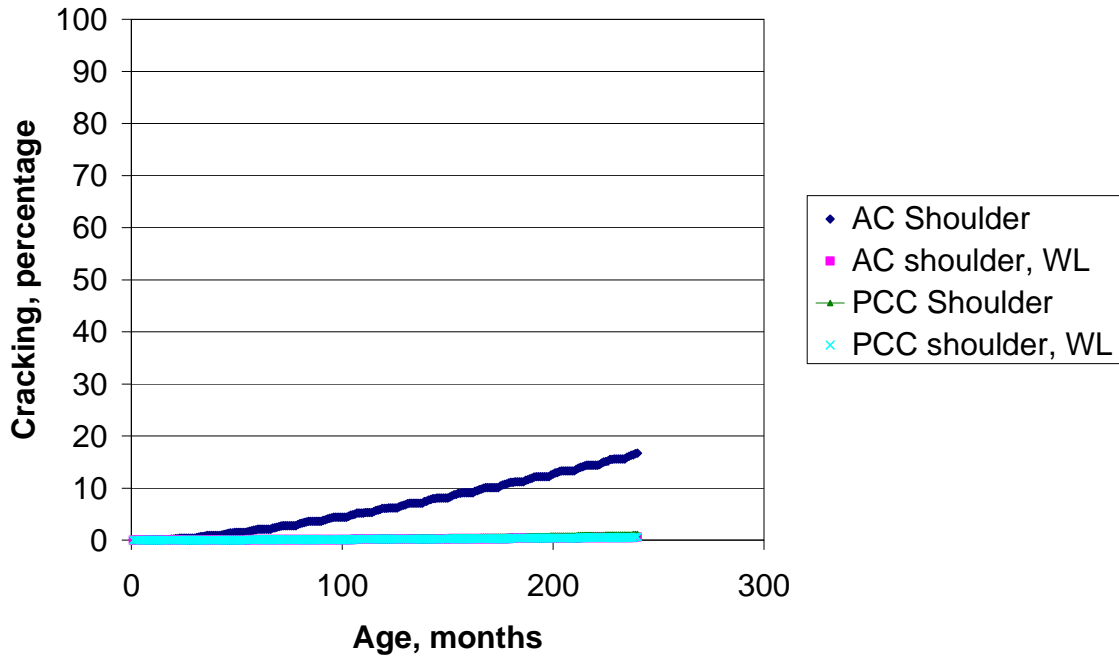


Figure 39 Effect of Edge Support on cracking. Location -Rochester, AADTT=500, HPCC =9, COTE =0.0000048, MR=500, HBase=6, Base -Class 5, Joint Spacing =15, Dowel D = none, Subgrade - A-6

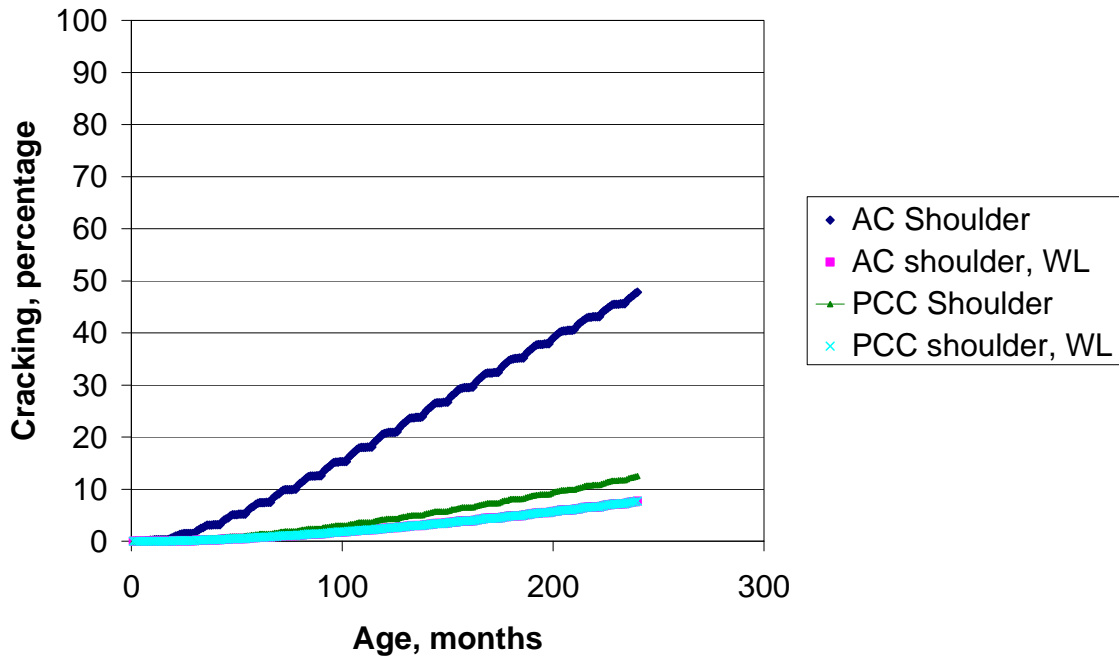


Figure 40 Effect of Edge Support on cracking. Location -Rochester, AADTT=500, HPCC =10, COTE =0.0000048, MR=500, HBase=6, Base -Class 5, Joint Spacing =20, Dowel D = none, Subgrade - A-6

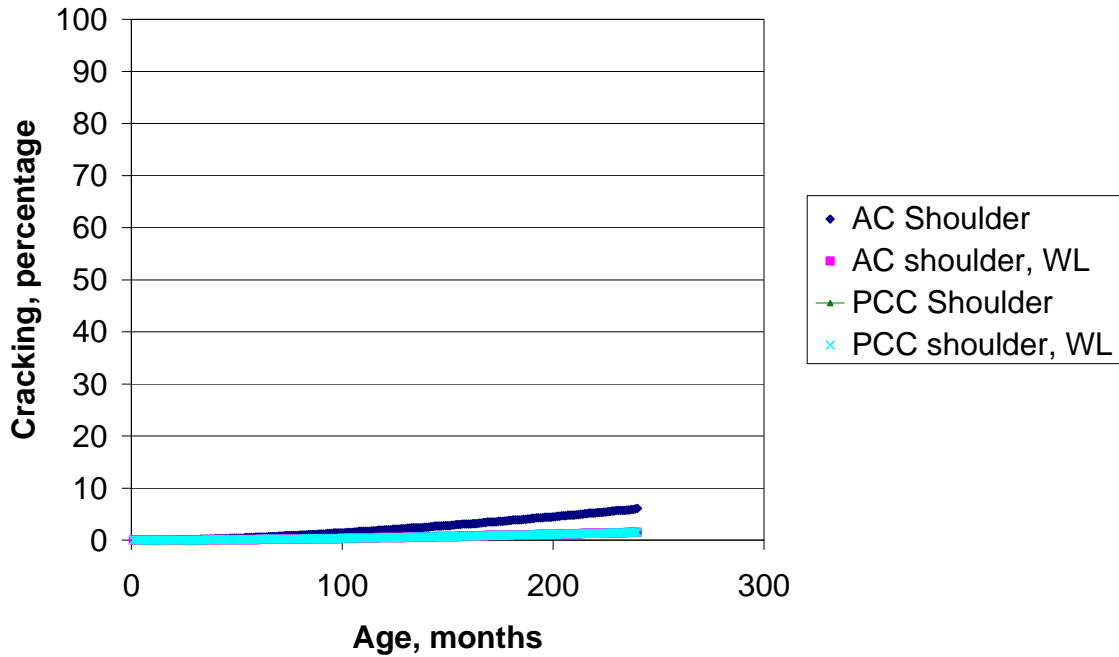


Figure 41 Effect of Edge Support on cracking. Location -Rochester, AADTT=500, HPCC =12, COTE =0.0000048, MR=500, HBase=6, Base -Class 5, Joint Spacing =20, Dowel D = none, Subgrade - A-6

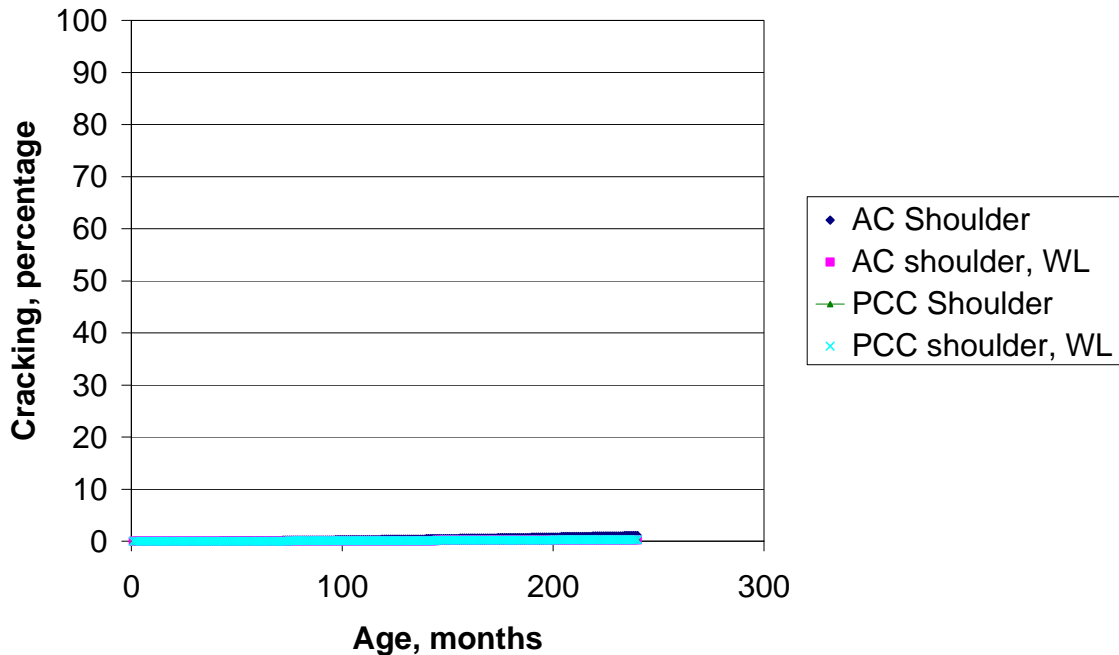


Figure 42 Effect of Edge Support on cracking. Location -Rochester, AADTT=500, HPCC =14, COTE =0.0000048, MR=500, HBase=6, Base -Class 5, Joint Spacing =20, Dowel D = none, Subgrade - A-6

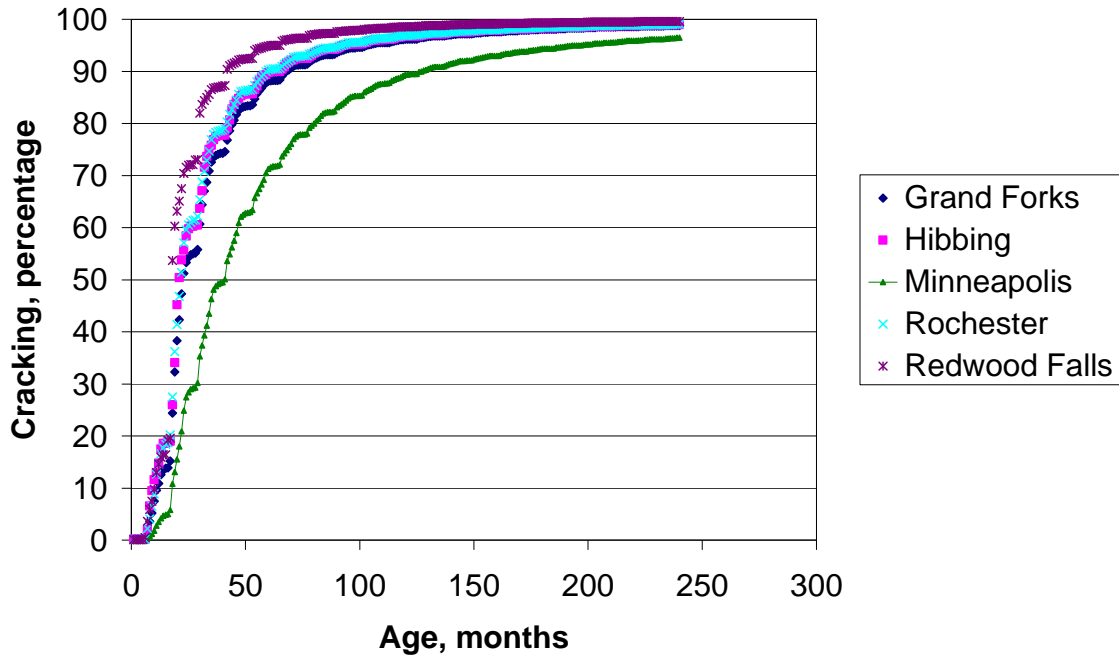


Figure 43 Effect of Location (Climatic Zone) on cracking. AADTT=500, HPCC =6, COTE =0.0000048, MR=500, HBase=6, Base -Class 5, Lane Width =12, Joint Spacing =15, Dowel D = none, Shoulders - AC, Subgrade - A-6

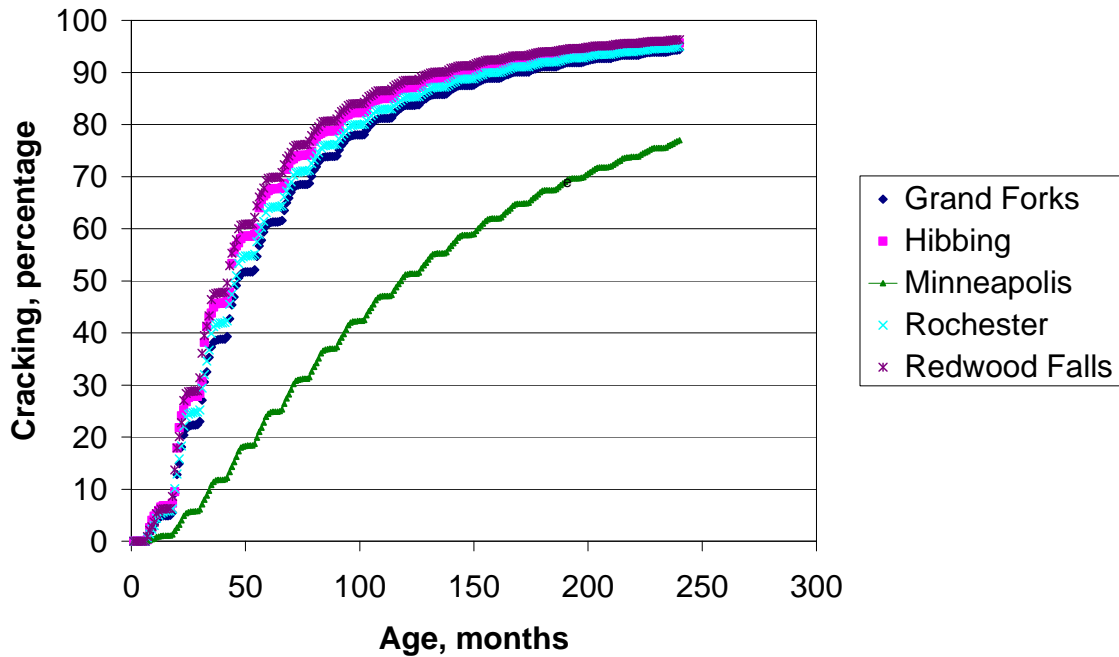


Figure 44 Effect of Location (Climatic Zone) on cracking. AADTT=500, HPCC =7, COTE =0.0000048, MR=500, HBase=6, Base -Class 5, Lane Width =12, Joint Spacing =15, Dowel D = none, Shoulders - AC, Subgrade - A-6

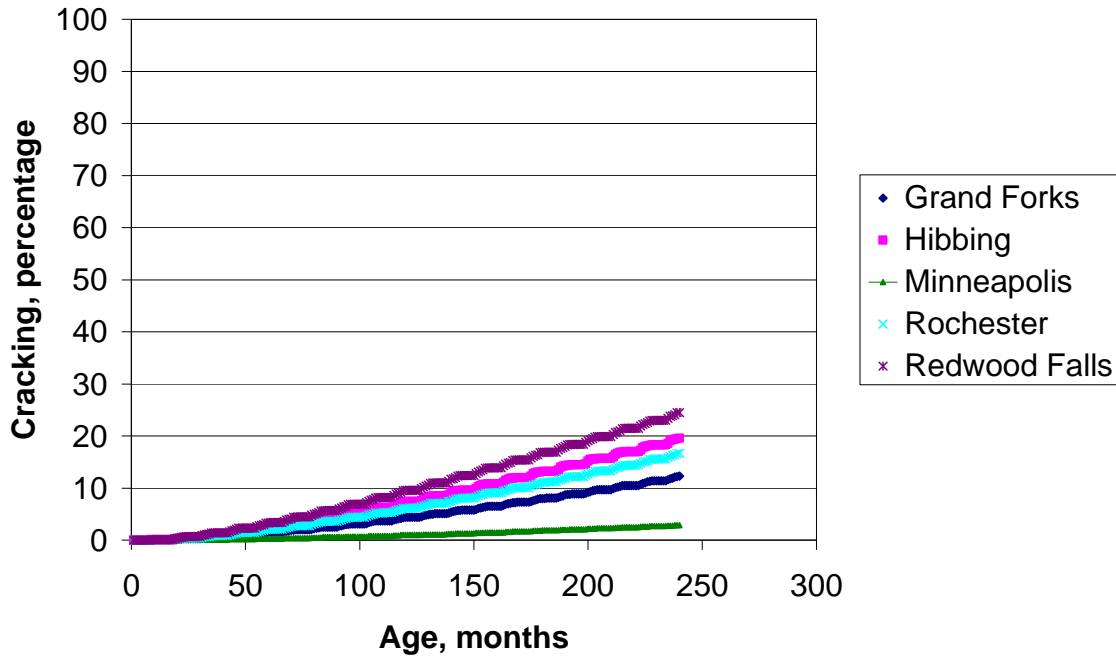


Figure 45 Effect of Location (Climatic Zone) on cracking. AADTT=500, HPCC =9, COTE =0.0000048, MR=500, HBase=6, Base -Class 5, Lane Width =12, Joint Spacing =15, Dowel D = none, Shoulders - AC, Subgrade - A-6

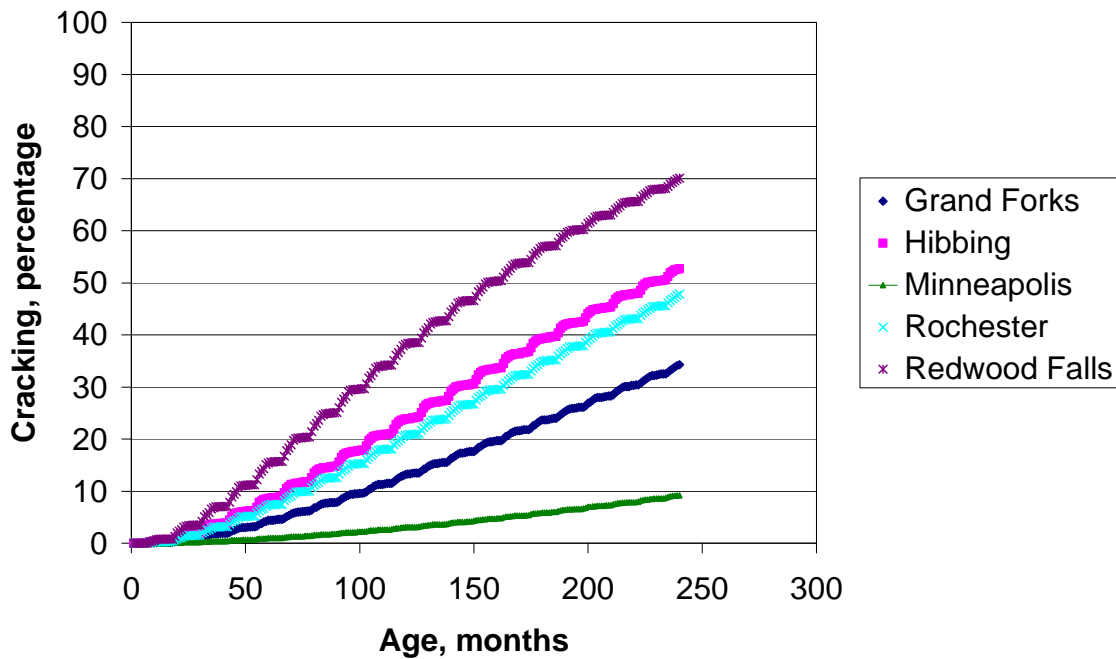


Figure 46 Effect of Location (Climatic Zone) on cracking. AADTT=500, HPCC =10, COTE =0.0000048, MR=500, HBase=6, Base -Class 5, Lane Width =12, Joint Spacing =20, Dowel D = none, Shoulders - AC, Subgrade - A-6

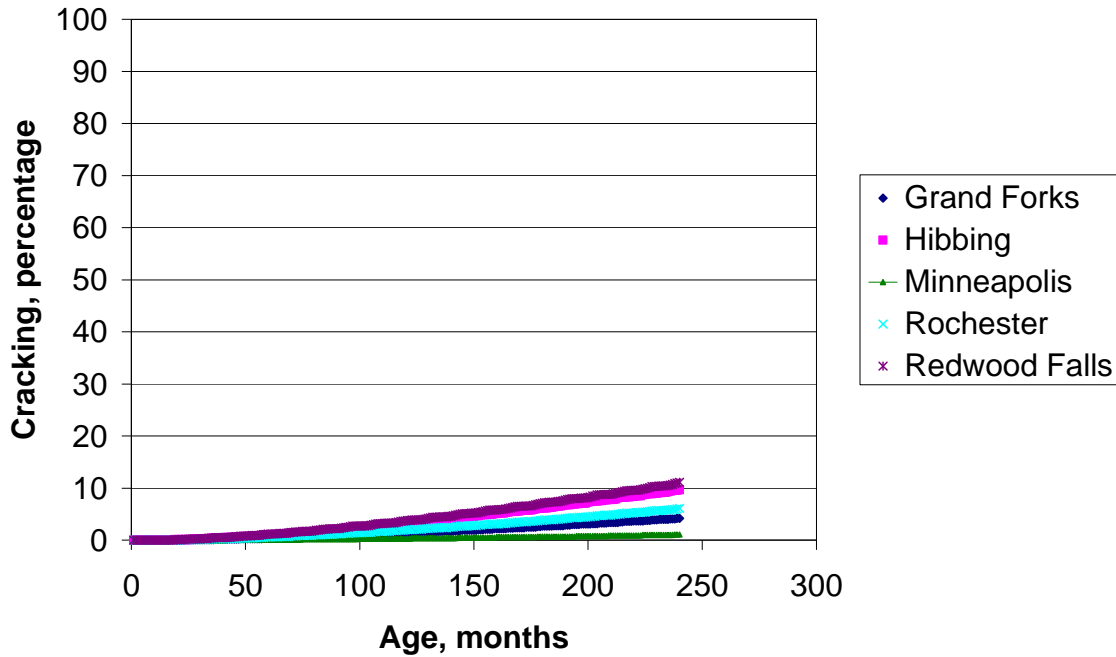


Figure 47 Effect of Location (Climatic Zone) on cracking. AADTT=500, HPCC =12, COTE =0.0000048, MR=500, HBase=6, Base -Class 5, Lane Width =12, Joint Spacing =20, Dowel D = none, Shoulders - AC, Subgrade - A-6

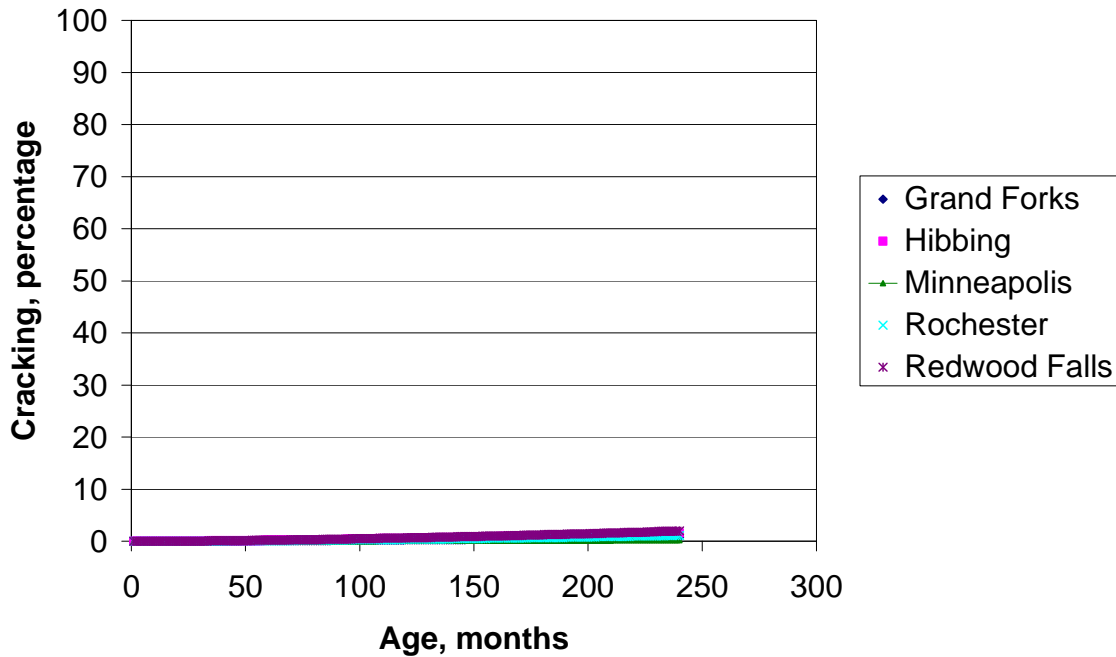


Figure 48 Effect of Location (Climatic Zone) on cracking. AADTT=500, HPCC =14, COTE =0.0000048, MR=500, HBase=6, Base -Class 5, Lane Width =12, Joint Spacing =20, Dowel D = none, Shoulders - AC, Subgrade - A-6

Predicted Faulting Charts

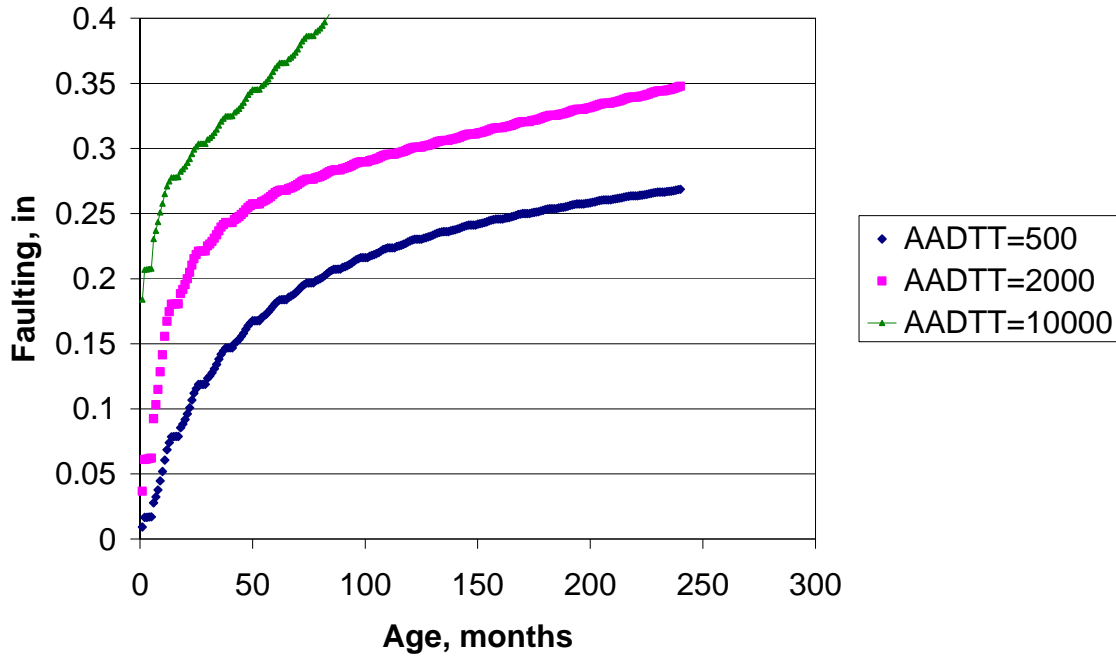


Figure 49 Effect of Traffic on faulting. Location -Rochester, HPCC =6, COTE =0.0000055, MR=700, HBase=6, Base -Class 5, Lane Width =12, Joint Spacing =15, Dowel D = 0, Shoulders - AC, Subgrade - A-6

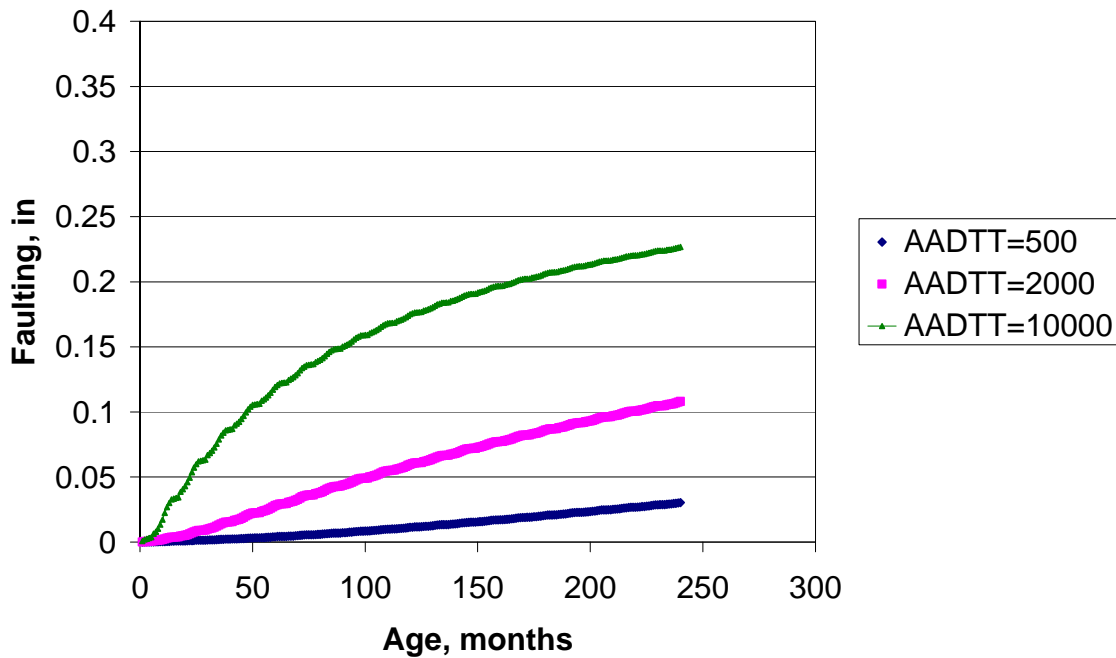


Figure 50 Effect of Traffic on faulting. Location -Rochester, HPCC =6, COTE =0.0000055, MR=700, HBase=6, Base -Class 5, Lane Width =12, Joint Spacing =15, Dowel D = 1, Shoulders - AC, Subgrade - A-6

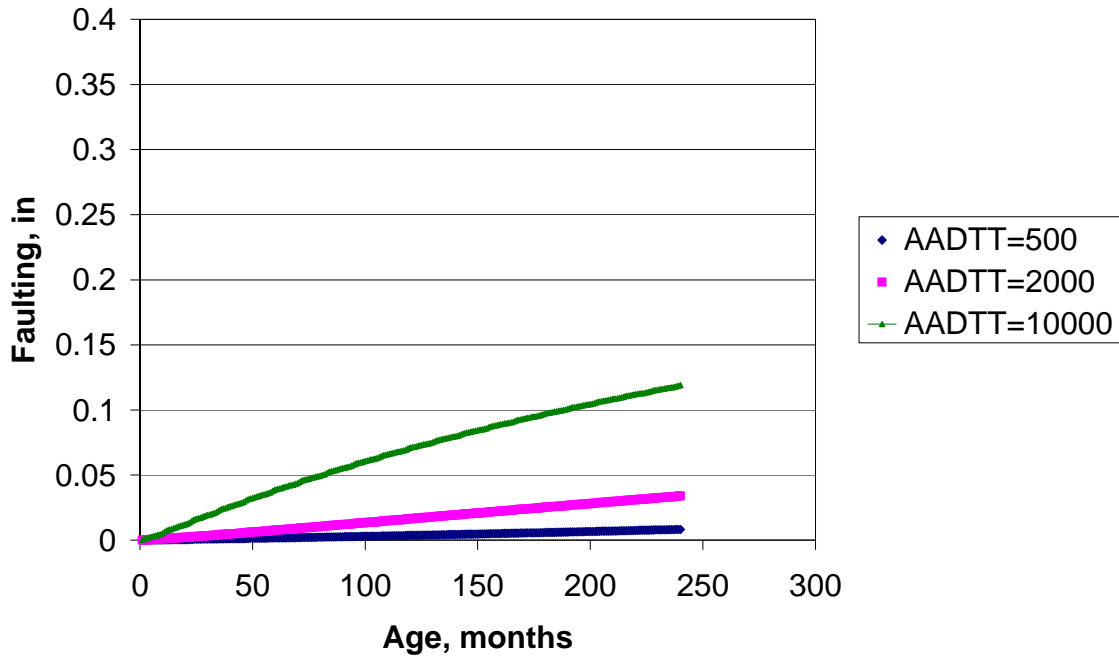


Figure 51 Effect of Traffic on faulting. Location -Rochester, HPCC =6, COTE =0.0000055, MR=700, HBase=6, Base -Class 5, Lane Width =12, Joint Spacing =15, Dowel D = 1.25, Shoulders - AC, Subgrade - A-6

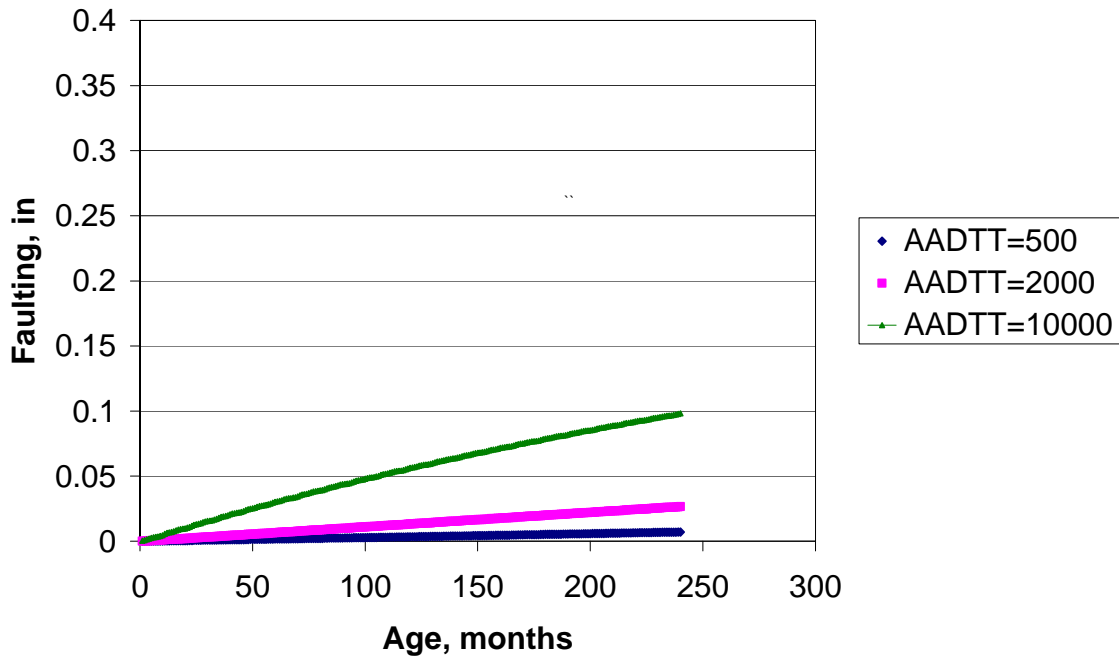


Figure 52 Effect of Traffic on faulting. Location -Rochester, HPCC =6, COTE =0.0000055, MR=700, HBase=6, Base -Class 5, Lane Width =12, Joint Spacing =15, Dowel D = 1.5, Shoulders - AC, Subgrade - A-6

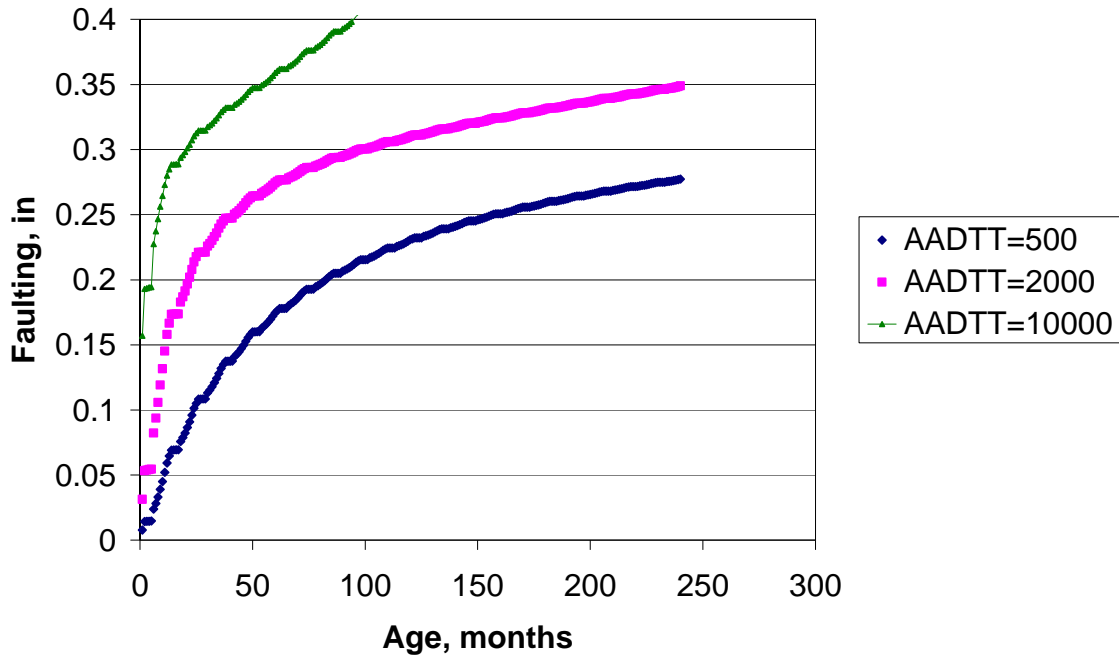


Figure 53 Effect of Traffic on faulting. Location -Rochester, HPCC =7, COTE =0.0000055, MR=700, HBase=6, Base -Class 5, Lane Width =12, Joint Spacing =15, Dowel D = 0, Shoulders - AC, Subgrade - A-6

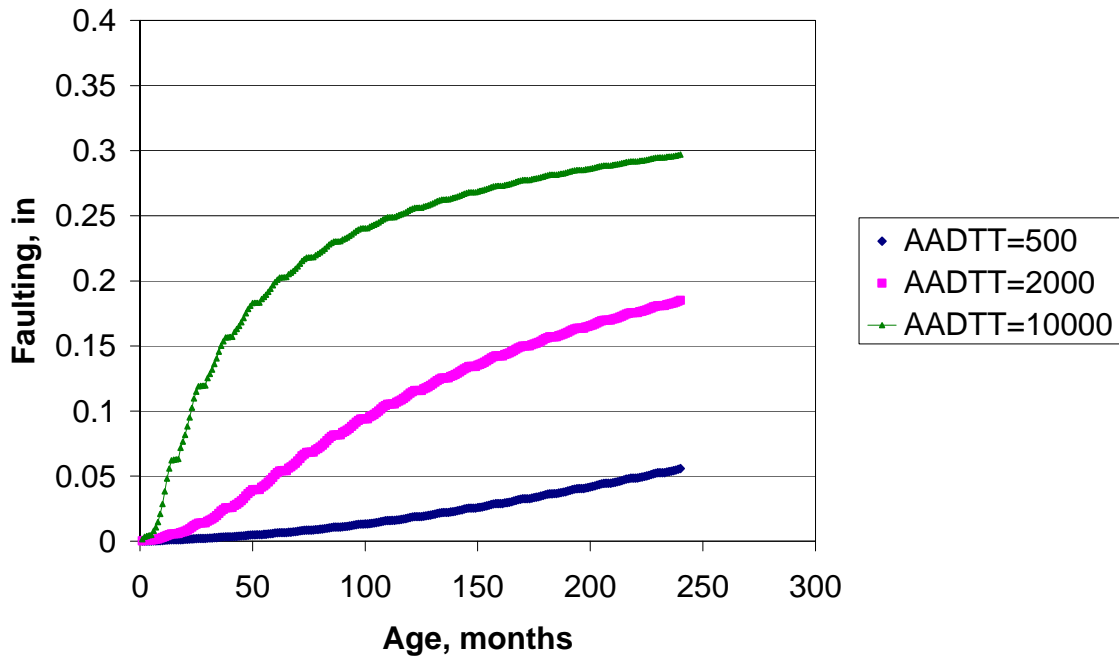


Figure 54 Effect of Traffic on faulting. Location -Rochester, HPCC =7, COTE =0.0000055, MR=700, HBase=6, Base -Class 5, Lane Width =12, Joint Spacing =15, Dowel D = 1, Shoulders - AC, Subgrade - A-6

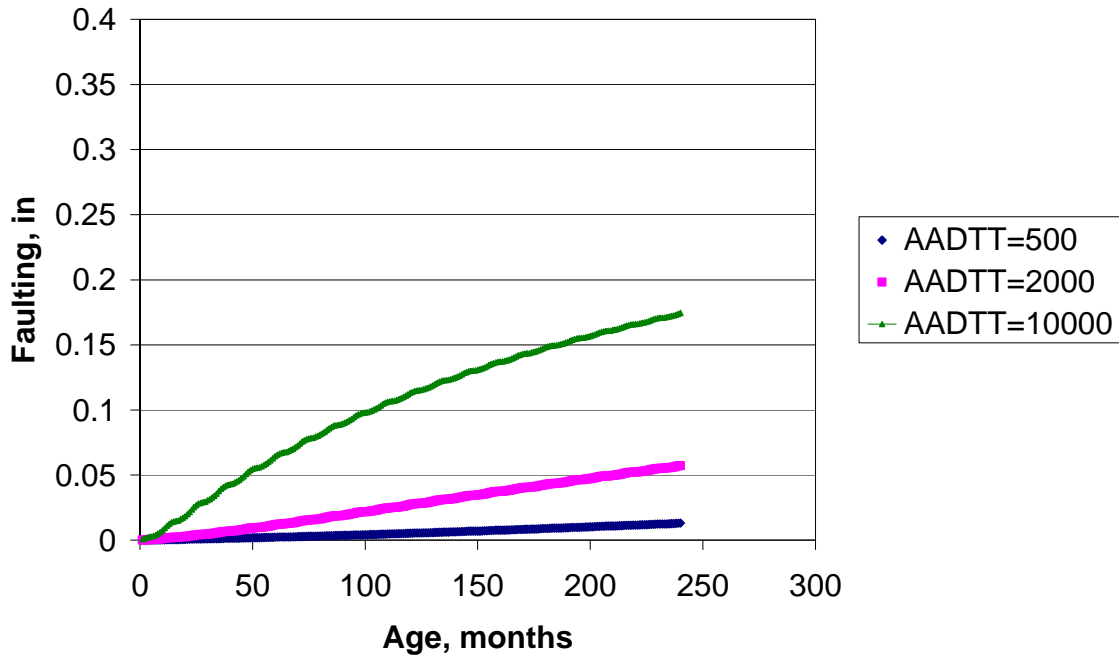


Figure 55 Effect of Traffic on faulting. Location -Rochester, HPCC =7, COTE =0.0000055, MR=700, HBase=6, Base -Class 5, Lane Width =12, Joint Spacing =15, Dowel D = 1.25, Shoulders - AC, Subgrade - A-6

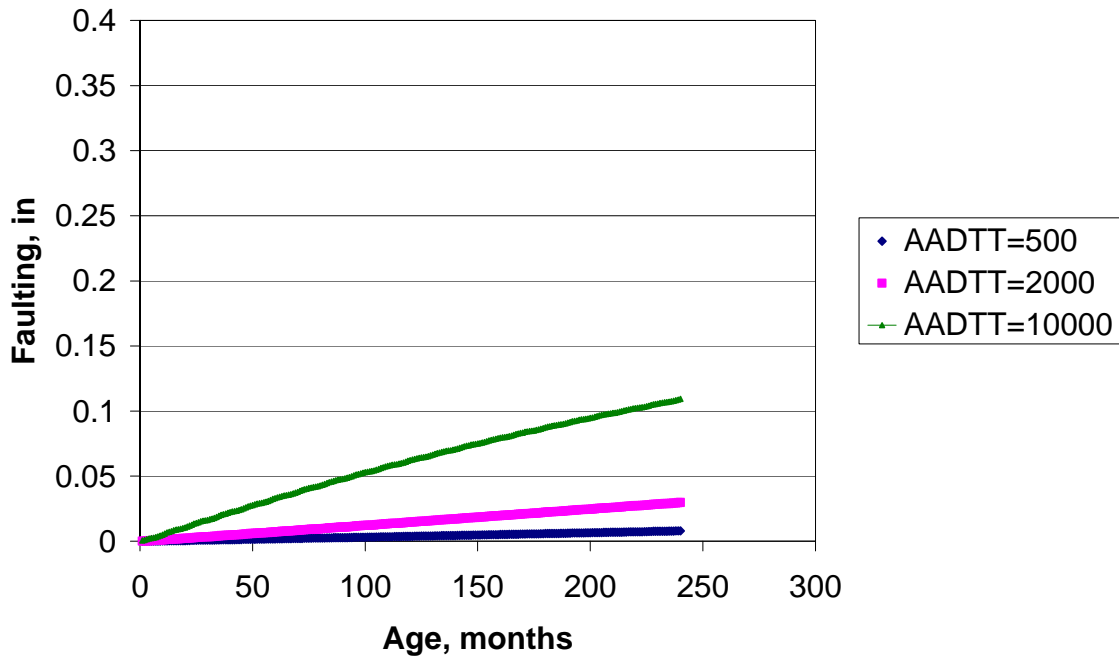


Figure 56 Effect of Traffic on faulting. Location -Rochester, HPCC =7, COTE =0.0000055, MR=700, HBase=6, Base -Class 5, Lane Width =12, Joint Spacing =15, Dowel D = 1.5, Shoulders - AC, Subgrade - A-6

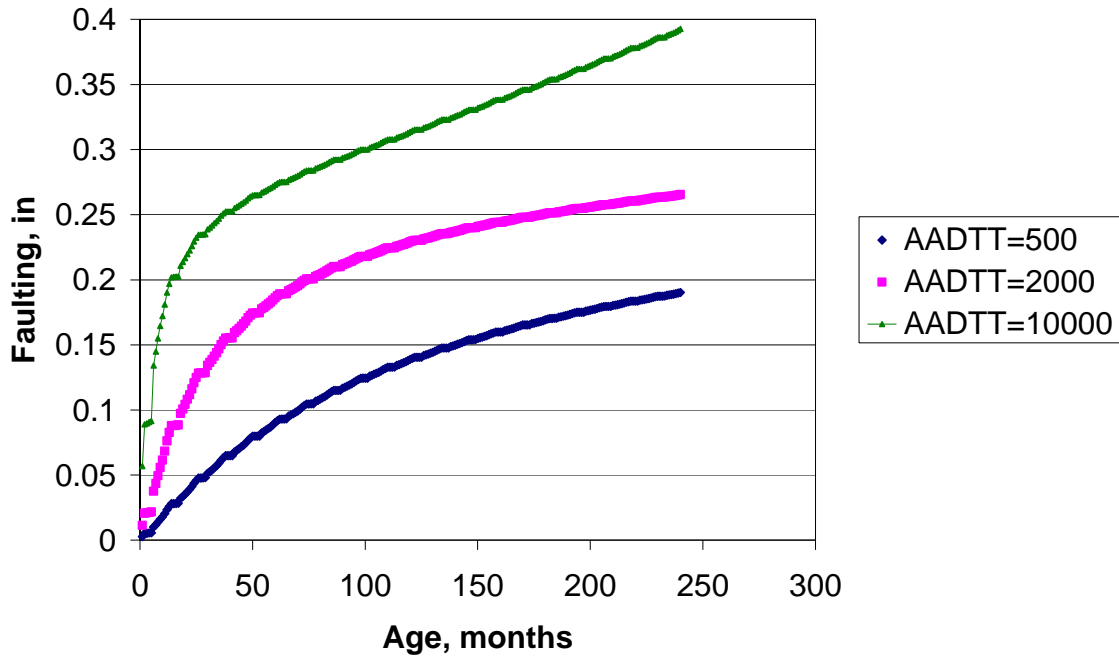


Figure 57 Effect of Traffic on faulting. Location -Rochester, HPCC =9, COTE =0.0000055, MR=700, HBase=6, Base -Class 5, Lane Width =12, Joint Spacing =15, Dowel D = 0, Shoulders - AC, Subgrade - A-6

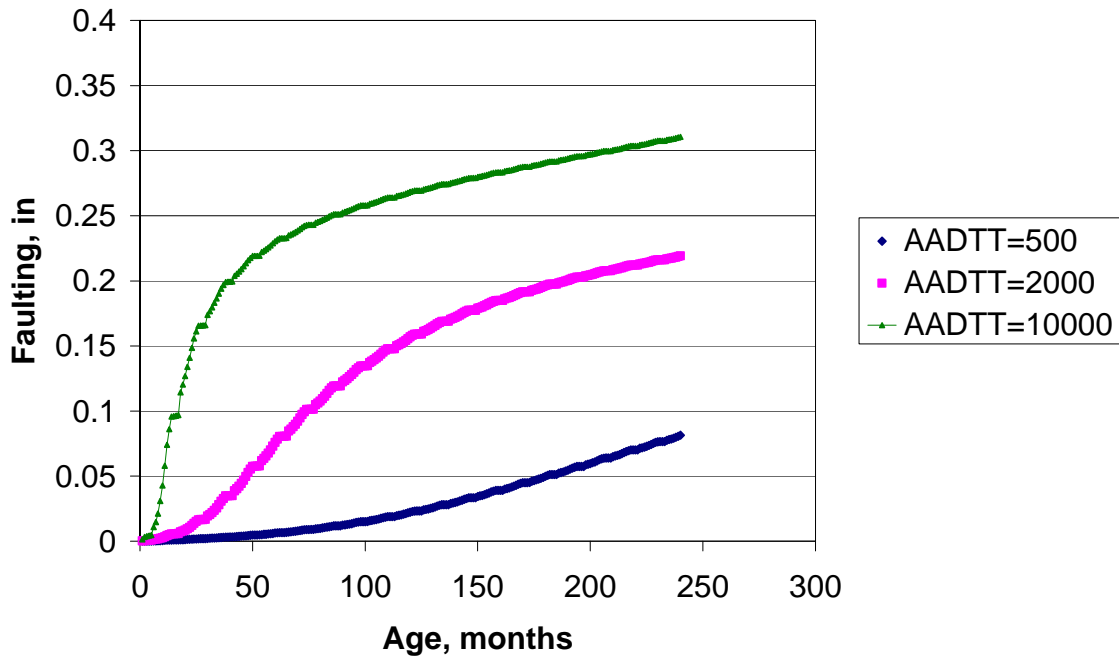


Figure 58 Effect of Traffic on faulting. Location -Rochester, HPCC =9, COTE =0.0000055, MR=700, HBase=6, Base -Class 5, Lane Width =12, Joint Spacing =15, Dowel D = 1, Shoulders - AC, Subgrade - A-6

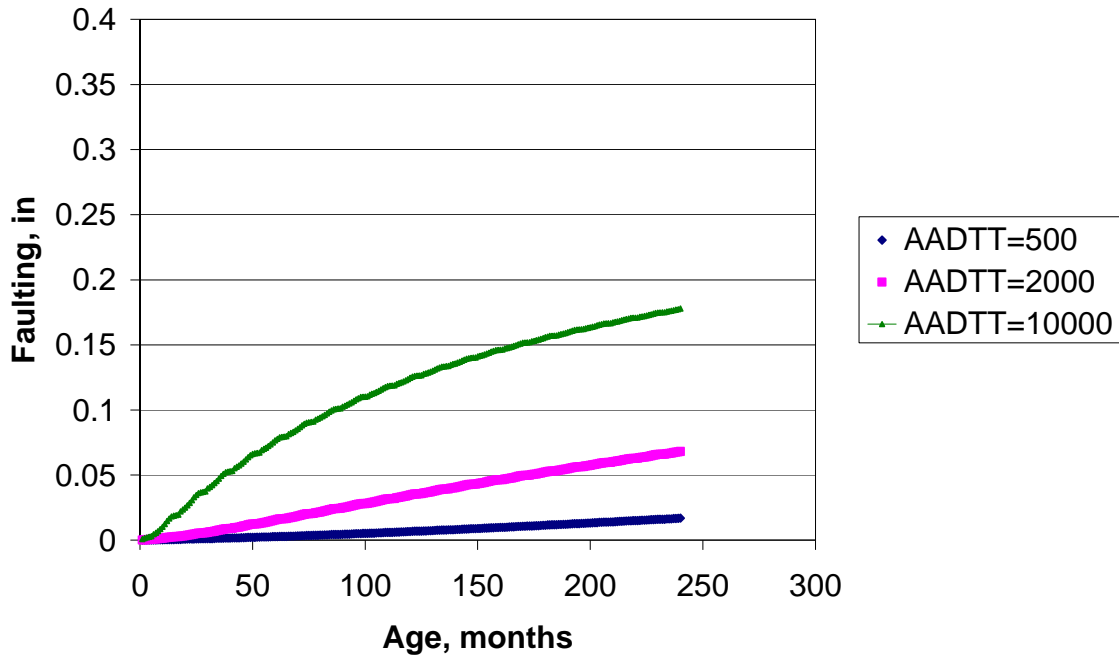


Figure 59 Effect of Traffic on faulting. Location -Rochester, HPCC =9, COTE =0.0000055, MR=700, HBase=6, Base -Class 5, Lane Width =12, Joint Spacing =15, Dowel D = 1.25, Shoulders - AC, Subgrade - A-6

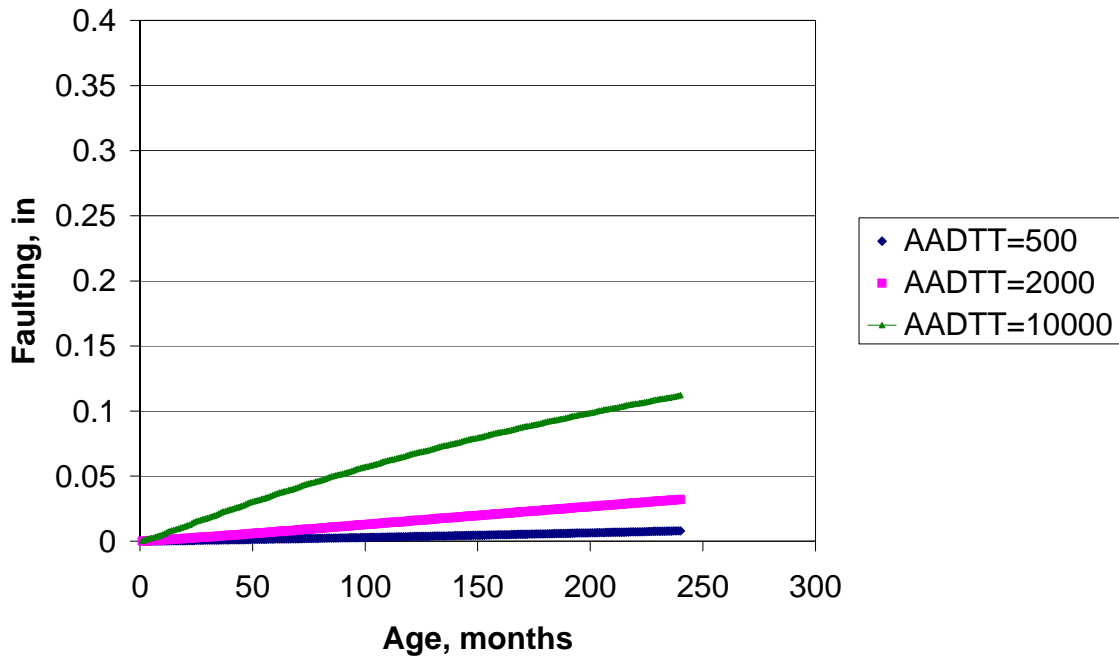


Figure 60 Effect of Traffic on faulting. Location -Rochester, HPCC =9, COTE =0.0000055, MR=700, HBase=6, Base -Class 5, Lane Width =12, Joint Spacing =15, Dowel D = 1.5, Shoulders - AC, Subgrade - A-6

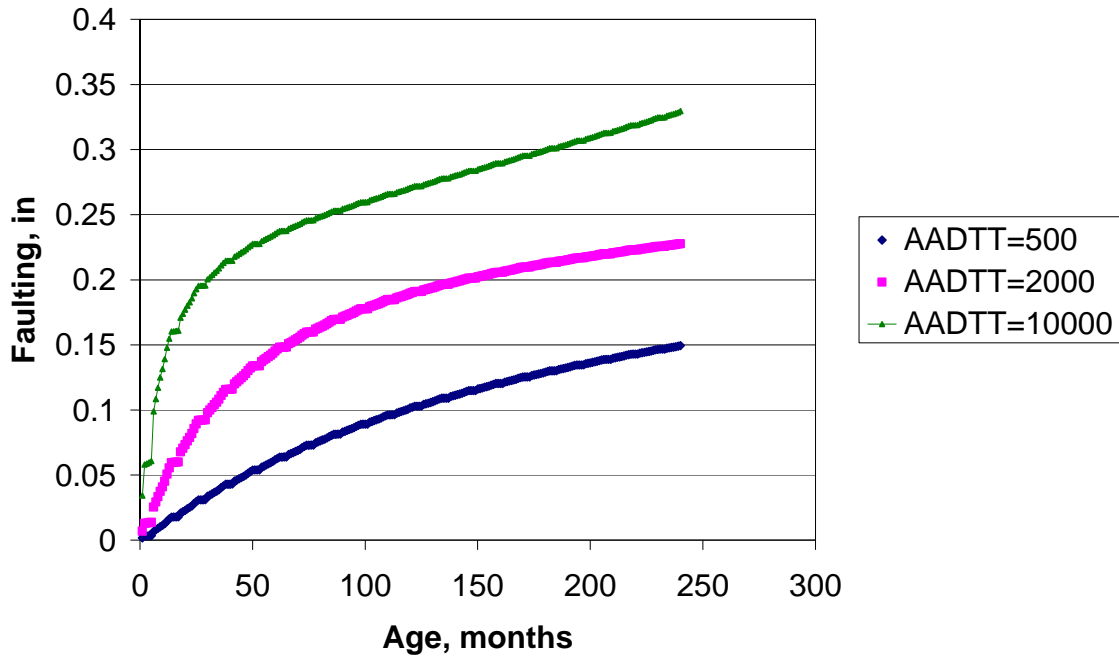


Figure 61 Effect of Traffic on faulting. Location -Rochester, HPCC =10, COTE =0.0000055, MR=700, HBase=6, Base -Class 5, Lane Width =12, Joint Spacing =15, Dowel D = 0, Shoulders - AC, Subgrade - A-6

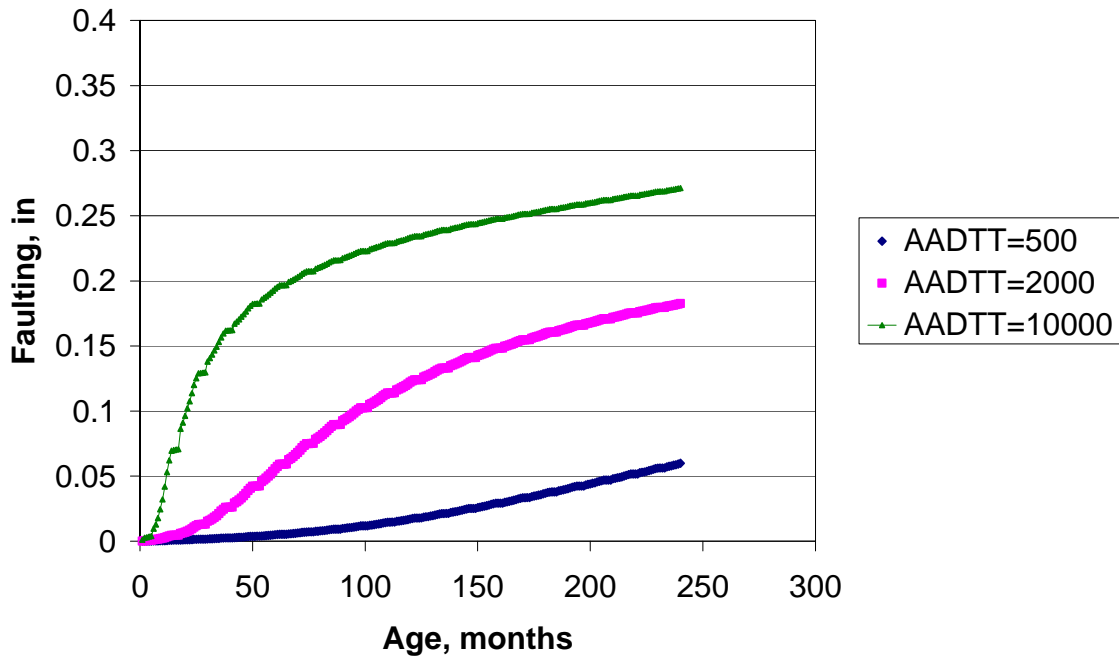


Figure 62 Effect of Traffic on faulting. Location -Rochester, HPCC =10, COTE =0.0000055, MR=700, HBase=6, Base -Class 5, Lane Width =12, Joint Spacing =15, Dowel D = 1, Shoulders - AC, Subgrade - A-6

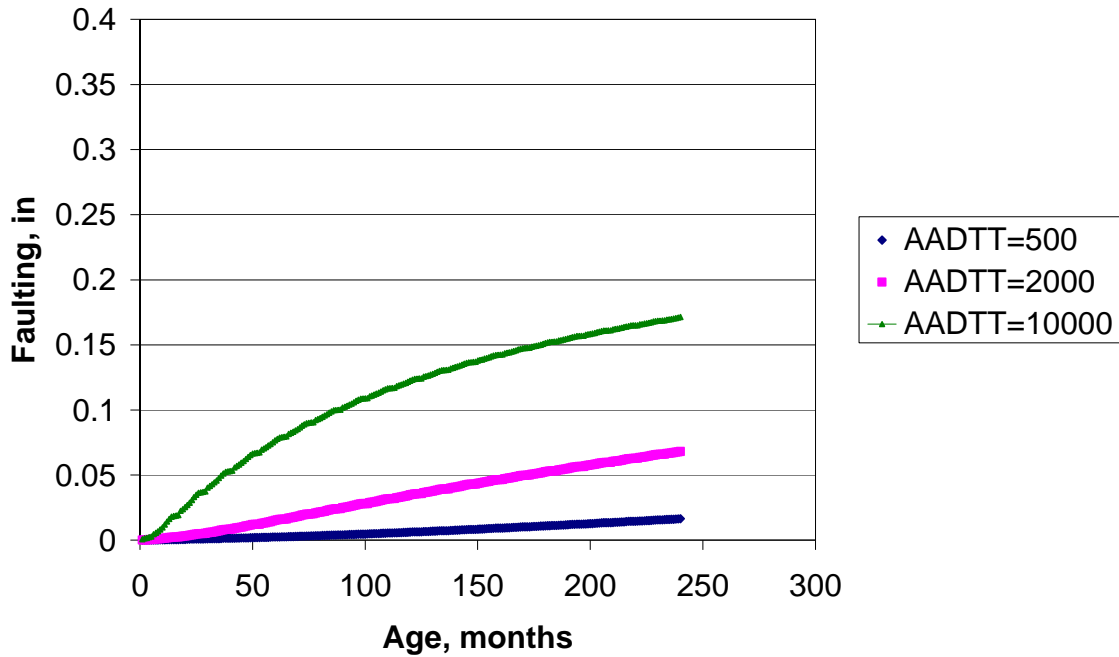


Figure 63 Effect of Traffic on faulting. Location -Rochester, HPCC =10, COTE =0.0000055, MR=700, HBase=6, Base -Class 5, Lane Width =12, Joint Spacing =15, Dowel D = 1.25, Shoulders - AC, Subgrade - A-6

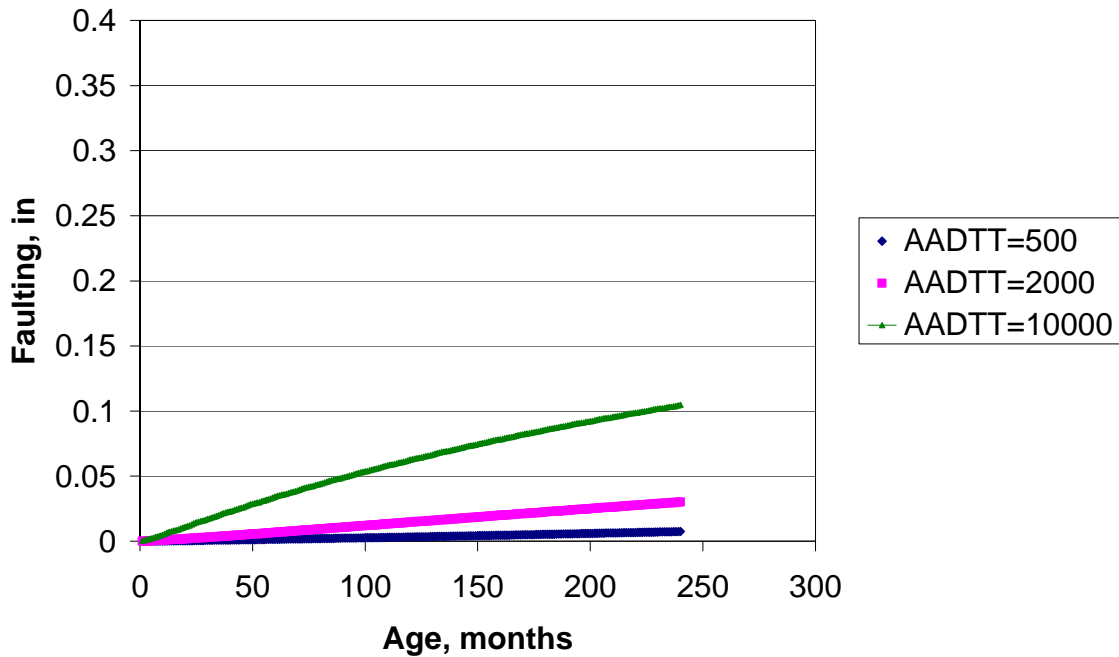


Figure 64 Effect of Traffic on faulting. Location -Rochester, HPCC =10, COTE =0.0000055, MR=700, HBase=6, Base -Class 5, Lane Width =12, Joint Spacing =15, Dowel D = 1.5, Shoulders - AC, Subgrade - A-6

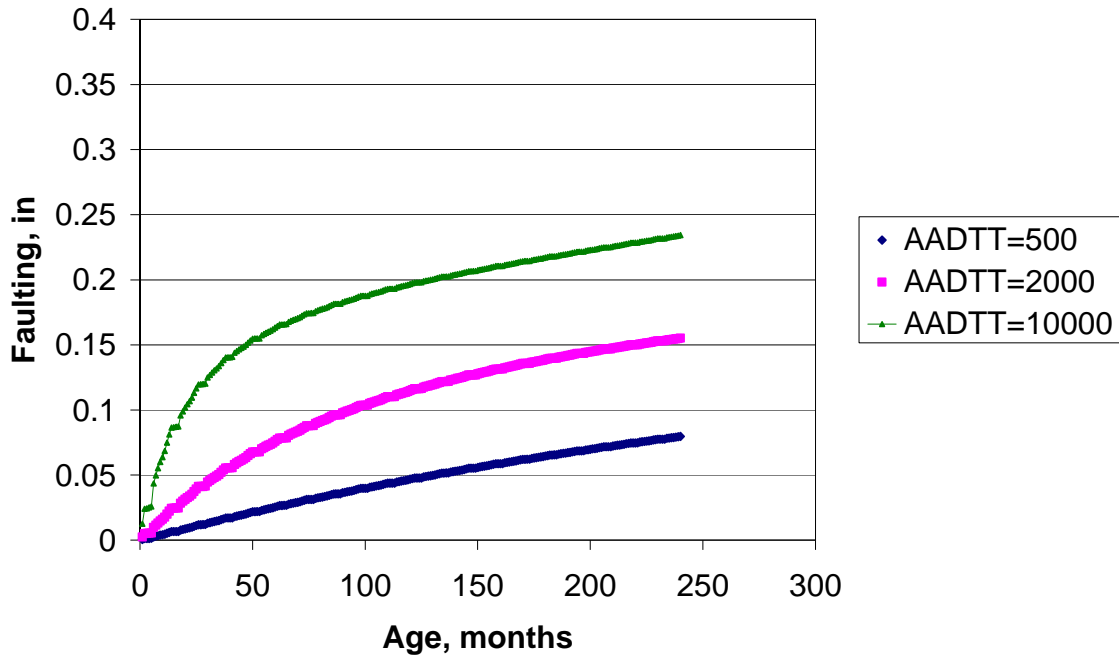


Figure 65 Effect of Traffic on faulting. Location -Rochester, HPCC =12, COTE =0.0000055, MR=700, HBase=6, Base -Class 5, Lane Width =12, Joint Spacing =15, Dowel D = 0, Shoulders - AC, Subgrade - A-6

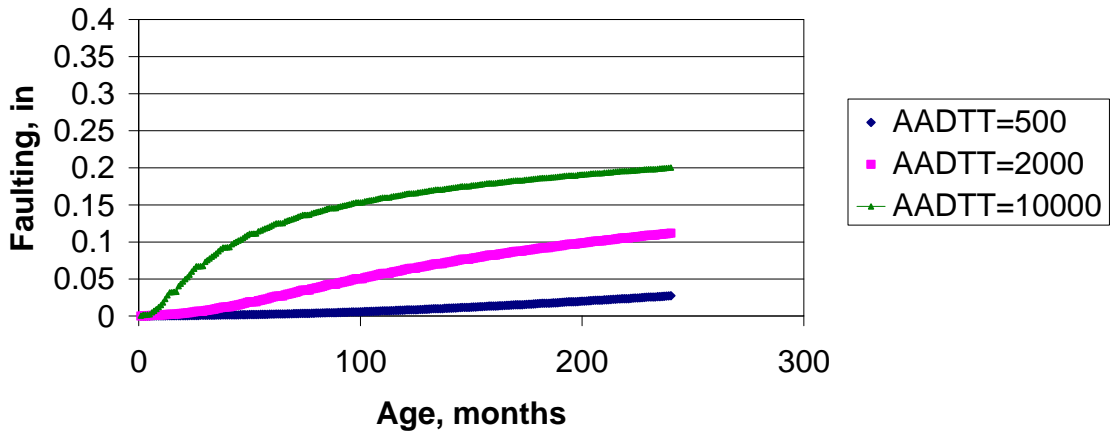


Figure 66 Effect of Traffic on faulting. Location -Rochester, HPCC =12, COTE =0.0000055, MR=700, HBase=6, Base -Class 5, Lane Width =12, Joint Spacing =15, Dowel D = 1, Shoulders - AC, Subgrade - A-6

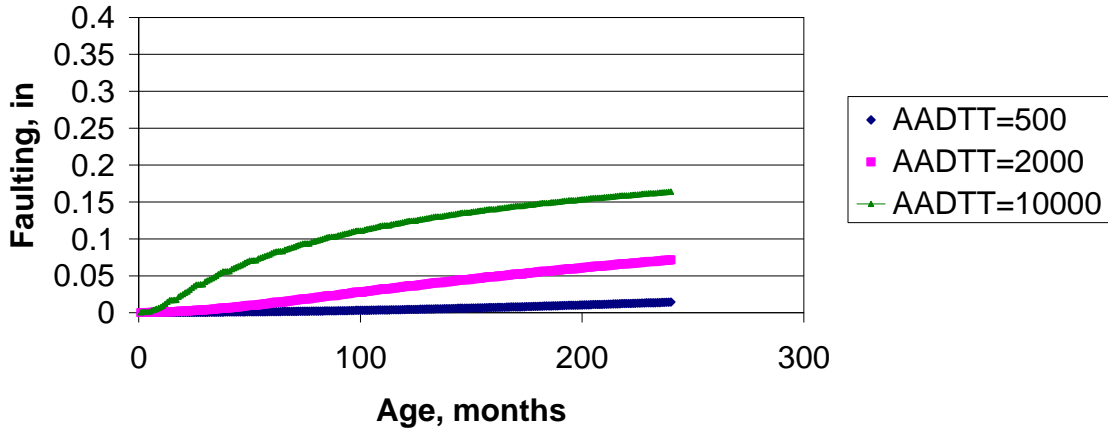


Figure 67 Effect of Traffic on faulting. Location -Rochester, HPCC =12, COTE =0.0000055, MR=700, HBase=6, Base -Class 5, Lane Width =12, Joint Spacing =15, Dowel D = 1.25, Shoulders - AC, Subgrade - A-6

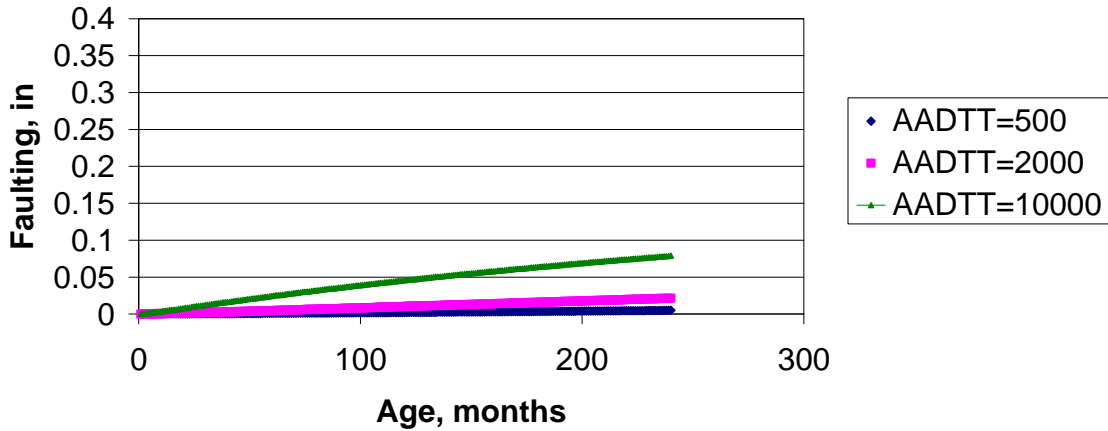


Figure 68 Effect of Traffic on faulting. Location -Rochester, HPCC =12, COTE =0.0000055, MR=700, HBase=6, Base -Class 5, Lane Width =12, Joint Spacing =15, Dowel D = 1.5, Shoulders - AC, Subgrade - A-6

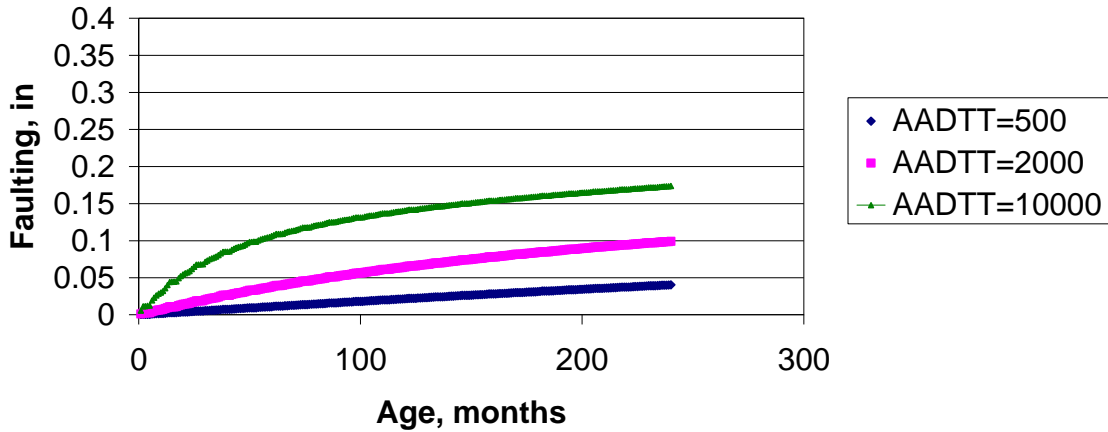


Figure 69 Effect of Traffic on faulting. Location -Rochester, HPCC =14, COTE =0.0000055, MR=700, HBase=6, Base -Class 5, Lane Width =12, Joint Spacing =15, Dowel D = 0, Shoulders - AC, Subgrade - A-6

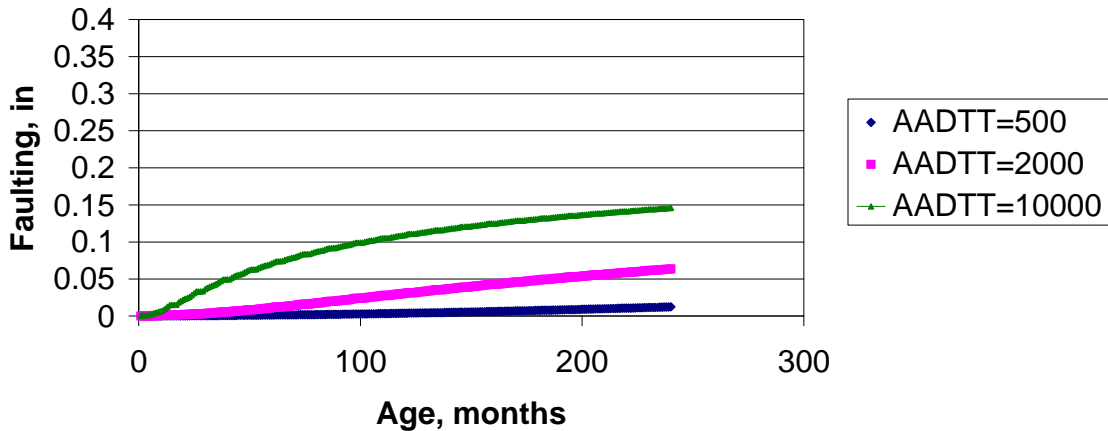


Figure 70 Effect of Traffic on faulting. Location -Rochester, HPCC =14, COTE =0.0000055, MR=700, HBase=6, Base -Class 5, Lane Width =12, Joint Spacing =15, Dowel D = 1, Shoulders - AC, Subgrade - A-6

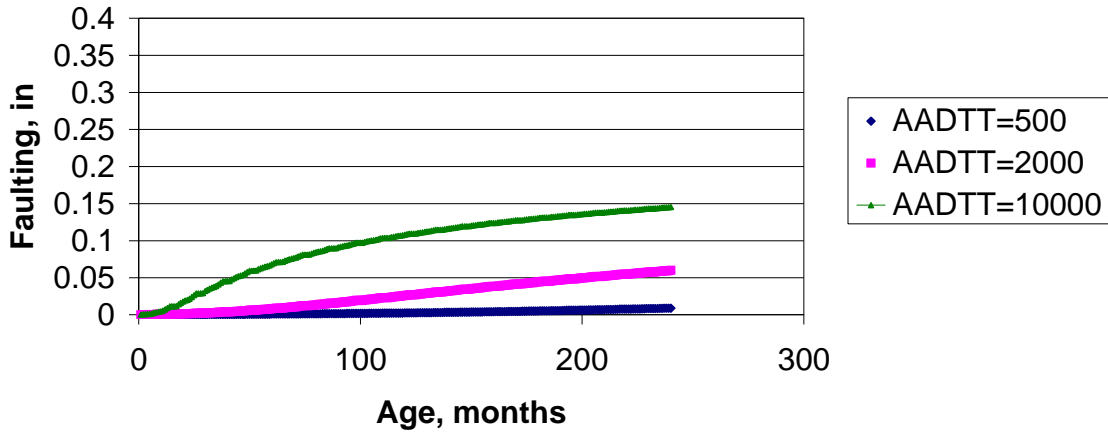


Figure 71 Effect of Traffic on faulting. Location -Rochester, HPCC =14, COTE =0.0000055, MR=700, HBase=6, Base -Class 5, Lane Width =12, Joint Spacing =15, Dowel D = 1.25, Shoulders - AC, Subgrade - A-6

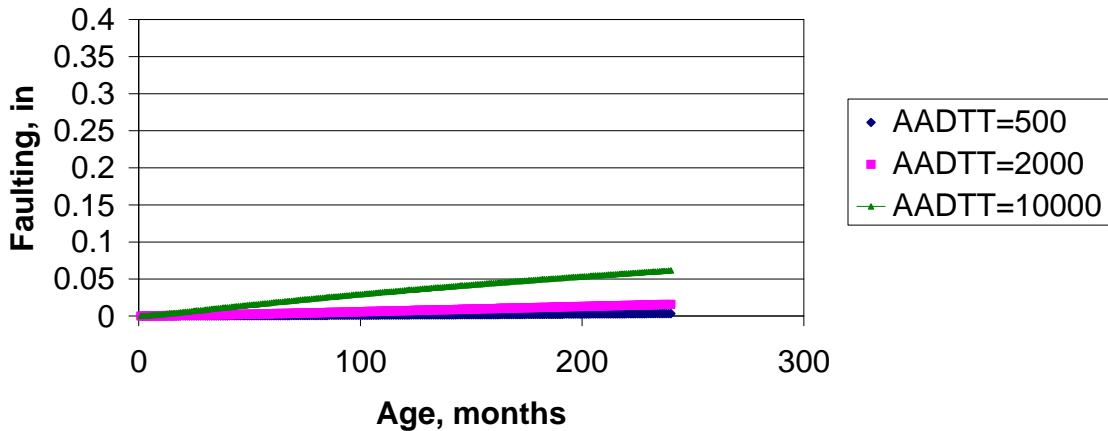


Figure 72 Effect of Traffic on faulting. Location -Rochester, HPCC =14, COTE =0.0000055, MR=700, HBase=6, Base -Class 5, Lane Width =12, Joint Spacing =15, Dowel D = 1.5, Shoulders - AC, Subgrade - A-6

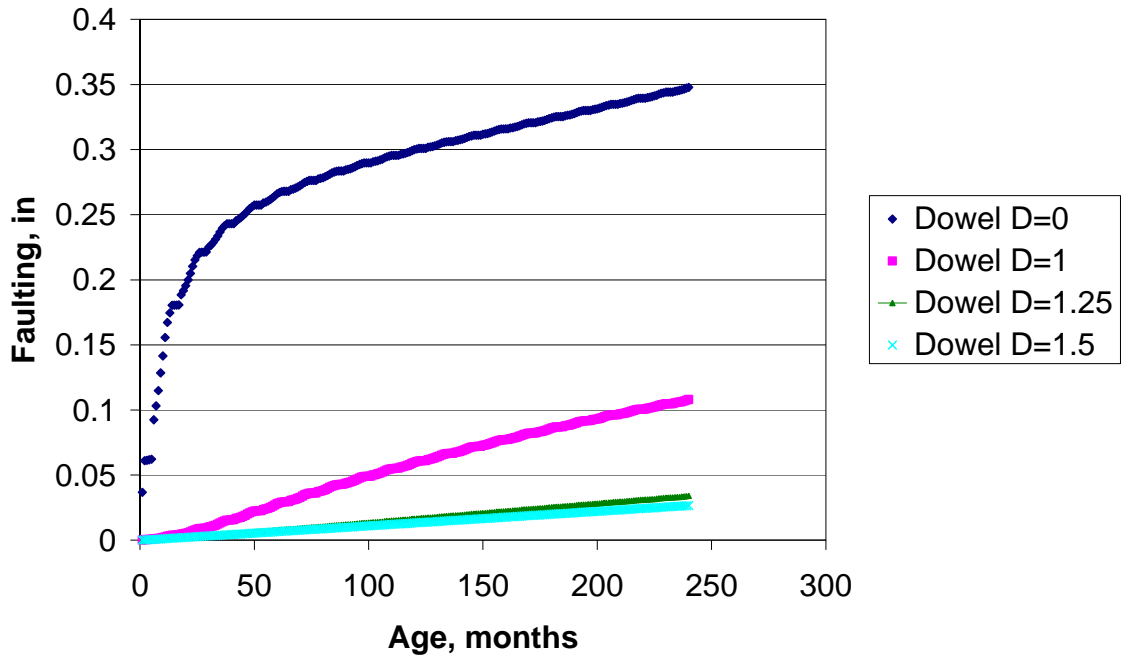


Figure 73 Effect of Dowel Diameter on faulting. Location -Rochester, AADTT=2000, HPCC =6, COTE =0.0000055, MR=700, HBase=6, Base -Class 5, Lane Width =12, Joint Spacing =15, Shoulders - AC, Subgrade - A-6

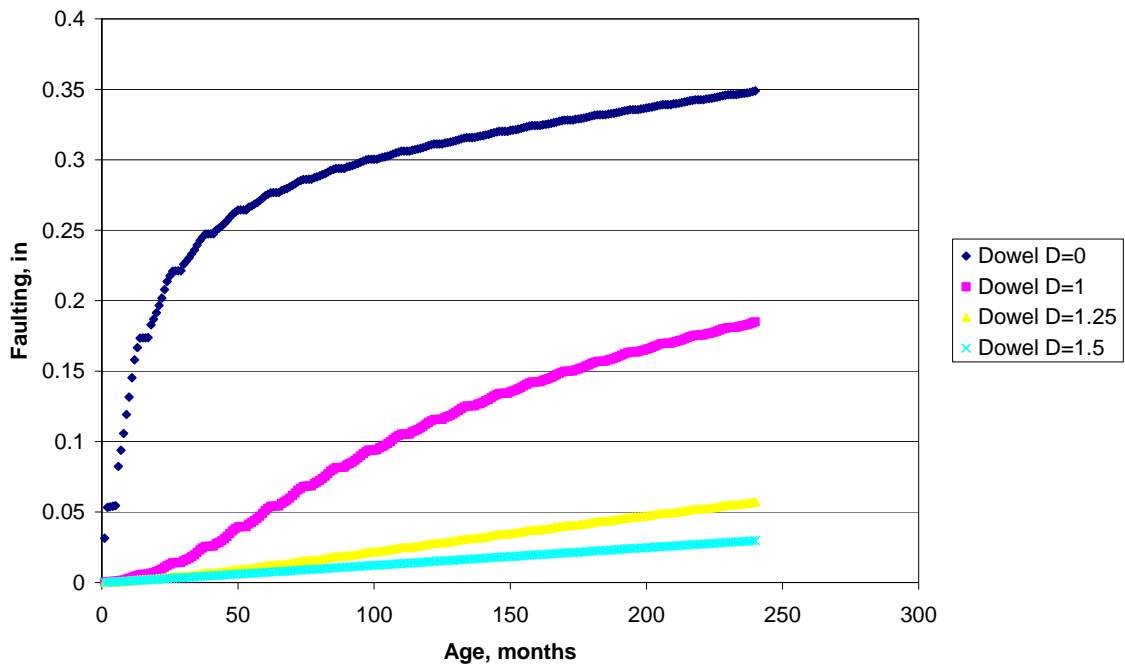


Figure 74 Effect of Dowel Diameter on faulting. Location -Rochester, AADTT=2000, HPCC =7, COTE =0.0000055, MR=700, HBase=6, Base -Class 5, Lane Width =12, Joint Spacing =15, Shoulders - AC, Subgrade - A-6

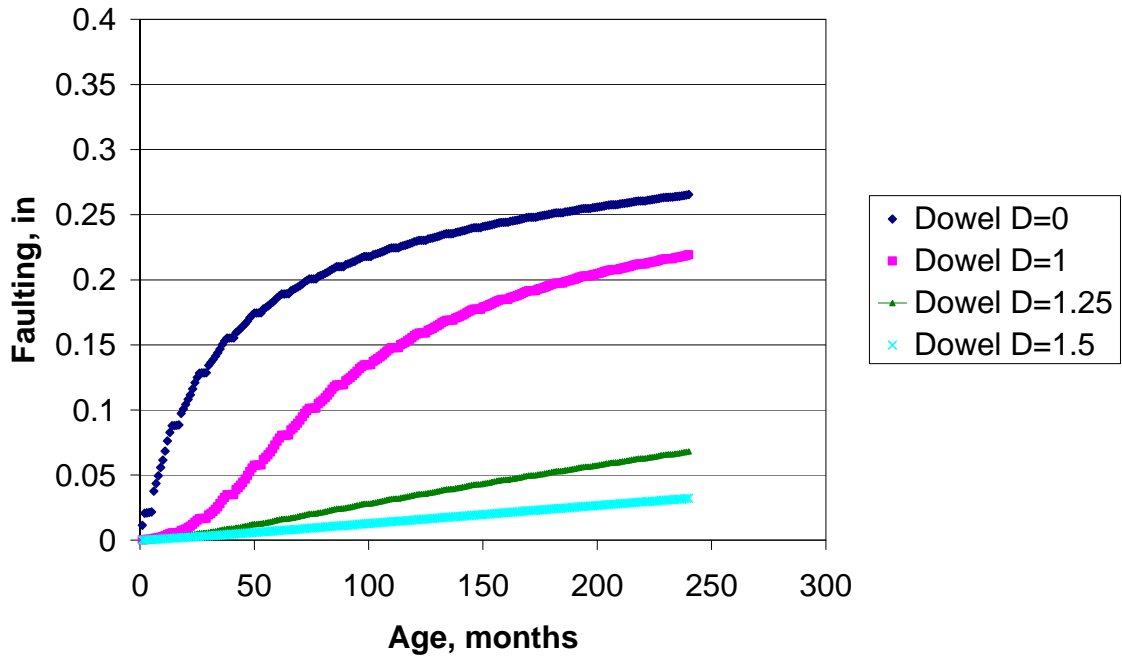


Figure 75 Effect of Dowel Diameter on faulting. Location -Rochester, AADTT=2000, HPCC =9, COTE =0.0000055, MR=700, HBase=6, Base -Class 5, Lane Width =12, Joint Spacing =15, Shoulders - AC, Subgrade - A-6

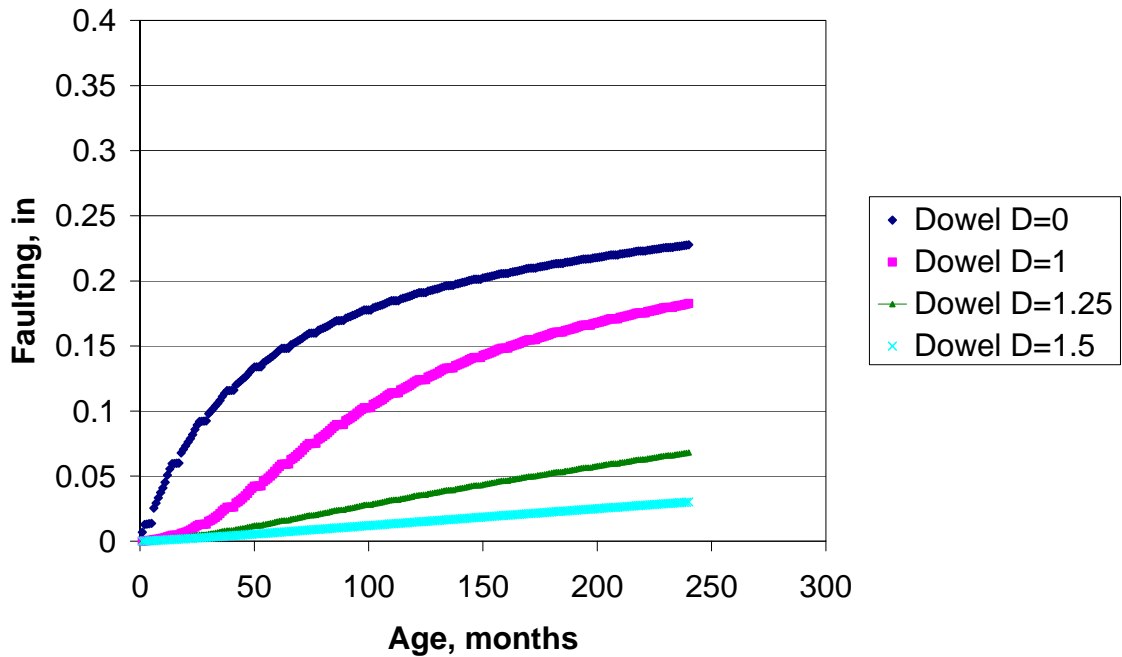


Figure 76 Effect of Dowel Diameter on faulting. Location -Rochester, AADTT=2000, HPCC =10, COTE =0.0000055, MR=700, HBase=6, Base -Class 5, Lane Width =12, Joint Spacing =15, Shoulders - AC, Subgrade - A-6

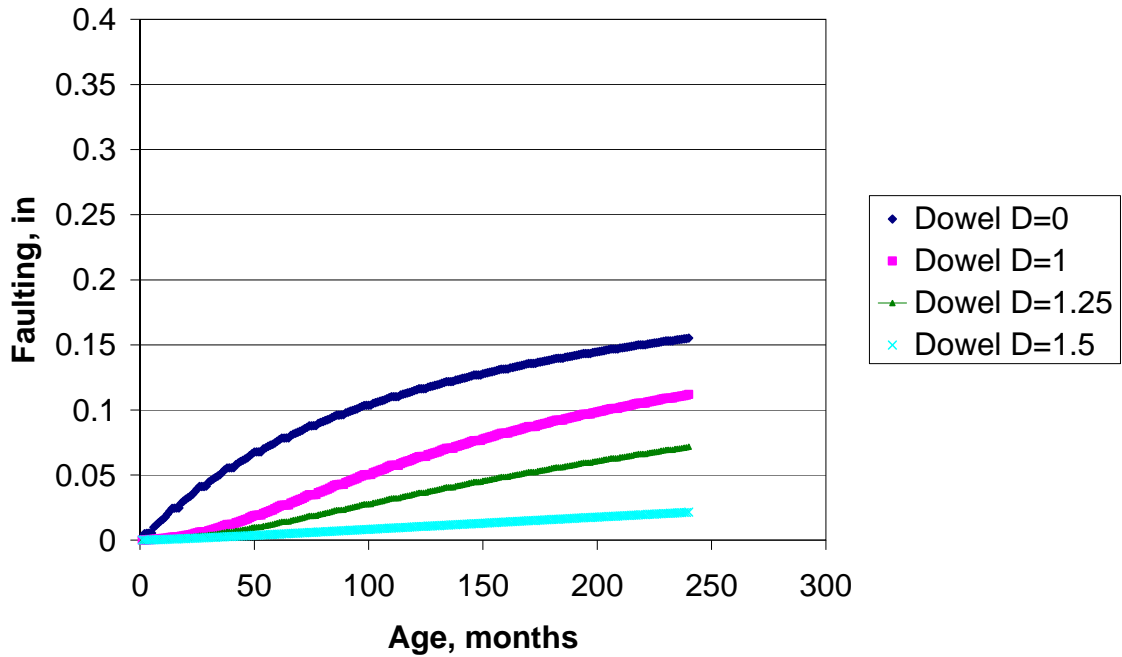


Figure 77 Effect of Dowel Diameter on faulting. Location -Rochester, AADTT=2000, HPCC =12, COTE =0.0000055, MR=700, HBase=6, Base -Class 5, Lane Width =12, Joint Spacing =15, Shoulders - AC, Subgrade - A-6

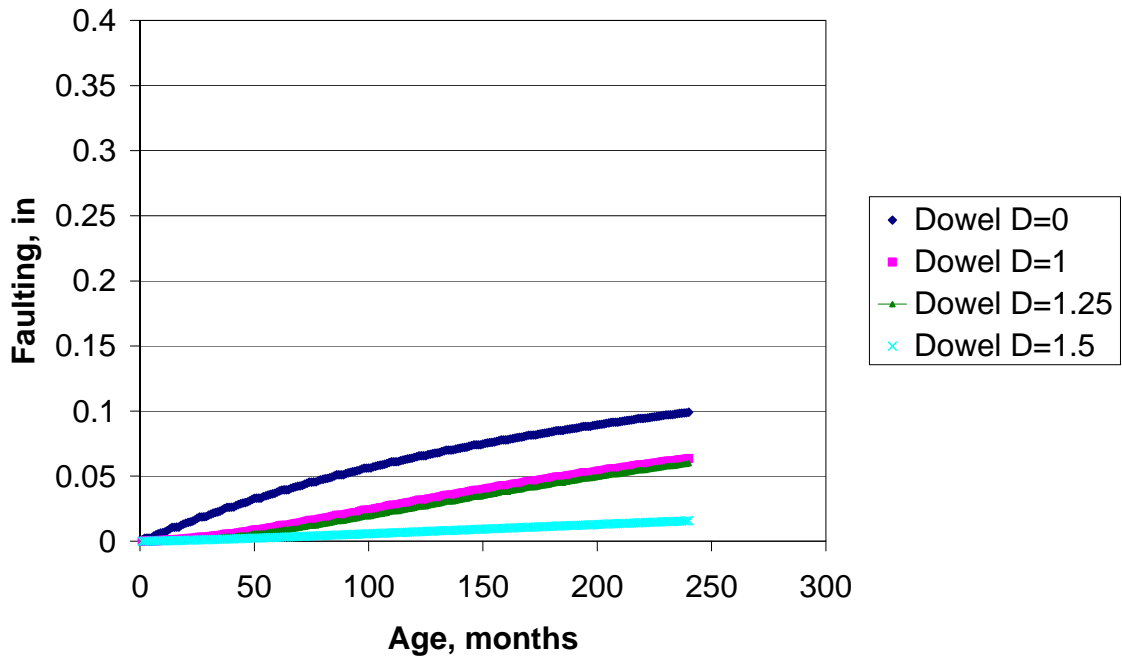


Figure 78 Effect of Dowel Diameter on faulting. Location -Rochester, AADTT=2000, HPCC =14, COTE =0.0000055, MR=700, HBase=6, Base -Class 5, Lane Width =12, Joint Spacing =15, Shoulders - AC, Subgrade - A-6

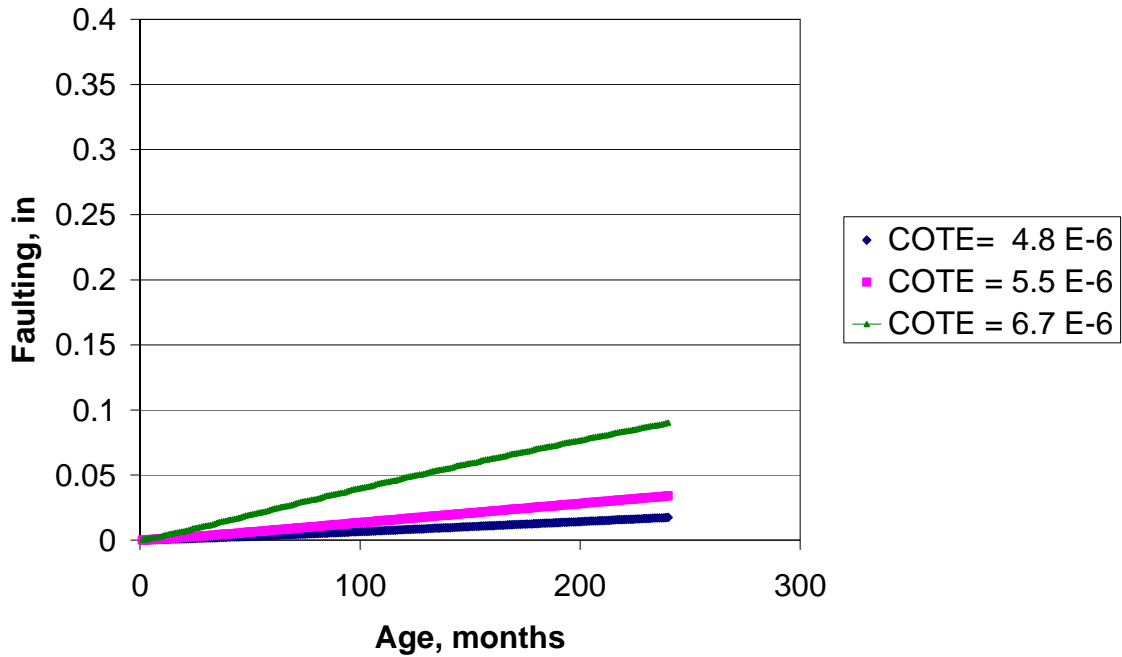


Figure 79 Effect of COTE on faulting. Location -Rochester, AADTT=2000, HPCC =6, MR=700, HBase=6, Base -Class 5, Lane Width =12, Joint Spacing =15, Dowel D = 1.25, Shoulders - AC, Subgrade - A-6

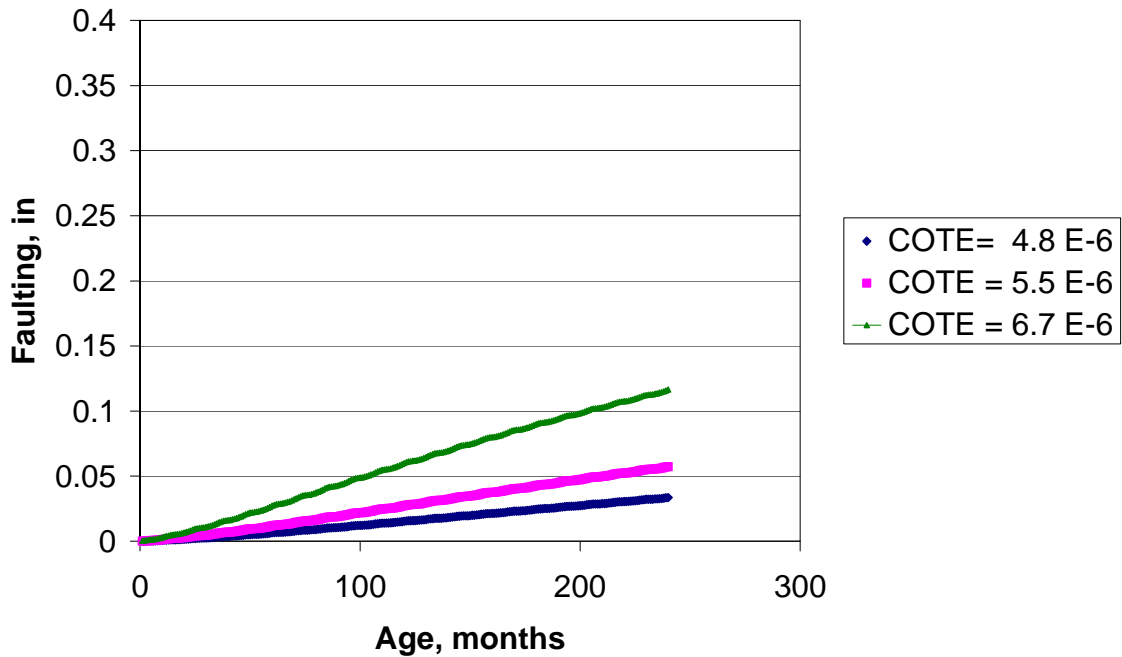


Figure 80 Effect of COTE on faulting. Location -Rochester, AADTT=2000, HPCC =7, MR=700, HBase=6, Base -Class 5, Lane Width =12, Joint Spacing =15, Dowel D = 1.25, Shoulders - AC, Subgrade - A-6

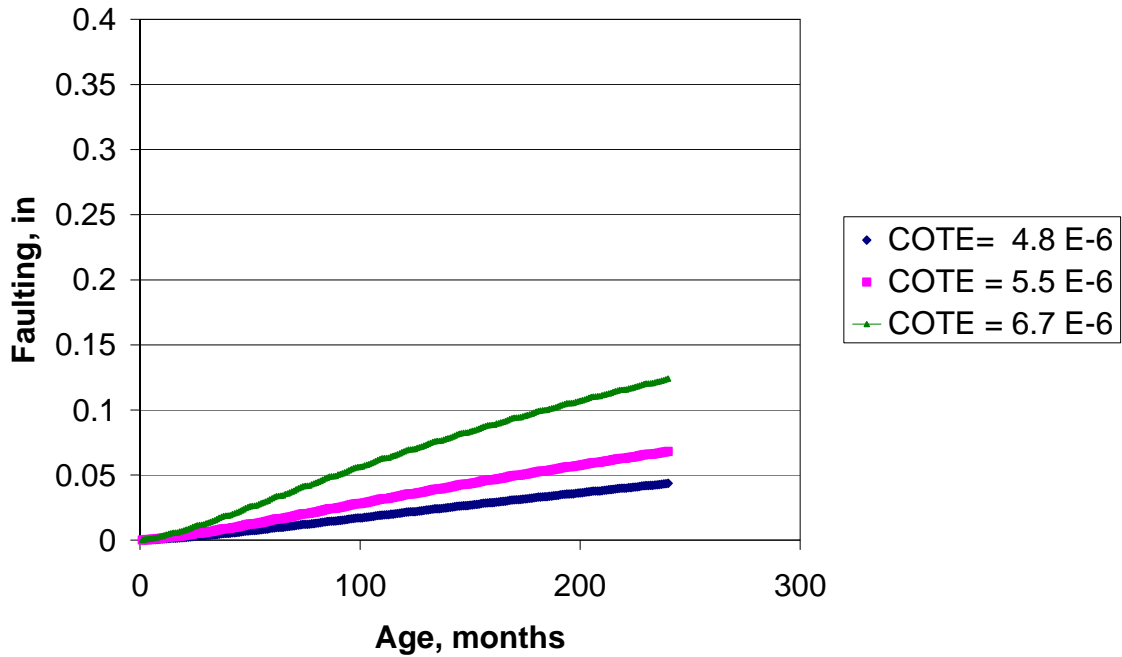


Figure 81 Effect of COTE on faulting. Location -Rochester, AADTT=2000, HPCC =9, MR=700, HBase=6, Base -Class 5, Lane Width =12, Joint Spacing =15, Dowel D = 1.25, Shoulders - AC, Subgrade - A-6

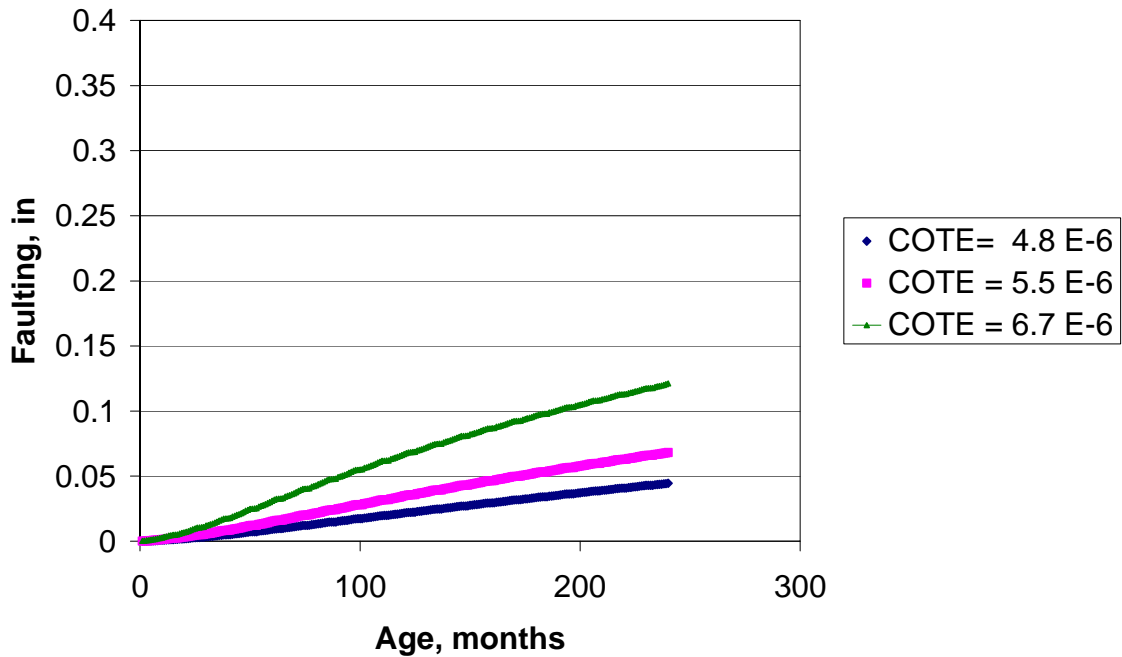


Figure 82 Effect of COTE on faulting. Location -Rochester, AADTT=2000, HPCC =10, MR=700, HBase=6, Base -Class 5, Lane Width =12, Joint Spacing =15, Dowel D = 1.25, Shoulders - AC, Subgrade - A-6

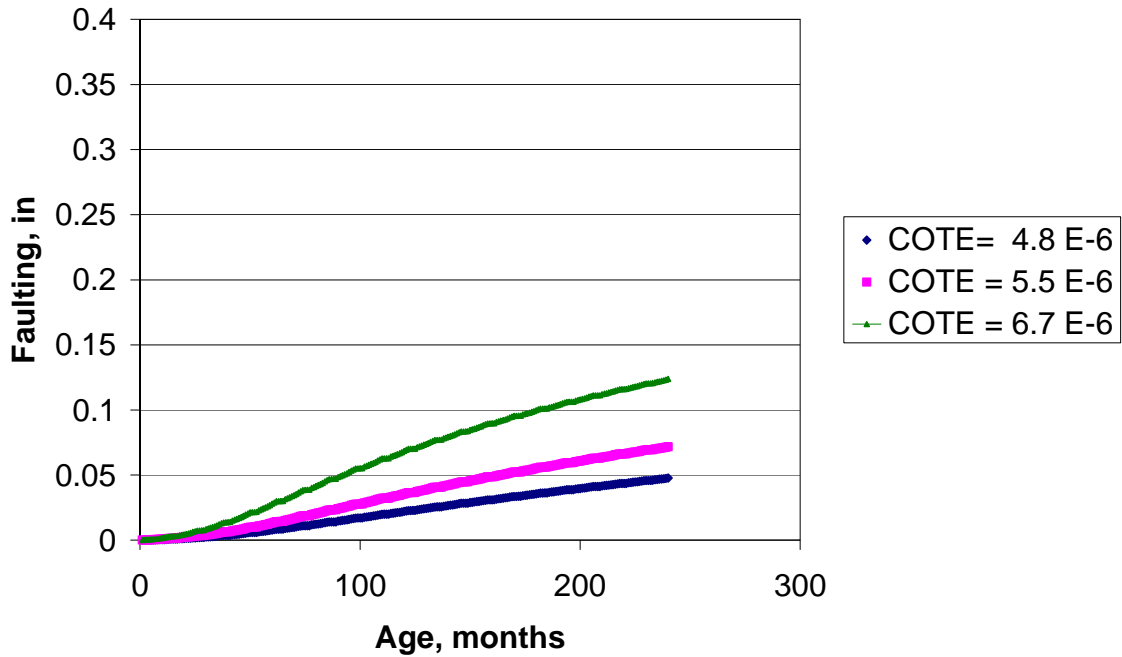


Figure 83 Effect of COTE on faulting. Location -Rochester, AADTT=2000, HPCC =12, MR=700, HBase=6, Base -Class 5, Lane Width =12, Joint Spacing =15, Dowel D = 1.25, Shoulders - AC, Subgrade - A-6

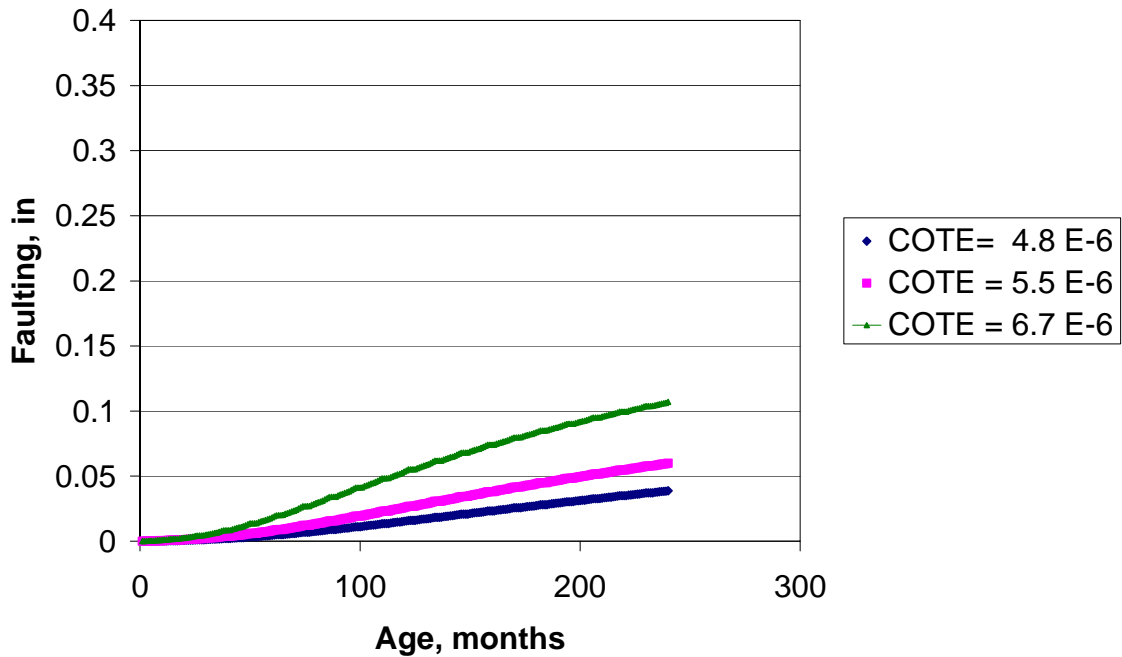


Figure 84 Effect of COTE on faulting. Location -Rochester, AADTT=2000, HPCC =14, MR=700, HBase=6, Base -Class 5, Lane Width =12, Joint Spacing =15, Dowel D = 1.25, Shoulders - AC, Subgrade - A-6

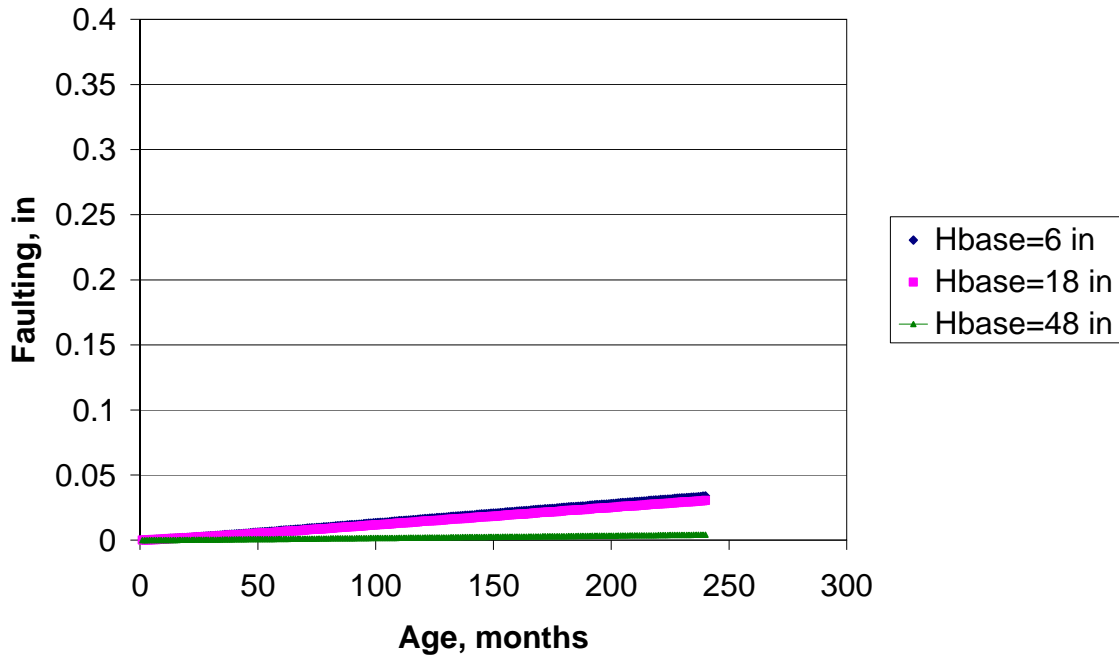


Figure 85 Effect of Base Thickness on faulting. Location -Rochester, AADTT=2000, HPCC =6, COTE =0.0000055, MR=700, Base -Class 5, Lane Width =12, Joint Spacing =15, Dowel D = 1.25, Shoulders - AC, Subgrade - A-6

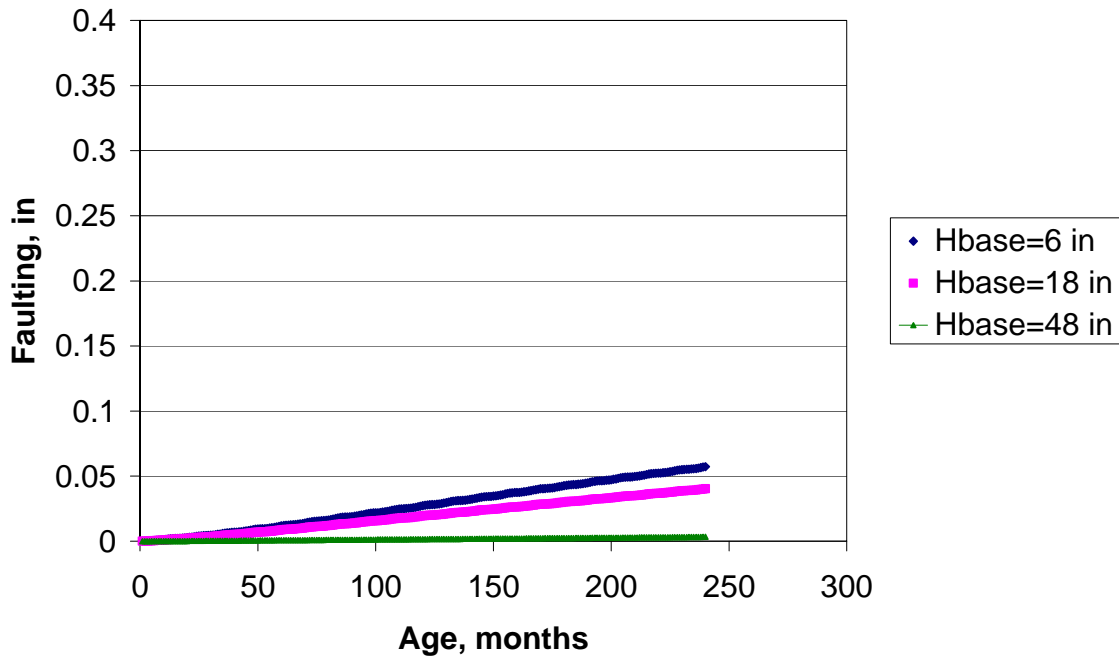


Figure 86 Effect of Base Thickness on faulting. Location -Rochester, AADTT=2000, HPCC =7, COTE =0.0000055, MR=700, Base -Class 5, Lane Width =12, Joint Spacing =15, Dowel D = 1.25, Shoulders - AC, Subgrade - A-6

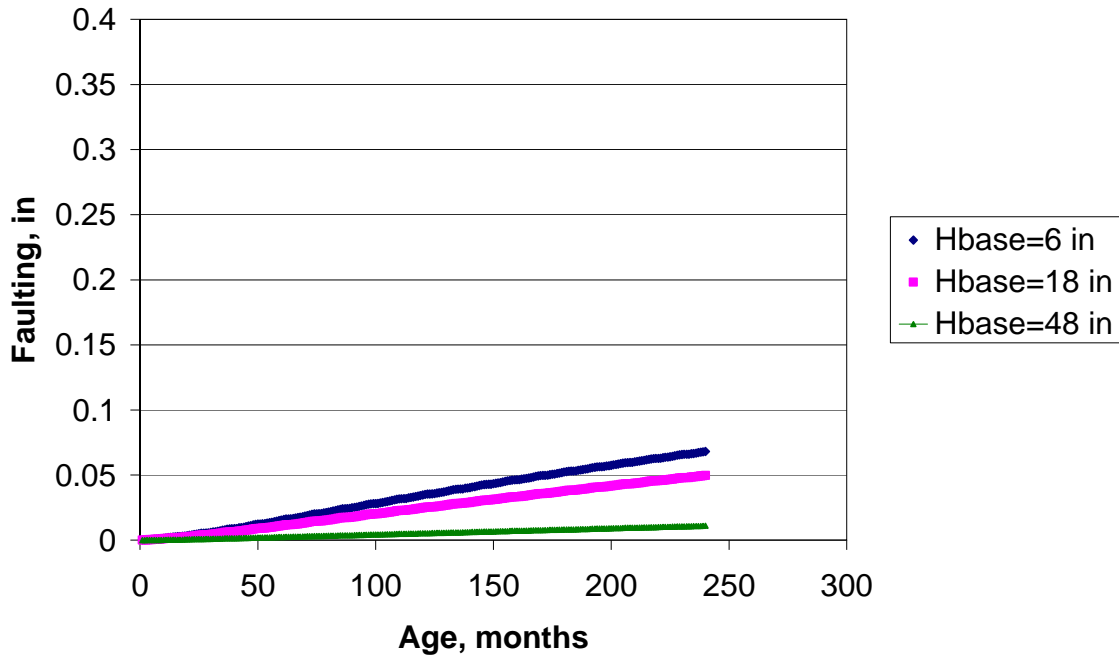


Figure 87 Effect of Base Thickness on faulting. Location -Rochester, AADTT=2000, HPCC =9, COTE =0.0000055, MR=700, Base -Class 5, Lane Width =12, Joint Spacing =15, Dowel D = 1.25, Shoulders - AC, Subgrade - A-6

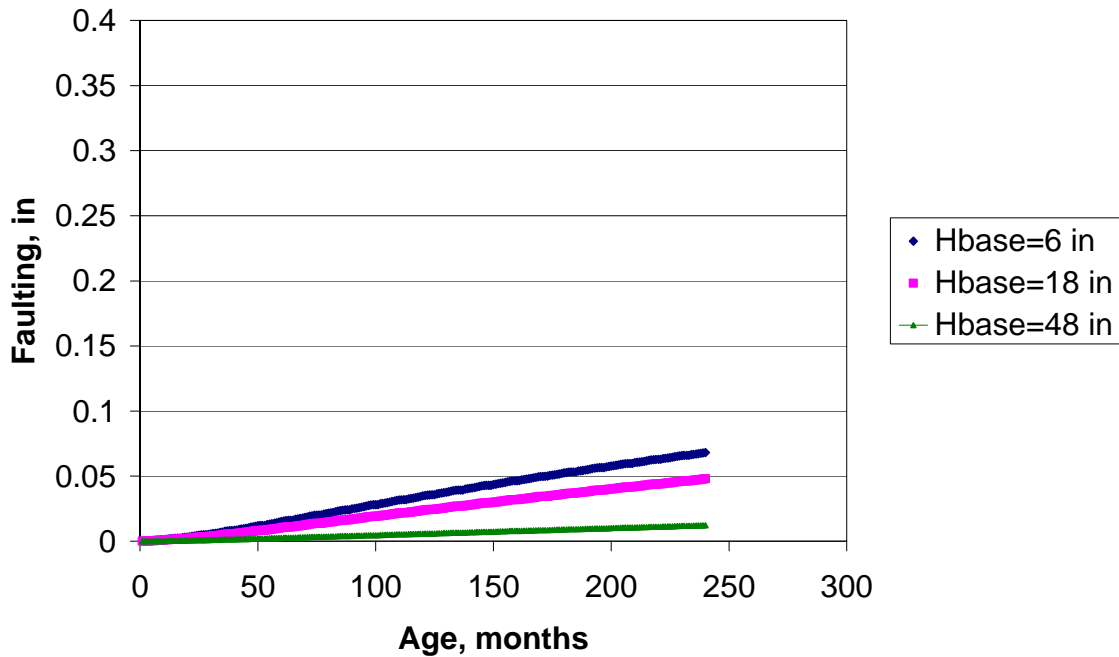


Figure 88 Effect of Base Thickness on faulting. Location -Rochester, AADTT=2000, HPCC =10, COTE =0.0000055, MR=700, Base -Class 5, Lane Width =12, Joint Spacing =20, Dowel D = 1.25, Shoulders - AC, Subgrade - A-6

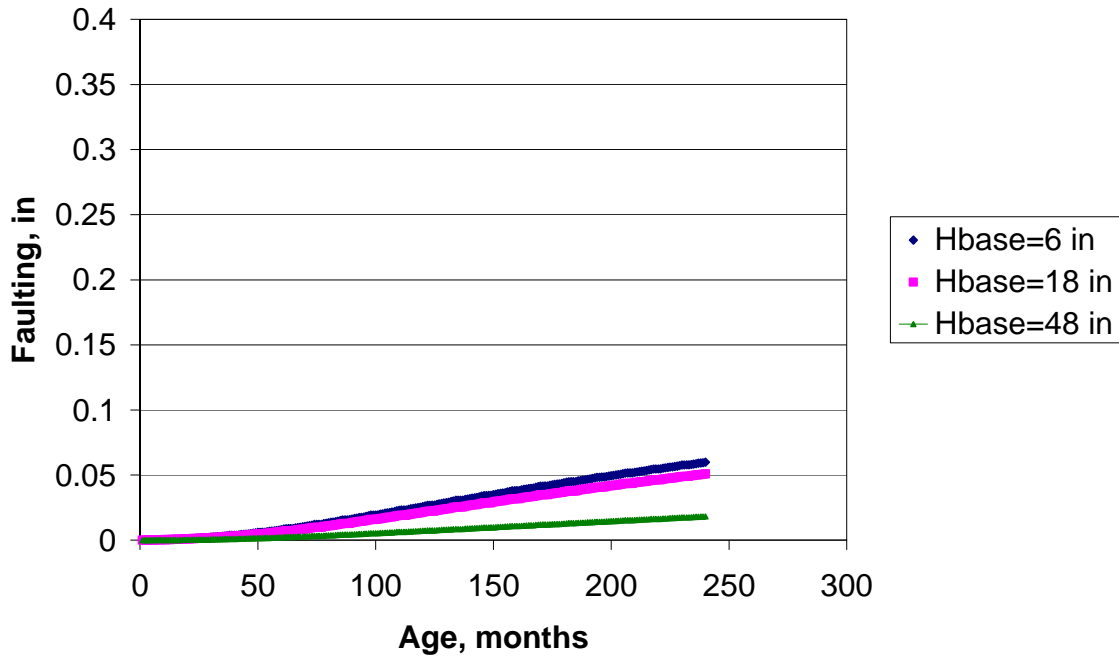


Figure 89 Effect of Base Thickness on faulting. Location -Rochester, AADTT=2000, HPCC =14, COTE =0.0000055, MR=700, Base -Class 5, Lane Width =12, Joint Spacing =20, Dowel D = 1.25, Shoulders - AC, Subgrade - A-6

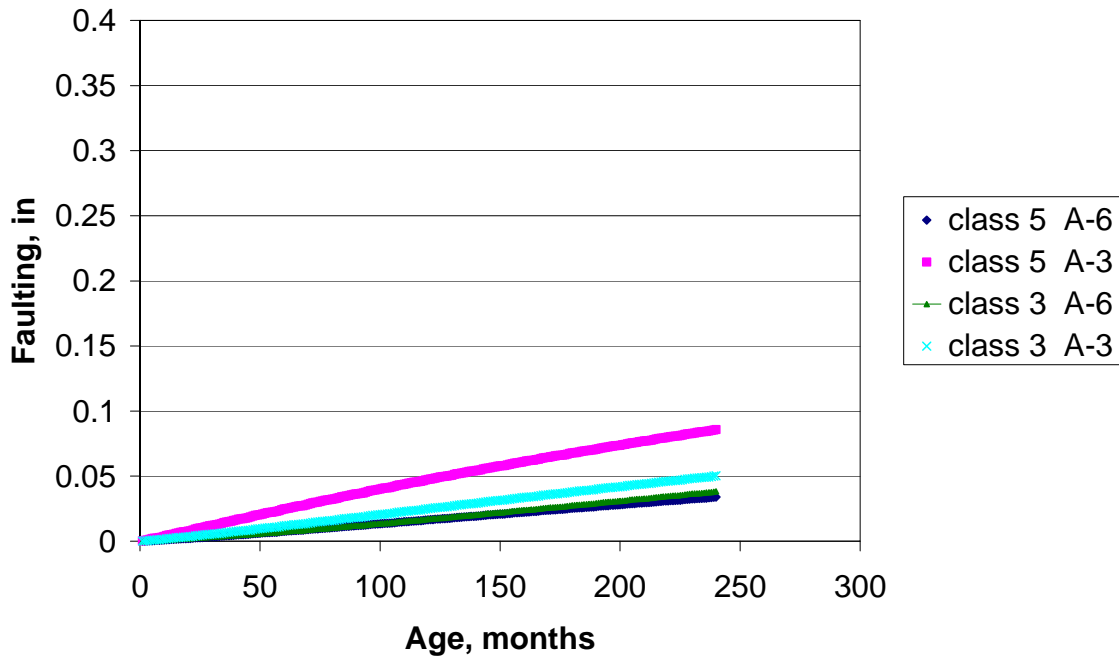


Figure 90 Effect of Base and Subgrade Material on faulting. Location -Rochester, AADTT=2000, HPCC =6, COTE =0.0000055, MR=700, HBase=6, Lane Width =12, Joint Spacing =15, Dowel D = 1.25, Shoulders - AC

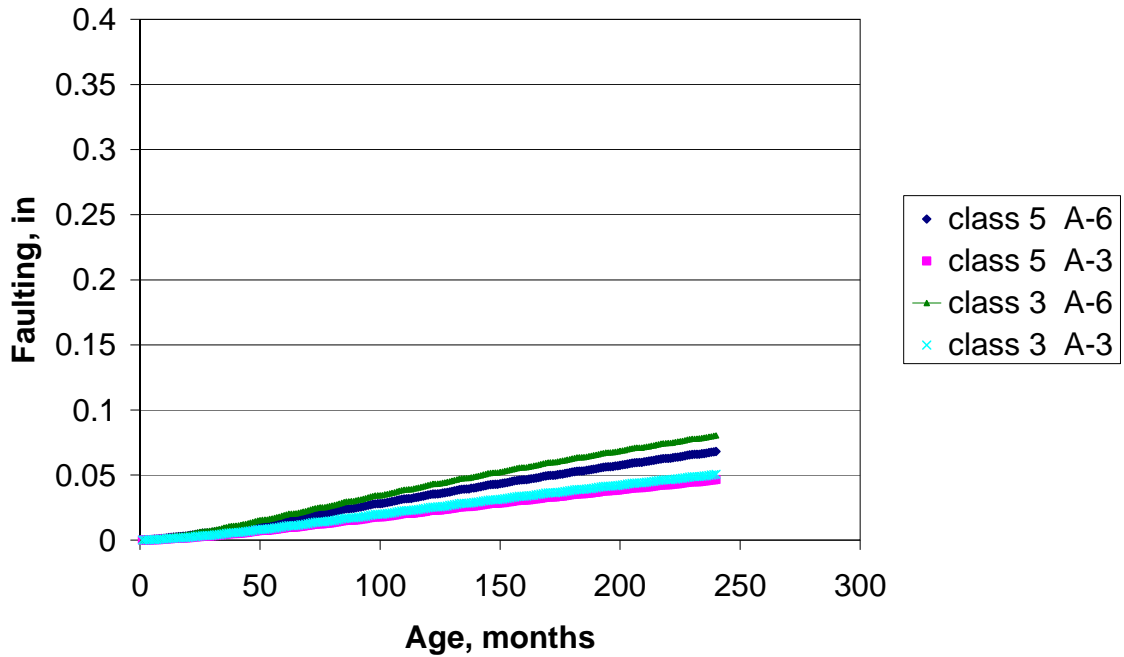


Figure 91 Effect of Base and Subgrade Material on faulting. Location -Rochester, AADTT=2000, HPCC =9, COTE =0.0000055, MR=700, HBase=6, Lane Width =12

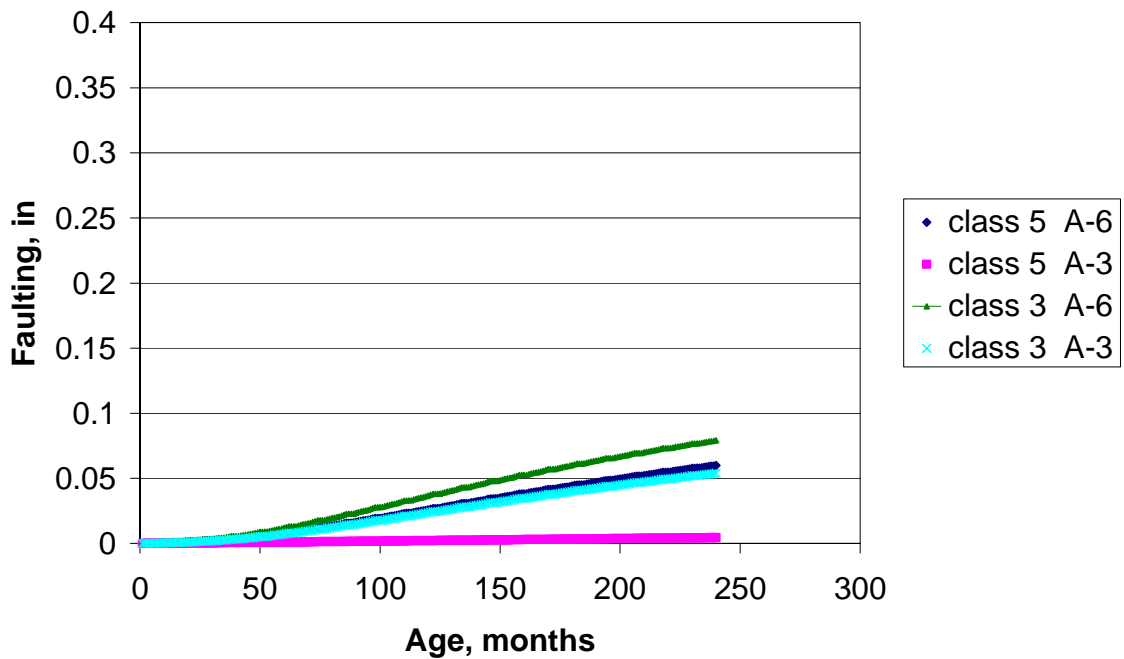


Figure 92 Effect of Base and Subgrade Material on faulting. Location -Rochester, AADTT=2000, HPCC =14, COTE =0.0000055, MR=700, HBase=6, Lane Width =12, Joint Spacing =20, Dowel D = 1.25, Shoulders - AC

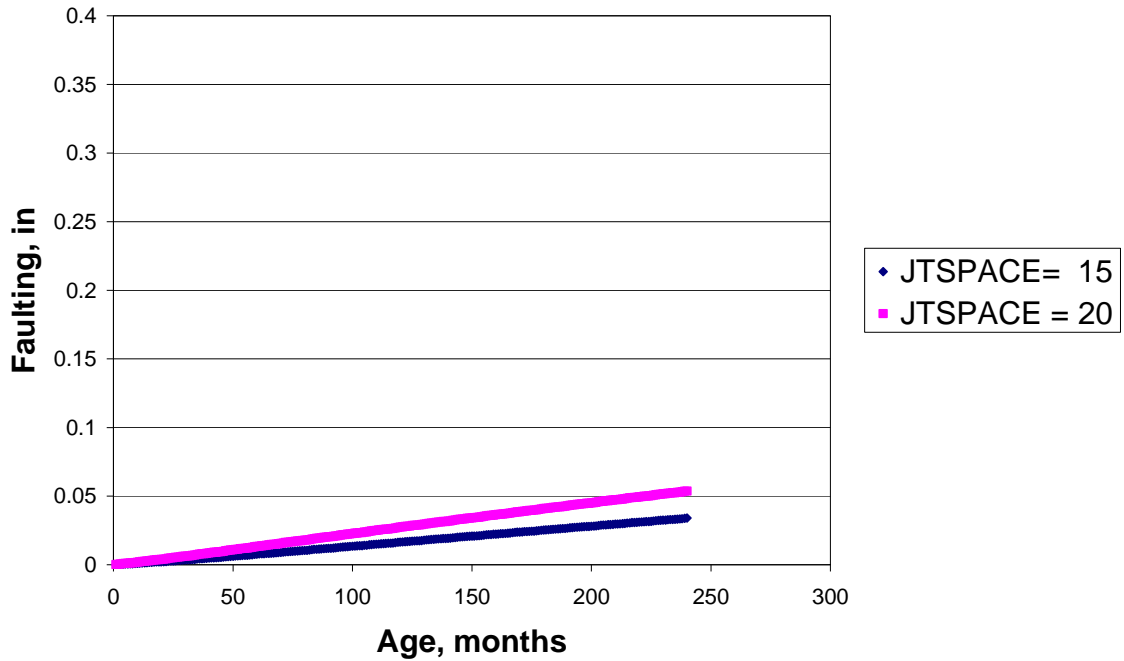


Figure 93 Effect of Joint Spacing on faulting. Location -Rochester, AADTT=2000, HPCC =6, COTE =0.0000055, MR=700, HBase=6, Base -Class 5, Lane Width =12, Dowel D = 1.25, Shoulders - AC, Subgrade - A-6

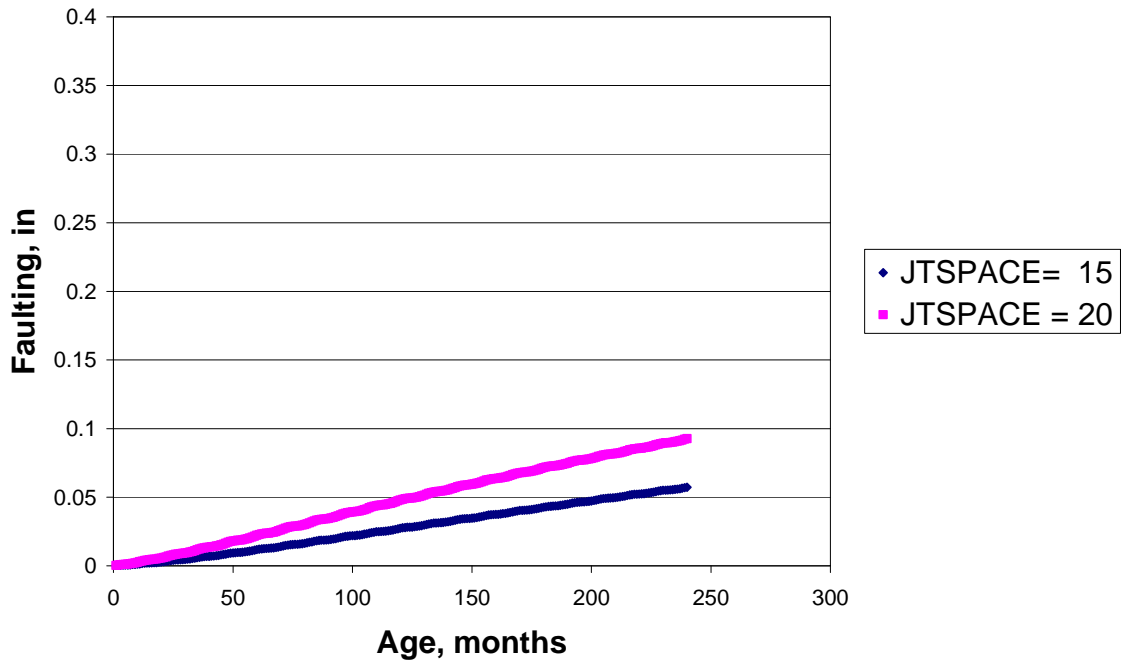


Figure 94 Effect of Joint Spacing on faulting. Location -Rochester, AADTT=2000, HPCC =7, COTE =0.0000055, MR=700, HBase=6, Base -Class 5, Lane Width =12, Dowel D = 1.25, Shoulders - AC, Subgrade - A-6

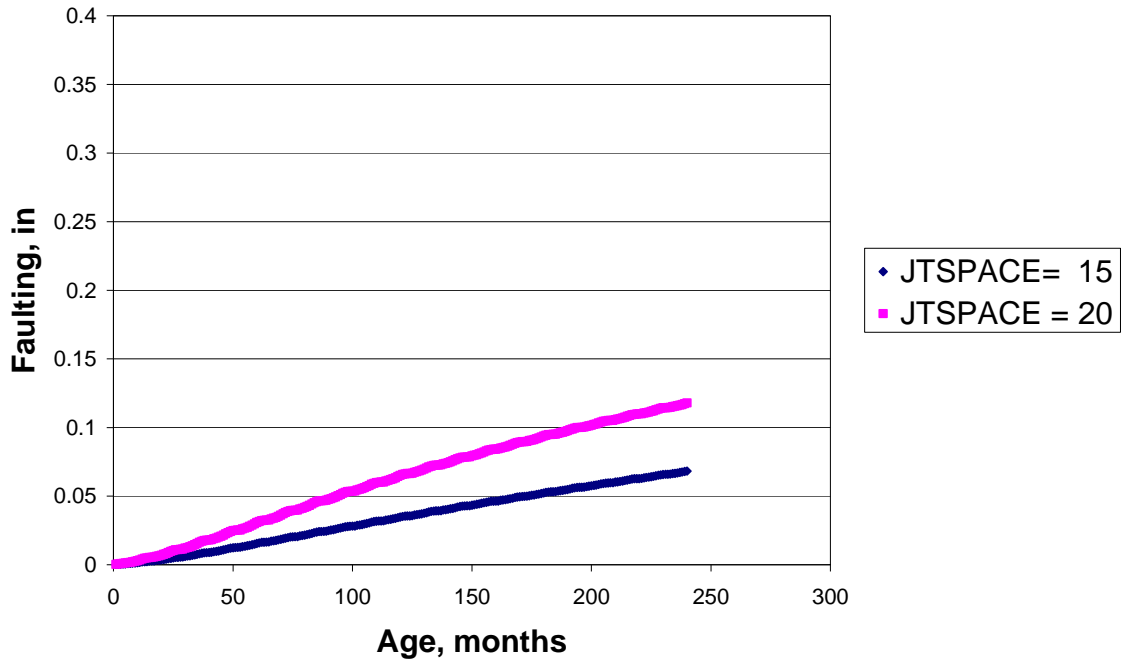


Figure 95 Effect of Joint Spacing on faulting. Location -Rochester, AADTT=2000, HPCC =9, COTE =0.0000055, MR=700, HBase=6, Base -Class 5, Lane Width =12, Dowel D = 1.25, Shoulders - AC, Subgrade - A-6

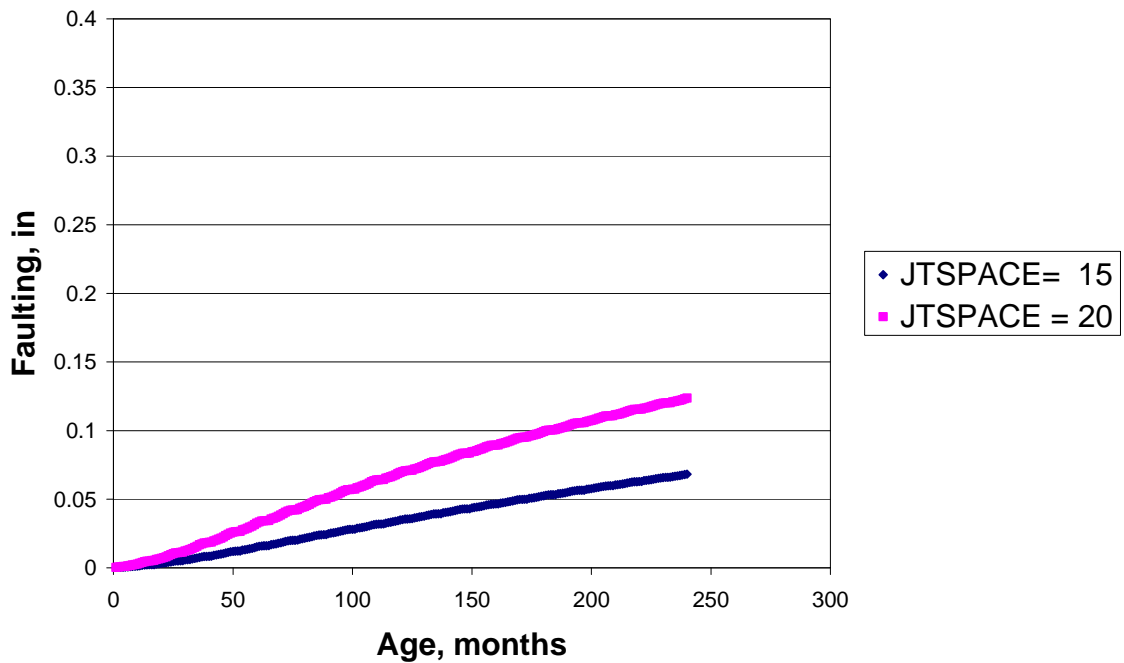


Figure 96 Effect of Joint Spacing on faulting. Location -Rochester, AADTT=2000, HPCC =10, COTE =0.0000055, MR=700, HBase=6, Base -Class 5, Lane Width =12, Dowel D = 1.25, Shoulders - AC, Subgrade - A-6

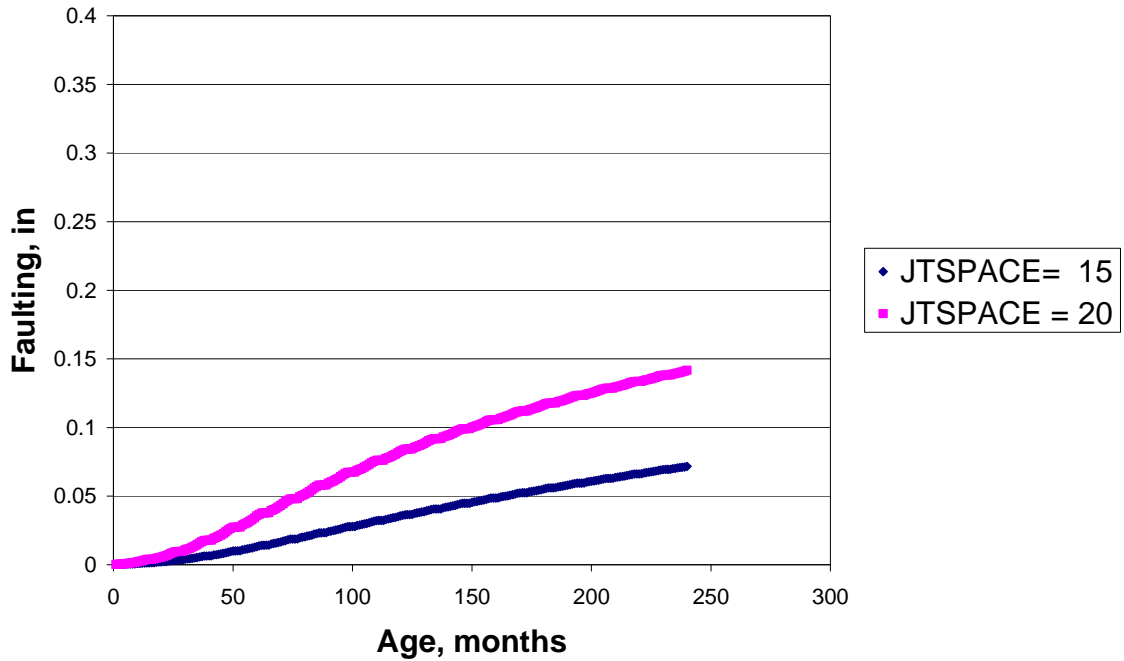


Figure 97 Effect of Joint Spacing on faulting. Location -Rochester, AADTT=2000, HPCC =12, COTE =0.0000055, MR=700, HBase=6, Base -Class 5, Lane Width =12, Dowel D = 1.25, Shoulders - AC, Subgrade - A-6

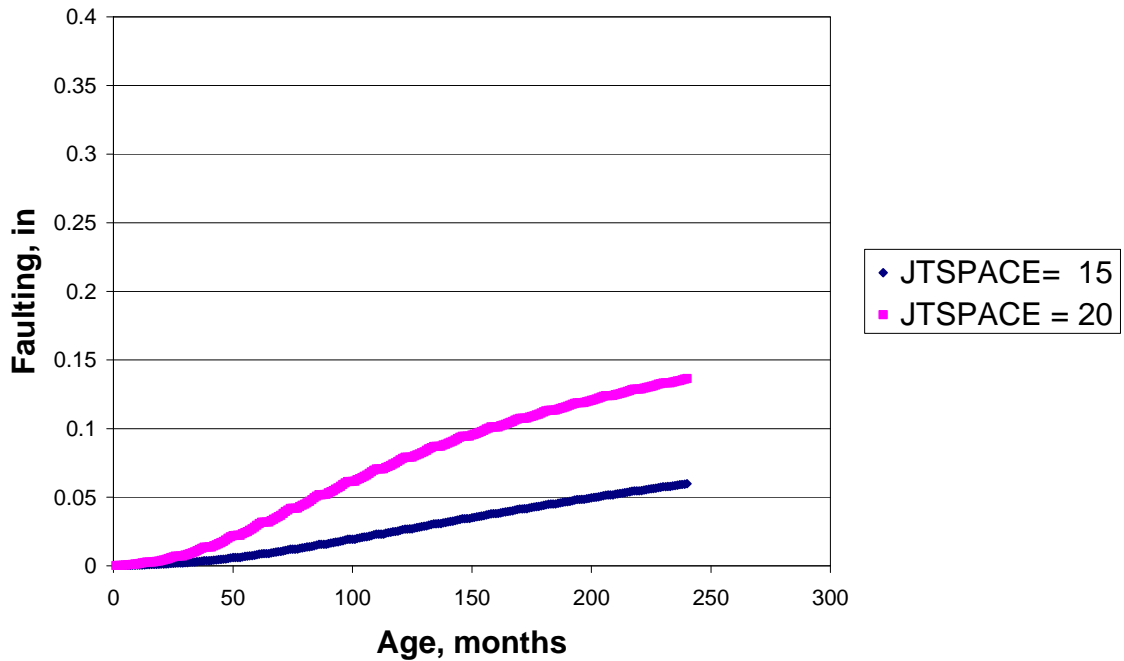


Figure 98 Effect of Joint Spacing on faulting. Location -Rochester, AADTT=2000, HPCC =14, COTE =0.0000055, MR=700, HBase=6, Base -Class 5, Lane Width =12, Dowel D = 1.25, Shoulders - AC, Subgrade - A-6

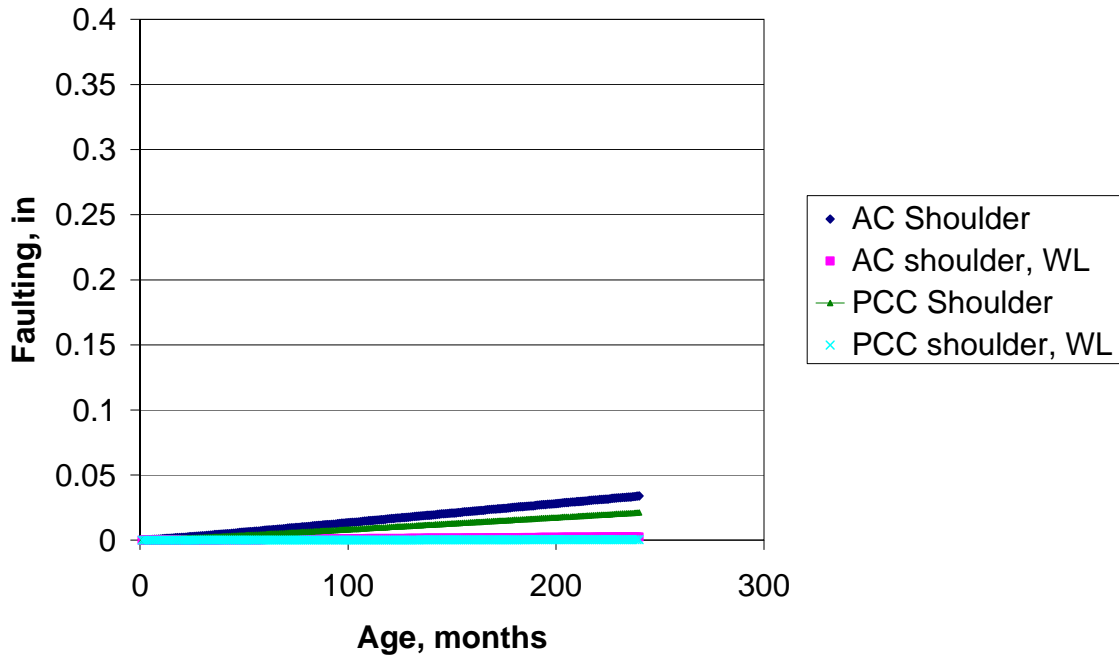


Figure 99 Effect of Edge Support on faulting. Location -Rochester, AADTT=2000, HPCC =6, COTE =0.0000055, MR=700, HBase=6, Base -Class 5, Joint Spacing =15, Dowel D = 1.25, Subgrade - A-6

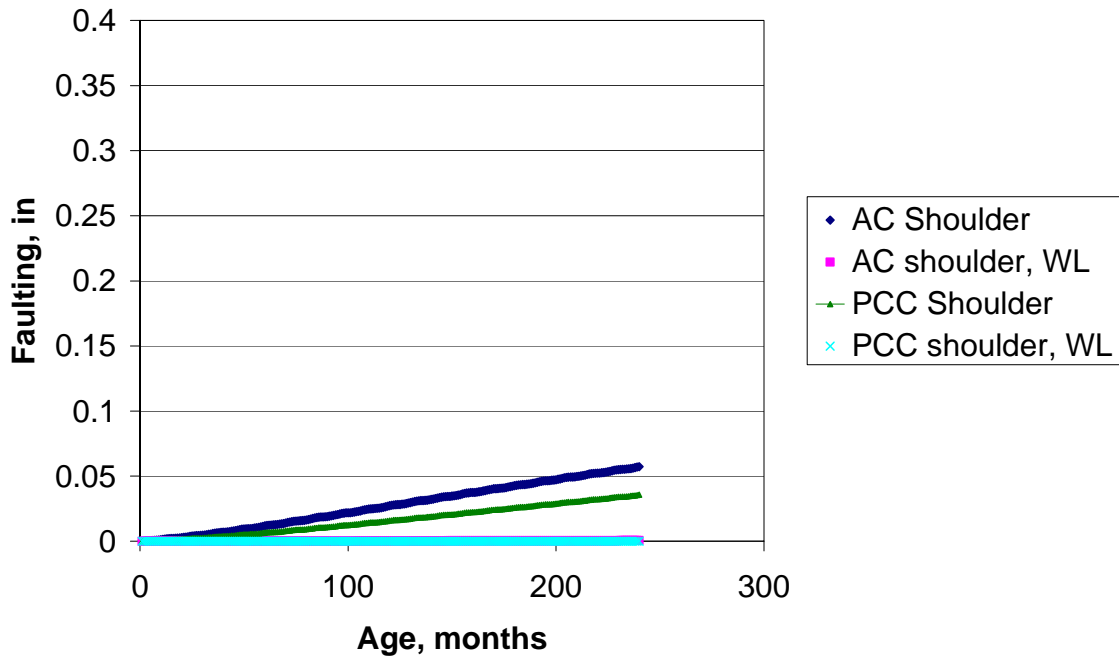


Figure 100 Effect of Edge Support on faulting. Location -Rochester, AADTT=2000, HPCC =7, COTE =0.0000055, MR=700, HBase=6, Base -Class 5, Joint Spacing =15, Dowel D = 1.25, Subgrade - A-6

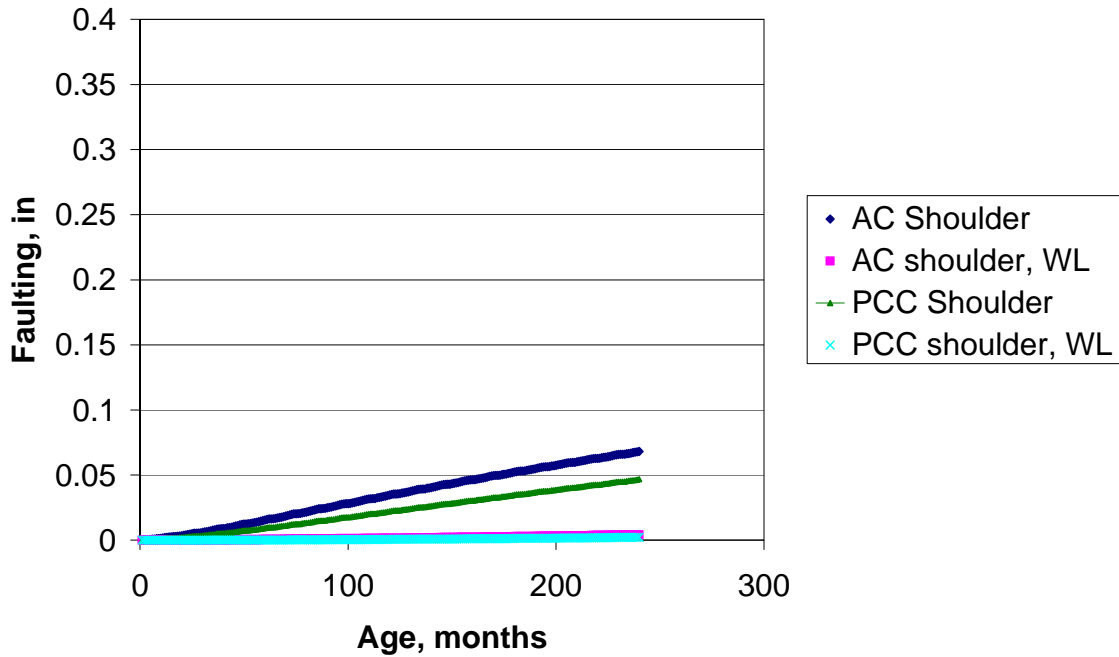


Figure 101 Effect of Edge Support on faulting. Location -Rochester, AADTT=2000, HPCC =9, COTE =0.0000055, MR=700, HBase=6, Base -Class 5, Joint Spacing =15, Dowel D = 1.25, Subgrade - A-6

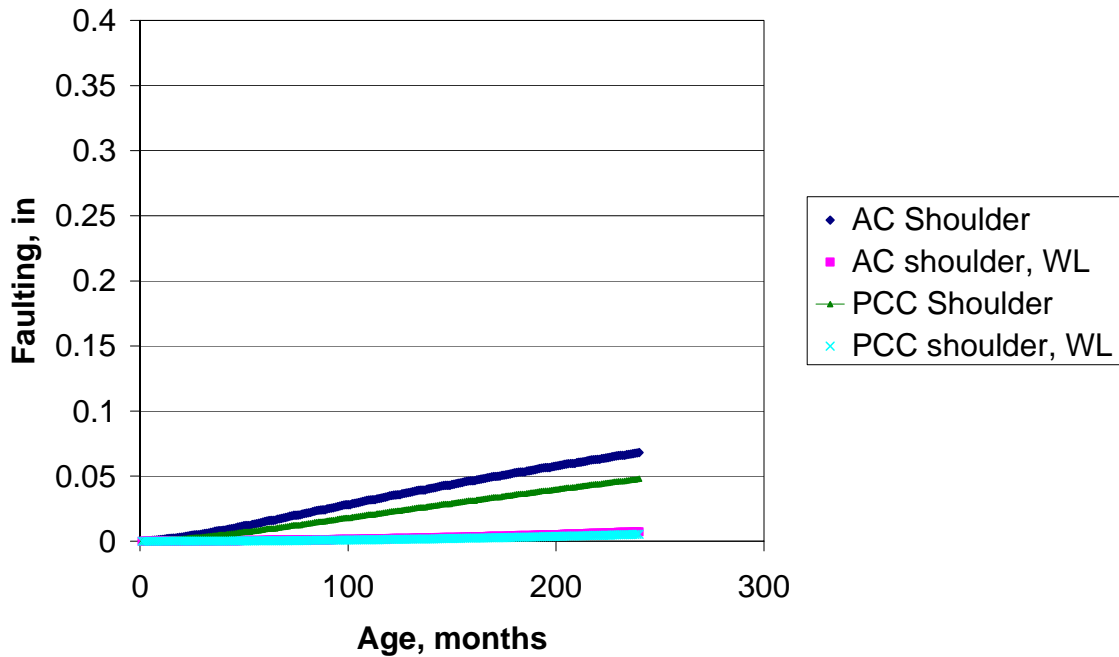


Figure 102 Effect of Edge Support on faulting. Location -Rochester, AADTT=2000, HPCC =10, COTE =0.0000055, MR=700, HBase=6, Base -Class 5, Joint Spacing =20, Dowel D = 1.25, Subgrade - A-6

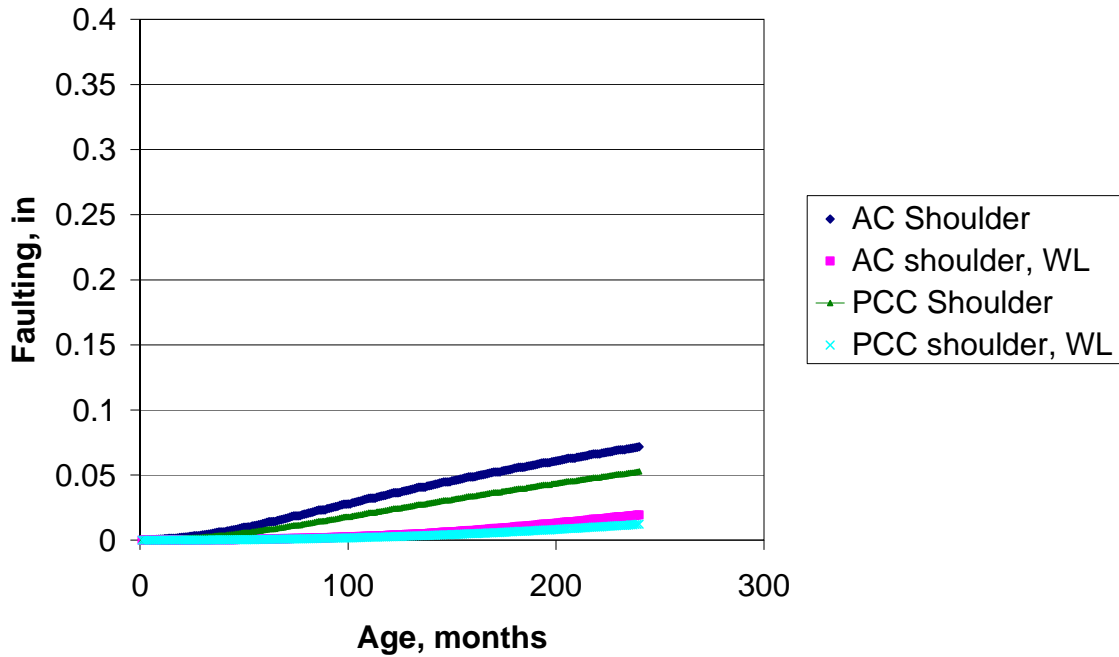


Figure 103 Effect of Edge Support on faulting. Location -Rochester, AADTT=2000, HPCC =12, COTE =0.0000055, MR=700, HBase=6, Base -Class 5, Joint Spacing =20, Dowel D = 1.25, Subgrade - A-6

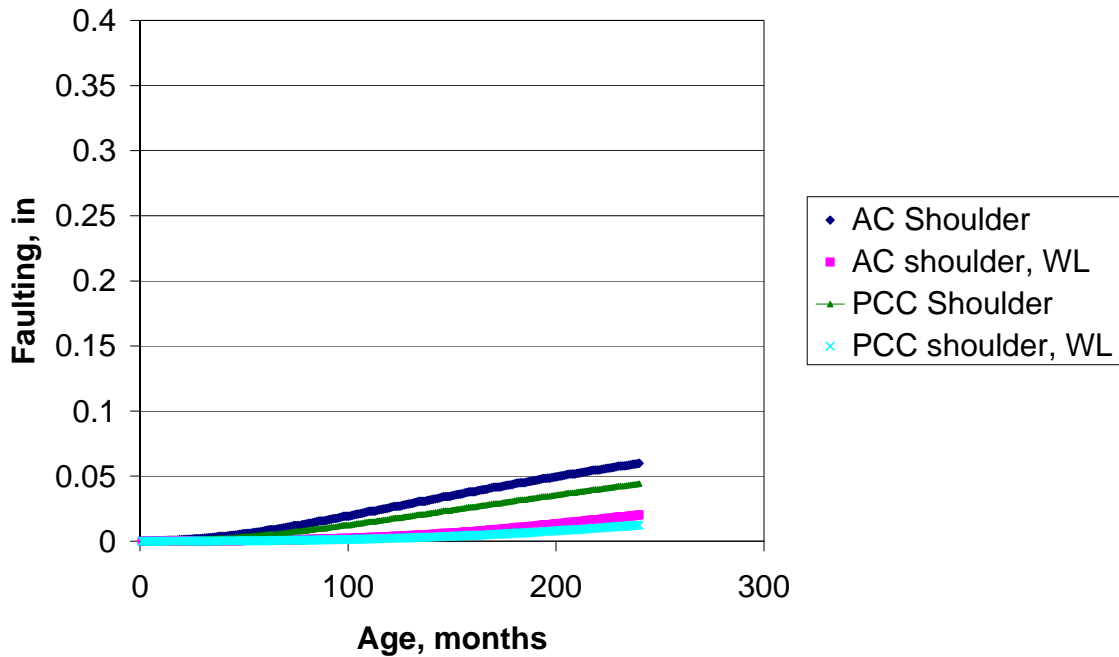


Figure 104 Effect of Edge Support on faulting. Location -Rochester, AADTT=2000, HPCC =14, COTE =0.0000055, MR=700, HBase=6, Base -Class 5, Joint Spacing =20, Dowel D = 1.25, Subgrade - A-6

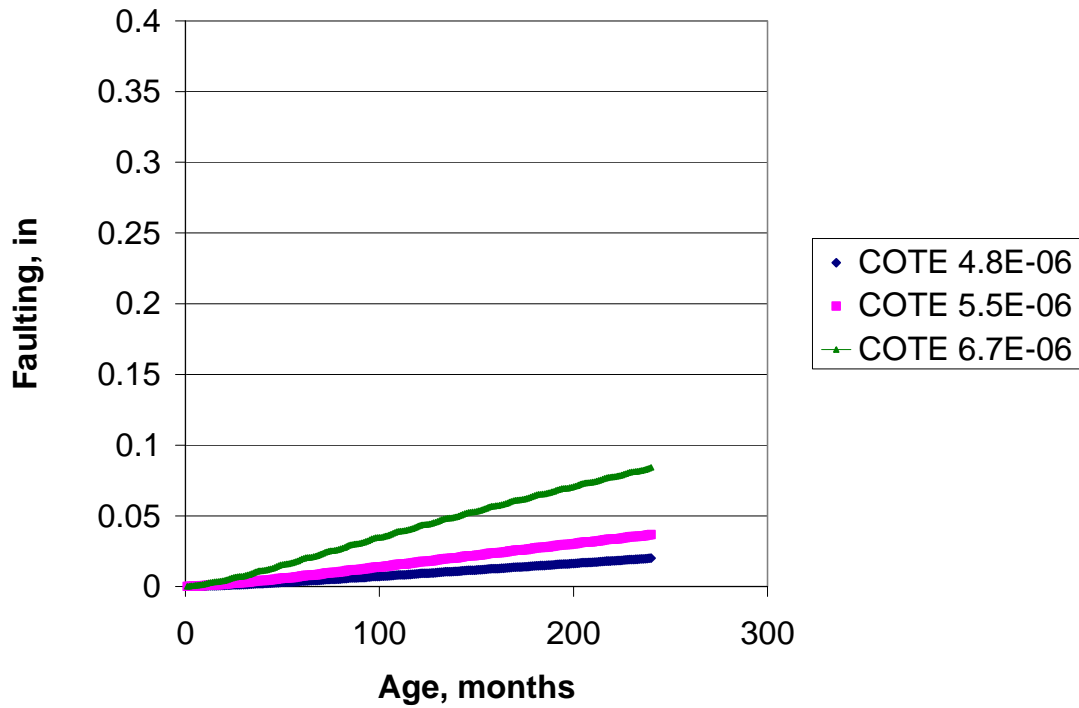


Figure 105 Effect of MR on faulting. Location -Rochester, AADTT=2000, HPCC =14, MR=500, HBase=6, Base -Class 5, Lane Width =12, Joint Spacing =15, Dowel D = 1.25, Shoulders - AC, Subgrade - A-6

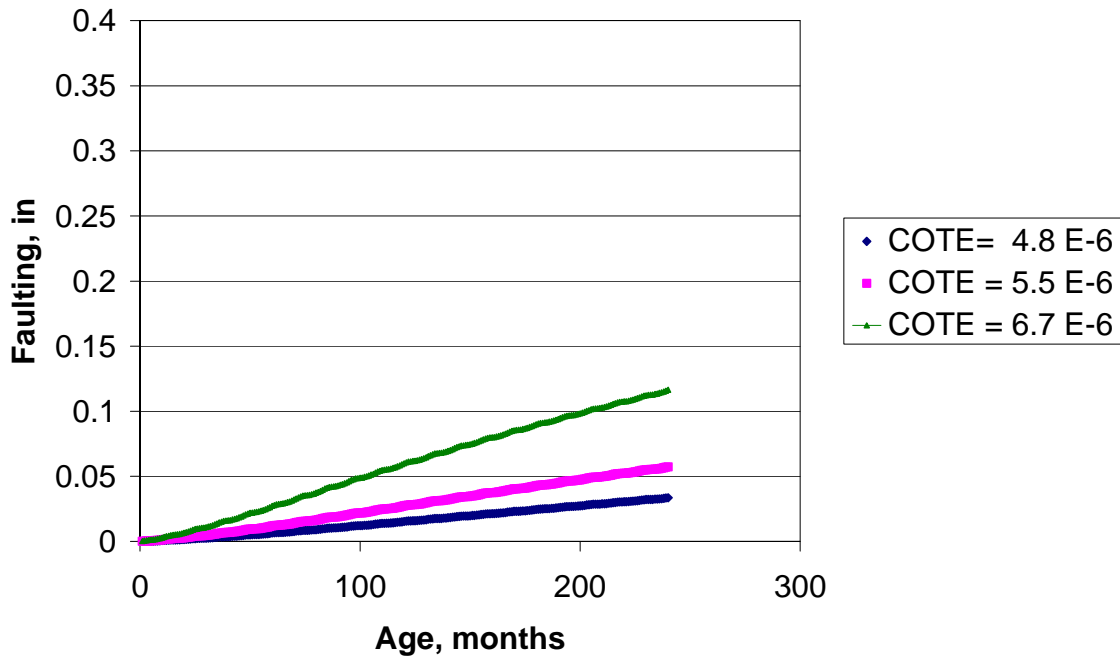


Figure 106 Effect of MR on faulting. Location -Rochester, AADTT=2000, HPCC =14, MR=700, HBase=6, Base -Class 5, Lane Width =12, Joint Spacing =15, Dowel D = 1.25, Shoulders - AC, Subgrade - A-6

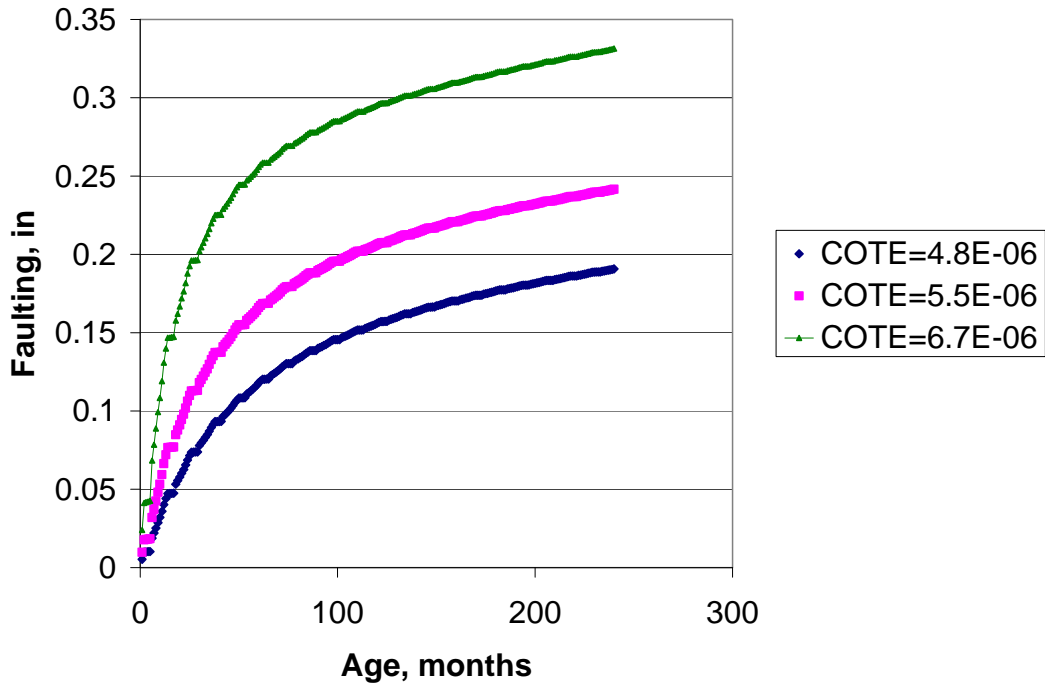


Figure 107 Effect of MR on faulting. Location -Rochester, AADTT=2000, HPCC =14, MR=500, HBase=6, Base -Class 5, Lane Width =12, Joint Spacing =15, Dowel D = 0, Shoulders - AC, Subgrade - A-6

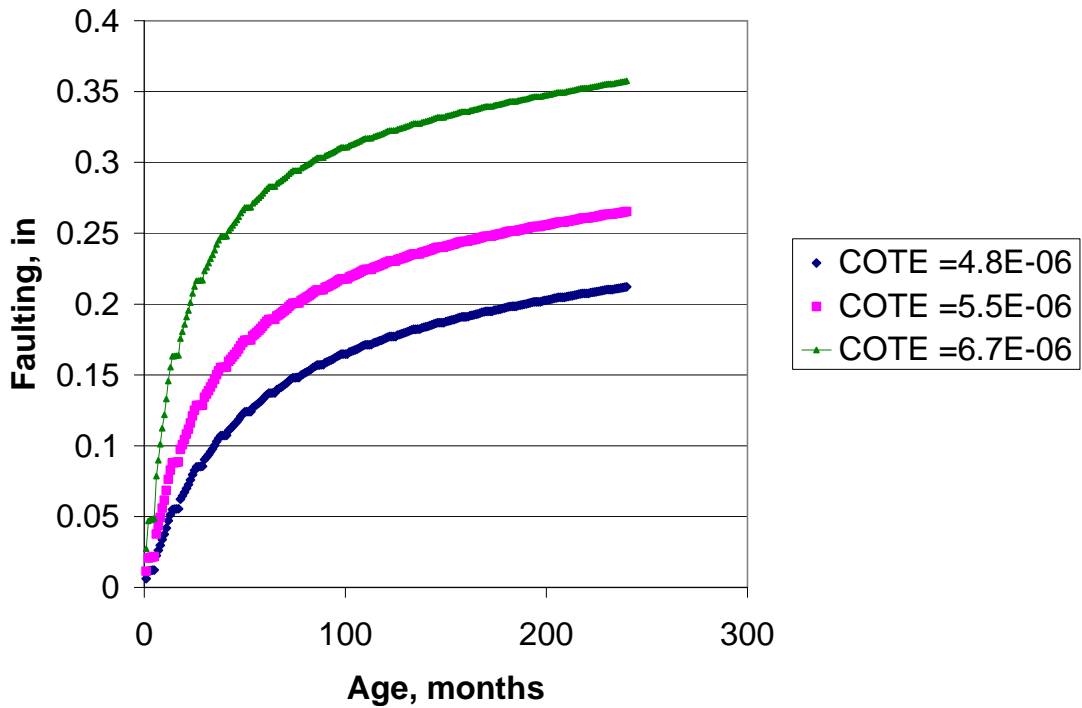


Figure 108 Effect of MR on faulting. Location -Rochester, AADTT=2000, HPCC =14, MR=700, HBase=6, Base -Class 5, Lane Width =12, Joint Spacing =15, Dowel D = 0, Shoulders - AC, Subgrade - A-6